



University of
Strathclyde
Glasgow

Influence of scour on the dynamic behaviour and seismic response of bridges

Ph.D. Thesis

Christos Antonopoulos

Department of Civil and Environmental Engineering

University of Strathclyde, Glasgow

08/05/2025

This thesis is the result of the author's original research. It has been composed by the author and has not been previously submitted for examination which has led to the award of the degree. The copyright of this thesis belongs to the author under the terms of the United Kingdom Copyright Acts as qualified by the University of Strathclyde Regulation 3.50. Due acknowledgement must always be made of the use of any material contained in, or derived from this thesis.

Abstract

Earthquake and scouring are the leading causes of bridge failure worldwide, resulting not only in casualties and fatalities but also in enormous societal and economic losses. A great number of bridges in earthquake-prone countries cross rivers and have shallow foundations, which renders them highly vulnerable to the combined effects of earthquake and flood-induced scour.

This thesis investigates the problem through a combination of experimental and numerical studies that shed light on the effect of scour on the dynamic behaviour and seismic response of structures with shallow foundations. The numerical simulation of the behaviour of the soil-foundation-structural system is conducted in the linear viscoelastic domain using the substructure approach, which allows to decouple the behaviour of the superstructure from the one of the soil-foundation system. The proposed approach, validated against available results from experimental tests carried out on a structural prototype subjected to scour, is used to conduct extensive parametric analyses.

The study results shed light on the effects of scour on the dynamic properties and fundamental frequency of vibration of bridges with shallow foundations and have important implications on the development of inverse techniques for scour identification based on the evaluation of the changes in the bridge modal properties. They also contribute to quantify the impact of scour on the seismic response of bridges with shallow foundations.

Acknowledgements

I would like to thank my supervisor, Enrico Tubaldi, for his guidance throughout my PhD studies and for offering me valuable opportunities which contributed to my professional development. Throughout this journey, I had the chance to collaborate and discuss with experts in the civil engineering field, that contributed significantly to my academic growth by providing their knowledge and publishing together the novelties of my research to academic journals. Specifically, I am grateful to Sandro Carbonari, Fabrizio Gara, Francesca Dezi, Stergios-Aristoteles Mitoulis, Sotirios Argyroudis, Laura Ragni, Athanasios Vratsikidis, Dimitris Pitilakis and Anastasios Anastasiadis.

Further, I would like to thank my close friends, Thanos, Haifa and Georgia for all the fun moments and experiences in and out of the University. Last but not least, I would like to thank my partner, Jonathan, for believing in me and reminding me to rest.

Contents

Abstract.....	i
Acknowledgements.....	ii
Contents	iii
List of figures.....	v
List of tables.....	viii
Main symbols and abbreviations.....	ix
1. Introduction.....	1
1.1 Objectives	2
1.2 Outline	2
1.3 List of Publications.....	3
References.....	4
2 Review of bridge scour and monitoring approaches.....	5
2.1 Bridge scour mechanisms	5
2.2 Local scour.....	6
2.2.3.1 Empirical approaches.....	12
2.2.3.2 Experimental tests.....	13
2.2.3.3 Computational fluid mechanics approaches.....	13
2.2.3.4 Finite element modelling and soil-structure interaction.....	13
2.3 Scour monitoring techniques	14
2.3.1.1 Float-out device.....	15
2.3.1.2 Tethered buried switch	15
2.3.1.3 Time domain reflectometry (TDR)	16
2.3.1.4 Ground penetrating radar (GPR).....	17
2.3.1.5 Fibre-Bragg Grating (FBG)	17
2.3.1.6 Magnetic Sliding Collar (MSC).....	18
2.3.1.7 Sonars.....	18
2.3.1.8 Electrical conductivity devices	20
2.3.1.9 Sounding Rods	20
2.3.2.1 Accelerometers and vibration-based monitoring techniques	21
2.3.2.2 Tilt sensors	23
2.3.2.3 Global Positioning System (GPS).....	23
2.3.2.4 Space-borne synthetic aperture radar interferometry	24
References.....	26
3 Review of combined effects of scour and earthquakes	32
3.1 Introduction.....	32

3.2 Multi-hazard risk analysis and current codes.....	33
3.2.1.1 Fragility analysis.....	35
3.2.1.2 Life-cycle cost and risk assessment	36
3.2.2.1 Impact of climate change on scour.....	37
3.2.2.2 Adaptation strategies for multi-hazard risk.....	37
3.3 Review of studies on the topic	38
3.4 Research gaps.....	39
References.....	40
4 Dynamic behaviour of soil-foundation-structure systems subjected to scour.....	43
4.1 Numerical evaluation of impedance functions	43
4.2 Influence of scour on dynamic behaviour of SFS system	50
4.3 Parametric study	53
4.4 Conclusions	58
Appendix A.....	59
Appendix B.....	55
References.....	57
5 Field tests and numerical analysis of the effects of scour on a full-scale soil-foundation-structural system	58
5.1 Field test setup.....	59
5.2 Numerical modelling strategy	62
5.3 Free-field tests results and comparison with the numerical studies.....	68
5.4 Model updating.....	74
5.5 Conclusions	77
References.....	79
6 Dynamic behaviour and seismic response of scoured bridge piers.....	81
6.1 Model description.....	81
6.2 Soil-foundation system impedance functions.....	86
6.3 Dynamic behaviour of SFS model.....	92
6.4 Seismic response of SFS systems under scour hazard.....	96
6.5 Conclusions	103
References.....	105
7 Conclusions and future work	106
Data availability	108

List of figures

Figure 2-1: i) Different types of scour on a bridge [18] ii) Scour hole around a circular pier due to flowing water [19].....	6
Figure 2-2: Vortex systems around a bridge pier [22].....	7
Figure 2-3: Variation of local scour depth for increasing flow velocity and time [18].....	8
Figure 2-4: Cylinders differing in cross-sections shape, but having the same projected width to the flow [36].....	9
Figure 2-5: Variation on K_θ for increasing values of θ [37].....	10
Figure 2-6: Variation of local scour depth over time [35].....	11
Figure 2-7: i) Float-out device [55], ii) Schematic of float-out device [54]	15
Figure 2-8: Tethered buried switch [56].....	16
Figure 2-9: Typical TDR system [60].	16
Figure 2-10: Schematic of waterbone GPR arrangement.	17
Figure 2-11: Typical GPR profile [62].....	17
Figure 2-12: FBG scour monitoring systems developed by [63].	18
Figure 2-13: i) Manual read out magnetic sliding collar device, ii) Automated read out sliding collar system [65].....	19
Figure 2-14: Schematic of a sonar scour monitoring system [66].	19
Figure 2-15: Schematic of electrical conductivity prove [67].	20
Figure 2-16: Sounding rods installed at a bridge pier [69].	20
Figure 2-17: Reduction in stiffness caused by scour [56].....	21
Figure 2-18: Schematic of tilt sensor device [54].	23
Figure 2-19: Schematic of GPS deployment on a bridge [82].	24
Figure 3-1: Multiple hazards and their corresponding intensity measures to infrastructure systems [11].	34
Figure 3-2: Fragility surfaces for the pier (left column) and the abutment (right column) exposed to scour and earthquake hazards [22].....	35
Figure 3-3: Fragility curve for a bridge with different levels of scour and PGA[23].	36
Figure 4-1: FE model developed in Abaqus of the soil domain with infinite elements at boundaries, (ii) Rigid-body constraint used to simulate the massless rigid strip foundation.	45
Figure 4-2: (i) Forces and (ii) displacements of the strip foundation.....	45
Figure 4-3: Comparisons of impedance functions between those obtained from Abaqus with the analytical solution developed by Hryniewicz [1] (i) k_{zz} , (ii) d_{zz} , (iii) k_{xx} , (iv) d_{xx} , (v) k_{ryry} , (vi) d_{ryry}	47
Figure 4-4: Geometry of the 3 different scour hole scenarios investigated.	47
Figure 4-5: Comparisons of the calculated impedance functions for different scour scenarios (i) k_{zz} , (ii) d_{zz} , (iii) k_{xx} , (iv) d_{xx} , (v) k_{ryry} , (vi) d_{ryry} , (vii) k_{xry} , (viii) d_{xry}	48
Figure 4-6: Ratios $k_{ijscour}/k_{ijno\ scour}$, $d_{ijscour}/d_{ijno\ scour}$ for different scour scenarios.	49
Figure 4-7: Comparisons of the damping factors for different scour scenarios related to (i) k_{zz} and d_{zz} , (ii) k_{xx} and d_{xx} , (iii) k_{ryry} and d_{ryry} , (iv) k_{xry} and d_{xry}	50
Figure 4-8: Ratio $\xi_{scour}/\xi_{no\ scour}$ for different scour scenarios related to direction (i) k_{zz} and d_{zz} , (ii) k_{xx} and d_{xx} , (iii) k_{ryry} and d_{ryry} , (iv) k_{xry} and d_{xry}	50
Figure 4-9: Model of the SFS system.	51
Figure 4-10 : Fundamental vibration frequency of the SFS system for four different scour scenarios.52	52
Figure 4-11: Variation of Π_ω with $\Pi\omega_0$ for different values of Π_h and Π_s for the case of (i) NS, (ii) TS1/4, (iii) TS3/8, (iv) TS1/2.	54
Figure 4-12: Ratio of the natural frequency of the system with and without scour for different levels of Π_h and Π_s for (i) TS1/4, (ii) TS3/8, (iii) TS1/2.	55
Figure 4-13: Ratio of the natural frequency of the system with and without scour for different levels of $\Pi\omega_0$ and (i) $\Pi_h=1$, (ii) $\Pi_h=2$, (iii) $\Pi_h=3$, (iv) $\Pi_h=4$	56

Figure 4-14: Geometry and dimensions of the bridge pier case study.....	57
Figure 4-15: Variation of the fundamental vibration frequency of the bridge using the results of the parametric study and the analytical estimate.	57
Figure 5-1: Geometry and characteristics of EuroProteas [2].....	59
Figure 5-2: Multi-span bridge with simply supported deck exposed to scour.	59
Figure 5-3: Subsoil characteristics from the 30-meter deep borehole BH-02 (left), N_{SPT} blow count from BH-02 (middle), and shear wave velocity profile (right) for cases (a) DH-01: DH test before EuroProteas' construction, (b) V_s values at a site approximately 50 m south of EuroProteas [10], (c) reference model of the valley cross-section from updated geophysical, geotechnical and numerical modelling [11], (d) profile from detailed geotechnical and geophysical surveys [12]. Adapted from Pitilakis et al. [2].	60
Figure 5-4: Installed accelerometers on EuroProteas.....	61
Figure 5-5: (i) Excavation of the soil under the foundation, (ii) Scour hole shape at the end of the final test.	62
Figure 5-6: Superstructure used in fixed-base model.	62
Figure 5-7: Model of SFS system with soil domain (in blue) and absorbing boundary conditions (in yellow) and the structure (in red).....	63
Figure 5-8: Simulation of scour hole at the soil domain of the model i) SFS_1, ii) SFS_1_TS, and iii) SFS_1_SS.	64
Figure 5-9: Geometry and simulation of the scour hole around the embedded foundation for the model i) SFS_1_RS_E and ii) SFS_1_TS_E.	65
Figure 5-10: Shape of the triangular scour holes considered within the two-dimensional modelling approach.....	67
Figure 5-11: Model of the SFS_3 system.	67
Figure 5-12: Singular values (SVs) of the PSD matrix of the response to ambient vibration in the case of no scour.....	69
Figure 5-13: Experimental modal shapes for system with no scour, and normalised scour widths $2s/2b_f = 0.1$ m and $2s/2b_f = 0.25$ m. Plan view of top and base horizontal displacements.....	69
Figure 5-14: Variation of the vibration frequencies of the i) first, ii) second and iii) third monitored mode with the normalized scour width $2s/2b_f$ according to experimental and numerical results from the models SFS_1, SFS_2 and SFS_3.	71
Figure 5-15: Comparison of monitored modes between the models SFS_1, SFS_1_TS and SFS_1_SS.	71
Figure 5-16: Comparison of the normalised vibration frequencies for increasing scour width between the models SFS_1, SFS_1_TS, SFS_1_RS_E and SFS_1_TS_E.....	72
Figure 5-17: Vertical stresses distribution of the soil of the model SFS_1 for i) $2s/2b_f = 0$ and ii) $2s/2b_f = 0.25$ (unit of MPa).....	73
Figure 5-18: Comparison of the non-dimensional ratio $f_{scour}/f_{no\ scour}$ between EuroProteas and Rubbianello bridge.....	74
Figure 5-19: Contact area of soil-foundation interface for i) the case of no scour and for scour width ii) $2s = 0.3$ m iii) $2s = 0.6$ m and iv) $2s = 0.75$ m.	75
Figure 5-20: Numerical modal shapes for system with no scour, and normalised scour widths $2s/2b_f = 0.1$ m, $2s/2b_f = 0.2$ m and $2s/2b_f = 0.25$ m. Plan view of top and base horizontal displacements.	76
Figure 5-21: Variation of the vibration frequencies of the monitored modes with the normalized scour width $2s/2b_f$ derived by the updated SFS_1 model and experiments.....	77
Figure 6-1: (i) Forces and (ii) displacements of the strip foundation.....	82
Figure 6-2: Rigid body constraint used to simulate the massless rigid strip foundation for the case of i) no embedment and ii) embedment depth.	83
Figure 6-3: Geometry of the considered triangular scour hole for a i) no-embedded, ii) embedded foundation.	83
Figure 6-4: i) Considered bridge pier, ii) geometry of the system components.....	84

Figure 6-5: SFS system modelling.....	85
Figure 6-6: Scour scenarios investigated for different embedded depth i) $d_f/b_f = 0$, ii) $d_f/b_f = 0.3$ iii) $d_f/b_f = 0.7$ iv) $d_f/b_f = 1.0$	87
Figure 6-7: Comparisons of the calculated impedance functions of the case of embedded depth $d_f/b_f = 0$ for different scour scenarios i) k_{xx} ii) k_{xry} iii) k_{ryry} iv) d_{xx} v) d_{xry} vi) d_{ryry}	88
Figure 6-8: Comparisons of the calculated impedance functions of the case of embedded depth $d_f/b_f = 0.3$ for different scour scenarios i) k_{xx} ii) k_{xry} iii) k_{ryry} iv) d_{xx} v) d_{xry} vi) d_{ryry}	88
Figure 6-9: Comparisons of the calculated impedance functions of the case of embedded depth $d_f/b_f = 0.7$ for different scour scenarios i) k_{xx} ii) k_{xry} iii) k_{ryry} iv) d_{xx} v) d_{xry} vi) d_{ryry}	89
Figure 6-10: Comparisons of the calculated impedance functions of the case of embedded depth $d_f/b_f = 1.0$ for different scour scenarios i) k_{xx} ii) k_{xry} iii) k_{ryry} iv) d_{xx} v) d_{xry} vi) d_{ryry}	89
Figure 6-11: Comparison of the impedance functions of the case of NS for different embedded depths i) k_{xx} ii) k_{xry} iii) k_{ryry} iv) d_{xx} v) d_{xry} vi) d_{ryry}	90
Figure 6-12: Comparison of the impedance functions of the case of TS1/4 for different embedded depths i) k_{xx} ii) k_{xry} iii) k_{ryry} iv) d_{xx} v) d_{xry} vi) d_{ryry}	90
Figure 6-13: Comparison of the impedance functions of the case of TS3/8 for different embedded depths i) k_{xx} ii) k_{xry} iii) k_{ryry} iv) d_{xx} v) d_{xry} vi) d_{ryry}	91
Figure 6-14: Comparison of the impedance functions of the case of TS1/2 for different embedded depths i) k_{xx} ii) k_{xry} iii) k_{ryry} iv) d_{xx} v) d_{xry} vi) d_{ryry}	91
Figure 6-15: Variation of Π_{ω} for increasing values of $\Pi_{\omega 0}$ for various values of Π_{df} and Π_h	94
Figure 6-16: Ratio of the natural frequency of the system with and without scour for various levels of Π_{df} , $\Pi_{\omega 0}$ and Π_h	95
Figure 6-17: Vibration frequency estimates of the two investigated SFS systems for various scour and embedded depth scenarios and i) $V_s = 300$ m/s, ii) $V_s = 500$ m/s, iii) $V_s = 700$ m/s.....	96
Figure 6-18: Response spectrums of the ground motion records and corresponding scale factors (SF).	97
Figure 6-19: Seismic response of the examined SFS systems under Cubuklu earthquake for various scour and embedded depth scenarios and for $V_s = 500$ m/s.....	98
Figure 6-20: Contribution ratio of the rotational foundation displacement ($\phi_f h_{total}$) to the total deck displacement (u_d) of the SFS systems for i) $V_s = 300$ m/s, ii) $V_s = 500$ m/s and iii) $V_s = 700$ m/s.	101
Figure 6-21: Contribution ratio of the foundation displacement (u_f) to the total deck displacement (u_d) of the SFS systems for i) $V_s = 300$ m/s, ii) $V_s = 500$ m/s and iii) $V_s = 700$ m/s.	102
Figure 6-22: Contribution ratio of the $u_d - u_f - \phi_f h_{total}$ to the total deck displacement (u_d) of the SFS systems for i) $V_s = 300$ m/s, ii) $V_s = 500$ m/s and iii) $V_s = 700$ m/s.	102

List of tables

Table 1-1: Journal publications and corresponding chapters and objectives of this Ph.D. thesis.	3
Table 2-1: Comparison of local scour depths for the pier shapes shown in Figure 2-4 [36].	9
Table 2-2: Shape factors for uniform piers [19].	10
Table 2-3: Mandatory and desirable criteria for successful monitoring of scour conditions on bridges [53].	14
Table 2-4: Comparison of scour monitoring techniques	25
Table 4-1: Vibration frequency of the SFS system for different levels of scour	53
Table 4-2: Units and dimensions of the involved variables	53
Table 4-3: Scour width and results of the parametric study.	57
Table 5-1: Types and names of the installed accelerometers on EuroProteas.	61
Table 5-2: Fundamental frequency of vibration for different structural configurations (case without scour).	68
Table 5-3: Fundamental vibration frequencies of the models SFS_1, SFS_1_TS, SFS_1_RS_E and SFS_1_TS_E for increasing scour width.	72
Table 5-4: Reduction of the vibration frequencies for increasing scour widths with respect to the case of no scour.	73
Table 5-5: MAC values between the experimental mode vectors and the matched numerical mode vectors.	76
Table 6-1: Units and dimensions of the involved parameters.	92
Table 6-2: Assumed values and expressions of the investigated non-dimensional parameters.	93
Table 6-3: Geometry and properties of the examined SFS systems.	96
Table 6-4: Details of the picked ground motions via Rexel [6].	97
Table 6-5: Average peak response values of the SFS system for $h_p = 5$ m and $V_s = 300$ m/s under various scour and embedded depth scenarios.	99
Table 6-6: Average peak response values of the SFS system for $h_p = 5$ m and $V_s = 500$ m/s under various scour and embedded depth scenarios.	99
Table 6-7: Average peak response values of the SFS system for $h_p = 5$ m and $V_s = 700$ m/s under various scour and embedded depth scenarios.	100
Table 6-8: Average peak response values of the SFS system for $h_p = 15$ m and $V_s = 300$ m/s under various scour and embedded depth scenarios.	100
Table 6-9: Average peak response values of the SFS system for $h_p = 15$ m and $V_s = 500$ m/s under various scour and embedded depth scenarios.	100
Table 6-10: Average peak response values of the SFS system for $h_p = 15$ m and $V_s = 700$ m/s under various scour and embedded depth scenarios.	101

Main symbols and abbreviations

Symbols

Latin letters

A	Foundation area in contact with soil
Al	Parameter describing the alignment of the pier with respect to the approach flow
a	Transverse pier width or diameter for a circular pier
b_c	Width of pier cap
b_f	Half foundation width
\mathbf{C}	Damping matrix
c'	Soil cohesion
c_{ij}	Imaginary parts of the impedance functions for the foundation response in i -th direction due to excitation in the j -th direction
d	Pier diameter
d_{50}	Median sediment diameter
d_{ij}	Frequency dependent imaginary parts of the impedance functions for the foundation response in i -th direction due to excitation in the j -th direction
d_w	Water depth
f	Vibration frequency
f_{max}	Maximum frequency of interest
Fr	Froude number
G	Shear modulus
g	Gravity acceleration
h	Total structure height
h_f	Half foundation height
h_s	Superstructure height
I_f	Foundation moment of inertia
k_{ij}	Frequency dependent real parts of the impedance functions for the foundation response in i -th direction due to excitation in the j -th direction
\mathbf{K}	Stiffness matrix
\bar{k}	Impedance function containing both the real and imaginary parts of the impedances
k_s	Superstructure lateral stiffness
l_{max}	Maximum element size
L	Pier length
l_c	Length of pier cap
l_f	Half foundation length
\mathbf{M}	Mass matrix
M	Mass
$M(\omega)$	Moment dependent on frequency of excitation
m_f	Foundation mass
m_s	Superstructure lumped mass
N_{SPT}	Number of strokes in SPT test
$P(\omega)$	Vertical force dependent on frequency of excitation
P_f	Probability of failure
$Q(\omega)$	Horizontal force dependent on frequency of excitation
Re	Reynolds number
s	Half width of the scour-foundation interface
Sh	Pier shape
T	Time
t	Time
t^*	Equilibrium time scale
\mathbf{U}	Vector collecting the degrees of freedom

$\bar{\mathbf{U}}$	Fourier transform of the vector \mathbf{U}
U_c	Critical velocity of bed material required to initiate grain motion
U_f	Flow velocity
u_f	Foundation translation
u_0	Horizontal displacement amplitude
u_s	Relative displacement of the superstructure mass with respect to the base
V_{La}	Lysmer's shear wave velocity
V_s	Soil shear wave velocity
w_0	Vertical displacement amplitude
y_s	Equilibrium scour depth

Greek letters

a_0	Non-dimensional frequency
E	Soil elastic modulus
E_s	Steel Young's modulus
Θ	Kinematic viscosity
θ	Angle of attack
θ_f	Foundation rotation
λ_{min}	Minimum shear wavelength
μ	Friction coefficient
ν	Soil Poisson's ratio
ν_c	Concrete Poisson's ratio
ν_s	Steel Poisson's ratio
ζ	Radiation damping factor
ζ_s	Hysteric damping ratio
Π	Dimensionless parameter according to Buckingham theorem
ρ	Soil density
ρ_f	Fluid density
ρ_{sed}	Sediment density
σ_g	Uniformity of particle size
Φ	Soil friction angle
φ	Upstream scour slope
φ_0	Rotation amplitude
φ_q	Mode vector
φ_r	Mode vector
ω	Circular frequency of excitation
$\tilde{\omega}$	Natural frequency of a Soil-Foundation Structure system
ω_0	Natural frequency of the fixed base system

Abbreviations

3D	Three-Dimensional
ABCs	Absorbing Boundary Conditions
BH	Borehole
CINPE4	Four node finite elements in ABAQUS
CPE4	Four node plane-strain elements in ABAQUS
CPT	Cone Penetration Testing
CS	Cross Section
DH	Downhole
FB	Fixed Base
FBG	Fibre-Bragg Grating
FDD	Frequency Domain Decomposition
FFT	Fast Fourier Transforms

FHWA	Federal Highway Administration
GPR	Ground Penetrating Radar
GPS	Global Positioning System
IC	Including Coupling
MAC	Modal Assurance Criterion
MDOF	Multi Degree of Freedom
NC	Neglecting Coupling
NS	No Scour
PGA	Prak Ground Acceleratiron
SFS	Soil-Foundation-Structure
SFS_1	Structure with soil modelled as a continuum with absorbing boundaries
SFS_1_RS_E	SFS_1 model with rectangular shape scour hole, removing additionally soil elements at both sides of the foundation
SFS_1_SS	SFS_1 model using ‘surface to surface’ contact interface between the soil and foundation
SFS_1_TS	SFS_1 model considering a triangular prism shape of the scour hole
SFS_1_TS_E	SFS_1 model with triangular shape scour hole, removing additionally soil elements at both sides of the foundation
SDOF	Single Degree of Freedom
SF	Scale Factor
SPT	Standard Penetration Testing
SPSS	Soil-Pile-Structure system
TDR	Time Domain Reflectometry
TS	Triangular shaped scour
TS1/4	Triangular shaped scour with a width beneath the foundation equal to 1/4 of the width of the foundation
TS1/2	Triangular shaped scour with a width beneath the foundation equal to 1/2 of the width of the foundation
TS3/8	Triangular shaped scour with a width beneath the foundation equal to 3/8 of the width of the foundation
ÖBB	Austrian Federal Railways

1. Introduction

Bridges are critical components of transport infrastructure networks. Their failure can lead to significant losses: beyond the deaths, injuries, and the costs of replacing the structure, the failure of a single bridge can affect the movement of people and goods in a region for long times [1].

The functioning and stability of bridges can be undermined by various threats. Several studies have investigated and analysed the causes of bridge failure (see e.g. [2] or [4]). Floods and earthquakes are among the most critical natural hazards that can lead to bridge collapse. Among the different actions exerted by the flow of rivers during floods, scour is the most severe one. Scour results in the removal of the soil surrounding the foundations of bridge piers and abutments that are located underwater. The main effects of this action are 1) a reduction of the load bearing capacity of foundation-soil systems, and 2) changes in their stiffness, which manifest themselves with settlements and also variations of dynamic behaviour of the bridge. Structures with shallow foundations are more vulnerable to these actions compared to structures with piled foundations.

Under severe floods, scour could lead directly to structural failure, but in many other circumstances scour could reduce only by a small amount the foundation support and it may not be noticed in post-flood inspections, particularly if the scour hole has refilled. Under these circumstances, other hazards such as earthquakes may impact the bridge. Thus, it is of extreme interest to carry out a multi-hazard analysis to investigate how scour affect the dynamic behaviour and seismic response of bridges. Most of the research carried out to date has focused on the case of bridges with piled foundations (see e.g. [4] for a recent review of the literature), whereas very few studies have analysed the performance of bridges with shallow foundations exposed to scour and earthquakes.

The novelty of this research is based on the investigation of the effects of scour and earthquake hazards on bridges with shallow foundations through both experimental and numerical approaches. The proposed methodologies allow the detection and quantification of the changes of bridge dynamics due to scour and earthquake hazards and can be used for early hazard identification and decision-making. This study presents a non-dimensional framework that simplifies the analysis of scour effects on bridges with shallow foundations. It integrates the scour effects within seismic analysis, enabling more accurate assessment of bridges. This integration is crucial to predicting vulnerabilities and enhancing bridge resilience in multi-hazard scenarios. The findings provide critical insights for updating bridge design codes, particularly in flood and earthquake prone regions. This study fills the gap by developing advanced numerical modelling strategies for dynamic impedance functions and validating these methods against experimental results from free-field tests on a full-scale prototype. These full-scale experiments address the critical research gap of limited experimental studies on how scour affects the dynamic behaviour of bridges, and therefore their seismic response. Furthermore, it highlights the progressive nature of local scour and its quantifiable impact on modal properties, providing a robust framework for real-time monitoring and predictive maintenance. The results demonstrate that the vibration-based monitoring methodologies developed can replace expensive, invasive, and time-consuming traditional scour monitoring techniques by offering accurate, quick, and cost-effective solutions to estimate the scour extent and the dynamic behaviour and seismic response of bridges under scour. Importantly, the effects of scour on the natural frequencies of bridges are presented in a non-dimensional form, enabling quick and easy prediction of scour extent.

This research provides practical tools in addition to the theoretical contribution for bridge management and safety. The proposed non-dimensional framework allows engineers to assess efficiently bridge safety under combined scour and earthquake hazards, and spot quickly high-risk structures. The proposed remote monitoring methodologies enable timely and targeted maintenance by reducing

unnecessary inspections. These advancements are especially valuable for flood and earthquake prone regions, contributing to the sustainability of transport systems.

1.1 Objectives

The PhD study aimed to fill the above knowledge gap, through a combination of experimental and numerical studies that shed light on the effect of scour on the dynamic behaviour and seismic response of structures with shallow foundations. The main objectives (Obj.s) of the PhD study are:

Obj 1: To investigate the fundamental processes of bridge scour, exploring its causes, progression, and impact on seismic response of bridge piers, along with a thorough evaluation of modern scour monitoring techniques and modelling.

Obj 2: To investigate the impact of the progressive nature of local scour on the modal properties of bridge piers, aimed at evaluating the extent of scour.

Obj 3: To analyse and model with different strategies the results of vibration tests conducted on a structural prototype subjected to bridge scour.

Obj 4: To develop and apply a numerical modelling strategy for the analysis of the dynamic behaviour and seismic response of bridges previously exposed to scour.

1.2 Outline

This manuscript is organized into seven chapters. Chapter 2 reviews the mechanisms responsible for the development of scour at bridge foundations, with a particular focus on local scour, and the approaches available for monitoring scour. Chapter 3 summarises and reviews the studies in the literature that have already focused on the topic of combined bridge scour and earthquake action on bridges. Chapter 4 illustrates the numerical modelling strategy developed to investigate the dynamic behaviour of soil-foundation-structure systems subjected to scour. The proposed strategy is based on the development of dynamic impedance functions for shallow foundations under increasing levels of scour, which allow to analyse separately the soil-foundation system and the superstructure. It is specifically addressed to bridges with shallow foundations, although it can be applied in principle to any type of foundations. The results of this study provide useful insight into the effect of scour in terms of variation of the fundamental vibration frequency of bridges, which could be estimated applying vibration-based identification techniques. Chapter 5 analyses the results obtained from field tests carried out on a full-scale structural prototype that has been subjected to increasing levels of scour, with ambient vibrations measured by means of accelerometers. An operational modal analysis technique, the Frequency Domain Decomposition method, has been employed to extract the modal periods and shapes of the system, and numerical analyses employed different strategies have been carried out to interpret the obtained results. Chapter 6 illustrates the extension of the modelling strategy of Chapter 5 to investigate the seismic response of bridges previously exposed to scour. The developed strategy considers a more complex bridge model, and can describe foundations with different embedment depths. The analysis of the seismic response of two representative bridge prototype shed light on the impact of scour on the time history and maximum response of the various degrees of freedom that contribute to the top displacement demand. Chapter 7 provides the overall conclusions of this thesis, highlighting its key contributions, limitations and directions for future work.

The outlined methodology bridges the gap between theoretical and practical advances by integrating experimental validation with advanced numerical modelling. The results of this research work highly contribute to changing bridge engineers' approach on scour monitoring, multi-hazard analysis and seismic design of bridge with shallow foundations, enhancing transport systems against future scour and earthquake events.

1.3 List of Publications

Below is the full list of peer reviewed journal publications that resulted from the study, and their relationship with the chapters and objectives of this thesis mentioned in section 1.1.

Table 1-1: Journal publications and corresponding chapters and objectives of this Ph.D. thesis.

	Journal Publication	Related Chapter	Objective No.
1.	C. Antonopoulos, E. Tubaldi, S. Carbonari, F. Gara, F. Dezi, "Influence of scour on dynamic impedances of bridge shallow foundations", <i>In Proceedings 8th ECCOMAS Thematic Conference on Computational Methods in Structural Dynamics and Earthquake Engineering</i> , Athens, Greece, 2021, pp. 3658-3670.	Chapter 4	2
2.	C. Antonopoulos, E. Tubaldi, S. Carbonari, F. Gara, F. Dezi, "Dynamic behavior of soil-foundation-structure systems subjected to scour", <i>Soil Dynamics and Earthquake Engineering</i> , vol. 152, 106969, 2022. https://doi.org/10.1016/j.soildyn.2021.106969 .	Chapter 4	2
3.	E. Tubaldi, C. Antonopoulos, S.A Mitoulis, S. Argyroudis, F. Gara, L. Ragni, S. Carbonari, F. Dezi, A. Vratsikidis, D. Pitolakis, A. Anastasiadis, "Field Tests and numerical analysis of the effects of scour on a full-scale soil-foundation-structural system", <i>Journal of Civil Structural Health Monitoring</i> , vol. 13, issue 8, pp. 1461-1481, 2023. https://doi.org/10.1007/s13349-022-00608-x .	Chapter 5	3
4.	C. Antonopoulos, E. Tubaldi, S. Carbonari, F. Gara, F. Dezi, "Dynamic behaviour and seismic response of scoured bridge piers", Accepted in <i>Infrastructures</i> .	Chapter 6	4

References

- [1] J.M. Adam, N. Makoond, B. Riveiro, M. Buitrago, “Risks of bridge collapses are real and set to rise – here’s why”, *Nature*, 2024; vol. 629, issue 8014, pp. 1001-1003, 2024.
- [2] L. Deng, W. Wang, Y. Yu, “State-of-the-Art Review on the Causes and Mechanisms of Bridge Collapse”, *Journal of Performance of Constructed Facilities*, vol 30, issue 2, 04015005, 2016.
- [3] G. Zhang, Y. Liu, J. Liu, S. Lan, J. Yang, “Causes and statistical characteristics of bridge failures: A review”. *Journal of traffic and transportation engineering (English edition)*, vol. 9, issue 3, pp. 388-406, 2022.
- [4] M. Badroddin, Z. Chen, “Probabilistic Understanding of Seismic Performance of River-Crossing Bridges with Scour Effects: A Critical Review and Investigation of Seismic-Scour Damage Effects”, *International Journal of Civil Engineering*, vo. 21, issue 6, pp. 915-931, 2023.

2 Review of bridge scour and monitoring approaches

Bridge scour, defined as the removal of sediments around bridge piers and abutments due to flowing water, is the leading cause of bridge failure worldwide [1]-[3]. It causes fatalities and significant socio-economic losses to transportation networks in terms of operational disruptions, high traffic, increased labour demands due to temporary closure, fuel expenditure, detours to the network road, and reconstruction works [4]-[9]. For example, the Austrian Federal Railways (ÖBB) had to deal with more than 100 million EUR financial losses due to flooding [10]. Notably, the Morava River flood of 2006, resulted in severe damage of the Northern Railway with repair cost exceeding EUR 41.4 [10]. This catastrophe led to a complete shutdown of passenger and freight services for several months along the Austrian Northern Railway [11],[12]. Another catastrophic flooding in 2013 had even more significant financial losses for ÖBB over EUR 75 million. These losses stemmed from significant direct damage to multiple track sections and service disruptions, exacerbated by subsequent rainfall-induced events such as debris flows [10]. In the United Kingdom, after heavy flood events, the condition of approximately 1600 flood-induced structures was inspected and it was conducted that more than 20 road bridges were partially or completely collapsed causing significant disruption to the network. It must be mentioned that due to high water levels the Highways and Transport Division started the inspection of the structures after a few hours of the event [13]. According to Lamp et al. [5] scour causes approximately 8.2 million disrupted passenger journeys in Britain rail network, corresponding to economic consequences of between £6 million and £60 million annually. In 2015, winter storms led to a severe damage of bridges throughout Scotland, notably impacting the Lamington viaduct. This event resulted in the closure of the West Coast mainline connecting Glasgow and London for nearly two months due to scour at one of its piers [14]. The subsequent recovery cost exceeded £6 million. Transport Scotland holds responsibility for approximately 1600 bridges, and 8% of them need meticulous consideration, necessitating potential monitoring and scour protection measures. Particularly, approximately £3.5 million must be allocated for identified scour repairs and scour resilience works [15]. In 1987, a 32-year old bridge spanning Schoharie Creek in New York collapsed due to pier scour undermining its foundation. This incident, which resulted in fatalities, prompted the Federal Highway Administration (FHWA) to urge state departments of transportation to evaluate overwater bridges against scour. A decade long investigation revealed that 62.4% of these bridges posed a low risk of scour failure, 20% had unknown foundations, 13.5% were susceptible to scour, and 3.5% were deemed scour critical (approximately 17000 bridges), indicating a high likelihood of failure if subjected to a 100-year flood [16]. Another notable incident in 1987 was the collapse of the Granrhyd Bridge in Wales, which carried the Central Wales line over the River Towy. Investigation concluded that the collapse was caused by local scour at one of the piers, resulting in four fatalities, with channel instability potentially contributing to the failure [17]. In 2009, the Feltham Bridge, a railway bridge over the River Crane, collapsed due to local scour at one of its abutments. Debris in the river redirected water flow towards the abutments, leading to scour during a period of high river flows[17].

Section 2.1 Bridge scour mechanisms explains in detail the different types of bridge and their mechanisms. Section 2.2 Local scour focuses specifically on local scour, examining key factors influencing the scour depth, the importance of scour hole shape and its assumptions in earlier studies, and existing scour modelling approaches in the literature. Section 2.3 Scour monitoring techniques highlights the importance of scour monitoring techniques for early hazard mitigation and provides an extensive literature review of available scour monitoring methods.

2.1 Bridge scour mechanisms

Commonly, there are three types of scour [6]: general, contraction and local scour. General scour is irrespective of a bridge presence and can be either long-term or short-term. It entails the erosion of the

sediment from the bed and banks across the whole or a substantial portion of the of the channel width. On the other hand, contraction and local scour are directly linked to bridge presence. Contraction scour arises from the acceleration of flow induced by a constriction, such as a bridge, and it is generally limited to the immediate vicinity of the constriction, extending only a short distance upstream or downstream, compared to general scour. Local scour is usually the most critical one and occurs due to local features (e.g. bridge piers or abutments) that obstruct the flow, resulting in turbulence and formation of vortices, which in turn lead to local sediment movement and erosion around underwater foundations [18]. Figure 2-1 illustrates the three different types of scour can occur in a bridge and the formation of vortices due to flowing water to a circular pier, and hence the formation of a scour hole. In many cases, the most significant contribution to total scour is due to local scour. Thus, the next subsection provides a more in-depth description of the phenomenon and of the parameters that affect it.

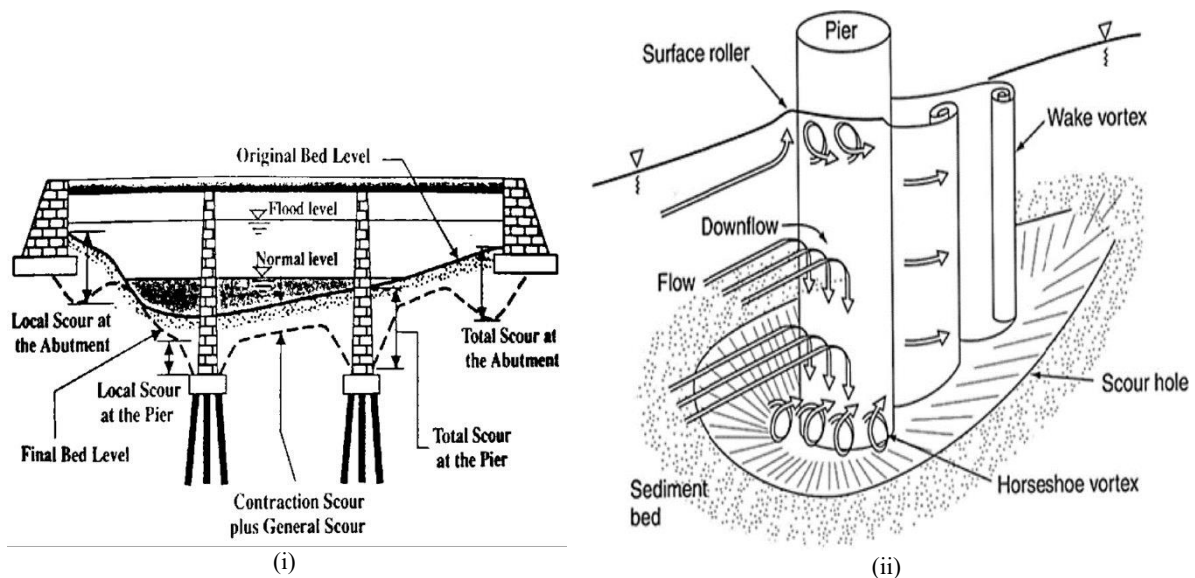


Figure 2-1: i) Different types of scour on a bridge [18] ii) Scour hole around a circular pier due to flowing water [19].

2.2 Local scour

Breusers et al. [20] defines scour as a natural phenomenon resulting from the flowing water, which removes and erodes material from the bed and bank of streams, but also from the surrounding areas of bridge piers and abutments. According to Chiew [21] the scour around an obstruction, such as a bridge pier, is caused by the system of vortices developed around the obstruction, which can divide into the followings:

1. Horseshoe vortex combined with the downflow in front of the pier
2. Vortex shedding (wake vortex) at the back of the pier
3. Trailing vortex (only if the pier is completely submerged in water)

The basic mechanism causing local scour at piers is the down-flow at the upstream face of the pier and formation of vortices at the base. As the flow approaches the pier, it gradually decelerates until it comes to rest at the pier face. At the upstream side of the pier, the approach flow velocity diminishes to zero leading to an associated increase in pressure at the pier face. The pressures are highest near the water surface, where the deceleration is greatest, and reduce with depth [23]. Given the gradual reduction in velocity from the water surface to the bed, the pressure exerted in the pier face similarly reduces, thereby forming a downward pressure gradient. Consequently, this pressure gradient propels the flow downward along the pier face, resembling that of a vertical jet. The resulting downward flow impacts the streambed, creating a scour hole in the vicinity of the pier base. The downflow impacting the bed is the

main factor responsible for scour [23]. Figure 2-2 illustrates the flow and scour patterns surrounding a pier under current action. The robust vortex dynamics engendered by the pier presence lead to bed sediments within the vicinity of the pier base. Subsequently, the downflow rolls up forming a hole, and evolves into a complex vortex system through interaction with the upcoming flow. The vortex propagates downstream along the sides of the pier, commonly referred to as a horseshoe vortex due to its resemblance to the shape of a horseshoe [20]. The horseshoe vortex demonstrates considerable efficacy in transporting displaced particles beyond pier's vicinity. The horseshoe vortex strength reduces for increasing scour depth, resulting in a reduction of the sediment transport from the pier base [24]. Downstream the base of the pier, there are also the vertical vortices, known as wake vortices, which arise from the separation of the water flow at the sides of the pier [25]. These vortices are unstable, alternately shedding from either side of the pier. Both types of vortices contribute to the erosion of material at the base of the pier. However, the intensity of wake vortices decreases significantly with increasing distance downstream, leading to sediment deposition immediately downstream of the pier [26].

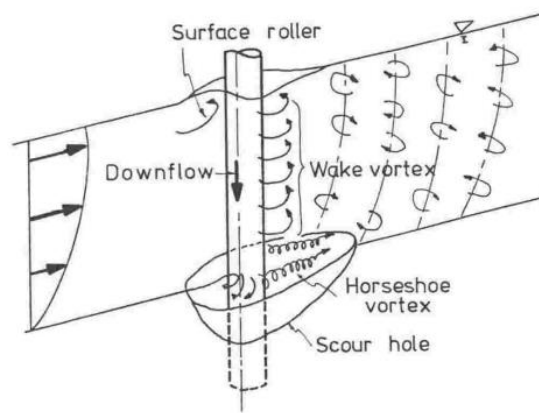


Figure 2-2: Vortex systems around a bridge pier [22].

2.2.1 Factors influencing local scour depth

Scour is a complex phenomenon whose geometry and rate are affected by multiple factors, including hydraulic conditions, sediment characteristics, channel morphology and bridge design. Understanding these factors is vital for providing not only accurate scour prediction approaches, but also a safe design of effective scour mitigation measures. Hence, establishing such equilibrium requires a certain amount of time, which holds particular significance during flood events. The equilibrium scour depth depends on the following parameters [27]:

$$y_s = f \left[\begin{array}{l} \text{Fluid properties } (\rho_f, \vartheta, U_f, d_w, g, \theta); \text{ Pier geometry } (a, L, Sh, K_{sh}, Al); \\ \text{Sediment properties } (d_{50}, \sigma_g, U_c, \rho_{sed}); \text{ Time } (t) \end{array} \right] \quad (2.1)$$

where ρ_f is the fluid density, ϑ is the kinematic viscosity, U_f is the flow velocity, d_w is the water depth, g is the acceleration due to gravity, θ is the angle of attack for the fluid properties. When it comes to pier geometry, a is the transverse pier width or the diameter for a circular pier, L is the pier length, Sh is the pier shape, K_{sh} is the pier shape factor, and Al is a parameter describing the alignment of the pier with respect to the approach flow. Subsequently, sediment properties are described by the median sediment diameter d_{50} , the uniformity of particle size σ_g , the critical velocity of bed material required to initiate grain motion U_c , and the sediment density ρ_{sed} .

Equation 2.2 indicates the dimensionless parameters used in most scour estimation methods. The most experimental studies undertaken under laboratory conditions investigate scour by means of Equation

2.2 using fixed values of pier shape for high values of flow Reynolds number (Re), subcritical Froude number (Fr) and approach flow aligned with the pier [27].

$$\frac{y_s}{a} = f\left[\frac{d_w}{a}, \frac{U_f}{U_c}, \frac{a}{d_{50}}, \frac{L}{a}, Sh, Re, Fr, \frac{t}{t^*}\right] \quad (2.2)$$

Flow shallowness, d_w/a

Melville and Coleman [18] classified the flow field by using the flow shallowness factor (d_w/a). The piers are classified as narrow when $d_w/a > 1.4$, as intermediate when $0.2 \leq d_w/a \leq 1.4$, and lastly as wide when $d_w/a < 0.2$. More in detail, scour depth for narrow piers increases for increasing a and is independent of d_w , while increases for increasing d_w and is independent of a for wide piers. For intermediate piers, the scour depth depends on both a and d_w . Jalal et al. [28] analysed different pier shapes with various flow shallowness ratio (0.197, 0.984, and 2.953) and resulted that for $d_w/a < 0.2$ scour decreases, while for $d_w/a > 1.4$, scour depth reaches a climax and depends primarily on pier width.

Relative coarseness, a/d_{50}

In the same study, it was concluded that the impact of sediment is negligible when $a/d_{50} > 50$, while Lee and Strum [29] showed that the relative coarseness has a limited effect on d_{se} due to the scaling of the sediment size for $a/d_{50} > 100$, which is aligned with the recently obtained results by Misuriya et al. [30]. The uniformity of the particle size (σ_g) is inversely proportional of the ratio d_{se}/a , while its effect on the scour hole is minor for high values of U_f .

Flow intensity, U_f/U_c

Local scour around bridge piers can be formed either under clear-water or live-bed conditions. More in detail, local scour under clear-water conditions typically occurs when the flow velocity around a pier or a structure remains below the threshold required to mobilise sediment in the riverbed ($U_f/U_c < 1$), and therefore no additional sediment is supplied from upstream, resulting in a gradual erosion around the structure. Oppositely, live-bed scour occurs when sediment is continuously supplied to the scour hole, and there is a dynamic equilibrium between sediment supply and the transport of sediment out of the scour hole due to flowing water ($U_f/U_c > 1$). Figure 2-3 illustrates the variation of local scour depth around piers for increasing flow velocity.

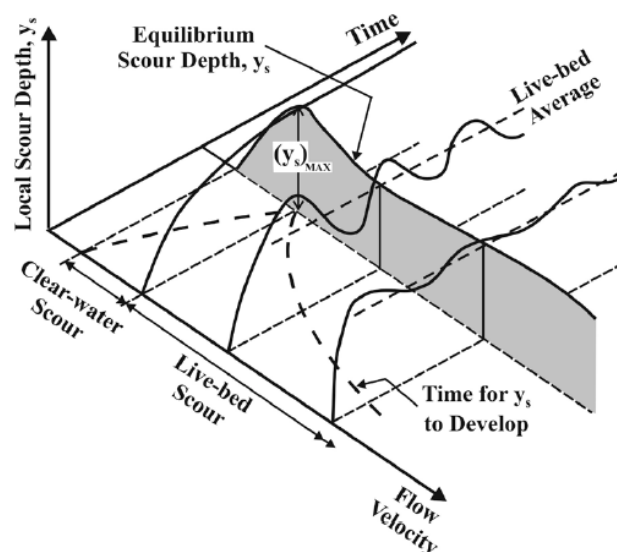


Figure 2-3: Variation of local scour depth for increasing flow velocity and time [18].

In terms of local scour under clear-water conditions, a few researchers (e.g. [18],[31]) have investigated how different sediment types affects scour depth. The comparison of scour depth resulting from different sediment types (uniform or non-uniform) reveals that the scour depth in non-uniform sediments tends to be shallower than that in uniform sediments. This difference is attributed to the accumulation of larger particles at the bottom of the scour hole, forming an armour layer that necessitates higher flow velocities to erode [31]. The local scour depth in uniform sediment increases almost linearly for increasing velocity, reaching its maximum value at the threshold velocity.

The local scour depth under live-bed conditions is dependent on the size and steepness of bed at specific flow velocities [21], [32]-[36]. Deeper and steeper bed features result in lower scour depth because the sediment delivered by a passing bedform is not completely removed from the scour hole before the next bedform arrives. The maximum scour depth occurs around the transition to a flatbed condition, characterised by elongated bedforms of negligible height [37].

Pier aspect ratio, L/a

Size of the pier is the main factor affecting scour depth [28]. The frequency of the vortex shedding and wake vortices are directly linked to the pier width. Mostafa [38] investigated the influence of the aspect ratio L/a on the scour depth for various shaped piers (Figure 2-4) and concluded that the scour depth can increase dramatically, and particularly for the rectangular shaped piers compared to the circular ones under the same conditions. For the sake of thoroughness, Table 2-1 summarises the findings of the study.



Figure 2-4: Cylinders differing in cross-sections shape, but having the same projected width to the flow [37],[38].

Table 2-1: Comparison of local scour depths for the pier shapes shown in Figure 2-4 [37],[38].

Shape (Figure 2-4)	L/a	Projected width of pier (mm)	$\frac{y_{s(non\ circular)}}{y_{s(circular)}}$
A	4		1.50
B	4		1.33
C	1		1.29
D	200	140	1.28
E	1		1.28
F	1		1.07
G	1		1.00

Omara et al. [39] experimentally investigated various scoured rectangular piers with varying L/a ratios. The results of this study show that as L/a increases beyond 4.5, scour depth continues to increase but at a reduced rate.

Pier shape, Sh

The shape of the pier plays a vital role in the estimation of the scour depth as different shapes lead to different interactions between the approach flow and the pier. Additionally, the formation of horseshoe and wave vortices is influenced by the shape of the pier [21]. Shape effects are usually described by the multiplying factor K_{sh} , which subsequently describes the difference in local scour between a particular

pier shape and a simple circular pier [37]. Table 2-2 shows recommended values of K_{sh} for different pier shapes.

Table 2-2: Shape factors for uniform piers [19].

Pier Shape	K_{sh}
Circular	1.0
Round Nosed	1.0
Square Nosed	1.1
Sharp Nosed	0.9

Pier Alignment, θ

The extent of local scour around various shapes of pier, excluding circular ones, is significantly affected by the pier alignment (θ) relative to the approaching flow. There is an increasing scour depth for increasing values of θ due to the increasing effective frontal width of the pier. The effects of pier alignment are usually taken into account by means of the multiplying factor K_θ .

The effects of pier alignment have been studied by Laursen and Torch [40] for rectangular piers and concluded that the higher the ratio L/a , the higher the scour depth for increasing values of θ . In order to highlight the importance of the pier alignment on scour development, Figure 2-5 illustrates the variation of K_θ for increasing values of θ and L/a [40].

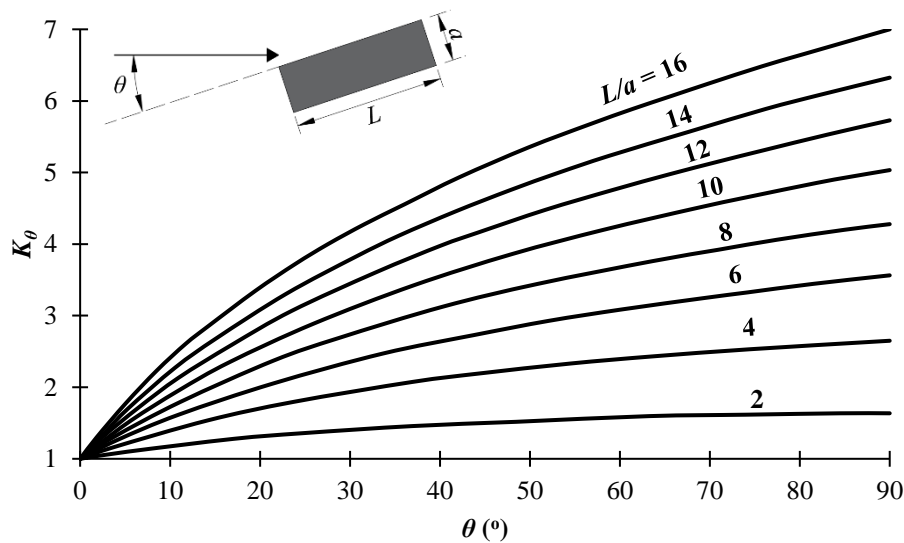


Figure 2-5: Variation on K_θ for increasing values of θ [40].

Richardson and Davis [19] suggested the following expression of K_θ that fits the curves obtained by Laursen and Torch [40].

$$K_\theta = (\cos \theta + L/a \sin \theta)^{0.65} \quad (2.3)$$

However, it must be mentioned that according to Richardson and Davis [19], K_θ should only be used if $\theta > 5^\circ$ and $2 \leq L/a \leq 16$. Fael et al. [41] showed alignment with the results obtained by [19] for $L/a = 4$, but tend to overestimate K_θ for $1.33 \leq L/a \leq 2$. Furthermore, Ettema et al. [42] showed that the curves obtained by the Laursen and Torch [40] are consistent with the new laboratory developed by Mostafa [38], but note that the maximum scour depth at skewed piers with low L/a occurs when θ is slightly higher than 90° .

Reynolds number, Re

Scour processes around bridge piers are significantly affected by the Reynolds number. As discussed in the previous sections, flow conditions play a significant role on the scour depth and sediment transport. The Reynolds number is a dimensionless parameter used to describe the flow regime and defined as follows:

$$Re = \frac{U_f a}{\nu} \quad (2.4)$$

Higher Re typically corresponds to turbulent flow conditions, which can result in increased scour depth due to greater energy dissipation and sediment transport capacity [35],[43],[44].

Froude number, Fr

The Froude number is a dimensionless parameter used to understand the flow conditions and their influence on sediment transport and scour processes around bridge piers and defined as follows:

$$Fr = \frac{U_f}{\sqrt{gd_w}} \quad (2.5)$$

The Froude number helps classify the flow regime as subcritical ($Fr < 1$), critical ($Fr = 1$) or supercritical ($Fr > 1$). Different flow regimes have varying effects on scour development and sediment transport. Changes in flow velocity, can impact the erosive power of the flow and consequently the scour depth.

Time

Time plays a fundamental role in shaping the development and extent of scour. Scouring is a gradual process wherein the geometry of sediment bed scour approaches its new equilibrium shape. Prolonged flood durations can increase sediment transport rates and erosive capacity, resulting in deeper scour depths and larger erosional volumes [45]. Furthermore, the temporal evolution of flow conditions during flooding affects scour initiation and progression. During the rising limb of a flood, high flow velocities initiate sediment entrainment and scour around hydraulic structures. This is very important as flood duration determines if the flood peak lasts long enough to establish the maximum scour depth [21], [46]. Subsequently, during the recession phase, while flow velocities decrease, scour processes may persist due to lingering sediment transport [19]. Figure 2-6 illustrates the variation of local scour depth over time.

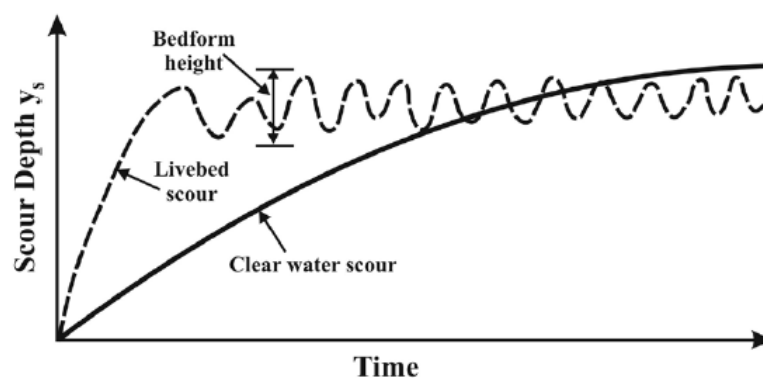


Figure 2-6: Variation of local scour depth over time [37].

Furthermore, it is worth noting that Melville and Chiew [45] showed that the equilibrium time scale (t^*) under clear water conditions depends on the flow intensity (U_f / U_c), flow shallowness (d_w/a) and

relative coarseness (a/d_{50}). Small scale laboratory experiments for clear-water conditions indicated that the scour depth was less than 50% of the equilibrium scour depth after 10-12 hours.

2.2.2 Local scour hole shape

The local scour hole is typically conical with the deepest point near the base of the pier and a gradual slope extending outward. The exact geometry of scour and extent around foundations are dependent on fluid properties, pier geometry, sediment properties and time (see section 2.2.1 Factors influencing local scour depth). The unsteady flow that generates vortices around the foundation creates a scour profile with varying slopes both upstream and downstream of the foundation [47].

As discussed in section 2.2.1 Factors influencing local scour depth , numerous experimental and numerical studies have investigated scour geometry providing recommendations and empirical scour depth. However, significant challenges persist due to the complexities associated with unsteady flow, scour mechanisms, bridge geometries compounded by the various erodible bed materials. Most of the developed empirical scour depth equations have significant assumptions (e.g. steady flow conditions or uniform bed material) or have focused only on a simple shape of bridge piers with or without considering scour development over time. Lee et al. [48] investigated experimentally scour development over time taking into account complex pier and foundation configurations, and various sediment sizes. It was concluded that most methods overestimate scour depth around bridge foundations.

Furthermore, for the sake of simplicity, scour geometry in numerical studies is generally considered symmetrical around a foundation, with equal upstream and downstream depth [49][54]. To the author's knowledge, only recently a more representative simulation of scour hole shape has started being taken into consideration. Zampieri et al. [55] investigated the effects of various symmetric and non-symmetric scour hole shapes to arch bridges assuming that both the upstream and downstream slope are equal to soil friction angle. In Tubaldi et al. [56], a refined scour geometry was developed, wherein the upstream slope of the scour hole was assumed to be at an angle equal to soil friction angle, while the downstream slope was set at half of that value. This assumption accounts for the energy dissipation within vortices generated by unsteady flow around the foundation, resulting in reduced force to the sediment immediately downstream. In the absence of external forces, soil naturally inclines at an angle equivalent to its frictional characteristics [57].

Consequently, further research on scour hole shape is imperative to investigate the effects of scour on bridges and understand scour development. Continued research on this is crucial not only for improving the design and maintenance of bridges, but also for the development of advance scour monitoring techniques. The present study aims to investigate the impact of scour hole shape on the dynamic properties and seismic response of bridges (see Chapter 6).

2.2.3 Scour modelling approaches

The accurate prediction of scour depth is essential for designing and maintaining safely bridge infrastructure. Various modelling approaches have been developed from empirical formulations to advanced machine-learning based techniques. This subsection discusses in detail the each of the developed approaches and highlights their advantages and limitations.

2.2.3.1 Empirical approaches

Empirical models (see e.g. [18],[19]) are widely used because of their simplicity and ease of implementation. Most of these models are based on laboratory experiments and field data, predicting scour depth as a function of hydraulic parameters, sediments characteristic, and bridge geometry (see section 2.2.1 Factors influencing local scour depth). HEC-18 developed by FHWA [26] is the most widely used model, providing design guidelines for scour estimation, incorporating empirical equations

derived from experimental datasets. However, most of the empirical models do not consider site specific variations and are unable to fully capture transient scour evolution, which may result in inaccurate scour depth estimates in complex flow conditions.

2.2.3.2 Experimental tests

Experimental tests are the most fundamental method not only for understanding scour mechanisms, but also for validating theoretical and numerical models. Breusers et al. [20] and Dargahi et al. [25] have provided valuable insights into the development of horseshoe vortices and wake vortex shedding around bridge piers during scour process. Large-scale physical tests (see e.g. [42]) have highlighted the significance of sediment gradation and pier shape on local scour depth. Although experimental studies benefit from high accuracy, they are often expensive, time-consuming, and influenced by scale effects, which can lead to discrepancies when applying the results to real-world bridges. Additionally, section 2.3.2.1 Accelerometers and vibration-based monitoring techniques discusses more in detail experimental approaches conducted by means of vibration-based techniques for scour identification.

2.2.3.3 Computational fluid mechanics approaches

Computational Fluid Dynamics (CFD) has enhanced scour modelling by enabling complex simulations of fluid-structure interactions. The Navier-Stokes equations solved by CFD models are able to capture flow turbulence, sediment transport and scour hole development. For example, Roulund et al. [58] provided high-resolution scour predictions by applying these methods to resolve complex flow around bridge piers. Even though CFD models often use advanced turbulence closure models to improve accuracy, such as Large Eddy Simulation and Averaged Navier-Stokes, they are characterised by high computational cost and require accurate calibration of sediment transport equations. These limitations often render this method impractical for large-scale bridge assessments.

2.2.3.4 Finite element modelling and soil-structure interaction

Finite Element Modelling (FEM) has been widely used to simulate scour-induced instabilities and assess the effects of soil-structure interaction on bridges. In these models, typically the soil is simulated as a continuum medium. A key aspect of the FEM-based scour modelling is the use of dynamic impedance functions, which represent the frequency-dependent stiffness and damping properties of the SFS system. Impedance functions have received considerable attention in the literature focused on scoured piled foundations, particularly in seismic and offshore engineering. Padrón et al. [59] examined the influence of footing-soil separation effects on the dynamic stiffness of piled foundations, demonstrating how scour-induced soil loss alters the foundation's response under dynamic loading. Dezi et al. [60] developed a three dimensional numerical model for the kinematic interaction of pile groups, later modified by Liang et al. [61] to include scour effects. Their results indicate that scour reduces lateral and rocking stiffness of the foundation, affecting bridge stability under dynamic loads. Carbonari et al. [62] developed lumped-parameter models for piled foundations, estimating the dynamic response through calibrated springs and dashpots. These studies highlight the significance of frequency-dependent foundation stiffness in numerical models to accurately capture the effects of scour on bridge dynamic behaviour.

While significant improvements have been achieved in recent decades, research on the impact of scour on the dynamic impedances of bridges with shallow foundations is limited. To the author's knowledge, only Guo [51] has investigated the changes of the impedance functions of shallow foundations under scour conditions, by taking the soil degradation due to scour into account. The results of this study show the scour has a significant impact on the modal properties of bridges, which may lead to increased instability. However, the lack both of numerical and experimental studies on this topic highlights a knowledge gap in the literature. Several recent studies have also explored the impact of scour on the dynamic response by means of FEM-based numeral models. Tubaldi et al. [56] and Scozzese et al. [63]

employed 3D simulations to evaluate the effect of scour on the modal properties of masonry arch bridges, considering the progressive soil erosion. Kariyawasam et al. [54] conducted centrifuge modelling for the validation of FEM predictions, underlying the importance of incorporating foundation flexibility into scour analyses. These studies provide essential insights into scour development mechanisms and their impact on bridges’ dynamic response. However, they focus on deep foundations or rigid bridge elements, leaving the impact of scour on shallow foundations inadequately addressed.

Given the current increased availability of real-time monitoring data, the integration of FEM with machine learning and artificial intelligence (AI) techniques is quite promising. While AI-based methods have shown a strong potential in their ability to predict scour extent [65],[66], their application in numerical models is still emerging.

2.3 Scour monitoring techniques

As already discussed in previous sections, scour is the leading cause of bridge failure worldwide. Consequently, effective monitoring of scour conditions is essential for early mitigation of potential damage and failure of bridge structures. This section discusses in detail all the currently available scour monitoring techniques developed so far, highlighting not only their principles and applications, but also their advantages and limitations.

Scour monitoring techniques are evaluated on criteria based on effectiveness, reliability, and practicality in assessing the soil erosion around bridge foundations. Table 2-3 summarises the mandatory and desirable criteria for a successful monitoring of scour [67].

Table 2-3: Mandatory and desirable criteria for successful monitoring of scour conditions on bridges [67].

Mandatory criteria	Desirable criteria
<ul style="list-style-type: none"> • Capability for installation on or near bridge pier or abutment • Ability to measure maximum scour depth within an accuracy of +/- 1 ft • Ability to obtain scour depth readings from above water or from a remote site • Operable during storm and flood conditions 	<ul style="list-style-type: none"> • Capability to be installed on most existing bridges or during construction of new bridges • Capability to operate in a range of flow conditions • Capability to withstand ice and debris • Relatively low cost • Vandal resistant • Operable and maintainable by highway maintenance personnel

Installation of scour monitoring infrastructure offers significant benefits by mitigating critical issues related to bridges’ integrity. These systems monitor scour progression, enabling timely inspections and reducing the risks of catastrophic bridge failures. Unlike periodic inspections, which may overlook rapid or unforeseen scour events, these systems provide continuous and detailed data on the condition of bridge foundations. Operationally, scour monitoring systems significantly contribute to safety by providing early warnings and detecting changes in sediment levels or structural integrity, allowing proactive measures, especially during extreme weather events where manual inspections can be unsafe. Furthermore, early detection not only reduces the cost of emergency repairs due to scour but also the transportation disruption. The detection of the location and scour extent by means of scour monitoring techniques allows targeted maintenance of bridge infrastructure, extending its lifespan and ensuring the reasonable use of maintenance budgets. By continuously tracking the health of bridge foundations, these systems help avert incidents that could risk human lives and disrupt transportation networks. Moreover, they significantly contribute to the effectiveness of existing scour protection measures, enabling timely

adjustments and reinforcements. In other words, the integration of scour monitoring systems with scour protection systems can offer an even more robust approach to transportation networks safety.

2.3.1 Direct scour measurement devices

2.3.1.1 Float-out device

Float-out device consists of a radio transmitter and are buried vertically into the soil in the close vicinity of piers and abutments at pre-determined depths. A receiver, installed near the bridge, listens continuously for signals emitted by an activated float-out device. When scour reaches the depth of the float-out device, the device floats up and it turns horizontally. Subsequently, the internal transmitter is activated, and transmits a signal to data acquisition system. Specifically, the transmitter transmits to the receiver either the value of 0 or 1, when the device is vertical or horizontal, respectively.

Float-out device is characterized by a simplicity and reliability on indicating if the scour depth has reached its installation depth. Nevertheless, it cannot provide any intermediate or maximum indication of the scour depth. Additionally, the installation process is expensive as it requires coring and drilling. Another disadvantage of the float-out device is the limited lifespan due to battery life, which lasts for approximately 9 years when the device is in an inactive state [68].

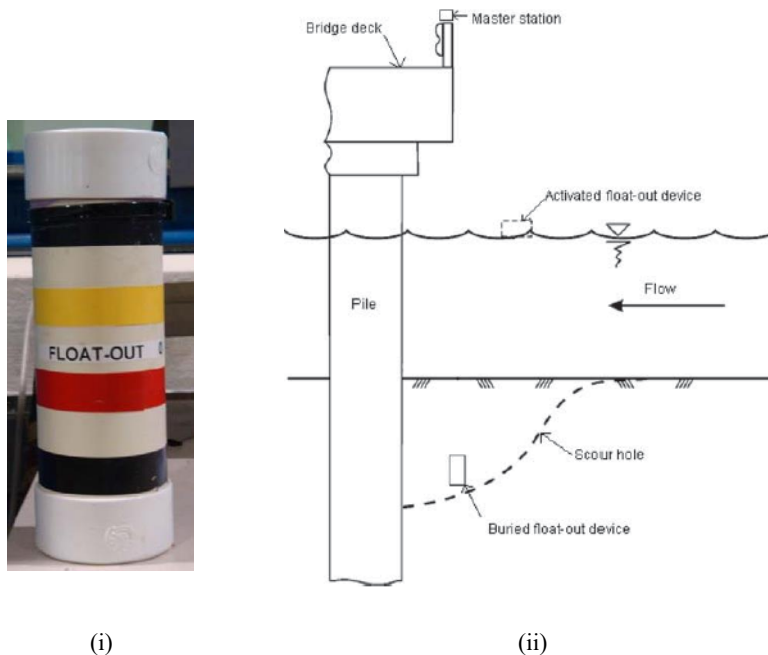


Figure 2-7: i) Float-out device [69], ii) Schematic of float-out device [68]

2.3.1.2 Tethered buried switch

The tethered buried switch is a type of float-out device which is buried vertically into the soil in the close vicinity of piers and abutments at pre-determined depths. It consists of a long aluminium rod with an internal electrical switch and it is hardwired to the data acquisition system. When scour reaches the depth of the tethered buried switch, it floats up and it turn horizontally. Similarly, as a float out device, the electrical switch triggers when the rod turns from vertical to horizontal position. Specifically, the electrical switch sends to the data acquisition system the value of 1 when the device is in position, the value of 2 when the device is floated out, and the value of 3 when the device is no operational.

The tethered buried switch benefits from a direct and simple indication of when scour reaches its installation depth. Nevertheless, it cannot provide any intermediate or maximum indication of the scour depth. The installation process is difficult and expensive, while the wire that connects the rod to the

data acquisition system is susceptible to vandalism and damage due to debris. Similarly with a float-out device, the tethered buried switch can be used only once for scour depth indication, however it is characterised by infinite lifespan when it is inactive due to its wire connection to data acquisition system.



Figure 2-8: Tethered buried switch [70].

2.3.1.3 Time domain reflectometry (TDR)

Time domain reflectometry (TDR) system is used to estimate the scour depth over time. A typical TDR system (Figure 2-9) consists of a TDR device (pulse generator and sampler), a connection cable, and a measurement probe [72]. The TDR technique operates by generating a fast-rise step or impulse and coupling it to a transmission line, which determines the water-soil interface, and hence the scour depth. The impulse propagates down the transmission line and it is reflected back to the source when it reaches the end of the transmission line or an intermediate discontinuity, for example a change of the system geometry or material dielectric permittivity [72],[73]. The TDR technique for scour monitoring is based on the significant difference of the dielectric constant of the water (approximately 81), and other materials such as air (1) or sediment solids (ranging between 2 and 7). Therefore, reflections occur when the impulse reaches the water-air or water-soil interface. The scour depth is estimated by measuring the time that the signal is reflected to the source.

Although TDR is a reliable technique for scour depth estimation, it is characterised as expensive and time consuming. This is due to the required installation of long probes into the riverbed at the location of interest.

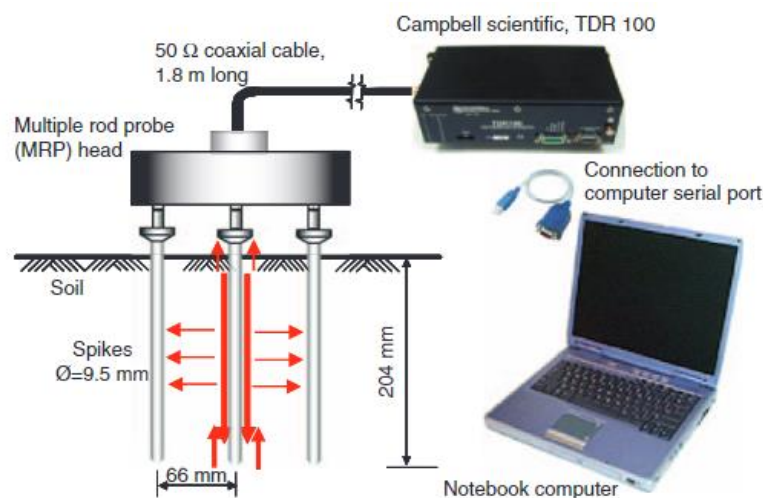


Figure 2-9: Typical TDR system [74].

2.3.1.4 Ground penetrating radar (GPR)

Ground penetrating radar is a widely used technique for the estimation of scour depth because of its easy implementation and reliability. It works in a similar way to TDR using mostly dielectric permittivity material properties. More in detail, GPR is an electromagnetic method that uses high-frequency (typically 100-2000 MHz) pulsed-radio waves that are generated by a transmitter antenna (TX). The pulsed-radio waves reflect back to a receiver antenna (RX) when they pass through materials with significantly different properties of dielectric permittivity. The waves will continue to propagate until they are reflected again or there is a complete energy dissipation [75]. Subsequently, the GPR is pulled along the water surface to image the subsurface by measuring the time required for the waves to reflect and be received by the receiver antenna. Figure 2-10 shows a schematic of a waterborne GPR arrangement, while Figure 2-11 shows an example of a GPR profile.

A drawback of this method is that the waterborne GPR is pulled manually, and therefore it cannot be used under extreme weather events or heavy-flood flow conditions. Moreover, GPR provides information about scour depth of a location only at the time of the deployment, and hence it cannot be used for a continuous scour monitoring technique [70].

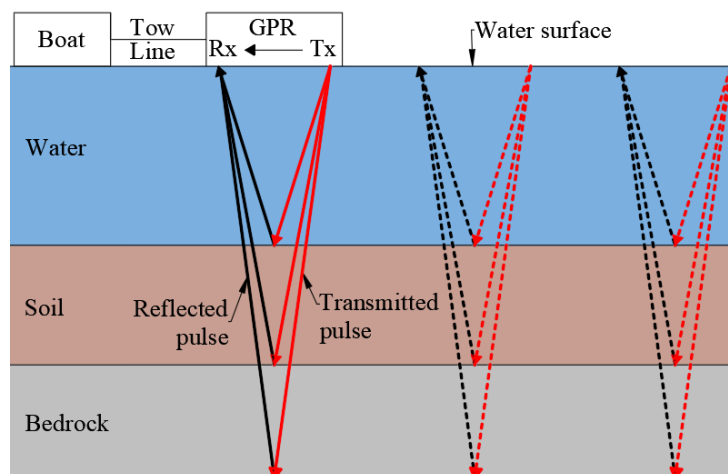


Figure 2-10: Schematic of waterborne GPR arrangement.

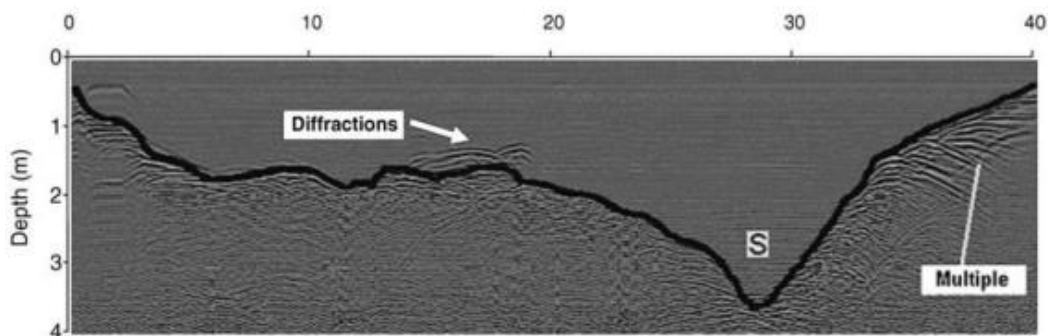


Figure 2-11: Typical GPR profile [76]

2.3.1.5 Fibre-Bragg Grating (FBG)

In the last years, techniques using Fiber Bragg Grating sensors have been developed for real-time scour monitoring as they benefit from long-term stability and reliability, resistance to environmental corrosion, and multiplexity along one single fibre compared to traditional sensors. FBG sensors function by measuring strain along embedded cantilever rods, generating electrical signals that indicate scour progression along the rod. A number of FBG sensors are mounted on different levels of the rod, which detect the strains developed on the bended rod when it is exposed to water. The sensors that are not

exposed to water and are still buried generate no or very small strains because that part of the rod is not bending. Consequently, the scour depth can be estimated by the number of the FBG sensors that are exposed to running water. However, the accuracy of the scour depth estimation depends on the number and space between the sensors mounted on the rod. Figure 2-12 shows two different models using FBG sensors for real-time scour monitoring developed by [77].

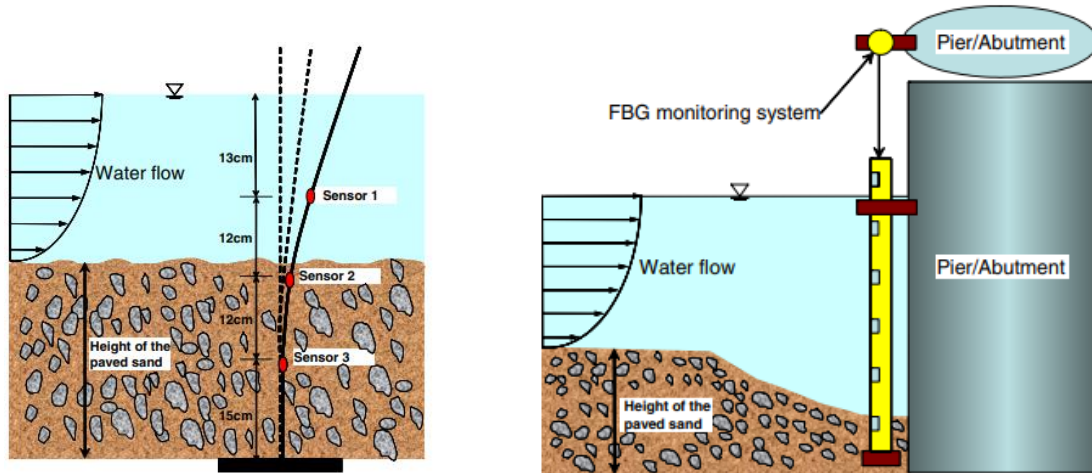


Figure 2-12: FBG scour monitoring systems developed by [77].

2.3.1.6 Magnetic Sliding Collar (MSC)

Magnetic sliding collars are attached to a bridge pier or abutments and consist of a rod and a ring driven or augured into the riverbed. As the sediment erodes due to flowing water, the collar slides down into the scour hole. Then magnetic triggers on the rod determines the collar's depth based on its position on the rod [78]. The data of magnetic sliding collars can be read either manually or automatically. Manually read magnetic sliding collars are characterized by inexpensive and easy installation during low-flow events. However, they are quite susceptible to debris damage, particularly during heavy-flow events due to the fact that the sensors require infrastructure in the form of metal tubing [70]. On the other hand, automatically read magnetic sliding collars consists of flexible cables attached to the system transmitting magnetic switch closures to a centralised data acquisition unit. Therefore, they are characterised by a higher cost and robustness than the manually read magnetic sliding collars. The main disadvantage of the magnetic sliding collars is that they cannot provide the infill scour process at a bridge, monitoring only the maximum scour depth. Figure 2-13 illustrates a schematic of the two different types of magnetic sliding collar.

2.3.1.7 Sonars

Sonar scour monitors are installed onto the bridge pier or abutment to assess streambed conditions. Presently, a variety of sonar monitors are available in the market, ranging from conventional fish finders to smart sonar transducers. The sonar transducer is interfaces with the sonar instrument or directly with a data logger. Employing sound wave propagation through water, the sonar instrument estimates the scour depth by measuring the time taken for the sound wave to travel from the transducer to the streambed and back. The data logger controls the sonar system operation and data collection functions and can be programmed to take measurements at predefined intervals. Sonar sensors normally conduct a sequence of rapid measurements to measure the distance from the transducer to the streambed. Sonars benefit from the fact that can be used both for scour and deposition monitoring [68]. Nevertheless, the measurements can be affected by aerated flow and bed load. On the other hand, the sonars might be installed to a variety of elevations in order not to interfere with debris.

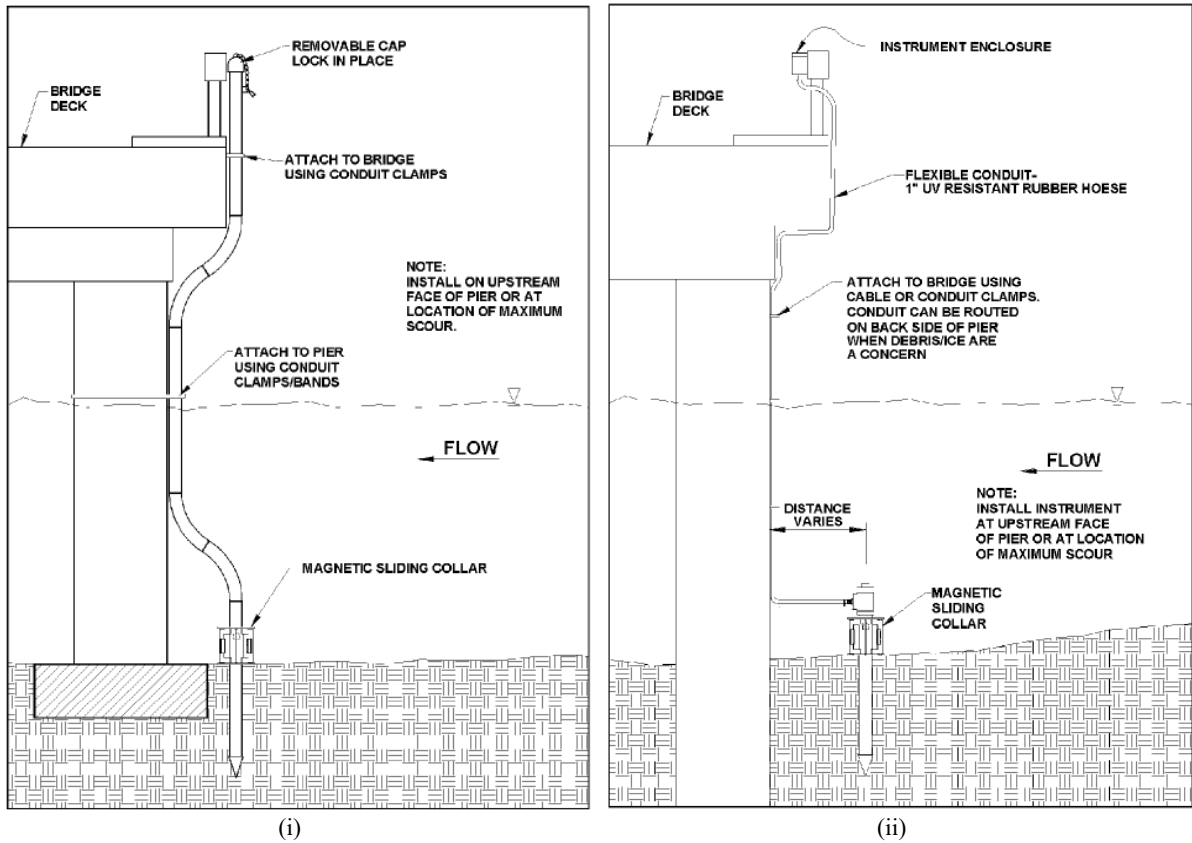


Figure 2-13: i) Manual read out magnetic sliding collar device, ii) Automated read out sliding collar system [79].

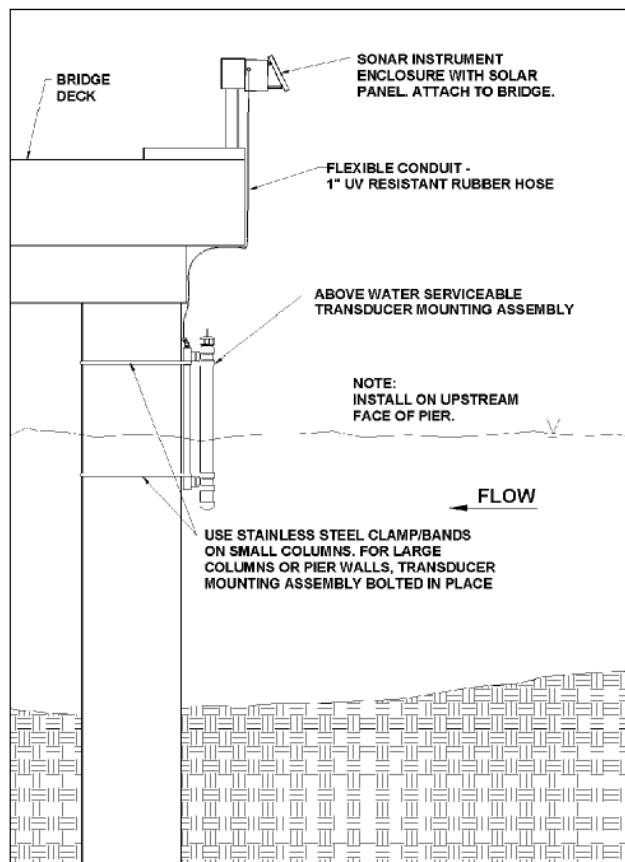


Figure 2-14: Schematic of a sonar scour monitoring system [80].

2.3.1.8 Electrical conductivity devices

An electrical conductivity probe consists of several sensors for measuring conductivity, spaced evenly along a rod. The rod is driven or jetted vertically into the riverbed at the location of interest (e.g bridge pier or abutment). Most of the sensors are installed below the riverbed, but at least one sensor remains above the riverbed in the surface-water flow. Sensors located above the riverbed measure the conductivity of the surface-water flow, while the sensors located below the riverbed measure the conductivity of the bed material and water. In a scour event, additional sensors will be exposed to surface-water flow, and hence the scour depth can be estimated by comparing historical riverbed and surface-water conductivity readings at each sensor [81].

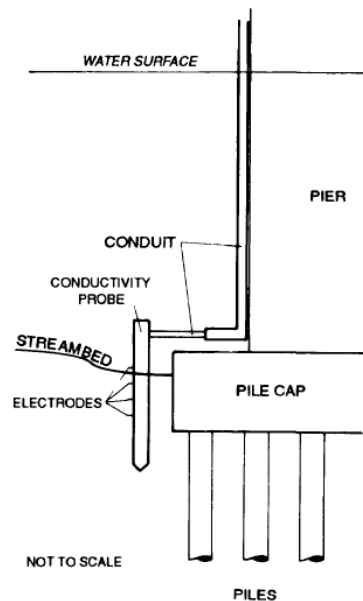


Figure 2-15: Schematic of electrical conductivity probe [81].

2.3.1.9 Sounding Rods

Sounding rods are manual or automated gravity based physical probes. The setup consists of a vertical or diagonal rod that connects the bridge structure with a metal base resting onto the riverbed. As scour progresses, the rod slides down to the riverbed, and therefore the developed scour depth can be measured. The metal base of the rod must be of sufficient size to prevent penetration into the streambed caused by the weight of the rod and the vibration of the rod from flowing [82]. Sounding rods benefit from simple and inexpensive installation, however the measurements are susceptible to debris and hydrodynamic forces.



Figure 2-16: Sounding rods installed at a bridge pier [83].

2.3.2 Indirect scour measurement devices

The direct scour measurement devices presented in the previous subsection are widely used for detecting and measuring scour at bridges. However, most of these devices require installation in the riverbed (e.g. scour probes), or they may have to be submerged (e.g. sonars). This may result in high installation costs, the need to request special permissions for installation, and also in exposure to the impact of floating debris that may damage them. For these reasons, in some cases it may be preferable to rely on indirect scour measurement devices that estimate the scour depth indirectly by monitoring the response of bridges and the changes on their dynamic response due to scour. The technologies and instruments available for indirect scour monitoring of bridges are presented in the following subsections.

2.3.2.1 Accelerometers and vibration-based monitoring techniques

Accelerometers have a great potential for supporting identification of scour. Scour leads to a significant reduction of the soil-foundation stiffness due to removal of soil around the foundation. Subsequently, this change on the soil-foundation system yields a change of the global stiffness of the Soil-Foundation-Structure (SFS) [49]. The natural frequencies of an SFS system, such as a bridge pier, can be estimated from accelerometers mounted on the structure using spectral analysis tools such as Fast Fourier Transforms (FFTs) or Frequency Domain Decomposition (FDD) [84]. Consequently, scour presence and extent can be detected by comparing the natural frequencies of an unscoured SFS system with the ones obtained by the accelerometers.

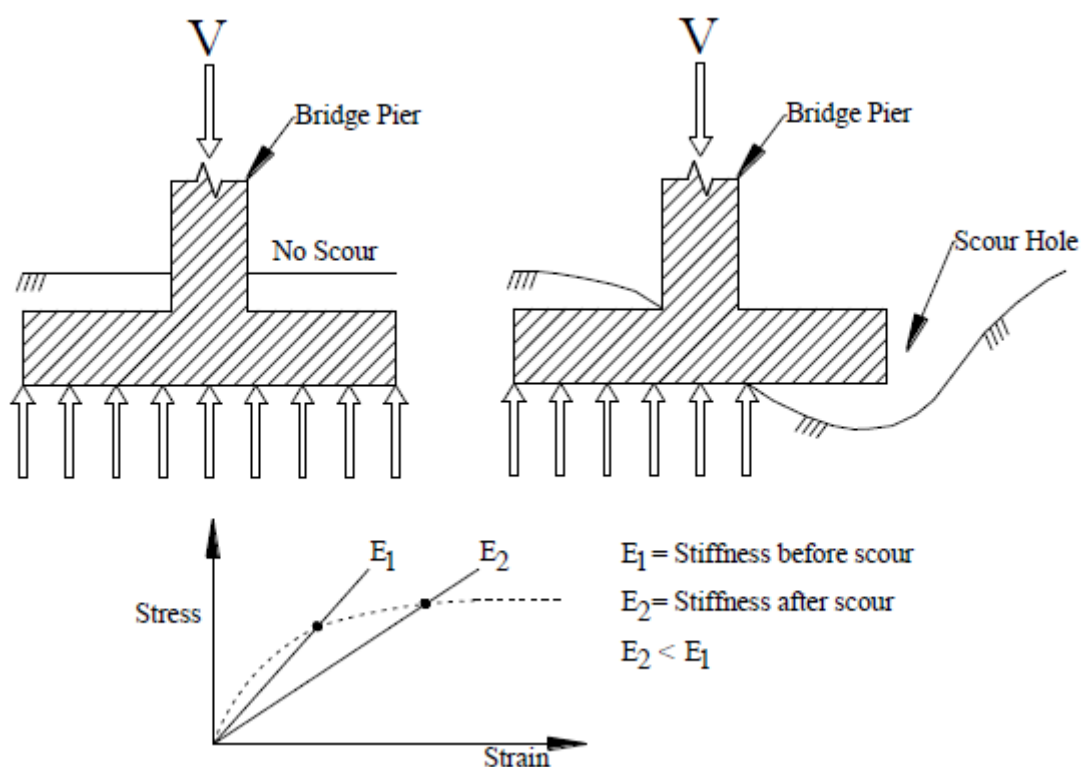


Figure 2-17: Reduction in stiffness caused by scour [70].

For these reasons, there are many studies in the literature that investigate the possibility of identifying the scour location and extent by means of vibration-based monitoring techniques, based on the evaluation of the changes of the bridge modal properties due to scour. Briaud et al. [69] focused on the use of accelerometers and tiltmeters to monitor scour, and carried out experiments on two large scale laboratory models with shallow and deep foundations. Subsequently, two individual monitoring

systems were designed and installed on two real bridges. The results of the experimental campaigns showed that the instruments could be successfully employed to provide warnings of potential bridge failure. However, there were shortcomings with regard to the accelerometers, which are related to lack of sufficient excitation from traffic and the high-power consumption required for the transmission of accelerometer data, for which typical solar panel and battery are not sufficient. Another study by Prendergast et al. [85] focused on single cantilever piles with the bottom part embedded in the soil, excited by a top impulse force, and on the development of a finite element model for capturing the effects of scour. The study showed that the effect of water on the measured natural frequencies of the cantilevers is negligible. Bao et al. [86] conducted similar experiments for vibration-based monitoring of scour and investigated the effect of the scour hole shape. This is usually assumed as symmetric in experiments, whereas in reality, it has often a non-symmetric shape (see section 2.2.2 Local scour hole shape). The experiments with unsymmetrical scour hole scenarios carried out from Bao et al. [86] demonstrated the importance of this factor for vibration-based scour detection. Foti and Sabia [87] proposed and evaluated two alternative techniques for monitoring foundation scour using measurements of traffic-induced vibrations. Similarly, Prendergast et al. [88] investigated the local sensitivity to scour of the vibration modes of a bridge, using a vehicle–bridge–soil dynamic interaction model for identifying both the occurrence and the location of the scour. Bao and Liu [89] developed a formula for predicting the predominant natural frequency of bridge piers under future higher scour widths by measuring only the response under a few small scour widths. Other recent numerical and experimental studies have been carried out on the use of ambient vibration recordings for scour identification [53], [90]-[92]. Even though many studies have investigated numerically and experimentally the changes of the dynamic behaviour of bridges with deep foundations subjected to scour, it is surprising that research on bridges with shallow foundations is scarce. This is probably because very often the simple problem of scour of a single monopile pier-system with circular diameter is considered in experimental flume studies on scour development and in studies investigating the changes of the dynamic properties of bridges. For this reason, there are not many studies investigating the geometry of the scour hole in case of pier on shallow foundations, with the exception of the recent work of Lee et al. [48]. As a result of this, many numerical and experimental studies investigating the effects of scour on bridges with shallow foundations introduced some simplifications in the description of scour (see, e.g., [49],[54],[93]). They also assumed scour profiles that are more representative of degradation scour rather than local scour, which is more critical for bridges. Experimental tests were carried out by Ruocci et al. [94] by imposing increasing levels of scour and applying damage detection techniques on a 1/2 scale model of a two-span bridge. Malekjafarian et al. [93] developed an approach to detect the vertical stiffness loss of multi-span bridges with shallow foundations due to scour based monitoring relative changes in vertical pier-mode shape amplitudes by means of recorded acceleration signals. Particularly, a scour monitoring indicator was proposed to compare the mode shape value of a given pier with those at the other piers. Kariyawasam et al. [54] carried out experimental centrifuge tests on a scaled bridge with shallow foundations to investigate the sensitivity of its natural frequency to scour, considering symmetric or triangular scour hole shapes that allow to treat the problem as a two-dimensional one, while local scour calls for the use of three-dimensional models. Scozzese et al. [63] studied the case of Rubbianello bridge, a multi-span masonry arch bridge with shallow foundations located in Central Italy, which suffered a partial collapse due to scour. They developed a three-dimensional model of the bridge, and simulated the development of a local scour hole shape at the base of a pier. They concluded that significant variations of modal properties occur only after the excavation reaches the foundation base and that monitoring the changes of vibration frequency may not provide sufficient warning of the risk of collapse due to scour for this type of bridges.

From the analysis of the literature of the problem, it is evident that most experimental studies on shallow foundations have been carried out in the laboratory, under controlled conditions, where it is impossible to fully recreate in-field conditions. As a consequence of this, there is also a lack of fully validated numerical strategies for simulating the effect of scour on the dynamic behaviour of soil–foundation–structure systems subjected to scour. Thus, further experimental and numerical research investigations on the problem are needed.

2.3.2.2 Tilt sensors

Tilt sensors, also known as inclinometers, can measure the pier and deck movement due to scour. Prendergast [70] provides a detailed description of the tiltmeter-based monitoring mechanism. A pair of tilt sensors are installed on the bridge deck to monitor the longitudinal and transverse movement of the bridge. Under a settlement event of the bridge foundation due to scour, the pair of the tilt sensors detect the movement of the bridge, which is likely to be not only a pure translation, but a rotation combined with a translation. When the movement of the bridge exceeds a predefined limit, the data system sends alert status messages. Recently, Faulkner et al [71] tracked bridge tilt behaviour using sensor fusion techniques. Specifically, they introduced gyroscopes as a complementary sensor for accelerometer rotational measurement and used sensor fusion techniques to combine the measurements from both sensors to get an optimised rotational result. Borlenghi et al. [95] applied MEMS-based tiltmeters combined with environmental sensors to isolate temperature effects and detect anomalies induced by scour. This study underlined the importance of integrating multivariable monitoring systems for accurate scour detection.

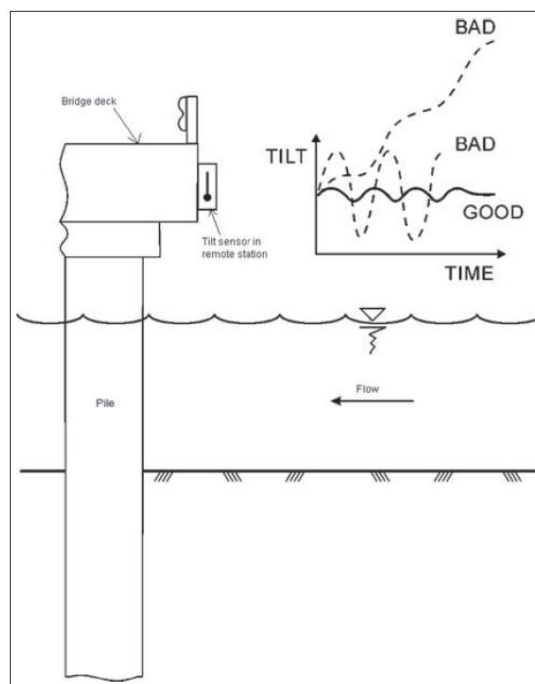


Figure 2-18: Schematic of tilt sensor device [68].

2.3.2.3 Global Positioning System (GPS)

Global Positioning System technology can be used to monitor the quasi-static movement and dynamic changes of a structure in real time. The GPS consists of 3 parts: satellites orbiting the Earth, control and monitoring stations on Earth, and the GPS receivers owned by the users also known as rovers [96]. The satellite constantly transmits information about its location by means of electromagnetic signals. The distance of the satellite to an unknown location on Earth is determined by the time that the electromagnetic signals are received by the GPS receiver.

GPS are often used to monitor slow movements with quite good accuracy. However, there is an increased use of GPS receivers for monitoring vibrations. It is noteworthy that this application is still limited by the capability of the GPS to record high frequency motion (i.e. higher than 10-20 Hz). Because of this, most of applications of GPS receivers are confined to flexible structures, such as long-span bridges [97]. However, higher rate GPS receivers (50 – 100 Hz) [98]-[100] have been developed that could be used to monitor stiffer structures like masonry arch bridges and detect changes of vibration frequency due to scour with good accuracy.

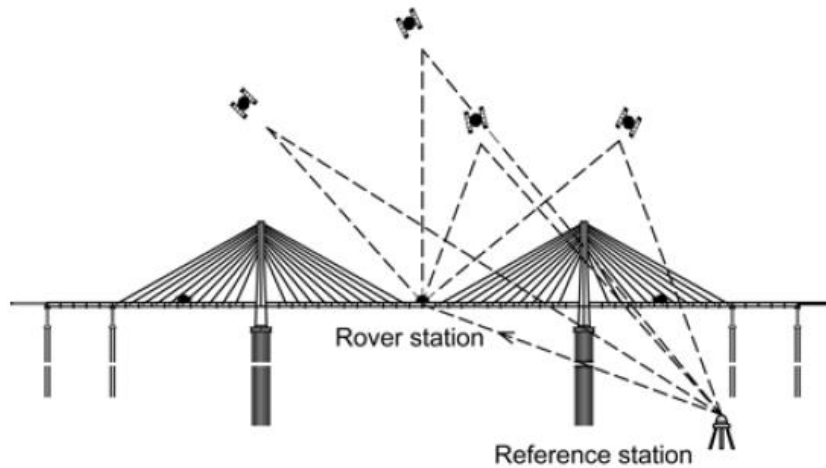


Figure 2-19: Schematic of GPS deployment on a bridge [96].

2.3.2.4 Space-borne synthetic aperture radar interferometry

Space-borne synthetic aperture radar (SAR) interferometry (InSAR) techniques have been recently proposed for scour monitoring purposes [101][103]. InSAR is an advanced processing technique used on radar images of the Earth's surface, capable of detecting very small movements in ground features, such as bridges. By means of applying InSAR techniques to a series of radar images of the same region, vertical and horizontal displacements of bridge elements caused by scour can be detected and define the scour extent indicating potential bridge damage. A major advantage of this technique is that is weather and darkness independent, while only one radar image can cover a major urban area of up to 100 km by 100 km, and consequently all the bridges in the area could be monitored cost effectively [104].

For the sake of completeness, Table 2-4 compares all the direct and indirect scour monitoring techniques discussed in this chapter, highlighting their advantages and disadvantages.

Table 2-4: Comparison of scour monitoring techniques

Technique	Easy to install and operate	Can be used during floods	Continuous monitoring	Able to measure refilling process	Affected by traffic or other hydraulic factors	Economic
Float-out device	Yes	Yes	No	No	No	Excellent
Tethered buried switch	Yes	Yes	No	No	No	Excellent
Time domain reflectometry (TDR)	Yes	Yes	Yes	Yes	No	Moderate
Ground penetrating radar (GPR)	Yes	No	No	No	No	Poor
Fibre-Bragg Grating (FBG)	No	Yes	Yes	Yes	No	Poor
Magnetic Sliding Collar (MSC)	Yes	Yes	No	No	No	Moderate
Sonars	Yes	Yes	Yes	Yes	No	Moderate
Electrical conductivity devices	Yes	Yes	Yes	Yes	No	Moderate
Sounding Rods	Yes	Yes	No	No	Yes	Excellent
Accelerometers	Yes	Yes	Yes	Yes	Yes	Excellent
Tilt sensors	Yes	Yes	Yes	Yes	Yes	Excellent
Global Positioning System (GPS)	Yes	Yes	Yes	No	Yes	Poor
Space-borne synthetic aperture radar interferometry	No	Yes	Yes	No	Yes	Poor

References

- [1] A.M. Shirole, R.C. Holt, “Planning for a comprehensive bridge safety assurance program”, Transportation Research Board, Washington, D.C., Transportation Research Record 1290, 1991, pp. 39-50.
- [2] J.L. Briaud, C.F.K. Ting, H.C. Chen, R. Gudavalli, S. Perugu, G. Wei, “SRICOS: prediction of scour rate in cohesive soils at bridge piers”, *Journal of Geotechnical and Geoenvironmental Engineering*, vol. 125, issue 4, pp. 234-246, 1999.
- [3] K. Wardhana, F.C. Hadipriono, “Analysis of recent bridge failures in the United States”, *Journal of Performance of Constructed Facilities*, vol.17, issue 3, pp. 144-150, 2003.
- [4] P.F. Lagasse, P.E. “Countermeasures to protect bridge piers from scour”, Transportation Research Board, Washington, D.C., NCHRP Report 593, 2007.
- [5] R. Lamb, P. Garside, P. Raghav, J.W. Hall, “A Probabilistic Model of the Economic Risk to Britain’s Railway Network from Bridge Scour During Floods”, *Risk Analysis*, vol. 39, issue 11, pp. 2457-2478, 2019.
- [6] A. Pizarro, S. Manfreda, E. Tubaldi, “The science behind scour at bridge foundations: a review”, *Water*, vol. 12, issue 2, 2020.
- [7] Z. Van Leewen, R. Lamp, “Flood and scour related failure incidents at railway assets between 1846 and 2013”, JBA Trust, W13-4224, 2014. Available: <https://www.jbatrust.org/wp-content/uploads/2016/01/JBA-Trust-Flood-and-scour-failure-at-railway-assets-1846-to-2013-W13-4224-FINAL.pdf>
- [8] M. Szönyi, M. Peter, R. Lamp, “Flooding after Storm Desmond”, Zurich Insurance Group, JBA Trust, 2015. Available: <https://www.jbatrust.org/wp-content/uploads/2016/08/flooding-after-storm-desmond-PUBLISHED-24-August-2016.pdf>
- [9] “Flooding and Scour Risk”, Safe Management of Railway Structures, Rail Safety Standards Board, London, United Kingdom, Report No. T554, 2005.
- [10] P. Kellermann, C. Schönberger, A.H. Thieken, “Large-scale application of the flood damage model RAILway Infrastructure Loss (RAIL)”, *Natural Hazards and Earth System Sciences*, vol. 16, issue 11, pp. 2357-2371, 2016.
- [11] A.P. Moran, A.H. Thieken, A. Schöbel, C. Rachoy, “Documentation of Flood Damage on Railway Infrastructure”, *In Data and Mobility: Transforming Information into Intelligent Traffic and Transportation Services Proceedings of the Lakeside Conference 2010*, Berlin, Heidelberg, Springer, 2010.
- [12] P. Kellermann, A. Schöbel, G. Kundela, A.H. Thieken, “Estimating flood damage to railway infrastructure – the case study of the March River flood in 2006 at the Austrian Northern Railway”, *Natural Hazards and Earth System Sciences*, vol. 15, pp. 2485-2496, 2015.
- [13] Cumbria Intelligence Observatory, “Cumbria floods November 2009: An impact Assessment”, Carlisle, United Kingdom, 2010.
- [14] Rail Accident Report. Structural failure caused by scour at Lamington viaduct, South Lanarkshire 31 December 2015, Report 22/2016, November 2016.
- [15] E. Tubaldi, C.J. White, E. Patelli, S. Mitoulis, G. De Almeida, J. Brown, M. Cranston, M. Hardman, E. Koursari, R. Lamb, H. McDonald, R. Mathews, R. Newell, A. Pizarro, M. Roca, D. Zonta, “Invited perspectives: Challenges and future direction in improving bridge flood resilience”, *Natural Hazards and Earth System Sciences*, vol. 22, issue 3, pp. 795-812, 2022.
- [16] R. Day, “SRICOS: Prediction of Scour Rate in Cohesive Soils at Bridge Piers”, *Journal of Geotechnical and Geoenvironmental Engineering*, vol. 126, issue 11, pp. 1028-1029, 2000.
- [17] B. Maddison, “Scour failure of bridges”, *Proceedings of the Institution of Civil Engineers-Forensic Engineering*, vol. 165, issue 1, 2012.
- [18] B.W. Melville, S.E. Coleman, *Bridge Scour*, Water Resources Publication, 2000.
- [19] E.V. Richardson, S.R. Davis, “Evaluating scour at bridges”, Federal Highway Administration, Washington D.C., FHWA-NHI-01-001, 2001.

- [20] H.N.C. Breusers, G. Nicollet, H.W. Shen, "Local scour around cylindrical piers", *Journal of Hydraulic Research*, vol. 15, issue 3, pp. 211-252, 1977.
- [21] Y.M. Chiew, "Local Scour at Bridge Piers", Ph.D. dissertation, Department of Civil Engineering, Auckland University, Auckland, New Zealand, 1984.
- [22] A.J. Raudkivi, A.J. Sutherland, "Scour at bridge crossings", Road Research Unit, National Roads Board, Wellington, New Zealand, Report No. 51, 1981.
- [23] B.W. Melville, A.J. Raudkivi, "Flow characteristics in local scour at bridge piers", *Journal of Hydraulic Research*, vol. 15, issue 4, pp. 373-380, 1977.
- [24] P.F. Lagasse, E.V. Richardson, "ASCE compendium of stream stability and bridge scour papers", *Journal of Hydraulic Engineering*, vol. 127, issue 7, pp. 531-533, 2001.
- [25] B. Dargahi, "Controlling mechanism of local scouring", *Journal of Hydraulic Engineering*, vol. 16, issue 10, pp. 1197-1214, 1990.
- [26] E.V. Richardson, S.R. Davis, "Evaluating scour at bridges", Federal Highway Administration, Hydraulic Engineering Circular 18, FHWA-IP-90-017, 1995.
- [27] M. Kharbeche, "The role of pier shape and aspect ratio on local scour with and without sacrificial piles", Master thesis, Department of Civil and Environmental Engineering, University of Windsor, Windsor, Ontario, Canada, 2022.
- [28] Jalal H.K., Hassan W.H., "Effect of bridge pier shape on depth of scour", *3rd International Conference on Engineering Sciences, IOP Conference Series: Materials Science and Engineering*, vol. 671, issue 012001, 2020.
- [29] S.O. Lee, T.W. Strum, "Effect of sediment size on physical modelling of bridge pier scour", *Journal of Hydraulic Engineering*, vol. 135, issue 10, pp. 793-821, 2009.
- [30] Misuyira G., Eldho T.I., Mazumder B.S., "Estimation of the local scour around the cylindrical pier over the gravel bed for a low coarseness ratio", *International Journal of River Basin Management*, vol. 22, no. 22, pp. 487-497, 2024.
- [31] Y. Chiew, B. Melville, "Local scour at bridge piers with non-uniform sediments", *Proceedings of the ICE*, vol. 87, issue 2, pp. 215-224, 1989.
- [32] R.K.W. Chee, "Live-bed scour at bridge piers", School of Engineering, University of Auckland, Auckland, New Zealand, Report No. 290, 1982.
- [33] B.W. Melville, "Live-bed scour at bridge sites", *Journal of Hydraulic Engineering*, vol. 110, issue 9, pp. 1234-1247, 1984.
- [34] A.J. Raudkivi, "Functional trends of scour at bridge piers", *Journal of Hydraulic Engineering*, vol. 112, issue 1, pp. 1-13, 1986.
- [35] B.W. Melville, A.J. Sutherland, "Design method for local scour at bridge piers", *Journal of Hydraulic Engineering*, vol. 114, issue 10, pp. 1210-1226, 1988.
- [36] D.M. Dongol, "Local scour at bridge abutments", Ph.D. dissertation, School of Engineering, University of Auckland, Auckland, 1994.
- [37] R. Ettema, G. Constantinescu, B. Melville, "Evaluation of Bridge Scour Research: Pier Scour Processes and Predictions", Transportation Research Board, Washington, D.C., NCHRP Web-Only Document 175, 2011
- [38] E.A. Mostafa, "Scour around skewed bridge piers", Ph.D. dissertation, Department of Civil Engineering, Alexandria University, Alexandria, Egypt, 1994.
- [39] Omara H., Ookawara S., Nassar K.A., Masria A., Tawfik A., "Assessing local scour at rectangular bridge piers", *Ocean Engineering*, vol. 266, 112912, 2022.
- [40] E. M. Laursen, A. Torch, "Scour around bridge piers and abutments", Bulletin No. 4, Iowa Highways Research Board, Ames, IA, 1956.
- [41] Fael C., Lanca R., Cardoso A., "Pier shape and alignment effects on local scour", In: *Proceedings small scale morphological evolution of coastal, estuarine and rivers conference*, Nantes, 2014.
- [42] R. Ettema, E.A. Mostafa, B.W. Melville, A.A. Yassin, "Local scour at skewed piers", *Journal of Hydraulic Engineering*, vol. 124, issue 7, pp. 756-760, 1998.

- [43] D.C. Froehlich, "Analysis of Onsite Measurements of Scour at Piers", In *Hydraulic engineering: proceedings of the 1988 national conference on hydraulic engineering*, Colorado Springs, CO, 1988, pp. 534-539.
- [44] Aly A.M., Dougherty E., "Bridge pier geometry effects on local scour potential: a comparative study", *Ocean Engineering*, vol. 234, 109326, 2021.
- [45] B.W. Melville, Y.M. Chiew, "Time scale for local scour at bridges", *Journal of Hydraulic Engineering*, vol. 125, issue 1, pp. 59-65, 1999.
- [46] B.W. Melville, "Pier and abutment scour – An integrated approach", *Journal of Hydraulic Engineering*, vol. 123, issue 2, pp. 125-136, 1997.
- [47] O. Link, C. Gobert, M. Manhardt, U. Zanke, "Effect of the horseshoe vortex system on the geometry of a developing scour hole at a cylinder", in *Fourth International Conference on Scour and Erosion*, 2008, pp. 162-168.
- [48] S.O. Lee, I. Abid, S.H. Hong, "Effect of complex shape of pier foundation exposure on time development of scour", *Environmental Fluid Mechanics*, vol. 21:2021; 21:103-127.
- [49] F. Federico, G. Silvagni, F. Volpi, "Scour Vulnerability of River Bridge Piers", *Journal of Geotechnical and Geoenvironmental Engineering*, vol. 129, issue 10, pp. 890-899, 2003.
- [50] S.E. Coleman, "Clearwater Local Scour at Complex Piers", *Journal of Hydraulic Engineering*, vol. 131, issue 4, pp. 330-334, 2005.
- [51] X. Guo, "Seismic Vulnerability analysis of scoured bridge systems", Ph.D. dissertation, University of Missouri-Kansas City, Kansas City, Missouri, 1993.
- [52] R. Mohammadpour, A. Ghani, N.A. Zakaria, T.A. Mohammed Ali, "Predicting scour at river bridge abutments over time", In *Proceedings of the Institution of Civil Engineers-Water Management*, vol. 170, issue WM1, pp. 15-30, 2017.
- [53] K.K.G.K.D. Kariyawasam, P.R.A. Fidler, J.P. Talbot, C.R. Middleton, "Field deployment of an ambient vibration-based scour monitoring system at Baildon Bridge, UK", In *International Conference on Smart Infrastructure and Construction 2019 (ICSIC) Driving data-informed decision-making*, ICE Publishing, 2019, pp. 711-719.
- [54] K.D. Kariyawasam, C.R. Middleton, G. Madabhushi, S.K. Haigh, J.P. Talbot, "Assessment of bridge natural frequency as an indicator of scour using centrifuge modelling", *Journal of Civil Structural Health Monitoring*, vol. 10, pp. 861-881, 2020.
- [55] P. Zampieri, M.A. Zanini, F. Faleschini, L. Hofer, C. Pellegrino, "Failure analysis of masonry arch bridges subject to local pier scour", *Engineering Failure Analysis*, vol. 79, pp. 371-384, 2017.
- [56] E. Tubaldi, L. Macorini, B.A. Izzuddin, "Three-dimensional mesoscale modelling of multi-span masonry arch bridges subjected to scour", *Engineering Structures*, vol. 165, pp. 486-500, 2018.
- [57] W.H. Hager, "Scour in hydraulic engineering", *Proceedings of the Institution of Civil Engineers-Water Management*, vol. 160, issue WM3, pp. 159-168, 2007.
- [58] A. Roulund, J.S. Andersen, B.M. Sumer, J. Fredsøe, "Numerical and experimental investigation of flow and scour around a circular pile", *Journal of Fluid Mechanics*, vol. 534, pp. 351-401, 2005.
- [59] L. A. Padron, G. E. Mylonakis, D. E. Beskos, "Importance of footing-soil separation on dynamic stiffness of piled embedded footings", *International Journal for Numerical and Analytical Methods in Geomechanics*, vol. 33, pp. 1439-1448, 2009.
- [60] F. Dezi, S. Carbonari, G. Leoni, "A model for the 3D kinematic interaction analysis of pile groups in layered soils", *Earthquake Engineering and Structural Dynamics*, vol. 38, issue 1, pp. 1281-1305, 2009.
- [61] F. Liang, H. Zhang, M. Huang, "Influence of flood-induced scour on dynamic impedances of pile groups considering the stress history of undrained soft clay", *Soil Dynamics and Earthquake Engineering*, vol. 96, pp. 76-88, 2017.
- [62] S. Carbonari, M. Morici, F. Dezi, G. Leoni, "A lumped parameter model for time-domain inertial soil-structure interaction analysis of structures on pile foundations", *Earthquake Engineering & Structural Dynamics*, vol. 47, issue 11, pp. 2147-2171, 2018

- [63] F. Scozzese, L. Ragni, E. Tubaldi, F. Gara, “Modal properties variation and collapse assessment of masonry arch bridges under scour action”, *Engineering Structures*, vol. 199, 109665, 2019.
- [64] F. Rahman, R. Chavan, “Machine learning application in prediction of scour around bridge piers: A comprehensive review”, *Archives of Computational Methods in Engineering*, 2024.
- [65] R. Abd El-Hady Rady, “Prediction of local scour around bridge piers: artificial-intelligence-based modeling versus conventional regression methods”, *Applied Water Science*, vol. 10, article no. 57, 2020.
- [66] I. Ahmadianfar, M. Jamei, “Prediction of local scour around circular piles under waves using a novel artificial intelligence approach”, *Marine Georesources and Geotechnology*, vol. 39, issue 1, 2021.
- [67] J. Marr, “Bridge Scour Monitoring Technologies: Development of Evaluation and Selection Protocols for Application on River Bridges in Minnesota”, Minnesota Department of Transportation, Research Services Section, Minnesota, USA, Report No. MN/RC 2010-14, 2010.
- [68] B.E. Hunt B, “Monitoring Scour Critical Bridges”, Transportation Research Board, Washington, D.C., NSHRP SYNTHESIS 396, 2009.
- [69] J.L. Briaud, S. Hurlebaus, K. Chang, C. Yao, H. Sharma, O. Yu, C. Darby, B.E. Hunt B, G.R. Price, “Realtime monitoring of bridge scour using remote monitoring technology”, Texas Transportation Institute, Texas, FHWA/TX-11/0-6060-1, 2011.
- [70] L.J. Prendergast, “Monitoring of scour around structures using changes on natural frequency of vibration”, Ph.D. dissertation, School of Civil, Structural & Environmental Engineering, University College Dublin, Dublin, Ireland, 2015.
- [71] K. Faulkner, J.M.W. Brownjohn, Y. Wang, F. Huseynov, “Tracking bridge tilt behaviour using sensor fusion techniques”, *Journal of Civil Structural Health Monitoring*, vol. 10, issue 4, pp. 543-555, 2020.
- [72] A.H.E. Elsaid, “Vibration based damage detection of scour in coastal bridges”, Ph.D. dissertation, North Carolina State University, Raleigh, North Carolina, 2012.
- [73] N.E. Yankielun, L. Zabilansky, “Laboratory investigation of time-domain reflectometry system for monitoring bridge scour”, *Journal of Hydraulic Engineering*, vol. 125, issue 12, pp. 1279-1284, 1999.
- [74] X. Yu, X. Yu, “Time Domain Reflectometry Automatic Bridge Scour Measurement System: Principles and Potentials”, *Structural Health Monitoring*, vol. 8, issue 6, pp. 463-476, 2009.
- [75] United States Environmental Protection Agency, *Waterborne Ground Penetrating Radar* [Online]. Available: <https://www.epa.gov/environmental-geophysics/waterborne-ground-penetrating-radar>
- [76] N. L. Anderson, A.M. Ismael, T. Thitimakorn. “Ground-Penetrating Radar: A Tool for Monitoring Bridge Scour”, *Environmental and Engineering Geoscience*, vol. 13, issue 1, pp. 1-10, 2007.
- [77] Y.B. Lin, J.C. Chen, K.C. Chang, J.C. Chern, J.S. Lai, “Real-time monitoring of local scour by using fiber Bragg grating sensors”, *Smart Materials and Structures*, vol. 14, issue 4, pp. 664-670, 2005.
- [78] Monitoring scour at bridges and offshore structures, Fondriest Environmental. Available: https://www.nexsens.com/pdf/Guide_Scour_Monitoring.pdf
- [79] J.D. Schall, G.R. Price, G.A. Fisher, O.F. Lagasse, E.V. Richardson, “Magnetic Sliding Collar Scour Monitor-Installation, Operation, and Fabrication Manual”, Transportation Research Board, Washington, D.C., NCHRP Report 397B, 1997.
- [80] J.D. Schall, G.A. Fisher, P.F. Lagasse, E.V. Richardson, “Sonar Scour Monitor-Installation, Operation, and Fabrication Manual”, Transportation Research Board, Washington, D.C., NCHRP Report 397A, 1997.
- [81] D.C. Hayes, F.E. Drummond, “Use of Fathometers and Electrical-Conductivity Probes to Monitor Riverbed Scour at Bridge Piers”, U.S. Geological Survey, Richmond, Virginia, Water-Resources Investigations Report 94-4164, 1995.
- [82] P.F. Lagasse, P.E. Clopper, J.E. Pagán-Ortiz, L.W. Zevenbergen, L.A. Arneson, J.D. Schall, L.G. Girard, “Bridge Scour and Stream Instability Countermeasures: Experience, Selection, and Design

- Guidance-Third Edition”, US Department of Transportation, National Highway Administration, Washington, D.C., USA, Technical Report FHWA-NHI-09-111, 2009.
- [83] G. Butch, “Evaluation of scour monitoring instruments in New York”, In *1996 ASCE North American Water and Environment Congress, Bridge Scour Symposium*, Anaheim, C.A., 1996.
- [84] R. Brincker, L. Zhang, P. Andersen. “Modal identification of output-only systems using frequency domain decomposition”, *Smart materials and structures*, vol. 10, issue 3, pp. 441, 2001.
- [85] L.J. Prendergast, D. Hester, K. Gavin, J.J. O’Sullivan, “An investigation of the changes in the natural frequency of a pile affected by scour”, *Journal of Sound and Vibration*, vol. 332, issue 25, pp. 6685-6702, 2013.
- [86] T. Bao, A.R. Swartz, S. Vitton, Y. Sun, Z.C. Liu, “Critical insights for advanced bridge scour detection using natural frequency”, *Journal of Sound and Vibration*, vol. 386, pp. 116-133, 2017.
- [87] S. Foti, D. Sabia, “Influence of foundation scour in the dynamic response of an existing bridge”, *Journal of Bridge Engineering*, vol. 16, issue 2, pp. 295-304, 2011.
- [88] L.J. Prendergast, K. Gavin, D. Hester, “Isolating the location of scour-induced stiffness loss in bridges using local modal behaviour”, *Journal of Civil Structural Health Monitoring*, vol. 7, pp. 483-503, 2017.
- [89] T. Bao, Z.L. Liu, “Bridge scour characteristic curve for natural frequency-based bridge scour monitoring using simulation-based optimization”, *Structural Control and Health Monitoring*, vol. 28, issue 8, e2773, 2021.
- [90] C.C Chen, W.H. Wu, F. Slih, S.W. Wang, “Scour evaluation for foundation of a cable-stayed bridge based on ambient vibration measurements of superstructure”, *NDT & E International*, vol. 66, pp. 16-27, 2014.
- [91] W. Xiong, C.S. Cai, B. Kong, X. Zhang, P. Tang, “Bridge scour identification and field application based on ambient vibration measurements of superstructures”, *Journal of Marine Science and Engineering*, vol. 7, issue 5, 2019.
- [92] C.W. Kim, K. Yoshitome, Y. Goi, F.L. Zhang, S. Kitagawa, M. Shinoda, H. Yao, Y. Hamada, “Scour detection of railway bridges by microtremor monitoring”, In *EASEC16: Proceedings of the 16th East Asia-Pacific conference on structural engineering and construction, 2019*. Springer Singapore, 2021, pp 97-107.
- [93] A. Malekjafarian, C. Kim, E.J. O'Brien, L.J. Prendergast, P.C. Fitzgerald, S. Nakajima, “Experimental demonstration of a mode shape-based scour monitoring method for multispan bridges with shallow foundations”, *Journal of Bridge Engineering*, vol. 25, issue 8, 04020050, 2020.
- [94] G. Ruocci, A. Quattrone, Z.L. Fragonara, R. Ceravolo, A. De Stefano, “Experimental testing of a masonry arch bridge model subject to increasing level of damage”, In *Proceedings of 4th international conference on advances in experimental structural engineering*, ISPRA, Lombardy, 2011.
- [95] P. Borlenghi, C. Gentile, M. D’Angelo, F. Ballio, “Long-term monitoring of a masonry arch bridge to evaluate scour effects”, *Construction and Building Materials*, 2024; 411:134580.
- [96] Y.I. TingHua, L.I HongNan, G.U. Ming, “Recent research and applications of GPS based technology for bridge health monitoring”, *Science China Technological Sciences*, vol. 53, pp. 2597-2610, 2010.
- [97] Moschas F., Stiros S. Measurement of the dynamic displacements and of the modal frequencies of a short-span pedestrian bridge using GPS and an accelerometer. *Engineering Structures*, 2011; 33: 10-17.
- [98] J.O. de Araújo Neto, J.L.A. Trabanco, A.P.C. Larocca, A.L. Cunha, M.C. dos Santos, “Rigid Bridges Health Dynamic Monitoring Using 100 Hz GPS Single-Frequency and Accelerometers”, *Positioning*, vol. 10, issue 2, pp. 17-33, 2019.
- [99] G.W. Roberts, E. Cosser, X. Meng, A. Dodson, “High frequency deflection monitoring of bridges by GPS”, *Journal of Global Positioning Systems*, 2004; vol. 3, issue 1-2, pp. 226-231, 2004.

- [100] J. Paziewski, R. Sieradzki, R. Baryla, “Detection of structural vibration with high-rate precise point positioning: case study results based on 100 Hz multi-GNSS observables and shake-table simulation”, *Sensors*, vol. 19, issue 22, 4832, 2019.
- [101] S. Selvakumaran, S. Plank, C. Geiß, C. Rossi, C. Middleton, “Remote monitoring to predict bridge scour failure using Interferometric Synthetic Aperture Radar (InSAR) stacking techniques”, *International Journal of Applied Earth Observation and Geoinformation*, vol. 73, pp. 463-470, 2018.
- [102] S. Selvakumaran, S. Plank, X. Geiß, C. Rossi, “Using InSAR stacking techniques to predict bridge collapse due to scour”, In *IGARSS 2018 – 2018 IEEE International Geoscience and Remote Sensing Symposium*, IEEE, 2018, pp. 866-869.
- [103] D. Tonelli, V.F. Caspani, A. Valentini, A. Rocca, R. Torboli, A. Vitti, D. Perissin, D. Zonta, “Interpretation of Bridge Health Monitoring Data from Satellite InSAR Technology”, *Remote Sensing*, vol. 15, issue 21, 5242, 2023.
- [104] J.J. Sousa, I. Hlaváčová, M. Bakoň, M. Lazecký, G. Patrício, P. Guimarães, A.M. Ruiz, L. Bastos, A. Sousa, R. Bento, “Potential of Multi-temporal InSAR Techniques for Bridges and Dams Monitoring”, *Procedia Technology*, vol. 16, pp. 834-841, 2014.

3 Review of combined effects of scour and earthquakes

Bridges shall be assessed and designed against multiple natural hazards to ensure sustainability and safety. Among the various threats to bridge stability, scour and earthquake hazards are the main causes of bridge failure worldwide due to their sudden and catastrophic nature [1]-[4]. As previously discussed in Chapter 2, bridge scour refers to the erosion of soil surrounding bridge supports, such as piers and abutments, caused by the flowing water. Scour compromises the structural integrity of bridges by reducing the support provided the soil surrounding underwater foundations, resulting in increased stresses and reduction of the soil-foundation stiffness and subsequently in a reduction of the overall stiffness of the SFS system. This stiffness reduction yields a significant change in the response of bridges to other dynamic loadings, such as earthquakes. When these two natural phenomena occur (more likely sequentially than simultaneously), their combined effects could amplify dramatically the risk of bridge failure. A great number of bridges with underwater foundations are located in earthquake-prone countries, highlighting the need of guidelines and procedures on the sustainable seismic design of bridges taking the scour effects into account. This chapter aims to explain the mechanism of these combined hazards on bridge stability, analyse the existing literature of numerical and experimental studies investigating the effects of scour on the seismic response of bridges, and discuss research gaps.

Section 3.1 Introduction introduces the combined effects of scour and earthquake hazards on bridges, highlighting their potentially catastrophic consequences. Section 3.2 Multi-hazard risk analysis and current codes reviews multi-hazard risk assessment frameworks, and current design codes, highlighting their limitations in accounting for both hazards simultaneously. Section 3.3 Review of studies on the topic presents an extensive literature review of both numerical and experimental studies on the effects of scour on the seismic response of bridges. Section 3.4 Research gaps identifies research gaps and the need of improved modelling approaches and their validation with experimental campaigns, especially for bridges with shallow foundations.

3.1 Introduction

Scour and earthquake events can have a detrimental effect on the serviceability of bridges, with the potential to cause even collapse. The damage nature of a bridge is strongly associated with the bridge and foundation typology. Scour at bridges with shallow foundations results in settlements, which could damage the superstructure. This type of damage can be particularly crucial for masonry bridges since it compromises arch integrity. Scour can also cause a loss of bearing capacity, which is a critical failure mode only for large portions of the foundation base undermined. Even when scour hole has not extended beneath a bridge's shallow foundation, soil stability issues of the remaining soil arise, worsening the flow conditions around the foundation [5]. Scour at bridges with piled foundations may result in various damage scenarios. The reduced lateral support due to scour increases the lateral displacements and bending moments on the piles, rendering them more susceptible to buckling, which can subsequently lead to total bridge collapse. Furthermore, scour reduces the shaft resistance of piles leading to differential settlement. Severe differential settlement of different foundations can cause cracking in the bridge superstructure, deck buckling, joint failures and possible collapse of bridge spans. When it comes to pile groups, block settlement can induce unacceptable tilting of the supported pier or abutment, leading to deck sliding or buckling. Moreover, severe scour can undermine the entire pile group, leading to block failure resulting in sudden and catastrophic collapse of a bridge component or span.

Earthquakes also pose a significant risk to the structural integrity of bridges. The dynamic forces developed during an earthquake can cause various failure modes, impacting different components of a bridge. Seismic forces induce excessive stresses and deformations in a bridge foundation, particularly

when it is not designed to withstand such loads, leading to settlement or tilting, and hence to a potential collapse. Pier and abutment failure is also a common damage scenario due to earthquakes. Bridge piers and abutments are subjected to high lateral forces when an earthquake occurs, which may exceed their design capacity resulting in cracking, spalling of concrete, buckling of reinforcement or shear failure. Additionally in a seismic event, bridge deck can undergo large displacements relative to the piers and abutments, which may result in deck unseating from its supports, and therefore in a bridge span collapse. Also, bearings can be dislodged or damaged causing misalignment and increased stresses of the bridge deck.

The scour and earthquake hazards are independent hazards, i.e., the occurrence of one event does not affect the probability of occurrence of another. However, as already discussed in Chapter 2, scour is a cumulative phenomenon and may be unnoticed for years. Thus, there is a non-negligible probability that an earthquake affects a bridge whose foundations are scoured. For example, just three weeks after the occurrence of a major flood event in the state of Washington, USA caused by the Pacific Northwest storm, an earthquake of magnitude Mw 4.5 hit the region on January 2009. Similarly in the region of Marche (Italy), a seismic sequence (largest magnitude Mw 5.5) was recorded in November 2022 following a very destructive flood that affected many bridges in September 2022. In some cases (see e.g. [6]), scour events could be recorded after a large earthquake occurrence, but this problem is out of the scope of this dissertation.

As mentioned earlier, scour decreases the soil-foundation stiffness and the foundation bearing capacity. Therefore, scour can strongly exacerbate the bridge damage scenarios caused by earthquakes. Particularly, scour can disrupt the intended failure hierarchy established by capacity design, potentially causing the various to collapse before the flexural failure of the bridge piers. Moreover, the reduction of the soil-foundation stiffness due to scour results in a stiffness reduction of the whole SFS system, resulting in a seismic response which can differ significantly from the case with no scour. However, in some cases, scour can be beneficial for the seismic response of bridges by inducing a reduction of inertial forces or a reduction of the bending and shear forces in the pier, due to increased rocking of the foundation. While these effects might be beneficial, the increased bridge flexibility due to scour may cause higher displacements during seismic events, increasing the likelihood of critical failures such as deck unseating. These contrasting effects emphasise the need for a systematic evaluation of the interactions between scour and earthquakes by balancing benefits and risks, hence ensuring robust multi-hazard design and maintenance strategies.

3.2 Multi-hazard risk analysis and current codes

According to the current design codes in the United States [7], foundations shall be designed for both service and strength limit states, and checked against extreme-event limit states. At the strength and limit states, foundations shall be designed with adequate bearing capacity and lateral resistance, assuming the sediments within the estimated scour depth. For extreme events, the stability of the foundations should be ensured with a scour depth estimated for an extreme flood event, not exceeding a 500-year flood. Furthermore, the NCHRP Report-489 [8] recognises the long-term nature of scour and takes the joint occurrence of scour and other extreme hazards into account. Specifically, NCHRP Report-489 recommends the load combination $1.25 DC + 1.00 EQ; 0.25 SC$, where DC stands for the dead load, EQ for the earthquake loads. The 0.25 SC indicates that the analysis should assume a scour depth equal to 0.25 of the design scour depth. Scour is treated as a partial reduction of the resistance of the foundation. Correspondingly, this assumption leads to a decrease in stiffness and bearing capacity of the foundation, which modifies the seismic response of SFS systems. The 0.25 factor is a conservative estimate to represent a partial degradation scenario where the scour effects have decreased the foundation's support capacity, while have not caused its failure. It is stated that relatively small combination factor of 0.25 is appropriate as long as a total washout of the foundation does not occur. This is because scoured bridge foundations may exhibit higher flexibility, thereby reducing inertial force

demands, which can be beneficial for the seismic response of bridges. At the same time, Eurocode 7 [9] for geotechnical design and Eurocode 8 [10] for earthquake-resistant design, provide guidelines for considering various loads and their combinations. However, there is no explicit load combination that simultaneously considers both scour and earthquakes. Instead, engineers are expected to account for these effects separately, while they are not provided with detailed guidelines.

Given the current changing climate and the increased rate of extreme weather events, analysing the risk of bridge failure due to multiple hazards is of paramount importance. Multi-hazard risk analysis is a relatively new area in structural engineering. This analysis is performed by combining the information on the joint statistics of the hazards with the information on the bridge vulnerability to these hazards. Figure 3-1 indicatively shows the potential multiple hazards and their corresponding intensity measures, highlighting the importance of multi-hazard [11]. Traditional single-hazard approaches may underestimate the risk by not accounting for the compounded effects of multiple hazards. Multi-hazard analysis addresses this gap by integrating the potential interactions between different hazards, leading to more accurate risk assessments and robust design frameworks [12][13].

Current management decisions regarding bridge infrastructure in the USA are evolving towards a bridge-by-bridge approach to mitigate scour-induced failures, independent of other bridges within the same regional transportation network [14]. Therefore, site-specific and scenario-specific investigations are crucial for developing a sustainable bridge management framework at the network level, as managing individual bridges on a case-by-case basis would be impractical. Wright et al. [15] explored the potential impacts of increased river flooding from climate change on bridge networks, identifying approximately 129,000 deficient bridges due to these effects. Consequently, to mitigate the risk of failure in these structures, assessment and design methodologies for bridges should anticipate potential increases in future flood hazards [16]. Various risk-based frameworks have been developed to incorporate uncertainties in river flow magnitudes at bridge locations [17]-[21], as climate change is expected to alter the statistical characteristics of maximum annual flow distributions regularly.

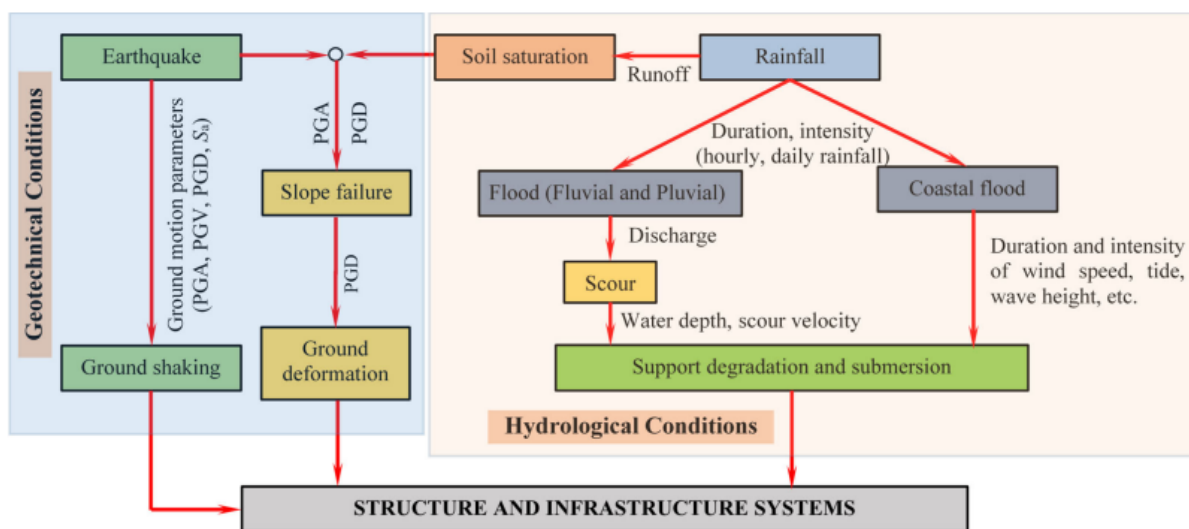


Figure 3-1: Multiple hazards and their corresponding intensity measures to infrastructure systems [11].

3.2.1 Probabilistic frameworks for multi-hazard analysis

Probabilistic frameworks are essential for assessing the vulnerability of bridges to multi-hazard analysis because they can quantify uncertainties and assess risks more robustly than deterministic methods. These approaches consider the variability in hazard intensity, frequency, and structural response under combined effects, offering a realistic evaluation of potential failure scenarios. The complex interactions

between scour and seismic events necessitate such methodologies to ensure the resilience and reliability of bridge structures.

3.2.1.1 Fragility analysis

Usually, the vulnerability is described by means of fragility surfaces, which describe the probability of exceedance of a given level of damage as a function of two parameters describing the intensity of the hazards (e.g. ground shaking intensity for the case of earthquakes and scour depth for the case of scour). For example, Argyroudis and Mitoulis [22] derived fragility curves for bridges exposed to floods and earthquakes for a typical three-span prestressed box-girder river-crossing bridge. Figure 3-2 shows the fragility surfaces obtained by evaluating the probability of exceeding different damage states for the pier (left column) and the abutment (right column) conditional to the scour depth and the peak ground acceleration.

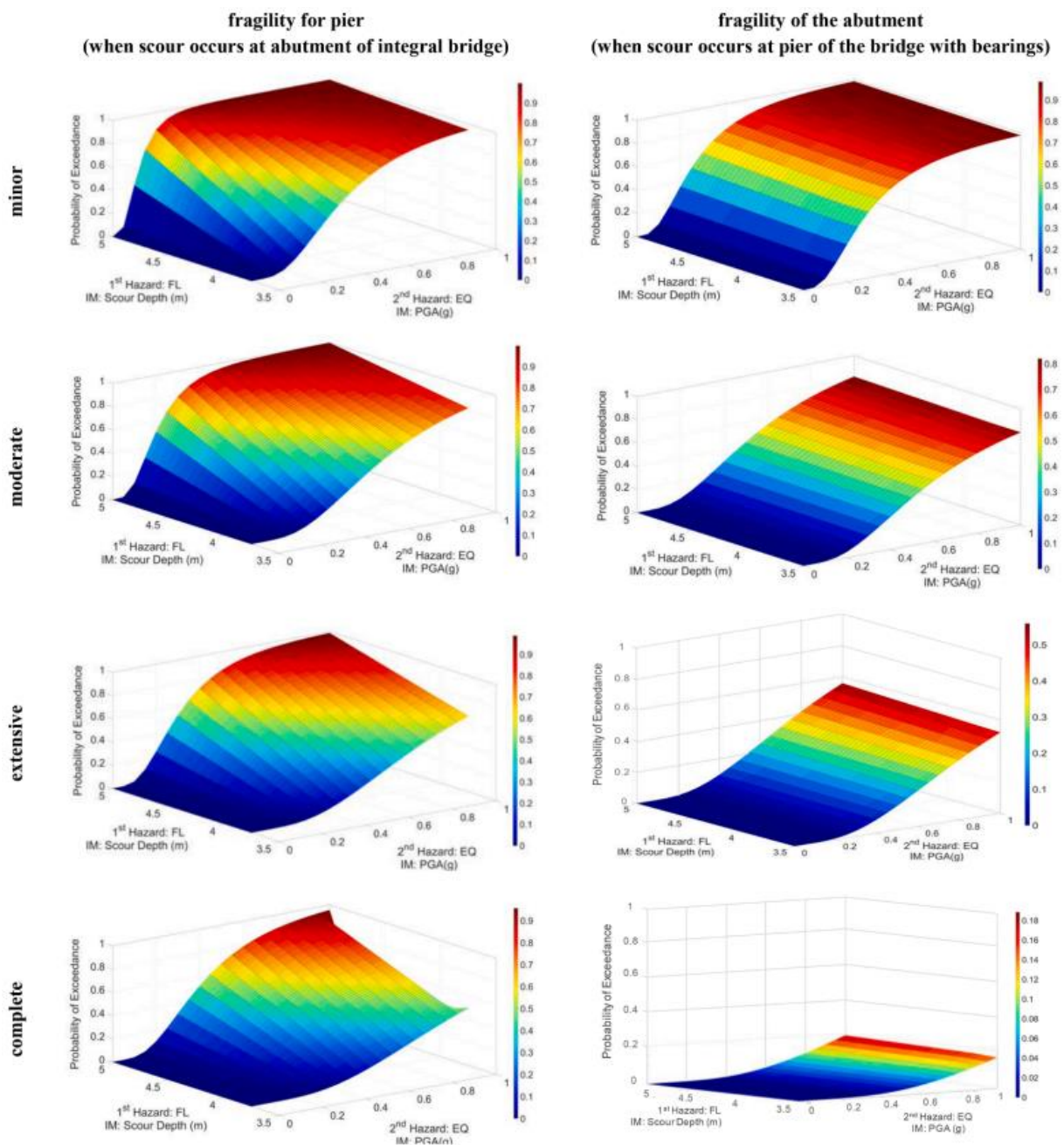


Figure 3-2: Fragility surfaces for the pier (left column) and the abutment (right column) exposed to scour and earthquake hazards [22].

Alternatively, multiple fragility curves could be derived by expressing the probability of damage exceedance for a given level of the intensity of one hazards, and for discrete levels of the intensity of the other hazard. For example, Figure 3-3 shows a typical fragility curve for the effect of Peak Ground Acceleration (PGA) for a bridge under various levels of scour [23].

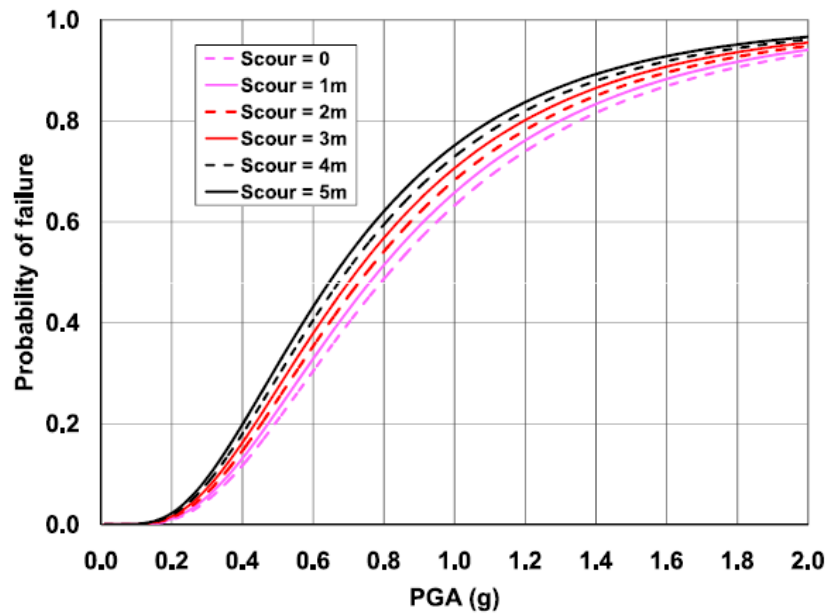


Figure 3-3: Fragility curve for a bridge with different levels of scour and PGA[23].

The risk of failure of a bridge due to multiple hazards can be evaluated by combining the information on the hazards and the information on the fragility as follows:

$$P_f = \int_0^{\infty} \int_0^{\infty} H[PGA > pga, S > s] dP_f(c, y) \quad (3.1)$$

Where $H[PGA > pga, S > s]$ is the hazard function describing the joint probability of PGA exceeding pga and S exceeding s , $P_f(c, y)$ is the probability of failure given $PGA = pga$ and $S = s$, and d is the differential operator.

3.2.1.2 Life-cycle cost and risk assessment

Multi-hazard assessment techniques are increasingly adopted in infrastructure systems, addressing their complexity by considering concurrent demands [12],[13]. The application of vulnerability and risk methodologies for estimating life-cycle costs has emerged as a practical area of interest for optimising the design and maintenance of structural integrity. Frameworks for risk assessment and life-cycle cost analysis have been developed for lifeline bridge structures in seismically active and flood-prone scenarios to quantify performance levels during operation [24][25]. Studies on life-cycle loss estimation have considered time-dependent hazards, aging effects, and the stochastic nature of hazard occurrence, as well as the structural performance and consequences associated with these hazards. Research has also advanced in assessing the resilience of bridge networks through retrofit techniques aimed at mitigating structural vulnerabilities under multiple hazard scenarios [26][27]. Argyroudis et al. [28] developed a framework for evaluating the resilience of infrastructure assets exposed to multiple hazards characterised by diverse nature impact and occurrence time. The proposed framework is applied to a case study, consisting of a multi-span highway bridge exposed to flood-induced scour followed by an earthquake. Statistical analyses have been conducted to evaluate the impact of retrofitting on seismic resilience in the context of flood-induced scour. Additionally, various mitigation measures have been proposed to reduce the probability of failure of bridge piers due to scour during seismic events.

Overall, the technical frameworks have revealed that traditional approaches inadequately accounted for the impacts of climate change, leading to underestimation or overestimation of future risks. The newly proposed risk-based frameworks are robust enough to assist bridge management services in making informed decisions regarding retrofitting to reduce failure probabilities under future flood hazards. These frameworks also provide quantitative measures to support decisions about bridge closures during flood events. Active control of data quality is crucial for understanding and managing bridge resilience in the context of future climatic conditions [29].

3.2.2 Climate change and multi-hazard risk

Climate change is expected to exacerbate the risks associated with scour and earthquakes, making it essential to consider these factors in bridge design and management. This section explores the impact of climate change on scour and discusses adaptation strategies for mitigating multi-hazard risks.

3.2.2.1 Impact of climate change on scour

Climate change is projected to significantly intensify the risk of scour, posing a critical threat to the structural integrity and longevity of bridge infrastructure. Rising global temperatures and shifting weather patterns are expected to increase the frequency and intensity of extreme weather events, including heavy rainfall and flooding [30]. These events lead to higher river flows and elevated water levels, which in turn intensify the scouring process around bridge foundations. Increased precipitation and runoff contribute to more aggressive and unpredictable erosion patterns, undermining the stability of bridge piers and abutments. Moreover, climate change-induced shifts in seasonal weather patterns can alter sediment transport dynamics in rivers, leading to changes in riverbed profiles and potentially exposing bridge foundations to unanticipated scouring depths [31]. The unpredictability and variability introduced by these climatic changes complicate the accurate prediction of scour depths, making traditional design and assessment methods increasingly inadequate [32]. Consequently, bridges that were originally deemed safe based on historical data may become vulnerable to scour under new climate conditions, necessitating a re-evaluation of existing infrastructure and adaptation of design standards [33]. In addition, the synergistic effects of climate change on scour can amplify the risks posed by other natural hazards, such as earthquakes, thereby compounding the overall threat to bridge stability and safety.

3.2.2.2 Adaptation strategies for multi-hazard risk

Adapting bridge infrastructure to withstand the combined impacts of scour and other natural hazards, such as earthquakes, requires a multifaceted approach that integrates advanced engineering practices, robust design standards, and proactive management strategies. One of the primary adaptation strategies involves the elevation of bridge foundations to account for anticipated increases in flood levels and scour depths. This approach, combined with the use of scour-resistant materials and innovative construction techniques, can significantly enhance the durability of bridge piers and abutments [34]. Implementing real-time monitoring systems equipped with sensors to detect early signs of scour and structural stress can provide critical data for timely interventions, helping to prevent catastrophic failures. Additionally, retrofitting existing bridges with advanced protective measures, such as riprap, collars, and scour countermeasures, can mitigate the impact of erosion [35]. Incorporating probabilistic risk assessment frameworks into the design process allows engineers to consider the combined probabilities of scour and seismic events, leading to more resilient structural designs. Furthermore, policy and regulatory changes that mandate the inclusion of climate change projections in infrastructure planning and development are essential for ensuring long-term resilience [36]. These measures, supported by increased funding for research and the development of innovative materials and technologies, can significantly reduce the vulnerability of bridge infrastructure to the compounded effects of multiple hazards. By adopting a holistic approach that encompasses engineering, policy, and

technology, it is possible to create a resilient and adaptive bridge infrastructure capable of withstanding the challenges posed by a changing climate and the associated increase in multi-hazard risks.

3.3 Review of studies on the topic

Many bridges with underwater foundations are located in earthquake-prone countries, and scour can not only directly affects the stability of these bridges but also makes them more susceptible to damage from earthquakes [37][39]. Bridge scour refers to the erosion of soil surrounding the supports of a bridge, such as its abutments and piers, caused by the movement of water [40],[41]. This phenomenon has a detrimental impact on the bridge's structural integrity by diminishing its foundation bearing capacity and by decreasing the overall stiffness of the Soil-Foundation-Structure (SFS) system. The stiffness reduction results in a different response of the structure to other dynamic loadings, such as earthquakes. Current codes lack comprehensive guidance for assessing and designing bridges to withstand the combined effects of earthquake and scour hazards (see section 3.2 Multi-hazard risk analysis and current codes).

Many researchers have investigated the issue in the last two decades. For example, Wang et al. [42] analysed the dynamic behaviour and seismic performance of different types of reinforced concrete girder bridges, such as multi-span simply supported, multi-span continuous and single frame bridges, under various scour conditions. They observed that scour can have a significantly different impact on the period elongation, and on the seismic response for different types of bridges, while enlarged shaft foundations can be effective in protecting bridges in earthquake and flood-prone areas. Prasad & Banerjee [43] evaluated the seismic performance of reinforced concrete bridges pre-exposed to various flood intensities and scour scenarios by means of nonlinear time history analyses. They concluded that the damageability of the bridge piers increases nonlinearly for increasing scour depth, and that even a low intensity flood causes a significant degradation of the seismic performance. Yilmaz et al. [44] assessed numerically the performance of two real-life California bridges under the multihazard condition of flood-induced scour and earthquake by means of fragility analysis. The results showed that the flood-events can increase the seismic vulnerability and risk of bridges, yet larger diameter foundations tend to reduce the impact of scour hazard on bridge seismic performance. Guo et al. [45] performed time-dependent fragility analyses to box-girder concrete bridge systems to investigate their seismic performance under combined seismic and scour hazards over their whole service life. Song et al. [46] developed an analytical approach to assess the earthquake damage potential of bridges with scoured foundation, showing that relatively low scour depths may cause foundation damage during an earthquake, even for bridges designed to provide satisfactory seismic performance. Fialko & Alipour [47] investigated the significance of non-uniform scour on the seismic performance of bridges. They concluded that for increasing scour depths scenarios, the amount of seismic energy experienced by the structure decreases, while the increasing flexibility of the foundation support results in an increasing displacement demand to other components of the structure. Han et al. [48] investigated the seismic response of a single pylon cable-stayed bridge founded on a pile group under various scour scenarios and they concluded that for increasing scour depths the bending moment on the piles increases whereas the bending moment demand of the pier decreases, and that the failure mode of the bridge move from the pier to the piles and the abutments. Zaky et al. [49] assessed the influence of scour on the seismic performance of the piled-foundation Boğaçay Bridge in Turkey. They concluded that increasing scour width leads to a significant increase of pier displacement demands, especially in the transverse direction of the bridge. Moreover, they observed that the internal forces of the pier decrease significantly because of the migration and spreading of plastic hinging from piers to piles due to scouring. Foti et al. [50] provided an overview of conventional approaches to assess the performance of scoured bridges against seismic actions, including an application to a SFS system with caisson foundations. They concluded that an advanced modelling of the impact of scour is essential, because of the drawback of the simplified conventional approaches' applicability to capture the decreasing foundation capacity for increasing scour geometries.

A significant number of experimental studies have also investigated the problem by performing tests on real systems or scaled models. Chang et al. [51] performed in-situ seismic tests of a bridge before its demolition due to accumulated scouring problem. The tests were conducted on three single columns and one caisson-type foundation. Specifically, one column with no exposed foundation, a column with exposed foundation, and one column which was excavated to study the effect of the scouring problem to the column performance. Based on the results, due to large dimension of the caisson foundation and the well graded gravel soil type that provided large lateral resistance, the seismic performance among the three columns had only minor differences. The column with the caisson-type foundation was examined experimentally, while a numerical parametric study was developed to predict its behaviour with different ground motions and different scour levels. Ciancimino et al. [52] performed scaled experiments to investigate the response of a bridge pier, supported on a cylindrical embedded foundation, subjected to general and local scour. They concluded that local scour has a minor effect on vertical bearing capacity and the lateral performance was dramatically decreased. The effect of general scour on the lateral performance was even more pronounced, while the rate of cyclic settlement accumulation was also much more severe compared to local scour, highlighting the importance of taking the scour geometry into consideration. Wang et al. [53] investigated both numerically and experimentally the seismic resonance behaviour of Soil-Pile-Structure systems (SPSS) with scour effects. They performed a series of shake-table tests to identify the resonance phenomena of scoured SPSS for different scour scenarios, while they developed a numerical model to account for effective stress effects at shallow depths. It was found that the resonance period of SPSS generally increases with increasing scour depth and excitation intensity, mainly due to the structural nonlinearity of SPSS.

3.4 Research gaps

Despite significant progress in understanding the collapse of bridges under concurrent hazard scenarios, numerous complex challenges remain unexplored. Firstly, bridge collapses are intricate processes typically resulting from a combination of diverse factors, making it highly challenging to pinpoint the primary factor directly leading to collapse. Secondly, conducting field tests to investigate the collapse of real-life bridges faces obstacles due to safety concerns and cost implications). Moreover, there is an impending need for research to develop probabilistic frameworks for assessing the sustainability of bridge networks under multiple hazards such as earthquakes and flood-induced scour [54]. Therefore, gaining a deeper understanding of these complexities is essential for formulating assessment strategies that offer reliable approaches to explicitly design lifeline bridge structures. This involves considering the interactions and return periods of various natural hazards—including earthquakes, flooding, and scour—throughout the service life of bridges.

Most of the numerical and experimental studies mentioned in Section 3.3 Review of studies on the topic focused on the case of bridges with deep foundations or caisson foundations, while bridges with shallow foundations, a more critical typology, have received attention only by few researchers. To the author's knowledge, only Guo [55] investigated the seismic performance of bridges with scoured shallow foundations, by evaluating the changes in the impedance functions, and used these in the seismic analysis of a simplified SFS system. Hence, further investigation in more complexed SFS systems is imperative. Other studies considering shallow foundations, have not investigated the seismic response but only the dynamic behaviour of bridges affected by scour (see e.g. [56]-[58]). Additionally, there is lack of numerical and experimental in-field studies on the seismic response of bridges under realistic scour conditions (see Section 2.2.2 Local scour hole shape).

From the analysis of the literature, it is evident that further research is needed to investigate the influence of scour on the dynamic behaviour and seismic response of bridges with shallow foundations. This dissertation aims to fill this knowledge gap, by addressing the problem with a series of novel experimental and numerical investigations, as described in detail in the next sections.

References

- [1] A.M. Shirole, R.C. Holt, “Planning for a comprehensive bridge safety assurance program”, Transportation Research Board, Washington, D.C., Transportation Research Record 1290, 1991, pp. 39-50.
- [2] J.L. Briaud, C.F.K. Ting, H.C. Chen, R. Gudavalli, S. Perugu, G. Wei, “SRICOS: prediction of scour rate in cohesive soils at bridge piers”, *Journal of Geotechnical and Geoenvironmental Engineering*, vol. 125, issue 4, pp. 237-246, 1999.
- [3] K. Wardhana, F.C. Hadipriono, “Analysis of recent failures in the United States”, *Journal of Performance of Constructed Facilities*, vol. 17, issue 3, pp. 144-150, 2003.
- [4] M. Yashinsky, J. Moehle, M. Eberhard, *Earthquake damage to bridges*, 2nd edition, Bridge Engineering Handbook-Seismic Design, 2014.
- [5] M.A Zanini, F. Faleschini, N. Ademovic, L.J. Prendergast, K. Gavin, M.P. Limongelli, “Structural Health Monitoring and Design Code compliance for performance assessment of bridges under scour and seismic hazards”, In *Proceedings of the Value of Structural Health Monitoring for the Reliable Bridge Management*, Zagreb, Croatia, 2017.
- [6] S. Stefanidou, A. Karatzetzou, G. Tsinidis, A. Mitoulis, S. Argyroudis, “Multi-hazard fragility assessment of bridges: Methodology and case study application”, In *3rd International Conference on Natural Hazards & Infrastructure*, Athens, Greece, 2022.
- [7] AASHTO LRFD Bridge Design Specifications, 9th Edition, Washington, D.C.: American Association of State Highway and Transportation Officials, 2020.
- [8] M. Ghosn, F. Moses, J. Wang, “Design of Highway Bridges for Extreme Events”, Transportation Research Board, Washington, D.C., NCHRP Report 489, 2003.
- [9] European Committee for Standardization. Eurocode 7: Geotechnical Design – Part 1: General Rules (EN 1997-1), Brussels: CEN, 2004
- [10] European Committee for Standardization. Eurocode 8: Design of Structures for Earthquake Resistance – Part 1: General Rules, Seismic Actions and Rules for Buildings (EN 1998-1), Brussels, CEN, 2004.
- [11] T. Roy, V. Matsagar, “Multi-hazard analysis and design of structures: status and research trends”, *Structure and Infrastructure Engineering*, vol. 19, issue 6, pp. 845-874, 2023.
- [12] M.M. Ettouney, S. Alampalli, A.K. Agrawal, “Theory of multihazards for bridge structures”, *Bridge Structures*, vol. 1, issue 3, pp. 281-291, 2005.
- [13] M. Ghosn, J. Wang, “Reliability model for bridge scour analysis”, In *Life-Cycle Performance of Deteriorating Structures: Assessment, Design and Management*, 2003, pp. 238-246.
- [14] L. Liu, D.M. Frangopol, A. Mandoro, D.Y. Yang, “Sustainability-informed bridge ranking under scour based on transportation network performance and multi-attribute utility”, *Journal of Bridge Engineering*, vol. 23, issue 10, 04018082, 2018.
- [15] L. Wright, P. Chinowsky, K. Strzepek, R. Jones, R. Streeter, J.B. Smith, J. Mayotte, A. Powell, L. Jantarasami, W. Perkins, “Estimated effects of climate change on flood vulnerability of U.S. bridges”, *Mitigation and Adaptation Strategies for Global Change*, vol. 17, pp. 939-955, 2012.
- [16] O. Khandel, M. Soliman, “Integrated framework for assessment of time-variant flood fragility of bridges using deep learning neural networks”, *Journal of Infrastructure Systems*, vo. 27, issue 1, 04020045, 2021.
- [17] D.K. Devendiran, S. Banerjee, A. Mondal, “Impact of climate change on multihazard performance of river-crossing bridges: Risk, resilience, and adaptation”, *Journal of Performance of Constructed Facilities*, vol. 35, issue 1, 04020127, 2021.
- [18] A. Ikpong, A. Bagchi, “New method for climate change resilience rating of highway bridges”, *Journal of Cold Regions Engineering*, vol. 29, issue 3, 04014013, 2015.
- [19] O. Khandel, M. Soliman, “Integrated framework for quantifying the effect of climate change on the risk of bridge failure due to floods and flood-induced scour”, *Journal of Bridge Engineering*, vol. 24, issue 9, 04019090, 2019.

- [20] A. Khelifa, L.A. Garrow, M.J. Higgins, M.D. Meyer, “Impacts of climate change on scour-vulnerable bridges: Assessment based on HYRISK”, *Journal of Infrastructure Systems*, vol. 19, issue 2, pp. 138-146, 2013.
- [21] D.Y. Yang, D.M. Frangopol, “Risk-based portfolio management of civil infrastructure assets under deep uncertainties associated with climate change: a robust optimization approach”, *Structure and Infrastructure Engineering*, vol. 16, issue 4, pp. 531-546, 2020.
- [22] S.A. Argyroudis, S.A. Mitoulis, “Vulnerability of bridges to individual and multiple hazards-floods and earthquakes”, *Reliability Engineering and System Safety*, vol. 210, 107564, 2021.
- [23] A. Alipour, B. Shafei, M. Shinozuka, “Reliability-Based Calibration of Load and Resistance Factors for Design of RC Bridges under Multiple Extreme Events: Scour and Earthquake”, *Journal of Bridge Engineering*, vol. 18, issue 5, pp. 362-371, 2013.
- [24] Z. Chen, X. Guo, “Multi-hazard life-cycle analysis of flood-scour effects on seismic bridge performance”, *Structures Congress 2015*, Portland, Oregon, 2015, pp. 1370-1379.
- [25] Y. Dong, D.M. Frangopol, “Probabilistic time-dependent multi-hazard life-cycle assessment and resilience of bridges considering climate change”, *Journal of Performance of Constructed Facilities*, vol. 303, issue 5, 04016034, 2016.
- [26] S. Chandrasekaran, S. Banerjee, “Retrofit optimization for resilience enhancement of bridges under multi-hazard scenario”, *Journal of Structural Engineering*, vol. 142, issue 8, C4015012, 2016.
- [27] A. Venkittaraman, S. Banerjee, “Enhancing resilience of highway bridges through seismic retrofit”, *Earthquake Engineering & Structural Dynamics*, vol. 43, issue 8, pp. 1173-1191, 2014.
- [28] S.A. Argyroudis, S.A. Mitoulos, L. Hofer, M.A. Zanini, E. Tubaldi, D.M. Frangopol, “Resilience assessment framework for critical infrastructure in a multi-hazard environment: Case study on transport assets”, *Science of the Total Environment*, vol. 714, 136854, 2020.
- [29] H. Dikanski, B. Imam, A. Hagen-Zanker, “Effects of uncertain asset stock data on the assessment of climate change risks: A case study of bridge scour in the UK”, *Structural Safety*, vol. 71, pp. 1-12, 2018.
- [30] Change, Intergovernmental Panel on Climate, *Climate change 2014-impacts adaptation and vulnerability*, part A: A global and sectoral aspects. Cambridge University Press, 2014.
- [31] J.L. Briaud J, H.C. Chen, Y. Li, P. Nurtjahyo, J. Wang, “SRICOS-EFA method for contraction scour in fine-grained soils”, *Journal of Geotechnical and Geoenvironmental Engineering*, vol. 131, issue 10, pp. 1283-1294, 2005..
- [32] B.W. Melville, S.E. Coleman, *Bridge scour*. Water Resources Publication, 2000.
- [33] S. Kameshwar, J.E. Padgett, “Multi-hazard risk assessment of highway bridges subjected to earthquake and hurricane hazards”, *Engineering Structures*, vol. 78, pp. 154-166, 2014.
- [34] E.V. Richardson, S.R. Davis, “Evaluating scour at bridges”, Federal Highway Administration, Washington, D.C., FHWA-NHI-01-001, 2001.
- [35] P.F. Lagasse, P.E., “Countermeasures to protect bridge piers from scour”, Transportation Research Board, Washington, D.C., NCHRP Report 593, 2007.
- [36] B.M. Ayyub, “Climate-Resilient Infrastructure: Adaptive Design and Risk Management”, Committee on Adaptation to a Changing Climate, American Society of Civil Engineers, 2018.
- [37] Z. Khan, K. Amanat, “Riverbed Scouring Effect in Bridge Pile Foundation during Earthquake”, *Advances in Soil Dynamics and Foundation Engineering*, 2014, pp. 343-352.
- [38] Z. Wang, W. Song, T. Li, “Combined fragility surface analysis of earthquake and scour hazards for bridge”, In *Proceedings, 15th World Conference on Earthquake Engineering*, Lisbon, Portugal, 2012, pp. 24-28.
- [39] S. Banerjee, G.G. Prasad, “Seismic Risk Assessment of Reinforced Concrete Bridges in Flood-Prone Regions”, *Structure and Infrastructure Engineering*, vol. 9, issue 9, pp. 952-968, 2013.
- [40] A.M. Kirby, M. Roca, A. Kitchen, M. Escarameia, O.J. Chesterto, *Manual on scour at bridges and other hydraulic structures*. 2nd edition, CIRIA742, London, 2015.

- [41] A. Pizarro, S. Manfreda, E. Tubaldi, “The Science behind Scour at Bridge Foundations: A Review”, *Water*, vol. 12, issue 2, pp. 374, 2020.
- [42] Z. Wang, L. Dueñas-Osorio, J.E. Padgett, “Influence of scour effects on the seismic response of reinforced concrete bridges”, *Engineering Structures*, vol. 76, pp. 212-214, 2014.
- [43] G.G. Prasad, S. Banerjee, “The Impact of Flood-Induced Scour on Seismic Fragility Characteristics of Bridges”, *Journal of Earthquake Engineering*, vol. 17, issue 6, pp. 803-828, 2013.
- [44] T. Yilmaz, S. Banerjee, P.A. Johnson, “Performance of Two Real-Life California Bridges under Regional Natural Hazards”, *Journal of Bridge Engineering*, vol. 121, issue 3, 04015063, 2015.
- [45] X. Guo, Y. Wu, Y. Guo, “Time-dependent seismic fragility analysis of bridge systems under scour hazard and earthquake loads”, *Engineering Structures*, vol. 121, pp. 52-60, 2016.
- [46] S.T. Song, C.Y. Wang, W.H. Huang, “Earthquake damage potential and critical scour depth of bridges exposed to flood and seismic hazards under lateral seismic loads”, *Earthquake Engineering and Engineering Vibration*, vol. 14, issue 4, pp. 579-594, 2015.
- [47] A. Fioklou, A. Alipour, “Significance of non-uniform scour on the seismic performance of bridges”, *Structure and Infrastructure Engineering*, vol. 15, issue 6, pp. 822-836, 2019.
- [48] Q. Han, J. Wen, X. Du, C. Huang, “Seismic Response of Single Pylon Cable-Stayed Bridge under Scour Effect”, *Journal of Bridge Engineering*, vol. 24, issue 6, 05019007, 2019.
- [49] A. Zaky, O. Özcan, Ö. Avşar, “Seismic failure analysis of concrete bridges exposed to scour”, *Engineering Failure Analysis*, vol. 115, 104617, 2020.
- [50] S. Foti, M. Aimar, A. Ciancimino, L. Giordano, “Influence of scour of foundations on the seismic performance of bridges”, In *SECED 2023 Conference*, Cambridge, United Kingdom, 2023.
- [51] K.C. Chang, Y.C. Sung, K.Y. Liu, P.H. Wang, Z.K. Lee, L.S. Lee, Witarto, “Seismic performance of an existing bridge with scoured caisson foundation”, *Earthquake Engineering and Engineering Vibration*, vol. 13, pp. 151-165, 2014.
- [52] A. Ciancimino, L. Jones, L. Sakellariadis, I. Anastasopoulos, S. Foti, “Experimental assessment of the performance of a bridge pier subjected to flood-induced foundation scour”, *Géotechnique*, vol. 72, issue 11, pp. 998-1015, 2022.
- [53] X. Wang, A. Alipour, J. Wang, Y. Shang, A. Ye, “Seismic resonance behavior of soil-pile-structure systems with scour effects: Shake-table tests and numerical analyses”, *Ocean Engineering*, vol. 289, 115052, 2023.
- [54] Y. Dong, D.M. Frangopol, D. Saydam, “Sustainability of bridge networks under flood-induced scour and earthquake”, In *11th International Conference on Structural Safety and Reliability, ICOSSAR 2013*, New York, USA, 2013, pp. 3575-3580.
- [55] X. Guo, “Seismic Vulnerability Analysis of Scoured Bridge Systems”, PhD dissertation, University of Missouri-Kansas City, Kansas City, Missouri, 2014.
- [56] A. Malekjafarian, C.W. Kim, E.J. O'Brien, L.J. Prendergast, P.C. Fitzgerald, S. Nakajima, “Experimental demonstration of a mode shape-based scour-monitoring method for multispan bridges with shallow foundations”, *Journal of Bridge Engineering*, vol. 25, issue 8, 04020050, 2020.
- [57] K.D. Kariyawasam, C.R. Middleton, G. Madabhushi, S.K. Haigh, J.P. Talbot, “Assessment of bridge natural frequency as an indicator of scour using centrifuge modelling”, *Journal of Civil Structural Health Monitoring*, vol. 10, pp. 861-881, 2020.
- [58] L.J. Prendergast L.J. “Monitoring of scour around structures using changes on natural frequency of vibration”, Ph.D. dissertation, School of Civil, Structural & Environmental Engineering, University College Dublin, Dublin, Ireland, 2015.

4 Dynamic behaviour of soil-foundation-structure systems subjected to scour

A great number of bridges in earthquake-prone countries cross rivers and have shallow foundations, which renders them highly vulnerable to the combined effects of earthquake and flood-induced scour. Thus, the research on the dynamic response of bridges with shallow foundations under scour and earthquake hazards is timely and imperative. This study investigates the problem through the development of a numerical model for evaluating the effect of scour on the impedance functions of a massless rigid strip foundation resting on a homogenous elastic half-space. The developed impedance functions are then used in an extensive parametric study analysing the changes of the fundamental frequency of bridge piers for different combinations of the geometrical and mechanical properties of the soil-structure-foundation system. The study results shed light on the effects of scour on the dynamic properties and fundamental frequency of vibration of bridges with shallow foundations and have important implications on the development of inverse techniques for scour identification based on the evaluation of the changes in the bridge modal properties.

Section 4.1 presents the numerical modelling strategy to estimate the foundation impedance functions under various scour scenarios, including its verification against analytical solutions and the derived impedance functions. Section 4.2 illustrates the investigated SFS system and presents the influence of considered scour conditions on the natural frequency of a case study. Section 4.3 presents the results of an extensive parametric study investigating the effects of scour on the fundamental vibration frequency on the examined SFS system, for a wide range of mechanical and geometric properties and soil conditions, revealing key trends and sensitivities. The findings of the parametric study are subsequently applied to a real-world scenario to quantify the effects of scour on the dynamic behaviour of bridges. Section 4.4 summarises the main findings of the study and future work needed. Appendix A supplements the results of this study by comparing the results of the impedance functions with and without coupling effects, while Appendix B presents the expanded mathematical formulation of the eigenvalue problem. The content of this chapter is based on peer-reviewed journal and conference publications, with minor modifications. The research was conducted in collaboration with Sandro Carbonari, Enrico Tubaldi, Fabrizio Gara, and Francesca Dezi (Table 1-1).

4.1 Numerical evaluation of impedance functions

This section describes in detail the modelling strategy developed in Abaqus for the calculation of impedance functions of shallow foundations subjected to scour. The case of a massless rigid strip foundation rigidly resting on a homogeneous elastic soil domain is considered, and a plane-strain problem assumption is made. Masonry bridges' piers are usually walls with aspect ratios that can allow this assumption. The modelling strategy is firstly validated by comparing the obtained impedance functions with those developed by Hryniewicz [1]. Subsequently, impedance functions are derived for various scour scenarios.

4.1.1 Modelling strategy

This subsection describes in detail the model developed in Abaqus for the derivation of the impedance functions. These can be expressed in non-dimensional form as a function of the non-dimensional frequency $a_0 = \omega b_f / V_s$, where ω is the circular frequency of the excitation, V_s is the soil shear wave velocity, and b_f is the half width of the foundation.

The developed model considers a finite domain, with infinite elements placed at the boundaries to satisfy the radiation condition preventing wave reflections. In particular, the foundation width and the

dimensions of the soil domain are assumed equal to $2b_f = 1$ m and 125×62.5 m, respectively. Four node plane-strain elements (CPE4) and plane strain solid continuum infinite elements (CINPE4) are used for the simulation of the model in the finite element code Abaqus (Figure 4-1i). The soil is assumed to behave linearly. It is noteworthy that the assumption of linear (or linear equivalent) behaviour for the soil is a necessary condition for employing the substructure approach for computing the natural frequency of SFS systems, as described in Section 4.2.1. The Young modulus and Poisson's ratio of the soil are assumed respectively equal to $E = 162.41$ MPa and $\nu = 0.25$, and the density is $\rho = 1600$ kg/m³. It is noted that for a given Poisson's ratio, the values of E , ρ and foundation geometry do not affect the results that are presented in nondimensional form. In other words, the nondimensional results verified by Hryniewicz's [1] analytical solutions are valid for $\nu = 0.25$.

The model mesh is developed based on the recommendations of [2][3] in order to accurately capture the propagation of waves in the model through a suitable number of nodes. In detail, the maximum element size l_{max} of the soil domain is chosen to satisfy the following equation:

$$l_{max} \leq \frac{\lambda_{min}}{10} \leq \frac{V_{s,min}}{10f_{max}} \quad (4.1)$$

where λ_{min} is the shear wavelength and f_{max} is the maximum frequency of interest, which, for seismic applications, is typically within the range 0–15 Hz. For a given element size, the maximum dimensionless excitation frequency a_0 satisfies:

$$a_0 \leq \frac{2\pi b_f}{10l_{max}} \quad (4.2)$$

It is noteworthy that this boundary condition of Eq. (4.1) is completely effective at absorbing body waves approaching the boundary at normal incidence, while it does not work perfectly for oblique angles [4]. Nevertheless, its use provides generally satisfactory results for earthquake engineering purposes, particularly if a relatively large margin is adopted between the boundary and the foundation, as done in the numerical study. To reduce numerical noise in the fluctuation of impedance functions, 1% hysteric damping is added to the soil elements. Around the left part of the foundation, a square mesh 0.005×0.005 (m) is used, while around the right side of the foundation the used mesh is 0.025×0.025 (m) for reducing the computational cost and facilitating the scour hole simulation at the next stages. In the rest of the soil domain, the mesh is developed with a bias towards to the boundaries from 0.005 to 0.3 m and 0.025–0.3 m, respectively. The infinite elements are long strips with length 62.5 m, which is equal to the half length of the physical domain. It is noteworthy that the massless rigid strip foundation in the model (see Section 4.1.4) is modelled through a rigid-body constraint applied to the set of nodes on the top of the soil domain for a length equal to the width of the foundation. Impedances of the soil-foundation system are defined as forces necessary to produce unit amplitude harmonic displacements of the foundation and can be obtained by means of steady-state analyses; the master node, where the displacements are applied and the corresponding reaction forces are monitored, is the one at the centre of this length (Figure 4-1ii).

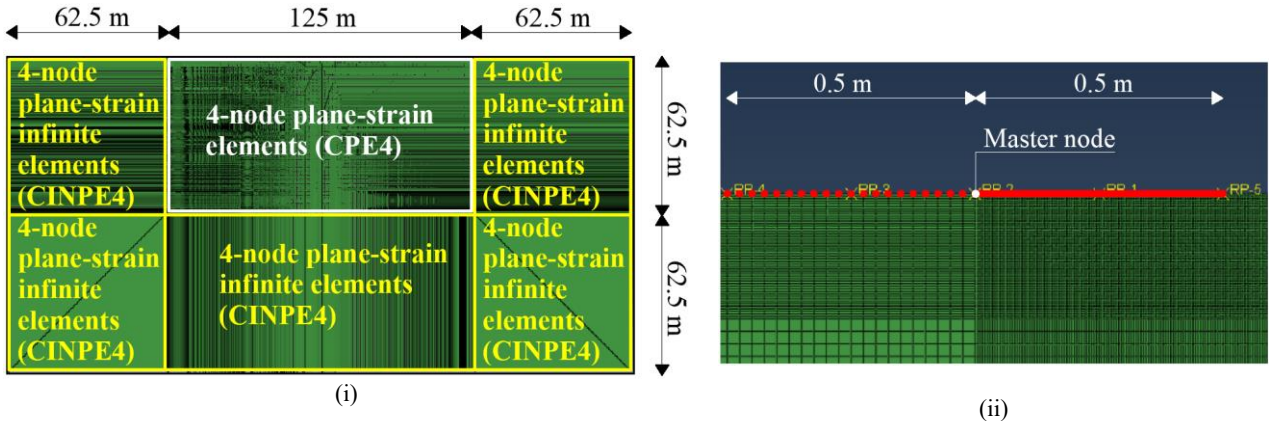


Figure 4-1: FE model developed in Abaqus of the soil domain with infinite elements at boundaries, (ii) Rigid-body constraint used to simulate the massless rigid strip foundation.

4.1.2 Numerical approach

The frequency-dependent impedance functions are numerically evaluated through steady-state analyses by subjecting the master node to harmonic unit amplitude displacements and by measuring the corresponding harmonic reaction forces. In the frequency domain, by suitably condensing the problem on the master node degrees of freedom, the following system of equations governs the dynamics of the strip foundation:

$$\begin{bmatrix} P(\omega) \\ Q(\omega) \\ M(\omega)/b_f \end{bmatrix} = \begin{bmatrix} k_{zz} + id_{zz} & 0 & 0 \\ 0 & k_{xx} + id_{xx} & k_{xr_y} + id_{xr_y} \\ 0 & k_{xr_y} + id_{xr_y} & k_{r_y r_y} + id_{r_y r_y} \end{bmatrix} \begin{bmatrix} w_0(\omega) \\ u_0(\omega) \\ \phi_0(\omega)b_f \end{bmatrix} \quad (4.3)$$

where w_0 , u_0 are the displacement amplitudes along the z and x directions, respectively, ϕ_0 is the rotation amplitude and k_{ij} , $d_{ij} = c_{ij}\omega$ are frequency-dependent quantities describing the real and the imaginary parts of the impedance functions, respectively, for the foundation response in the i -th direction due to the excitation in the j -th direction. Figure 4-2 illustrates forces and displacements along the various directions.

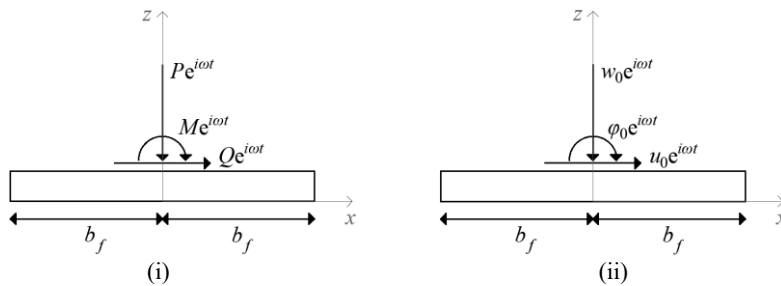


Figure 4-2: (i) Forces and (ii) displacements of the strip foundation.

The coefficients k_{ij} and d_{ij} evaluated numerically are presented as a function of the dimensionless frequency a_0 and compared with the analytical estimates obtained by Hryniewicz [1]. This procedure will be also repeated for three scour layouts, characterized by different geometries (see Section 4.2). For completeness, also the damping factors are evaluated to gain insight into the radiation damping. The damping factor ξ_{ij} is evaluated as:

$$\xi_{ij} = \frac{d_{ij}}{2k_{ij}} \quad (4.4)$$

4.1.3 Verification of numerical model

The numerical strategy described in the previous subsection is verified here by comparing the obtained impedance functions with those derived analytically by Hryniewicz [1]. The analytical impedance functions were obtained assuming zero off-diagonal terms, i.e., uncoupled horizontal and rotational response. Thus, to make the numerical model more compliant with the analytical one, the rotation at the foundation master node is not restrained when the horizontal displacement is imposed and vice-versa, the horizontal displacement is allowed when the rotation is imposed. The harmonic analyses are carried out for frequencies in the range between 3.2 Hz and 200 Hz, corresponding to values of the dimensionless frequency a_0 between 0.05 and 3.11. It is worth noting that the upper frequency bound is largely beyond that of interest in engineering applications and is chosen to demonstrate the overall reliability of the adopted numerical approach. Figure 4-3 compares the frequency-dependent coefficients k_{ij} and d_{ij} obtained from the numerical model with the Hryniewicz's analytical solution. The agreement between the curves is very good, except for the rotational behaviour (k_{rpy}). This may be due to differences in soil-foundation interface assumptions between the two models. Specifically, Hryniewicz [1] assumed a smooth soil-foundation contact, allowing for sliding, while the numerical model implicitly enforces a bonded contact through the applied rigid-body constraint to a set of nodes (Figure 4-1ii). This affects the transfer of tangential stresses and may explain the slightly higher values of k_{rpy} in the numerical results. Additionally, approximations introduced by Hryniewicz [1] for deriving the problem solution may also contribute to the observed differences. It is noteworthy that the maximum element size of the finite element soil domain is $l_{max} = 0.3$ m, and thus, according to Eq. (4.2), the maximum dimensionless frequency that could be accurately investigated with the adopted mesh is equal to $a_{0,max} = 1.05$. However, the use of a bias mesh, with elements with size significantly smaller than l_{max} around the foundation results in a satisfactory agreement with the theoretical solution for values of a_0 up to 3.11. For the sake of completeness, Figure 4-3 also shows the values of k_{ij} and d_{ij} derived by taking the coupling phenomenon into account, i.e., by restraining the rotations when the horizontal displacements are imposed, and by restraining the horizontal displacements when rotations are imposed. It can be observed that the coupling between the horizontal and the rotational behavior is not relevant and slightly affect the estimation of impedances, as assumed by Hryniewicz [1]. The effect of the coupling is investigated further in the next sections. The acronyms "NS", "NC" and "IC" denote the case of "No Scour", "Neglecting Coupling" and "Including Coupling", respectively.

4.1.4 Influence of scour on the dynamic impedance functions

Various models are considered for investigating the effect of scour on the dynamic impedance of the foundations, corresponding to different widths and depths of the scour hole shape beneath the right side of the foundation. In particular, in addition to the model with no scour (denoted as "NS"), the case of a scour hole with a "triangular" shape is investigated, for a width beneath the foundation equal to 1/4 of the width of the foundation (denoted as "TS1/4"), 3/8 the width (denoted as "TS3/8"), and 1/2 the width (denoted as "TS1/2"). Moreover, the upstream scour slope is assumed equal to $\phi = 30^\circ$, whereas the downstream scour slope is half of the upstream slope [5]. Figure 4-4 illustrates the geometry and dimensions of the scour holes for this case study. It must be mentioned that since the soil domain is discretized using quadrilateral elements, only an approximation of the scour hole of Figure 4-4 is obtained. However, having used a very refined mesh, the error stemming from this approximation is expected to be negligible.

Figure 4-5 illustrates the impedance functions obtained for the aforementioned models by taking into account the coupling between horizontal and rotational response. Moreover, the ratios $k_{ij}^{scour} / k_{ij}^{no\ scour}$, $d_{ij}^{scour} / d_{ij}^{no\ scour}$, $\xi_{scour} / \xi_{no\ scour}$ for each of the scoured cases are calculated to address the effect of scour on the impedance coefficients (Figure 4-6 and Figure 4-8).

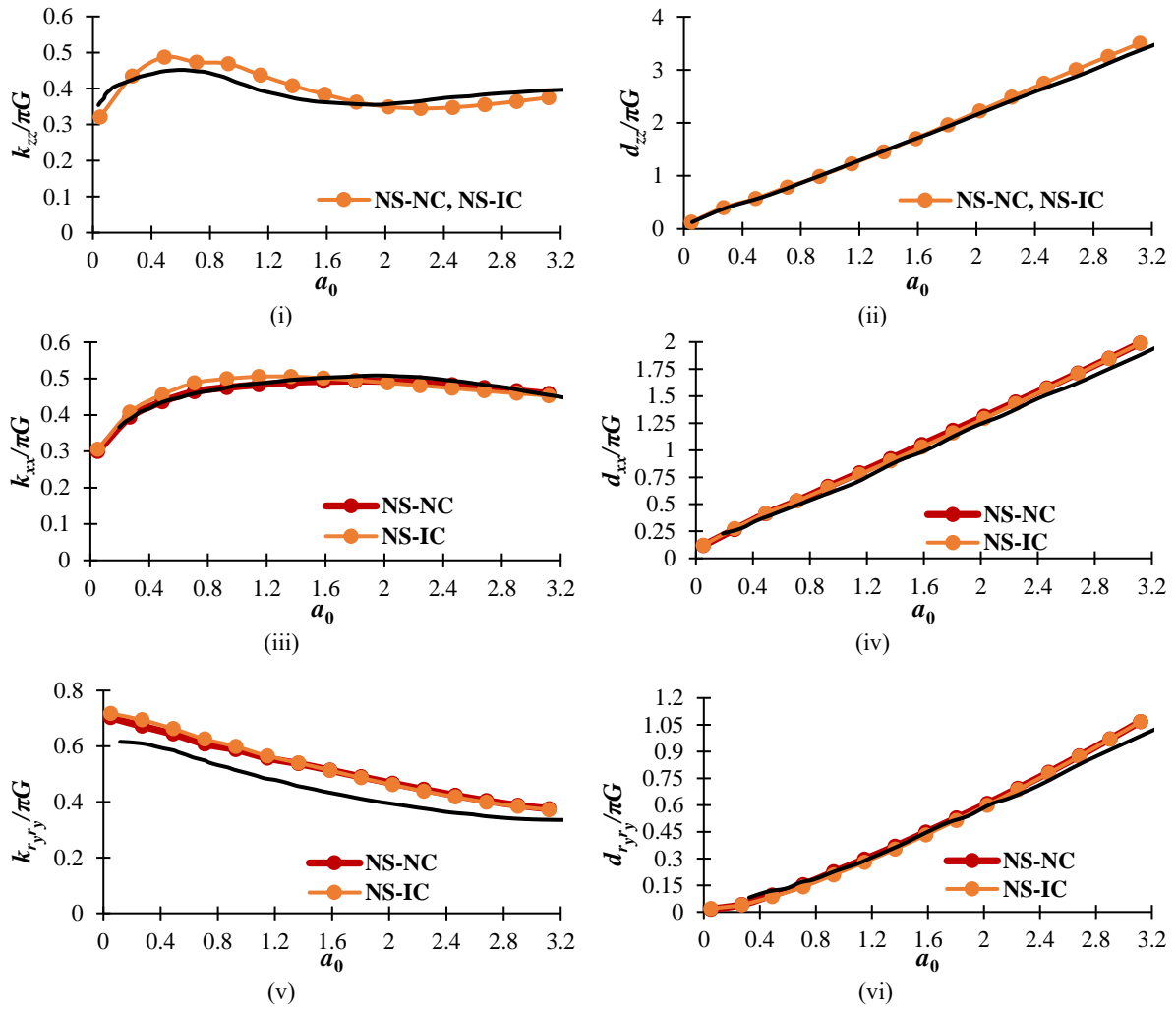


Figure 4-3: Comparisons of impedance functions between those obtained from Abaqus with the analytical solution developed by Hryniewicz [1] (i) k_{zz} , (ii) d_{zz} , (iii) k_{xx} , (iv) d_{xx} , (v) $k_{r,\gamma y}$, (vi) $d_{r,\gamma y}$.

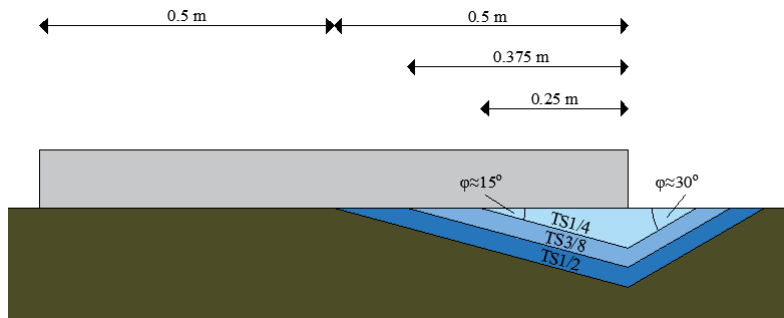


Figure 4-4: Geometry of the 3 different scour hole scenarios investigated.

In general, it can be observed that scour affects differently the various impedances, and that the effects of scour are different at the various frequencies. Increasing the scour width and depth results in a reduction of both the in-phase and out-of-phase components at low frequencies, while a different trend is observed at higher frequencies. For high values of a_0 , the effects of scour are different for the various components, particularly for the real part of the impedance function along the horizontal direction (k_{xx}). In the case of the vertical real component (k_{zz}), the value of a_0 beyond which increasing the scour hole does not result in a decrease of impedance is about 0.5, while for the other components it is generally higher (above 2). Scour also affects significantly the damping factors. In detail, the larger the scour hole, the higher the reduction of the damping factors related to the vertical, horizontal and rocking

components. An opposite trend is observed for the damping factor related to the coupling component (Figure 4-7).

A separate frequency-response analysis is carried out for each model by neglecting the coupling and the ratios of k_{ii} and d_{ii} obtained including and disregarding the coupling are displayed and compared to each other in Appendix A (Figure A.1) for completeness. These ratios are generally higher than or close to 1 for most of the investigated frequency range.

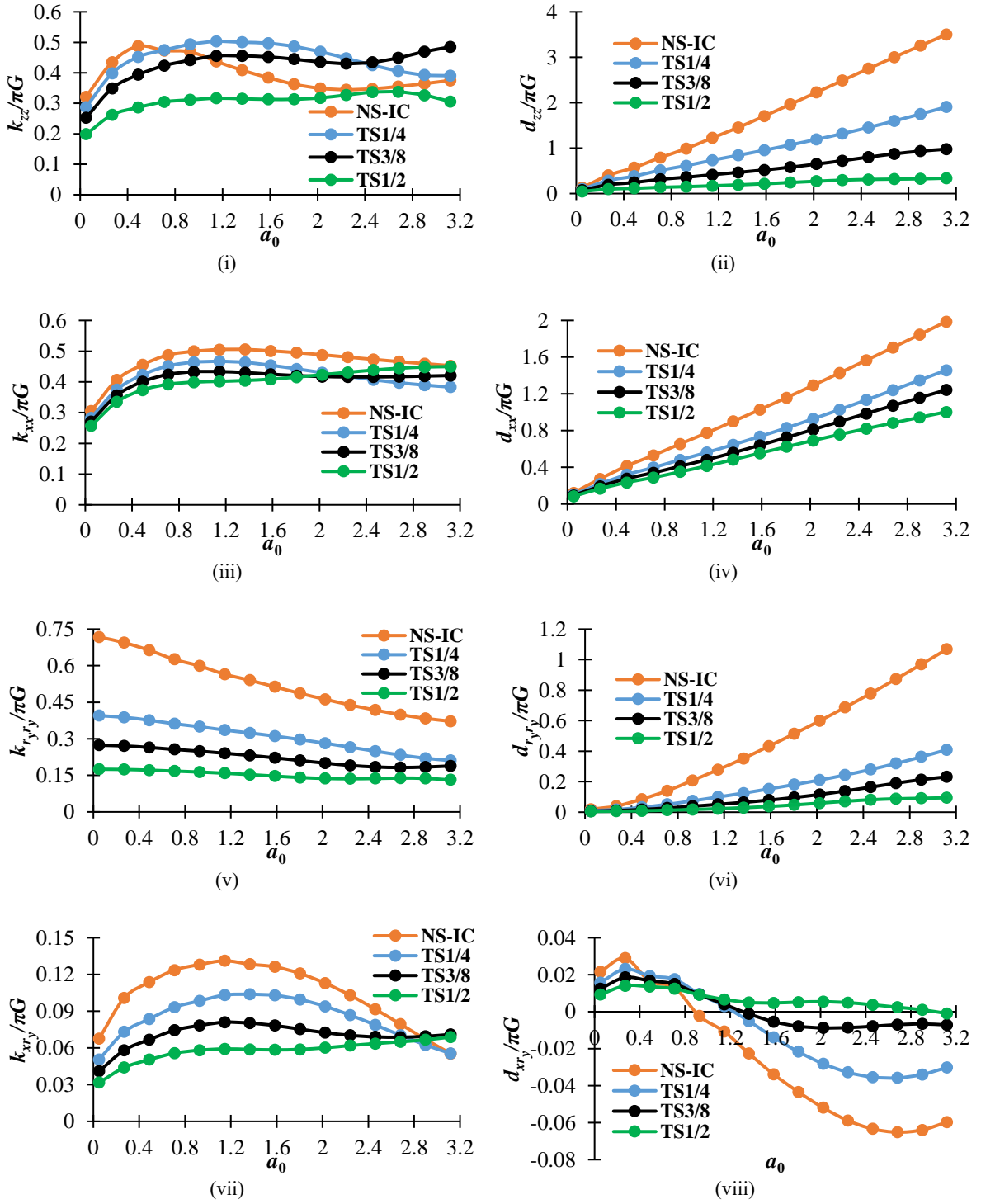


Figure 4-5: Comparisons of the calculated impedance functions for different scour scenarios (i) k_{zz} , (ii) d_{zz} , (iii) k_{xx} , (iv) d_{xx} , (v) $k_{r,y/y}$, (vi) $d_{r,y/y}$, (vii) $k_{x,r,y/y}$, (viii) $d_{x,r,y/y}$.

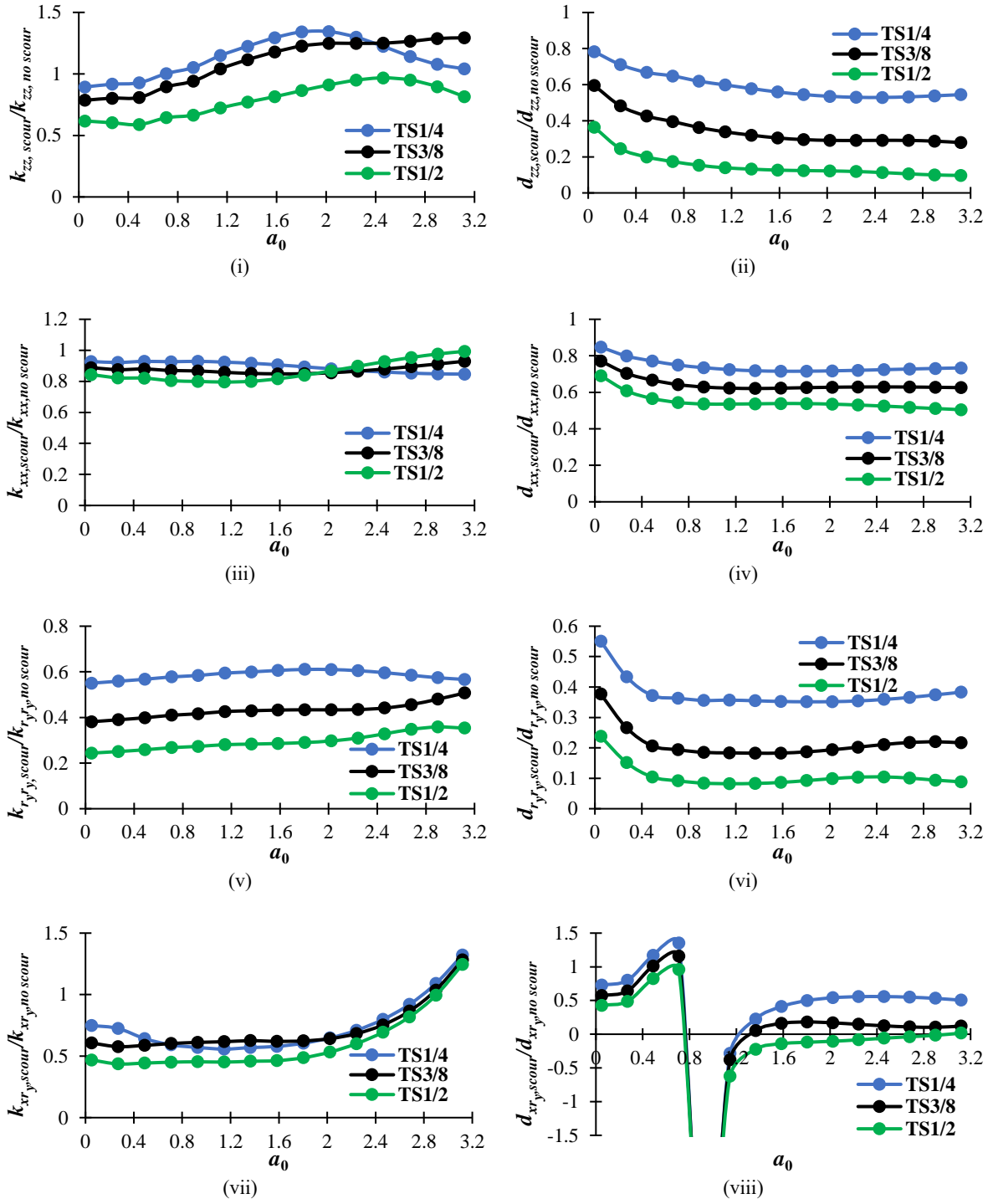


Figure 4-6: Ratios $k_{ij}^{scour} / k_{ij}^{no scour}$, $d_{ij}^{scour} / d_{ij}^{no scour}$ for different scour scenarios.

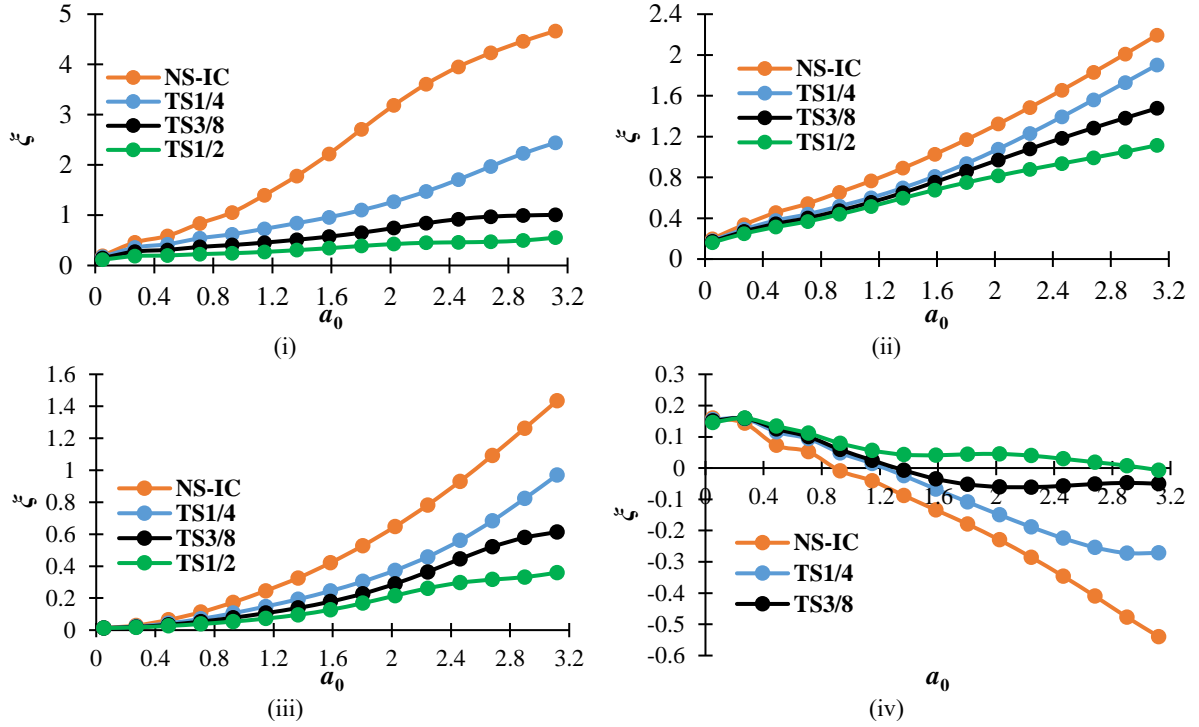


Figure 4-7: Comparisons of the damping factors for different scour scenarios related to (i) k_{zz} and d_{zz} , (ii) k_{xx} and d_{xx} , (iii) k_{ryry} and d_{ryry} , (iv) k_{xry} and d_{xry} .

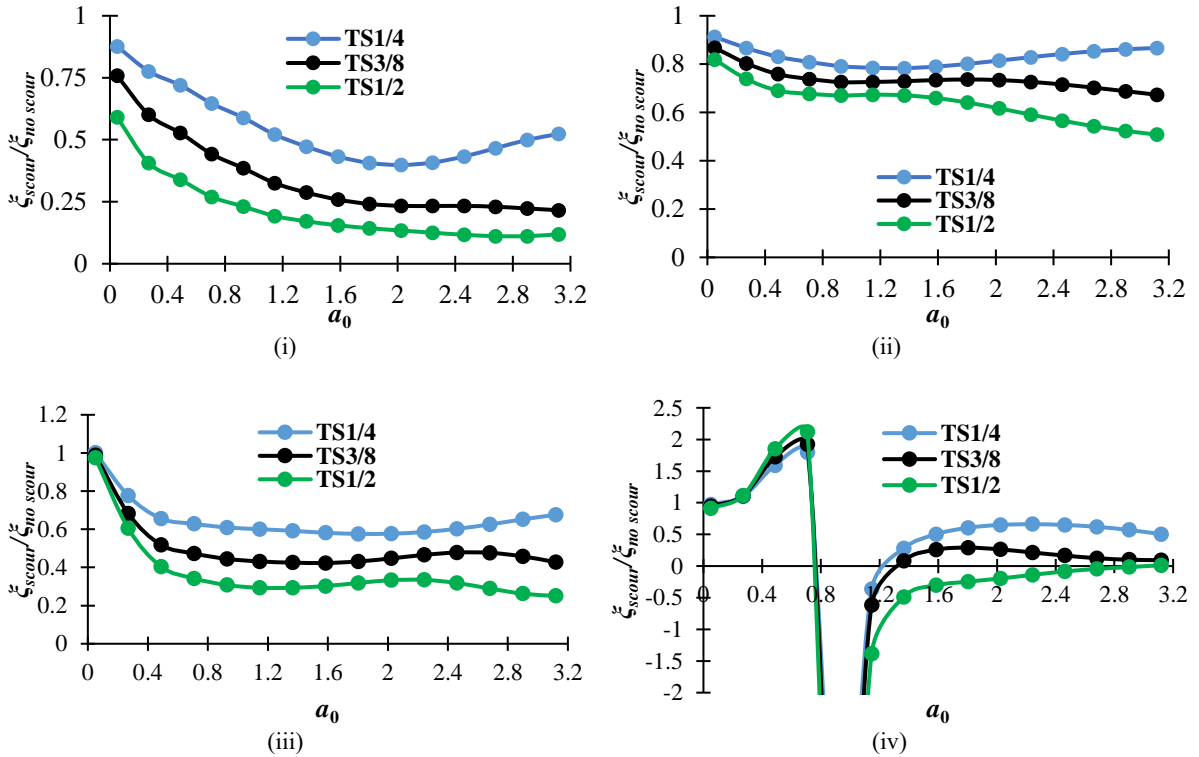


Figure 4-8: Ratio $\zeta_{scour}/\zeta_{no\ scour}$ for different scour scenarios related to direction (i) k_{zz} and d_{zz} , (ii) k_{xx} and d_{xx} , (iii) k_{ryry} and d_{ryry} , (iv) k_{xry} and d_{xry} .

4.2 Influence of scour on dynamic behaviour of SFS system

In this section, the impedance functions of scoured shallow foundations developed in Section 4.1 are used to evaluate the effect of scour on the natural frequency of SFS systems. Firstly, the dynamic problem formulation is presented and then the solution of the eigenvalue problem for a case study is

shown. The problem is thus made nondimensional with the aim of reducing the number of parameters to be considered in the subsequent parametric investigation (see Section 4.3).

4.2.1 Problem formulation for SFS system with scoured foundations

Figure 4-9 illustrates the SFS system considered in this study. The model consists of a superstructure with lumped mass m_s , height h_s and lateral stiffness k_s , based on a foundation of mass m_f , height $2h_f$, width $2b_f$ and mass moment of inertia I_f . The foundation is resting on a soil medium characterized by shear modulus G , mass density ρ and Poisson's ratio ν . The compliance of the soil-foundation system is described by means of the previously derived impedance functions.

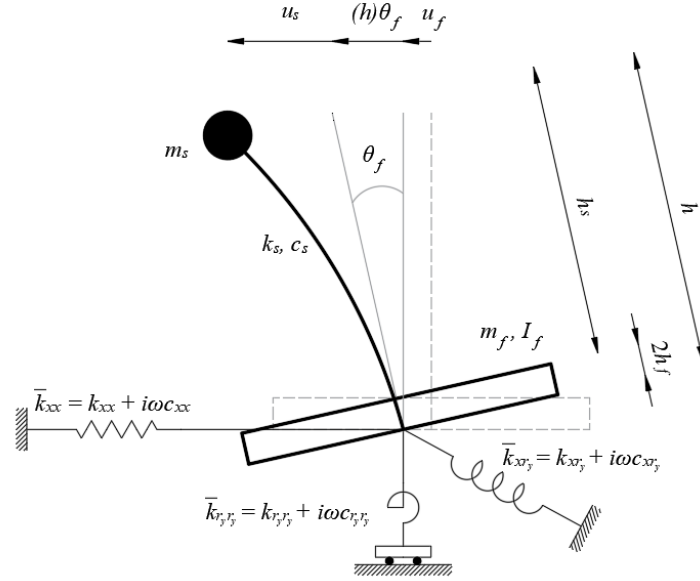


Figure 4-9: Model of the SFS system.

By assuming a linear behaviour for the superstructure, the free vibration equation of motion of the SFS system can be expressed in the frequency domain in a vector form as:

$$-\omega^2 \mathbf{M} \bar{\mathbf{U}} + i\omega \mathbf{C}(\omega) \bar{\mathbf{U}} + \mathbf{K}(\omega) \bar{\mathbf{U}} = 0 \quad (4.5)$$

where $\bar{\mathbf{U}}$ denotes the Fourier transform of the vector \mathbf{U} collecting the three degrees of freedom of the system, namely the foundation translation (u_f) and rotation (θ_f), and the relative displacement (u_s) of mass m_s with respect to the base. Furthermore, \mathbf{M} , \mathbf{C} and \mathbf{K} are the mass, damping and stiffness matrices of the system. These quantities are expressed as follows [6]:

$$\mathbf{U} = \begin{bmatrix} u_f & \theta_f & u_s \end{bmatrix}^T \quad (4.6)$$

$$\mathbf{M} = \begin{bmatrix} m_f + m_s & m_f h_f + m_s h & m_s \\ m_f h_f + m_s h & I_f + m_f h_f^2 + m_s h^2 & m_s h \\ m_s & m_s h & m_s \end{bmatrix} \quad (4.7)$$

$$\mathbf{C}(\omega) = \begin{bmatrix} c_{xx}(\omega) & b_f c_{xy}(\omega) & 0 \\ b_f c_{xy}(\omega) & b_f^2 c_{yy}(\omega) & 0 \\ 0 & 0 & c_s \end{bmatrix} \quad (4.8)$$

$$\mathbf{K}(\omega) = \begin{bmatrix} k_{xx}(\omega) & b_f k_{xy}(\omega) & 0 \\ b_f k_{xy}(\omega) & b_f^2 k_{yy}(\omega) & 0 \\ 0 & 0 & k_s \end{bmatrix} \quad (4.9)$$

The system resonance frequency is estimated by solving the eigenvalue problem of Eq. (4.5), which can be rewritten as (see Appendix B):

$$(\alpha + \beta + \gamma)\bar{u}_s = 0 \quad (4.10)$$

where α , β , γ are functions depending on ω , h , h_f , m_s , m_f , I_f , k_s , b_f , $\bar{k}_{xx}(\omega)$, $\bar{k}_{xy}(\omega)$, $\bar{k}_{yy}(\omega)$, and \bar{k} contains both the real and imaginary part of the impedances ($\bar{k}_{ij} = k_{ij} + i\omega c_{ij}$).

It is noteworthy that the impedance functions \bar{k}_{xx} , \bar{k}_{xy} , \bar{k}_{yy} are functions of the frequency of excitation and depend on G , V_s and b_f . Different approaches can be employed for solving the eigenvalue problem corresponding to Eq. (4.10) and evaluating the system resonance frequency $\tilde{\omega}$ (see e.g. [7][8]). The problem solution is herein illustrated considering a specific case study consistent with the EuroProteas' prototype [9] and characterized by the following values of the parameters: $h_s = 4.2$ m, $m_s = 6.11$ t/m, $k_s = 20672.16$ kN/m² and 5% structural damping for the superstructure. The strip foundation is described by a width $2b_f = 3$ m, thickness $2h_f = 0.4$ m, mass $m_f = 3.05$ t/m and moment of inertia $I_f = 2.33$ ton·m²/m. The soil beneath the foundation is described by a shear modulus $G = 31.47$ MPa and shear wave velocity $V_s = 130$ m/s.

Eq. (4.10) is solved repeatedly, considering each time the values of \bar{k}_{xx} , \bar{k}_{xy} , \bar{k}_{yy} that correspond to an excitation frequency ω . Each solution provides a value of the natural frequency $\tilde{\omega}$, and the correct one is that for which $\omega = \tilde{\omega}$. Figure 4-10 plots the fundamental vibration frequency of the above described SFS system for different scour scenarios (see Section 4.2), obtained by neglecting the coupling between the horizontal and rotational response of the foundation (denoted as "NC") and taking it into account (denoted as "IC"). It is observed that the vibration frequency of the system decreases linearly for increasing values of $2s/2b_f$. Accounting for the coupling between the translational and rotational responses results in higher values of the vibration frequency. Table 4-1 shows the exact values of the vibration frequency of the SFS system for each of the scour scenarios.

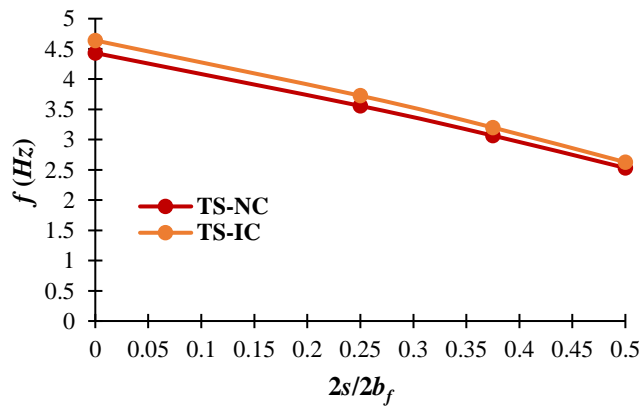


Figure 4-10 : Fundamental vibration frequency of the SFS system for four different scour scenarios.

Table 4-1: Vibration frequency of the SFS system for different levels of scour

Scour scenario	$2s/2b_f$	NC f (Hz)	IC f (Hz)
NS	0	4.43	4.64
TS1/4	0.25	3.56	3.73
TS3/8	0.375	3.07	3.20
TS1/2	0.5	2.53	2.63

4.3 Parametric study

This section describes the extensive parametric study aimed to investigate the effects of scour on the fundamental frequency of vibration of the SFS system. Firstly, a non-dimensional formulation of the problem is derived to reduce the number of parameters to be varied in the parametric study, then, results of the parametric investigation are presented.

4.3.1 Non dimensional formulation

The response of SFS systems has been thoroughly studied in the literature with a non-dimensional approach [10]-[16], but the case considered here, involving a strip foundation and described by Equation (Eq. (4.10)), has not been investigated yet. In most of the studies cited above, Buckingham theorem is applied to formulate an equation of n variables in terms of a set of $n-k$ non-dimensional variables, called Π -parameters, where k is the number of reference dimensions included in the equation.

The natural frequency of a SFS system ($\tilde{\omega}$) resting on a strip foundation can be expressed as a function of parameters describing the superstructure, foundation, and soil properties. Specifically, $\tilde{\omega}$ is dependent on 9 variables with 3 reference dimensions: length [L], time [T] and mass [M]:

$$\tilde{\omega}=f(\omega_0, h, h_f, m, m_f, b_f, \rho, V_s, \nu) \quad (4.11)$$

Table 4-2 describes the involved variables and corresponding units and dimensions.

Table 4-2: Units and dimensions of the involved variables

		Units	Dimensions
ω_0	natural frequency of the fixed base system	rad/s	[T ⁻¹]
h	total height of structure	m	[L]
h_f	half thickness of the foundation	m	[L]
m_s	superstructure mass	ton/m	[ML ⁻¹]
m_f	foundation mass	ton/m	[ML ⁻¹]
b_f	half width of the foundation	m	[L]
S	half width of the scour-foundation interface	m	[L]
P	soil density	ton/m ³	[ML ⁻³]
V_s	shear velocity	m/s	[LT ⁻¹]
ν	Poisson's ratio	-	-

According to Buckingham theorem, the number of the dimensionless Π -terms is equal to $10-3=7$ in the case of a foundation with no scour. In the case of a scoured foundation, another parameter must be introduced to describe the width of the scour (for a prefixed scour shape). Thus, an additional non-dimensional parameter (Π_s) must be considered. By choosing the variables b_f , ρ and V_s as the recurring set, the following Π -terms can be obtained:

$$\Pi_\omega = \frac{\tilde{\omega}}{\omega_0}, \Pi_h = \frac{h}{b_f}, \Pi_m = \frac{m_f}{m_s}, \Pi_{\omega_0} = \frac{\omega_0 b_f}{V_s}, \Pi_{h_f} = \frac{h_f}{b_f}, \Pi_{m_f} = \frac{m_f}{\rho b_f^2}, \Pi_s = \frac{2s}{2b_f}, \nu \quad (4.12)$$

4.3.2 Parametric study analysis and results

This subsection illustrates the results of the parametric study carried out to investigate the influence of the Π -terms of Eq. (4.10) on the fundamental frequency of vibration of SFS systems for various scour scenarios. To simplify the problem, it is assumed that the terms Π_{h_f} and Π_m are fixed with values 0.26 and 0.25 respectively, which are representative of many real conditions. The term Π_{m_f} is considered dependent on the term Π_{h_f} . Specifically, it is assumed that the ratio of the foundation density and soil density $\left(\frac{\rho_f}{\rho}\right)$ is approximately equal to 1.5, hence Π_{m_f} can be reformulated as $\Pi_{m_f} = \frac{m_f \rho_f}{\rho b_f^2 \rho} = 6 \frac{h_f}{b_f}$. The parameter Π_h is assumed to vary in the range 1–4 and Π_{ω_0} in the range 0–3. The Poisson's ratio is assumed equal to 0.25, to ensure consistency with the derived impedance function in Section 4.1.4, which were calculated using this value. Also, a 5% hysteric damping ratio (ζ_s) is added to the structure. The normalized circular frequency Π_ω is calculated for each of the scour scenarios (described by the scour shape and by Π_s) following the same procedure outlined in Section 4.2.1 (Figure 4-11).

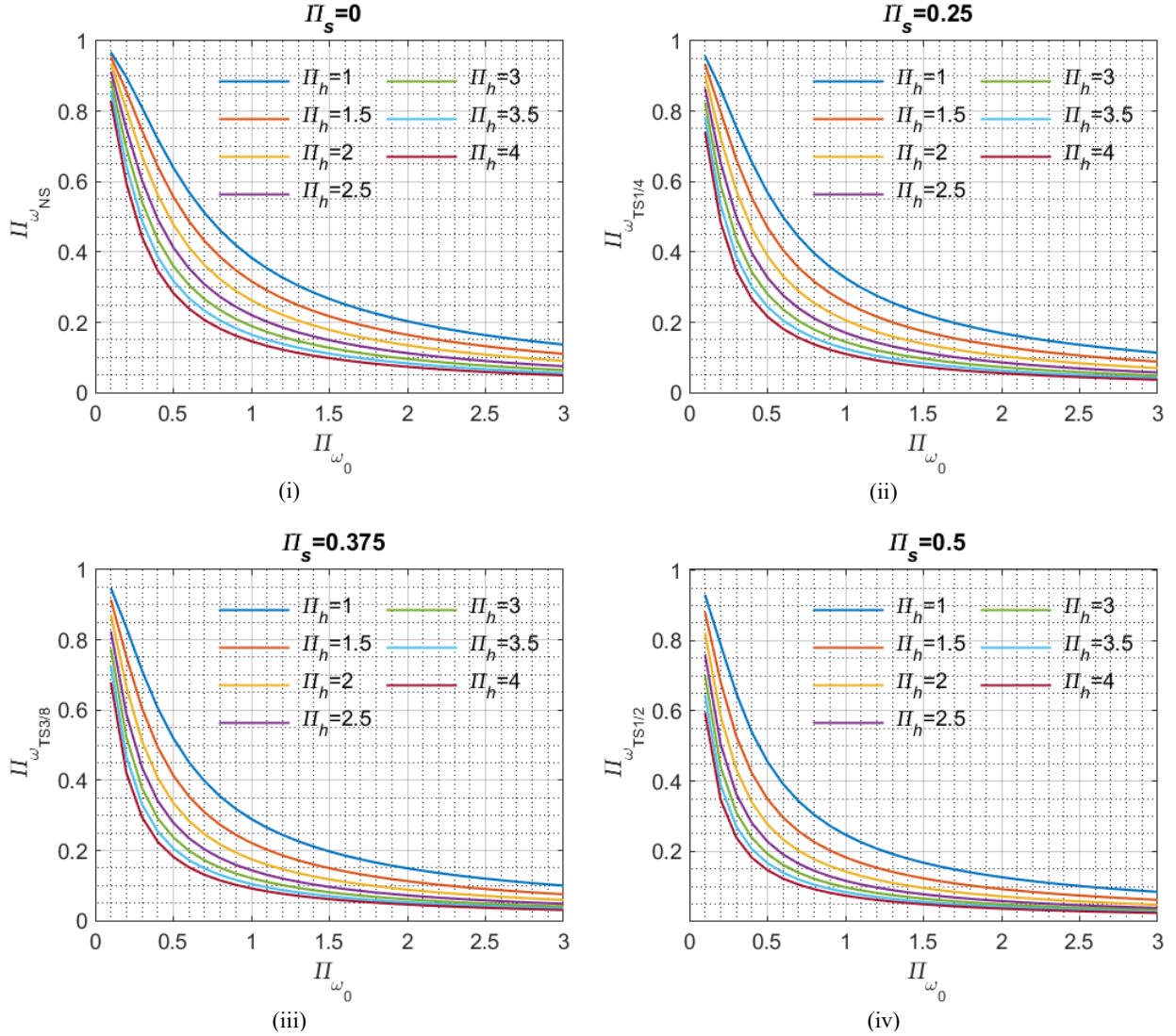


Figure 4-11: Variation of Π_ω with Π_{ω_0} for different values of Π_h and Π_s for the case of (i) NS, (ii) TS1/4, (iii) TS3/8, (iv) TS1/2.

Figure 4-12 illustrates the variation of the ratio of the natural frequencies of the system with and without scour for different levels of Π_h . According to Figure 4-12, both the terms Π_{ω_0} and Π_h significantly influence the dynamic behaviour of the system in presence of scour. In general, the reduction of vibration frequency due to scour is more important for high Π_{ω_0} and Π_h values. Specifically, for a fixed shear wave velocity V_s and width of foundation $2b_f$, the reduction of vibration frequency is higher for high values of h . On the other hand, for fixed values of h and b_f , the decrease of vibration frequency due to scour is more significant for high values of Π_{ω_0} , i.e, for high values of ω_0 or for low values of V_s . In other words, the softer the soil with respect to the structure, the higher the period elongation due to scour. For high values of Π_{ω_0} , the sensitivity of the changes of frequency of the system to Π_{ω_0} tends to decrease. Increasing the scour width Π_s results in more significant reductions of frequency, as expected.

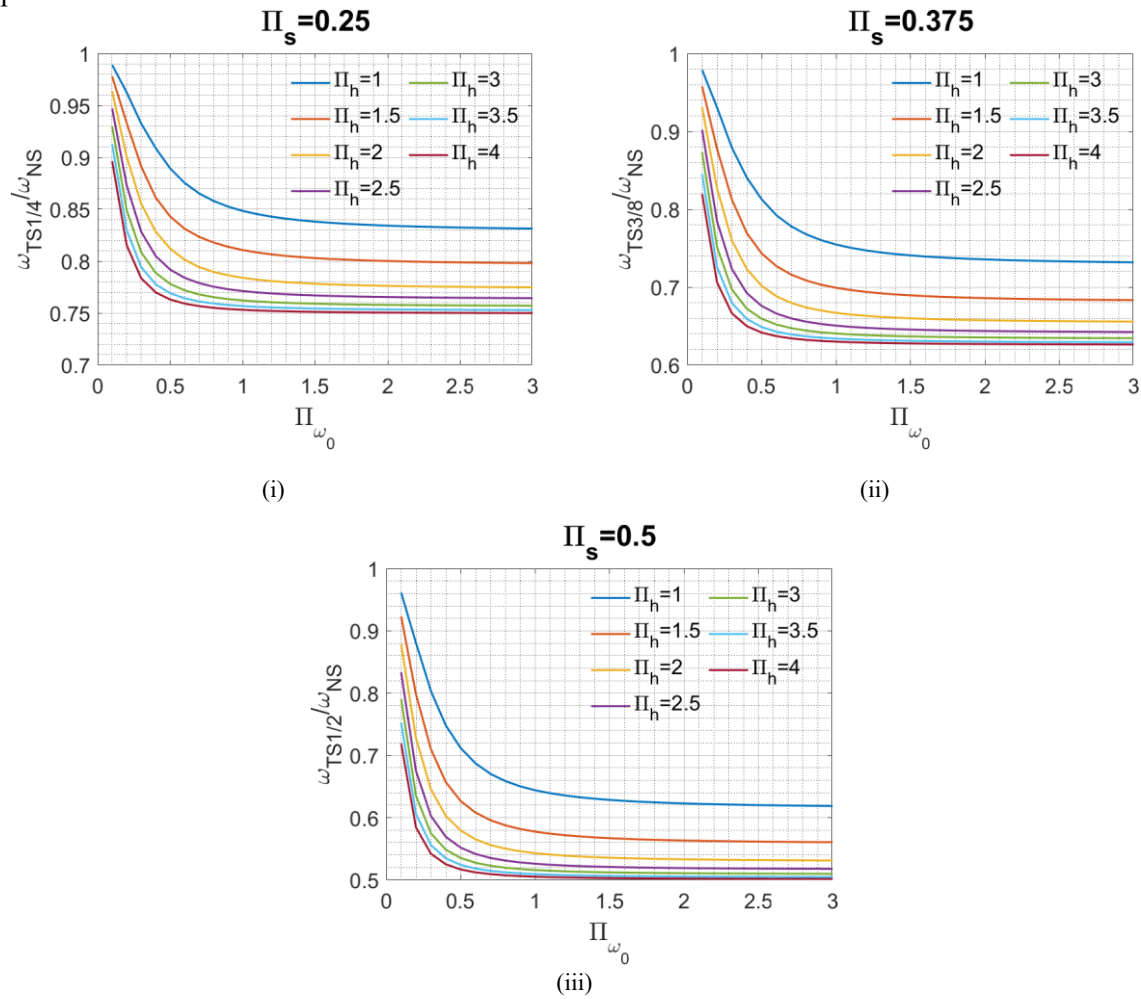


Figure 4-12: Ratio of the natural frequency of the system with and without scour for different levels of Π_h and Π_s for (i) TS1/4, (ii) TS3/8, (iii) TS1/2.

In order to better highlight the influence of Π_s on the effects of scour, Figure 4-13 plots the variation of the ratio of the natural frequency of the system with and without scour for increasing values of Π_s , and for fixed values of Π_{ω_0} and Π_h . For given Π_s and Π_h values, the normalized vibration frequency of the scoured system changes with Π_{ω_0} only for low Π_{ω_0} values. Thus, a self-similar behaviour is observed, with the decrease of the normalized frequency for increasing Π_s values that follows a master curve. In particular, a linear curve can be fitted to the observed trend for high Π_{ω_0} values, with the following expression:

$$\frac{\omega_{TS}}{\omega_{NS}} = 1 - 0.72 \Pi_h^{0.25} \Pi_s \quad (4.13)$$

This curve provides an approximate indication of the decrease of frequency for a given scour hole to foundation width.

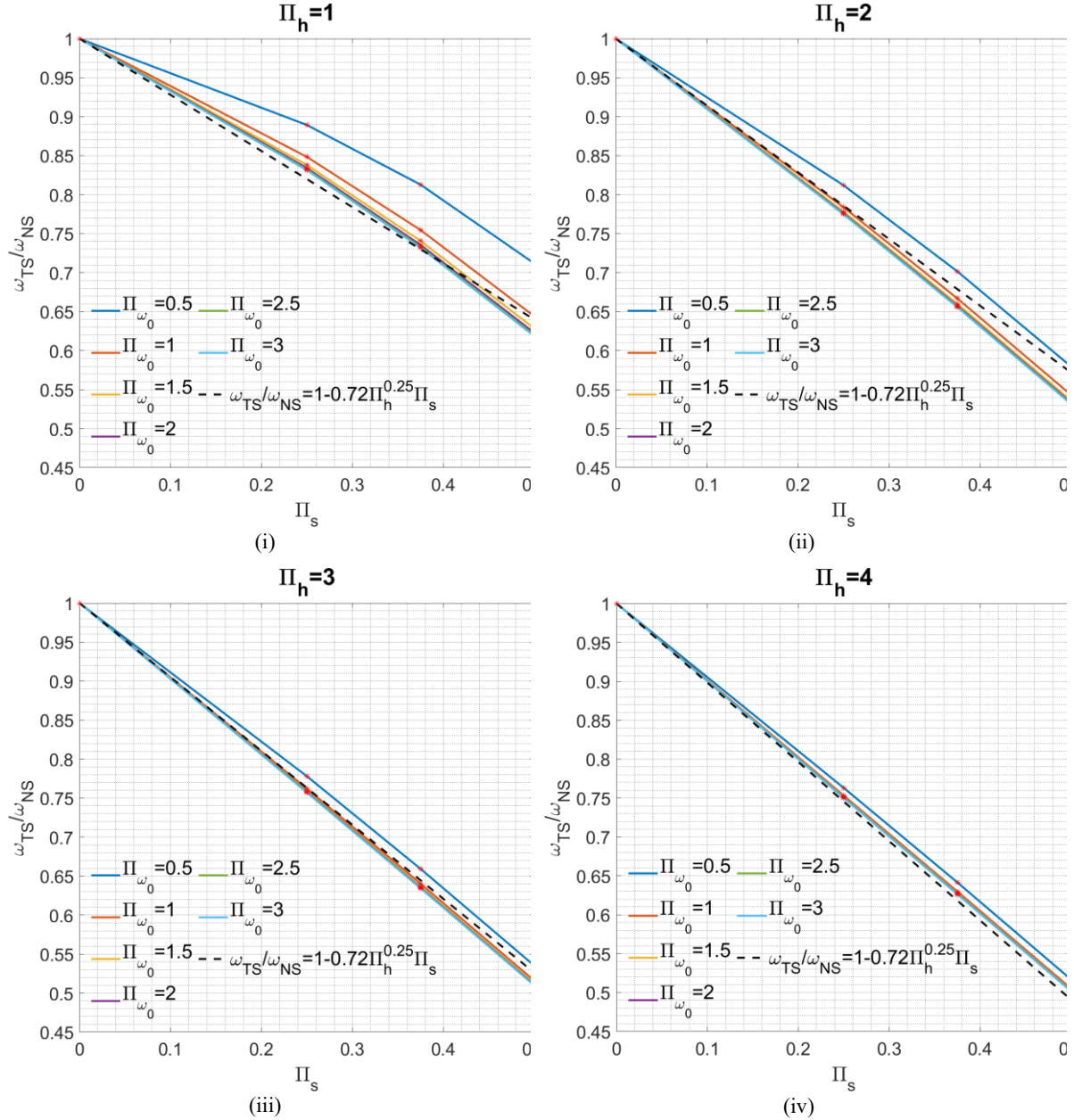


Figure 4-13: Ratio of the natural frequency of the system with and without scour for different levels of Π_{ω_0} and (i) $\Pi_h=1$, (ii) $\Pi_h=2$, (iii) $\Pi_h=3$, (iv) $\Pi_h=4$.

4.3.3 Application example

In this subsection, an application example is considered to illustrate how the results of the parametric study can be used to quantify the effects of scour on the dynamic behaviour of bridges. The application example (Figure 4-14) consists in a bridge pier loosely based on Ciampoli and Pinto [17]. The pier has a rectangular hollow cross section (4 m × 2 m × 0.3 m) and a height of 10 m. The square foundation mat has dimensions $2b_f = 7$ m and $2l_f = 5$ m along the transverse and longitudinal direction respectively, height $2h_f = 1.9$ m, and mass $m_f = 166.45$ t. The mat rests on a homogeneous soil characterized by a

shear modulus $G = 100$ MPa, soil density $\rho = 2000$ kg/m³ and Poisson's ratio $\nu = 0.25$. The span length is 30 m, while the weight per unit length of the deck is assumed equal to 200 kN/m. Thus, the tributary mass at the top of the pier is $m_s = 698$ t, which is about 4 times the foundation mass. The elastic modulus of the pier is $E = 32$ GPa, which corresponds to a concrete type C30/37. The lateral stiffness of the pier along the transverse direction is equal to $k_s = 646681.6$ kN/m, which corresponds to a circular frequency $\omega_0 = 30.43$ rad/s for the fixed base structure. According to the above data, the dimensionless Π -parameters can be calculated through Eq. (4.12) and are the following: $\Pi_h = 2.86$, $\Pi_m = 0.24$, $\Pi_{\omega_0} = 0.48$, $\Pi_{h_f} = 0.27$. As mentioned in Section 4.3.2 the parameter Π_{m_f} is assumed equal to $6 \cdot \Pi_{h_f}$ which corresponds to the value $\Pi_{m_f} = 1.63$. It must be mentioned that the parametric study in Section 4.3.2 was carried out for fixed values of $\Pi_{h_f} = 0.26$ and $\Pi_{h_f} = 0.25$, which are very close to those of the case study, and thus the results shown in Figure 4-11 to Figure 4-13 hold also for this system. Table 4-3 reports the values of Π_s considered in the parametric study and the values of Π_ω according to Figure 4-11, together with the corresponding values of the scour width $2s$, and of the system natural frequency. Figure 4-15 shows the variation of the frequency with the scour width, according to the parametric study results and to the expression of Eq. (4.13). This expression provides a quite good estimate of the effects of scour on the frequency of the system.

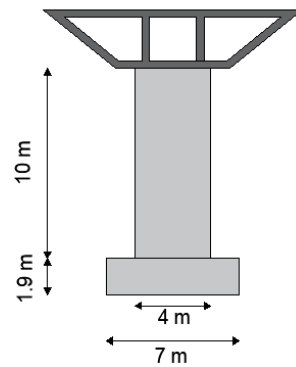


Figure 4-14: Geometry and dimensions of the bridge pier case study.

Table 4-3: Scour width and results of the parametric study.

$2s$	Π_s	Π_ω	f (Hz)
0	0	0.39	1.90
1.75	0.25	0.31	1.49
2.63	0.375	0.26	1.28
3.5	0.5	0.21	1.04

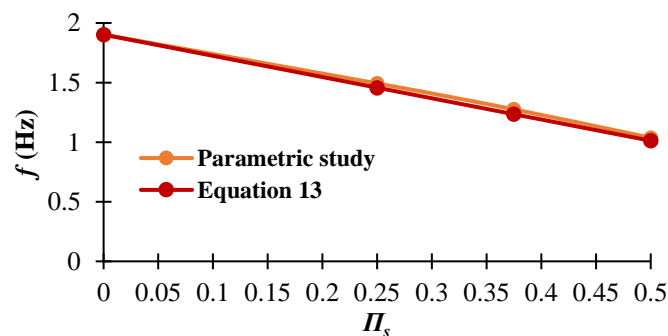


Figure 4-15: Variation of the fundamental vibration frequency of the bridge using the results of the parametric study and the analytical estimate.

4.4 Conclusions

This study analyses the effects of scour on bridges, by considering a soil-foundation-structure (SFS) system consisting of a single degree of freedom structure on a strip foundation rigidly resting on an elastic soil domain. First, a numerical model is developed in Abaqus for the calculation of the impedance functions of a massless strip foundation in the case of no scour. This model is validated by comparing the obtained impedance functions against analytically derived ones. Subsequently, the effect of various scour scenarios, characterized by increasing widths of the scour hole below the foundation, are investigated numerically, and the following conclusions are drawn based on the observed results:

- In general, scour affects differently the various impedances, and the effects are also different for the various frequencies investigated.
- For low frequencies, increasing the scour width (and thus depth) generally results in a reduction of both the in-phase and out-of-phase components of the foundation impedances. For high frequencies, the effects of scour differ for the various components, and do not follow a clear trend.
- Increasing scour width and depth also causes in general a reduction of the damping factors along the vertical, horizontal and rotational direction, while the damping factors related to the coupling components increase slightly due to scour.

In the second part of the paper, the derived impedance functions are employed to evaluate the influence of scour on the fundamental vibration frequency of a SFS system. For this purpose, the non-dimensional parameters governing the problem are identified, and an extensive parametric study is carried out to evaluate how scour affects the fundamental circular frequency of the SFS system for different combinations of these parameters. The following conclusions are drawn:

- In general, a roughly linear reduction of the normalized fundamental vibration frequency is observed for increasing depths of scour.
- The influence of scour on the fundamental period elongation is more significant for stiff but tall piers, resting on soft soils.

Results of this study have important implications for the development of inverse techniques aimed at evaluating the extent of scour at bridge foundations based on the evaluation of the changes of the vibration frequency of SFS systems. Future studies will be carried out using the same modelling strategy to investigate the influence of scour on the seismic response of bridges. It is important to note that the impedance functions and the study results are based on a linear model assumption for the soil and the structural system and thus are not expected to be accurate for the case of large scour widths, such that the stability of the foundation is compromised and nonlinear behaviour of the soil or of the structure may become significant. The linear elastic assumption does not capture specific soil behaviour, such as overconsolidation or slack zone formation, which may arise due to soil erosion or water-saturated conditions around scour hole. The limitations of the linear elastic model may also lead to incomplete predictions in scenarios where material degradation or long-term effects play a role. Although in this study a two-dimensional model is considered to limit the computational cost of the analyses and the parametric study, future studies will also investigate the effects of scour considering a more realistic three-dimensional description of the problem, as well as incorporating advanced soil models to better simulate the complex soil behaviour under scour conditions.

Appendix A

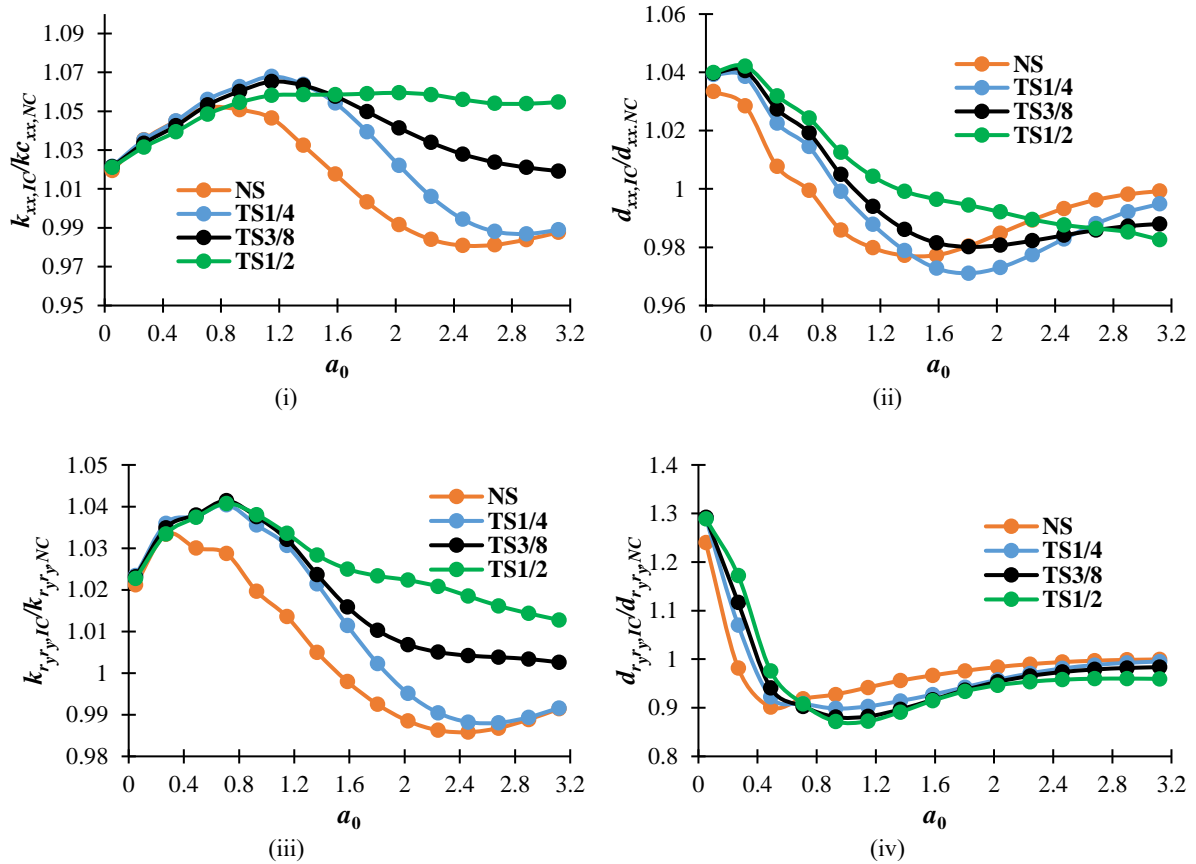


Figure A-1: Ratios k_{ij}^C/k_{ij}^{NC} and d_{ij}^C/d_{ij}^{NC} for comparison of the impedance functions by neglecting the coupling between the horizontal and rotational response.

Appendix B

Eq. 4.10 can be rewritten in expanded form as:

$$-\omega^2 m_s (\bar{u}_f + h\bar{\theta}_f + \bar{u}_s) - \omega^2 m_f (\bar{u}_f + h_f \bar{\theta}_f) + \bar{k}_{xx} \bar{u}_f + b_f \bar{k}_{xry} \bar{\theta}_f = 0 \quad (1A)$$

$$-\omega^2 m_s h (\bar{u}_f + h\bar{\theta}_f + \bar{u}_s) - \omega^2 I_f \bar{\theta}_f - \omega^2 m_f h_f (\bar{u}_f + h_f \bar{\theta}_f) + b_f \bar{k}_{xry} \bar{u}_f + b_f^2 \bar{k}_{ryry} \bar{\theta}_f = 0 \quad (2A)$$

$$-\omega^2 m_s (\bar{u}_f + h\bar{\theta}_f + \bar{u}_s) + \bar{k}_s \bar{u}_s = 0 \quad (3A)$$

Where \bar{k} contains both the real and imaginary part of the impedances ($\bar{k}_{ij}=k_{ij}+i\omega c_{ij}$).

Eq. 1A and Eq. 3A can be written as:

$$\bar{\theta}_f = -\frac{\omega^2 m_s (\bar{u}_f + \bar{u}_s) - \bar{k}_{xx} \bar{u}_f + \omega^2 m_f \bar{u}_f}{-b_f \bar{k}_{xry} + h\omega^2 m_s + h_f \omega^2 m_f} \quad (4A)$$

$$\bar{\theta}_f = \frac{\bar{k}_s \bar{u}_s - \omega^2 m_s (\bar{u}_f + \bar{u}_s)}{h\omega^2 m_s} \quad (5A)$$

Equating Eq. 4A and Eq. 5A one obtains:

$$\bar{u}_f = \frac{\frac{\bar{k}_s \bar{u}_s - \omega^2 m_s \bar{u}_s}{h\omega^2 m_s} + \frac{\omega^2 m_s \bar{u}_s}{-b_f \bar{k}_{xry} + h\omega^2 m_s + h_f \omega^2 m_f}}{\frac{1}{h} - \frac{\omega^2 m_f - \bar{k}_{xx} + \omega^2 m_s}{-b_f \bar{k}_{xry} + h\omega^2 m_s + h_f \omega^2 m_f}} \quad (6A)$$

Entering Eq. 6A into Eq. 5A yields:

$$\bar{\theta}_f = \frac{\bar{k}_s \bar{u}_s - \omega^2 m_s \left(\bar{u}_s + \frac{\frac{\bar{k}_s u_s - \omega^2 m_s \bar{u}_s}{h \omega^2 m_s} + \frac{\omega^2 m_s \bar{u}_s}{-b_f \bar{k}_{xry} + h \omega^2 m_s + h_f \omega^2 m_f}}{\frac{1}{h} - \frac{\omega^2 m_f - \bar{k}_{xx} + \omega^2 m_s}{-b_f \bar{k}_{xry} + h \omega^2 m_s + h_f \omega^2 m_f}} \right)}{h \omega^2 m_s} \quad (7A)$$

Entering Eq. 6A and Eq. 7A into Eq. 2A finally gives the following homogeneous equation:

$$(\alpha + \beta + \gamma) \bar{u}_s = 0 \quad (8A)$$

where:

$$\alpha = (-b_f \bar{k}_{xry} + h_f m_f \omega^2 + h m_s \omega^2) \delta \quad (9A)$$

$$\beta = \left(b_f^2 \bar{k}_{r,ry} - h^2 m_s \omega^2 - h_f^2 m_f \omega^2 - I_f \omega^2 \right) \frac{\bar{k}_s - m_s \omega^2 (1 - \delta)}{h m_s \omega^2} \quad (10A)$$

$$\gamma = -h m_s \omega^2 \quad (11A)$$

$$\delta = \frac{\frac{\bar{k}_s - m_s \omega^2}{h m_s \omega^2} - \frac{m_s \omega^2}{b_f \bar{k}_{xry} - h m_s \omega^2 - h_f m_f \omega^2}}{\frac{\bar{k}_{xx} - m_f \omega^2 - m_s \omega^2}{b_f \bar{k}_{xry} - h m_s \omega^2 - h_f m_f \omega^2} - \frac{1}{h}} \quad (12A)$$

References

- [1] Z. Hryniewicz, "Dynamic response of a rigid strip on an elastic half-space", *Computer Methods in Applied Mechanics and Engineering*, vol. 25, issue 3, pp. 355-364, 1981.
- [2] R.L. Kuhlemeyer, J. Lysmer, "Finite Element Method Accuracy for Wave Propagation Problems", *Journal of the Soil Mechanics and Foundations Division*, vol 99, issue 5, pp. 421-427, 1973.
- [3] C. Volpini, J. Douglas, A.H. Nielsen, "Guidance on Conducting 2D Linear Viscoelastic Site Response Analysis Using a Finite Element Code", *Journal of Earthquake Engineering*, vol. 25, issue 6, pp. 1153-1170, 2021.
- [4] A.H. Nielsen, "Absorbing boundary conditions for seismic analysis in ABAQUS" In *ABAQUS users' conference*, 2006, pp. 359-376.
- [5] G.J.C.M. Hoffmans, H.J. Verheij, *Scour manual*, Rotterdam, Netherlands, 1997.
- [6] S. Tileylioglu, J.P. Stewart, R.L. Nigbor, "Dynamic stiffness and damping of a shallow foundation from forced vibration of a field test structure", *Journal of Geotechnical and Geoenvironmental Engineering*, vol. 137, issue 4, pp. 344-353, 2011.
- [7] A. Maravas, G. Mylonakis, D.L. Karabalis, "Simplified discrete systems for dynamic analysis of structures on footings and piles", *Soil Dynamics and Earthquake Engineering*, vol. 61, pp. 29-39, 2014.
- [8] J. Fu, J. Liang, M. Todorovska, M. Trifunac, "Soil-structure system frequency and damping: estimation from eigenvalues and results for a 2D model in layered halfspace", *Earthquake Engineering & Structural Dynamics*, vol. 47, issue 10, pp. 2055-2075, 2018.
- [9] D. Pitilakis, E. Rovithis, A. Anastasiadis, A. Vratsikidis, M. Manakou, "Field evidence of SSI from full-scale structure testing", *Soil Dynamics and Earthquake Engineering*, vol. 112, pp. 89-106, 2018.
- [10] J.P. Wolf, *Foundation vibrational analysis using simple physical models*, Pearson Education, 1994.
- [11] N. Makris, C.J. Black, "Dimensional analysis of bilinear oscillators under pulse-type excitations", *Journal of Engineering Mechanics*, vol. 130, issue 9, pp. 1019-1031, 2004.
- [12] M.A. Ghannad, A. Amiri, S.F. Ghahari, "Effects of soil-structure interaction on response of structures subjected to near-fault earthquake records", In *AIP Conference Proceedings*, vol. 1010, issue 1, 2008, pp. 642-649.
- [13] J. Zhang, Y. Tang, "Dimensional analysis of structures with translating and rocking foundations under near-fault ground motions", *Soil Dynamics and Earthquake Engineering*, vol. 29, issue 10, pp. 1330-1346, 2009.
- [14] A.S. Veletsos, W.M. Meek, "Dynamic behaviour of building-foundation systems", *Earthquake Engineering & Structural Dynamics*, vol. 3, issue 2, pp. 121-138, 1974.
- [15] P.C. Jennings, J. Bielak, "Dynamics of building-soil interaction", *Bulletin of the Seismological Society of America*, col. 63, issue 1, pp. 9-48, 1973.
- [16] S. Carbonari, M. Morici, F. Dezi, G. Leoni, "A lumped parameter model for time-domain inertial soil-structure interaction analysis of structures on pile foundations", *Earthquake Engineering & Structural Dynamics*, vol. 47, issue 11, pp. 2147-2171, 2018.
- [17] M. Ciampoli, P.E. Pinto, "Effects of soil-structure-interaction on inelastic seismic response of bridge piers", *Journal of Structural Engineering*, vol. 121, issue 5, pp. 806-814, 1995.

5 Field tests and numerical analysis of the effects of scour on a full-scale soil-foundation-structural system

Scour is the prevailing cause of bridge failure worldwide, leading not only to traffic disruption, but also to social and economic losses and even to casualties. Many vibration-based monitoring techniques have been proposed for identifying the scour location and extent, based on the evaluation of the changes of the bridge modal properties due to scour. This study describes the experimental and numerical research carried out to investigate the effects of scour on the dynamic properties of structures with shallow foundations. Although these are the most vulnerable ones, they have received less attention compared to structures founded on pile foundations. To fill some existing knowledge gaps, field experiments were carried out on EuroProteas, a structural prototype with shallow foundation that was subjected to increasing levels of scour. The changes of the dynamic properties of the system are evaluated by postprocessing the ambient vibration recordings and by developing various models of the soil–foundation–structural system with different descriptions of the soil–structure interaction problem. The study results shed light on the effects of scour on systems with shallow foundations and on the accuracy of alternative modelling approaches. They are presented here to inform the development and validation of vibration-based techniques and modelling strategies for bridge scour identification.

From the analysis of the literature of the problem, it is evident that most experimental studies on shallow foundations have been carried out in the laboratory, under controlled conditions, where it is impossible to fully recreate in-field conditions. As a consequence of this, there is also a lack of fully validated numerical strategies for simulating the effect of scour on the dynamic behaviour of soil–foundation–structure systems subjected to scour. Thus, further experimental and numerical research investigations on the problem are needed. The DYMOBRIS EU project [1] was conceived with the objective of contributing to fill the knowledge gap in experimental evaluation and modelling of the effects of scour on systems with shallow foundations, which are the most vulnerable to scour. For this purpose, full-scale free and forced-vibration tests and recordings of ambient vibrations signals were carried out on the EuroProteas prototype [2][3] at EuroseisTest in June, 2019 to evaluate the effects of foundation scour on the dynamic properties of a SFS system. While the experiments were carried out by the DYMOBRIS EU project [1] team, the author of this thesis interpreted the experimental results and complemented them by numerical analyses, aimed to validate the numerical modelling strategies for describing the effects of scour on the dynamic behaviour of the SFS system. Section 5.1 describes the field test setup at EuroProteas and the investigated scour scenarios. Section 5.2 illustrates various modelling strategies developed to analyse the variation of dynamic properties of the in-field prototype due to scour, based on different description of the soil–structure interaction problem. Section 5.3 illustrates the ambient vibration test results and compares them with those obtained by the numerical models. Finally, Section 5.4 shows the updating of the numerical model to provide a better interpretation of the test results. It is noteworthy that the study results are useful not only for the development of vibration-based monitoring strategies for bridge scour, but they also contribute to improve the understanding of the effect of scour on the dynamic impedance of bridge foundations undergoing scour. This is of paramount importance for investigating the seismic response of bridges with scoured shallow foundation, which has received increased attention in the literature in the last decade [4][8]. The content of this chapter is based on a peer-reviewed journal publication, with minor modifications. The research was conducted in collaboration with Enrico Tubaldi, Stergios Aristoteles Mitoulis, Sotirios Argyroudis, Fabrizio Gara, Laura Ragni, Sandro Carbonari, Francesca Dezi, Athanasios Vratsikidis, Dimitris Pitilakis and Anastasios Anastasiadis (Table 1-1).

5.1 Field test setup

EuroProteas (Figure 5-1) is a double symmetric prototype structure, which simply rests on the ground surface. Its superstructure mass consists of two portable reinforced concrete slabs, bolted on four square hollow steel columns connected by steel X-braces. An identical reinforced concrete slab is used as a surface foundation of the model. The reconfigurable roof mass and bracing system allow achieving different values of the fixed base natural frequency of the structure and of the superstructure to soil stiffness ratio. The slabs mentioned above with dimensions $3.0 \times 3.0 \times 0.4$ m are made of concrete C20/25 and steel reinforcement of diameter 14 mm. The unit weight of the reinforced concrete is 25 kN/m^3 , leading to a mass of around 9.16 Mg for each slab. The four steel columns have cross sections QHS $150 \times 150 \times 10$ mm, length 3.8 m, and a total mass of approximately 0.68 Mg, while the X-braces have L cross sections $100 \times 100 \times 10$ mm and a total mass of approximately 0.41 Mg. The steel columns are fixed to the slabs using M20 steel bolts. The braces are conjoined to each other and to steel plates welded on the base of the columns by M16 bolts. The total height of EuroProteas is 5 m, whereas its total mass is approximately 28.5 Mg.

The considered prototype can provide a simplified representation of a stiff bridge pier of a multi-span simply supported deck, such that the deck does not contribute to the lateral stiffness of the system (Figure 5-2). It would have been more realistic to consider alternative prototypes with geometrical and mechanical properties matching the ones of real bridges. This study is characterised by potential limitations, namely, the relatively high ratio of the foundation mass to superstructure mass, the presence of solely granular soil under the foundation, and hence the consideration of drain conditions, and finally the absence of water in the field, which provides a contribution in terms of inertia and loads on submerged bridge piers. However, the main scope of this study is to validate numerical strategies for simulating the effect of scour on the dynamic properties of systems with the aid of large-scale field test results. Thus, the strategies developed, once validated, can be used to analyse other structures. The development of such a modelling strategy is essential for interpreting the results of any vibration-based monitoring strategy for scour measurement.

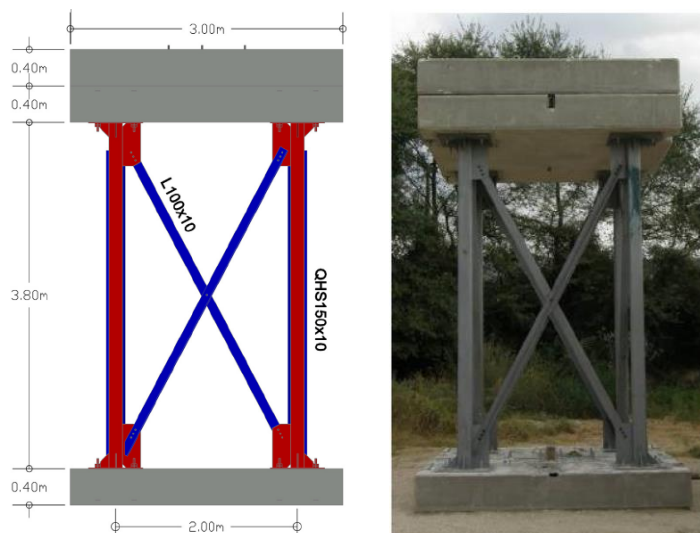


Figure 5-1: Geometry and characteristics of EuroProteas [2].

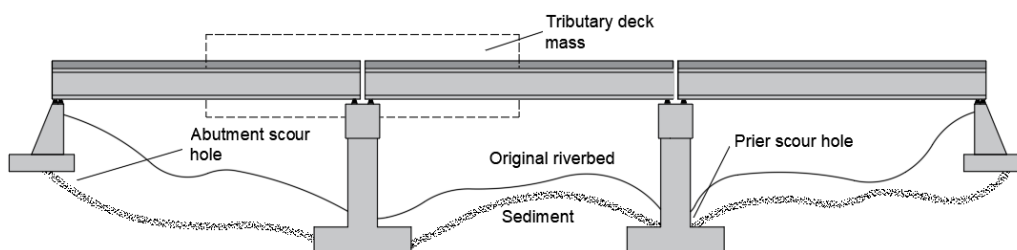


Figure 5-2: Multi-span bridge with simply supported deck exposed to scour.

5.1.1 Soil properties

EuroProteas is built at EuroseisTest experimental facility, whose soil and dynamic properties have been investigated thoroughly by earlier studies through comprehensive geotechnical and geophysical surveys [9]. Recently, Pitilakis et al. [2] carried out an array of additional geotechnical and geophysical field tests (drilling boreholes, down-hole measurements, and resonant column tests on representative soil specimens) to identify the exact soil conditions beneath EuroProteas. Laboratory tests were carried out for specimens from various depths and locations beneath the foundation providing detailed and valuable data before the construction of EuroProteas. Notably, a 12 m deep borehole (denoted as “BH-01”) was drilled at the eastern side of Euro-Proteas at a distance of 0.5 m of the foundation, while a 30 m deep borehole (denoted as “BH-02”) was drilled beneath the geometrical center of the foundation.

Figure 5-3 illustrates a comprehensive 30 m stratigraphy derived by the BH-02 and the low-strain shear wave velocity profile obtained by a down-hole test (denoted as “DH-01”) along with other V_s profiles in EuroProteas vicinity [10]-[12]. For the sake of completeness, the N_{SPT} profile corresponding to BH-02 is also provided. According to the data provided by the BH-02 (Figure 5-3), the top 7 m (unit A) of the soil consists mainly of silty clayey with sand, whereas for depths 7–22 m (unit B) and 22–30 m (unit C) of silty sand with gravels to clayey sand and of silty sand, respectively. Moreover, N_{SPT} does not exceed 6 in the upper 6 m, and the water level was found at 1.7 m below ground surface. Shear wave velocity ranges from 100 to 130 m/s in the upper 5 m and exceeds 300 m/s at 25 m depth.

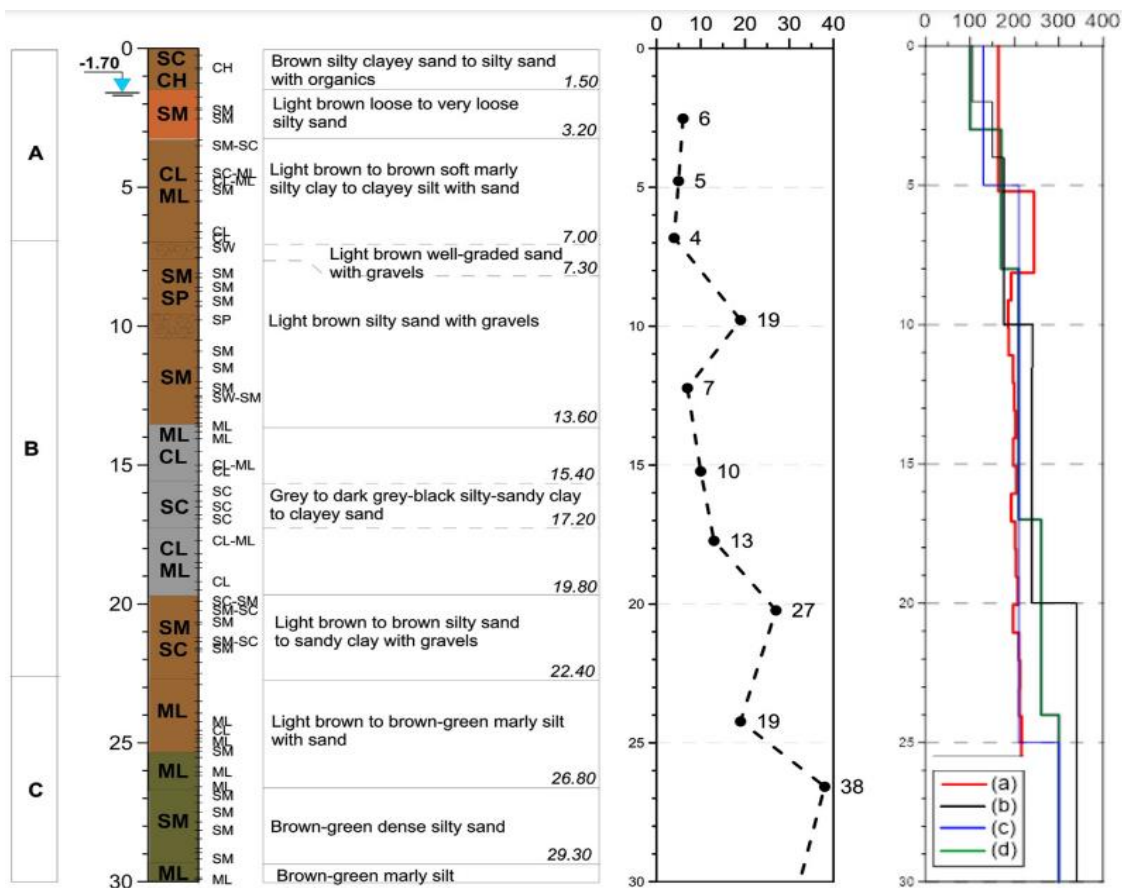


Figure 5-3: Subsoil characteristics from the 30-meter deep borehole BH-02 (left), N_{SPT} blow count from BH-02 (middle), and shear wave velocity profile (right) for cases (a) DH-01: DH test before EuroProteas' construction, (b) V_s values at a site approximately 50 m south of EuroProteas [10], (c) reference model of the valley cross-section from updated geophysical, geotechnical and numerical modelling [11], (d) profile from detailed geotechnical and geophysical surveys [12]. Adapted from Pitilakis et al. [2].

5.1.2 Sensor types and arrangement

Figure 5-4 shows the instrumentation installed on EuroProteas. Three triaxial accelerometers were placed on the roof slab, while another four triaxial accelerometers are placed on the top of the foundation slab (Table 5-1). All the accelerometers were oriented toward the positive x -direction of the structure, which forms a 30° angle with the magnetic North. There is no particular criterion regarding the disposition. In theory, three accelerometers should be sufficient to describe the motion of the rigid base and top slabs. The consideration of the same location of the accelerometers at the top and the bottom was not feasible due to the presence of a shaker onto the top slab for the application of forced-vibration tests, which will be part of a future study. The recordings from these accelerometers mentioned above are later used to identify the dynamic response and the modal shapes of EuroProteas structure under various scour scenarios (see Section 5.3).

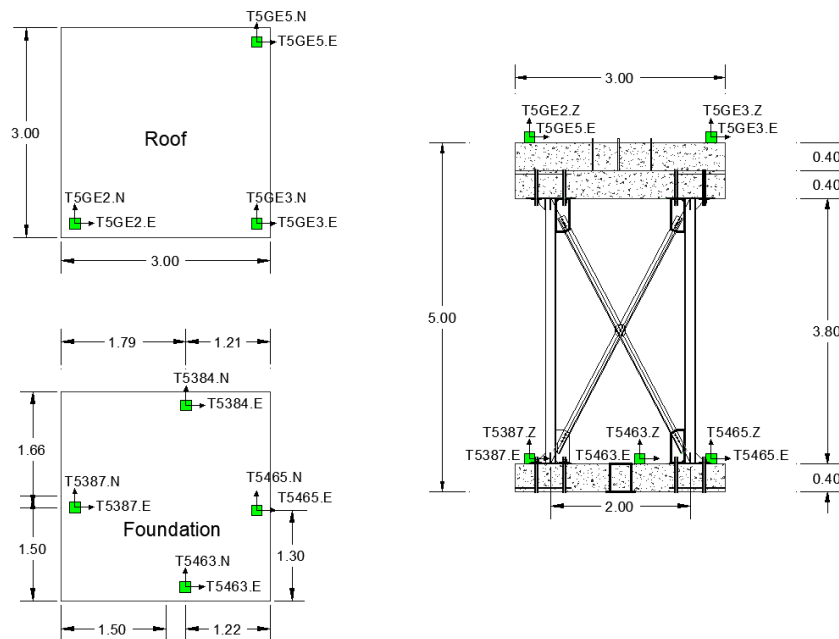


Figure 5-4: Installed accelerometers on EuroProteas.

Table 5-1: Types and names of the installed accelerometers on EuroProteas.

Accelerometers	
Type	Sensor
Güralp CMG-5T	T5463
Güralp CMG-5T	T5384
Güralp CMG-5T	T5465
Güralp CMG-5T	T5387
Güralp CMG-5TCDE	T5GE5
Güralp CMG-5TCDE	T5GE2
Güralp CMG-5TCDE	T5GE3

In addition to the prototype fully supported on the soil, two different scour scenarios were considered in the experimental campaign, corresponding to the scour widths $2s = 0.3$ m and $2s = 0.75$ m at the northern part of the foundation. Figure 5-5 depicts the excavated soil (i) during and (ii) at the end of the tests, after the superstructure was lifted. The considered scour hole shape can be assumed to be roughly representative of many scour holes that develop in real bridges with shallow rectangular foundation.



Figure 5-5: (i) Excavation of the soil under the foundation, (ii) Scour hole shape at the end of the final test.

Lee et al. [13] have investigated this issue by performing a series of flume tests considering different typologies of foundations, as opposed to cylindrical monopiles, and found that the scour develops upstream of the pier, with the maximum scour depth attained at the nose of the footing. Alternative scour hole shapes could have been considered, but some preliminary numerical analyses considering different scour hole shapes for the same portion of eroded soil beneath the foundation had shown that this has a minor influence on the dynamic behaviour of the system. The effect of the scour hole shape is investigated numerically in Section 5.2.

5.2 Numerical modelling strategy

This subsection illustrates three three-dimensional numerical models developed to design the experimental full-scale tests and to predict the effects of scour on the foundation response and the variations of the soil–foundation–structure (SFS) system dynamic properties. In particular, various models were built in the Finite Element code Abaqus [14], namely, the Fixed Base (FB) structure, the structure with a continuous semi-infinite soil domain (SFS_1), and the structure with the SFS modelled using linear springs and dashpots (SFS_2), which simulate the impedance functions. A simplified version of the SFS_2 model is also developed in Matlab [15], by employing a substructure approach and exploiting the impedance functions derived Chapter 4 using a two-dimensional soil model (SFS_3). The first two models developed in Abaqus share the same description of the superstructure (Figure 5-6), with two-node linear beam elements used to model the columns and the braces, and 20-node quadratic brick elements (C3D20) used to model the slabs. The columns are connected to the slabs using multipoint tie constraints, whereas the X-braces are connected to the column ends via a hinge connector. The connections between the two X-braces are based on joint connectors.

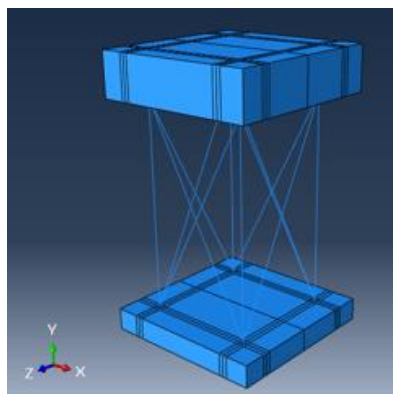


Figure 5-6: Superstructure used in fixed-base model.

The steel Young's modulus and Poisson's ratio are $E_s = 210,000$ MPa and $\nu_s = 0.2$, respectively, whereas the concrete mechanical properties are $E_c = 29,962$ MPa and $\nu_c = 0.2$. A 1% damping factor is assigned to both materials using the following Rayleigh model. The Rayleigh damping coefficients are calibrated

to achieve 1% damping factor in correspondence of the first and the third modes of vibration of the system, characterized by the highest participation of the superstructure masses along the x direction.

5.2.1 Fixed-base model (FB)

The FB model is obtained by restraining the displacements at the base of the foundation slab. This model, characterised by a fundamental vibration frequency of 9.26 Hz, is used to estimate the effects of Soil Structure Interaction (SSI) on the vibration properties by comparison with the other three designed models presented in the next subsections. The frequency of 9.26 Hz matches the ones evaluated in other studies on the same prototype [2].

5.2.2 Structure with soil modelled as a continuum with absorbing boundaries (SFS_1)

This sub-section describes the three-dimensional model including the semi-infinite soil-domain. This domain is modelled with solid elements with elasto-plastic behaviour. The elastic soil behaviour is described by assigning shear modulus $G = 31.6$ MPa, soil density $\rho = 1870$ kg/m³, shear wave velocity $V_s = 130$ m/s and Poisson's ratio $\nu = 0.3$. The aforementioned values are consistent with the soil properties derived from BH-02 (Figure 5-3) for the upper 5 m of the soil. It must be mentioned that the soil beneath EuroProteas mainly consists of sand, with the water level being 1.7 m under the ground surface. Therefore, for the sake of simplicity, a perfectly drained behaviour has been assumed for the entire soil domain. Furthermore, the soil strength parameters are estimated from available laboratory and field SPT and CPT tests reported in [16]. More in detail, the plastic behaviour is defined by the Mohr–Coulomb model, with a friction angle $\Phi = 30^\circ$, and cohesion $c' = 0.01$ MPa. The soil material damping is described through a 1% structural damping [14]. The interaction between the foundation and the soil is modelled using the “surface to surface” contact approach. The interface has a very high stiffness in compression to avoid penetration, can resist only compressive forces, and has a friction coefficient of $\mu = 0.6$ along the tangential direction. The soil is represented by a finite domain with local Absorbing Boundary Conditions (ABCs) to avoid reflection of outgoing waves (Figure 5-7). The length of the solid domain from the foundation slab outwards is 18 m; the absorbing elements are infinite brick elements, and their length is equal to that of the soil domain. To accurately model wave propagation, the mesh size satisfies the following relation [17]:

$$l_{max} \leq \left(\frac{1}{8} \sim \frac{1}{5}\right) \lambda_{min} \leq \frac{V_{s,min}}{8 f_{max}} \quad (5.1)$$

where l_{max} is the maximum element size, λ is shear wavelength, equal to 13 m, $V_{s,min}$ is the shear-wave velocity, equal to 130 m/s, and $f_{max} = 10$ Hz is the maximum frequency of interest.

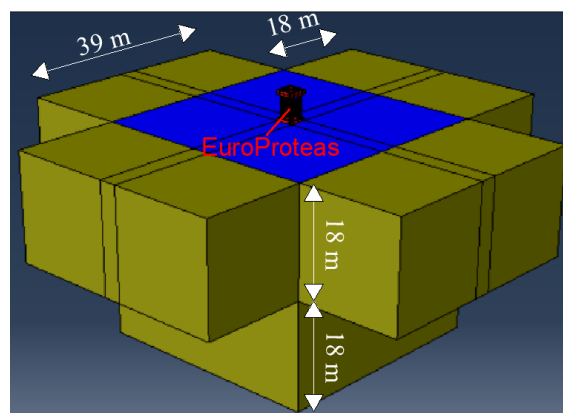


Figure 5-7: Model of SFS system with soil domain (in blue) and absorbing boundary conditions (in yellow) and the structure (in red).

In this model (denoted as “SFS_1”), scour is characterised by a rectangular prism shape and it is simulated by removing soil elements under the foundation slab. To investigate how the scour hole shape affects the changes in fundamental frequency of the system, two variations of this model are developed. The first one (denoted as “SFS_1_TS”) considers a triangular prism shape of the scour hole, which extends not only beneath, but also beside the foundation and it is more representative of real scour conditions (see, e.g., [18],[19]). The upstream scour slope is considered equal to $\phi = 30^\circ$, while the downstream scour slope half of the upstream slope. It must be mentioned that since the soil domain is discretized using hexahedron elements, the scour slopes are simulated only approximately using a very refined mesh. The second model (denoted as "SFS_1_SS) is developed by modifying the “surface to surface” contact interface between the soil and foundation, and removing the contact rather than soil elements beneath the foundation to simulate scour. In addition, the case of an embedded foundation is considered to represent not only more realistic conditions, where the foundation does not simply rest on the ground surface, but also an even more realistic scour hole shape based on the results of Lee et al. [13]. For this case, another two models are analysed, by removing not only the soil elements on the upstream side of the foundation (i.e., the one perpendicular to the flow), but also on the other two sides of the foundation (i.e., the ones parallel to flow), for a width of 0.3 m. For this case two models are considered, namely, “SFS_1_RS_E” and “SFS_1_TS_E”, representing, respectively, a rectangular and a triangular scour hole shape. Figure 5-8 depicts the soil and contact conditions of the models with non-embedded foundations SFS_1, SFS_1_TS and SFS_1_SS for a scour width of 750 mm, while Figure 5-9 illustrates the geometry and the simulation of the scour hole for the models with embedded foundations SFS_1_RS_E and SFS_1_TS_E.

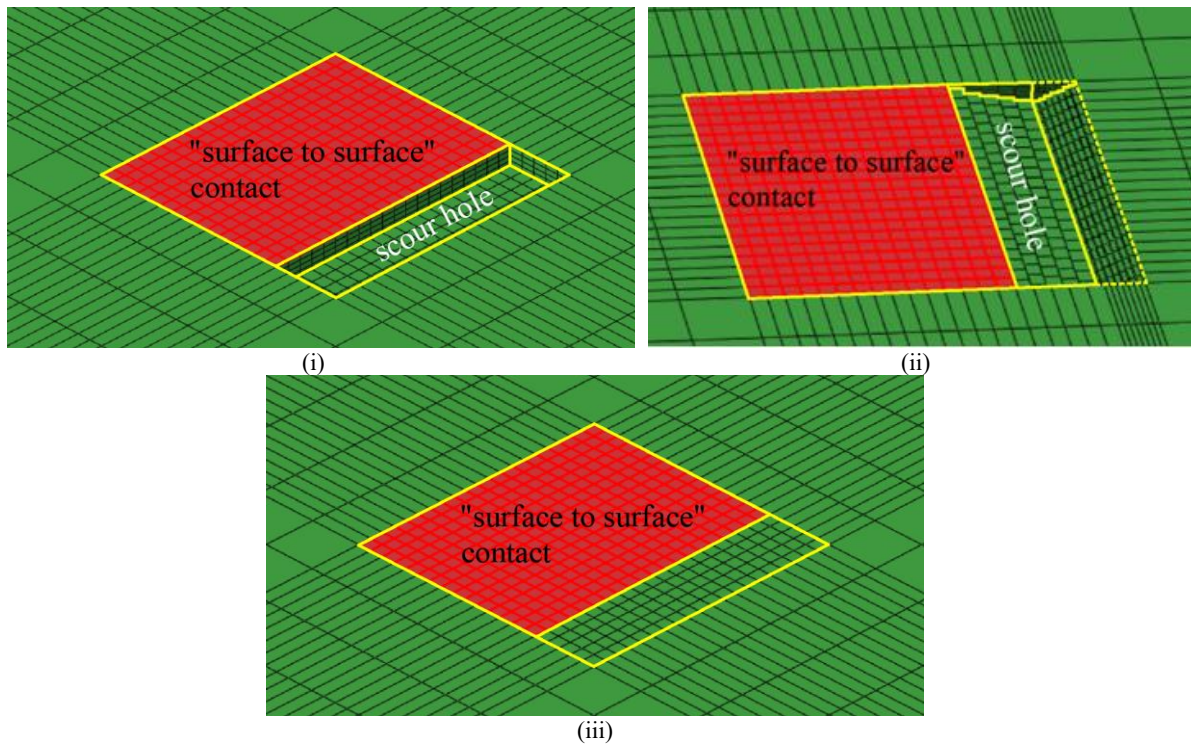


Figure 5-8: Simulation of scour hole at the soil domain of the model i) SFS_1, ii) SFS_1_TS, and iii) SFS_1_SS.

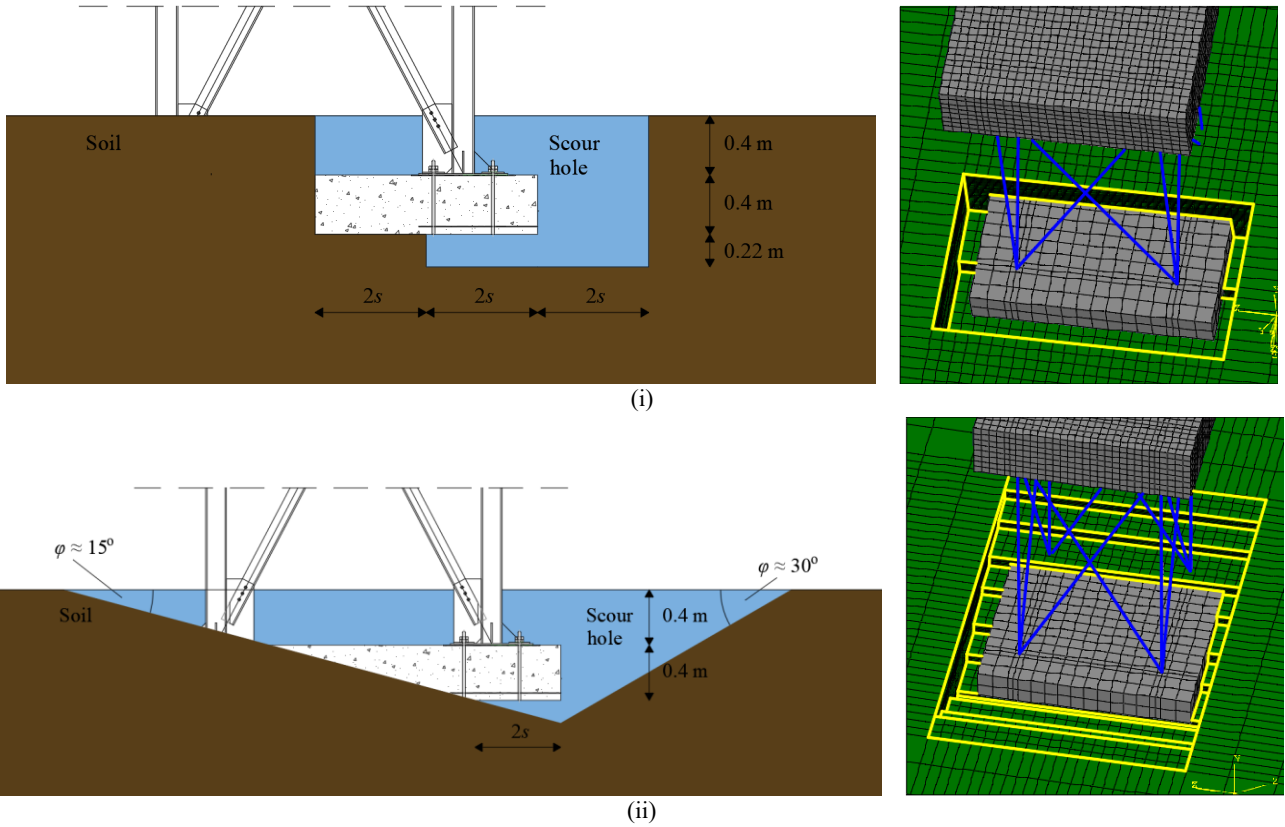


Figure 5-9: Geometry and simulation of the scour hole around the embedded foundation for the model i) SFS_1_RS_E and ii) SFS_1_TS_E.

5.2.3 Structure with soil modelled as simplified impedance function model (SFS_2)

In this model, the semi-infinite soil-domain is replaced by a set of distributed springs and dampers with the aim of obtaining a simplified description of the SSI problem. This approach is similar to the one followed in Tubaldi et al. [18] and Scozzese et al. [19], with zero-thickness cohesive interface elements resisting only compression stresses at the bottom of the foundation describing the soil reaction. The cohesive interface elements have a visco-elastic behaviour in compression, with properties based on the work of Gazetas [20]. The springs constants (stresses per unit displacements) have been evaluated as follows:

$$k'_{s,x} = \frac{k_{s,x}}{A_x}, \quad k'_{s,y} = \frac{k_{s,y}}{A_y}, \quad k'_{s,z} = \frac{k_{s,z}}{A_z} \quad (5.2)$$

where $k_{s,x}$, $k_{s,y}$ and $k_{s,z}$ are given by Gazetas [20] as a function of the shear modulus, $G = V_s^2 \rho = 31.6 \text{ MPa}$, the Poisson's ratio, $\nu = 0.3$, and of the foundation geometry, whereas A is the foundation area in contact with the soil.

The dashpots are in parallel with the springs and represent the soil radiation damping according to the following expression [20]:

$$c'_x \approx (\rho V_s) \cdot \tilde{c}_x, \quad c'_z \approx (\rho V_s) \cdot \tilde{c}_z \quad (5.3)$$

$$c'_y \approx (\rho V_{La}) \cdot \tilde{c}_y \quad (5.4)$$

where ρ is soil material density, V_{La} is Lysmer's shear wave velocity, related to V_s , and \tilde{c}_x , \tilde{c}_y and \tilde{c}_z are function of the foundation geometry and mechanical soil properties. A 5% hysteretic damping factor is

also considered to describe the energy dissipation within the soil domain. In this work, it is assumed that the springs and the dashpots are frequency independent, and the values of $k_{s,x}$, $k_{s,y}$, $k_{s,z}$ and of \tilde{c}_x , \tilde{c}_y , and \tilde{c}_z are those corresponding to the system natural frequency. A more sophisticated model could consider the variation with frequency of these parameters. The values of the subgrade reactions are $k'_{s,x}=27.9\cdot 10^6$ N/m³, $k'_{s,z}=27.9\cdot 10^6$ N/m³, and $k'_{s,y}=34.2\cdot 10^6$ N/m³. The values of the damping coefficients (including the hysteretic component) are $c'_x = 33.83\cdot 10^5$ N·s/m, $c'_z = 30.44\cdot 10^5$ N·s/m, and $c'_y = 30.44\cdot 10^5$ N·s/m. To simulate scour in Abaqus [14], the “model change” capability is employed, allowing to progressively eliminate the cohesive interface elements at the foundation–soil interface that represent the portion of eroded soil.

5.2.4 Two-dimensional structure and soil model (SFS_3)

A three-dimensional model with absorbing boundaries conditions is expected to provide a more accurate description of the behaviour of the system. However, it is computationally demanding. In this subsection, a simplified but robust numerical approach is employed for investigating the influence of scour on the dynamic response of systems with shallow foundation, which is based on two-dimensional description of the problem. This approach can be employed for a preliminary assessment of the effects of scour in terms of change of modal properties. The approach is based on the work presented in Chapter 4, where the influence of scour on the dynamic response of SFS systems was investigated by applying the substructure method [21]. In particular, non-dimensional frequency dependent impedance functions were obtained for a rigid strip foundation resting on an homogenous elastic soil domain for the case of no scour and for various scour hole shapes. The numerical model used to derive the impedance function was developed in Abaqus [14] using a plain–strain assumption, and it was validated based on the comparison between the impedance functions obtained numerically and the ones reported in Hryniewicz [22]. For the sake of clarification, Figure 5-10 illustrates the shape of the scour hole considered in Chapter 4. The derived impedance functions were used to evaluate the reduction of the fundamental vibration frequency of vibration of a simple SFS system (Figure 5-11) for increasing levels of scour. The same approach is adopted here to evaluate the effects of scour on the EuroProteas’ prototype. It must be noted that the impedance functions derived in Chapter 4 were obtained by assuming a linear soil behaviour. In contrast, the model SFS_1 considers elastoplastic soil behaviour and contact elements, introducing nonlinear effects. While taking these nonlinearities into account for the derivation of the impedance functions would be insightful, it would increase significantly computational demands and was beyond the scope of this thesis. The focus was placed on validating the response of SFS systems using the already derived impedance functions against experimental tests, proving a sound basis for future research including nonlinear scour effects.

The simplified model of EuroProteas consists of a superstructure with lumped mass $m_s = 18.32$ Mg, height $h_s = 4.2$ m, and lateral stiffness $k_s = 62,016.49$ kN/m, based on a shallow foundation of mass $m_f = 9.16$ Mg, height $2h_f = 0.4$ m, width $2b_f = 3$ m and mass moment of inertia $I_f = 6.99$ Mg m². The compliance of the soil-foundation system is described by means of the impedance functions \bar{k}_{xx} for the horizontal response, $\bar{k}_{r_y r_y}$ for the rotational response, and $\bar{k}_{x r_y}$ for the coupled roto-translational response of the foundation, where they are reported in non-dimensional form. Obviously, different impedances have to be considered for each investigated scour scenario. It must be noted the impedance functions derived in Chapter 4 and used in this study correspond to a soil Poisson’s ratio of $\nu = 0.25$. In contrast, a slightly higher Poisson’s ratio of $\nu = 0.3$ is applied to models SFS_1 and SFS_2, aligning with the soil properties derived from BH-02 (Figure 5-3) for the upper 5 m of the soil. This slight increase leads only to marginally higher impedance function values, allowing an accurate results comparison of the models.

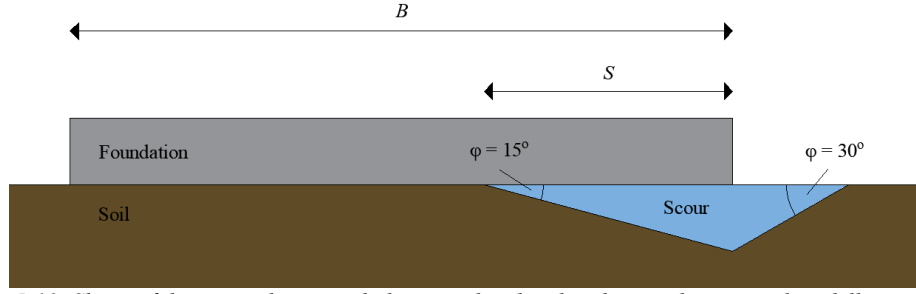


Figure 5-10: Shape of the triangular scour holes considered within the two-dimensional modelling approach.

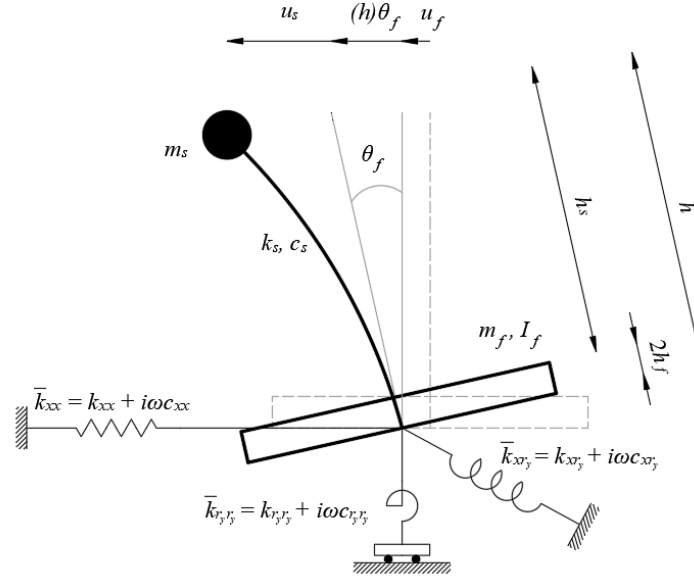


Figure 5-11: Model of the SFS_3 system.

The free vibration equation of motion of the SFS system can be expressed in the frequency domain in a vector form as:

$$-\omega^2 \mathbf{M} \bar{\mathbf{U}} + i\omega \mathbf{C}(\omega) \bar{\mathbf{U}} + \mathbf{K}(\omega) \bar{\mathbf{U}} = 0 \quad (5.5)$$

where $\bar{\mathbf{U}}$ denotes the Fourier transform of the vector \mathbf{U} collecting the three generalised displacements of the system in the time domain, namely, the foundation translation (u_f) and rotation (θ_f), and the relative displacement (u_s) of mass m_s with respect to the base (Figure 5-11). Furthermore, \mathbf{M} , \mathbf{C} and \mathbf{K} are the mass, damping and stiffness matrices of the system. These quantities are expressed as follows [23]:

$$\mathbf{U} = [u_f \quad \theta_f \quad u_s]^T \quad (5.6)$$

$$\mathbf{M} = \begin{bmatrix} m_f + m_s & m_f h_f + m_s h & m_s \\ m_f h_f + m_s h & I_f + m_f h_f^2 + m_s h^2 & m_s h \\ m_s & m_s h & m_s \end{bmatrix} \quad (5.7)$$

$$\mathbf{C}(\omega) = \begin{bmatrix} c_{xx}(\omega) & b_f c_{xy}(\omega) & 0 \\ b_f c_{xy}(\omega) & b_f^2 c_{yy}(\omega) & 0 \\ 0 & 0 & c_s \end{bmatrix} \quad (5.8)$$

$$\mathbf{K}(\omega) = \begin{bmatrix} k_{xx}(\omega) & b_f k_{xy}(\omega) & 0 \\ b_f k_{xy}(\omega) & b_f^2 k_{yy}(\omega) & 0 \\ 0 & 0 & k_s \end{bmatrix} \quad (5.9)$$

Equation (5.5) is solved repeatedly, considering each time the values of \bar{k}_{xx} , \bar{k}_{xy} , \bar{k}_{yy} that correspond to an excitation frequency ω . Each solution provides a value of the natural frequency $\tilde{\omega}$, and the correct one satisfies the equation $\omega = \tilde{\omega}$.

5.2.5 Eigenvalue analyses and validation of the modelling strategies

A preliminary validation of the developed modelling strategies was carried out before undertaking the experiments, based on the comparison of the eigenvalue analysis results with the experimental model properties obtained by an earlier experimental campaign [2] for the case of no scour. The experimental results were obtained by Ptilakis et al. [2] by recording ambient vibration signals by means of accelerometers located on the EuroProteas and applying the Frequency Domain Decomposition (FDD) method. Table 5-2 shows the estimated resonance frequencies of EuroProteas for each numerical model. These frequencies refer to the vibration in the horizontal direction. It can be noted that the resonant frequency of the system reduces significantly if soil–structure interaction effects are taken into account, and that there is a good agreement between the estimates of the frequency provided by the various models and the experimental one. Evaluating the modal frequencies of interest in Abaqus [14] is challenging, due to the presence of many modes involving only the 3D soil domain and not the superstructure, and the uncertainty in the contribution of the infinite elements at the boundaries. For this reason, the vibration frequency obtained from modal analysis of the model SFS_1 has been checked against that evaluated from free-vibration analysis.

Table 5-2: Fundamental frequency of vibration for different structural configurations (case without scour).

Structural configuration	Frequency [Hz]	
	Abaqus	Experimental
FB model	9.26	-
SFS_1 model	4.73	
SFS_1 model (Free vibration)	4.73	4.1
SFS_2 model	4.42	
SFS_3 model	4.64	

5.3 Free-field tests results and comparison with the numerical studies

Ambient vibrations signals were recorded by the accelerometers before inducing scour and for two different stages of scour, corresponding to the scour widths of $2s = 0.3$ m and $2s = 0.75$ m (see Figure 5-10 for definition of s). The identification of the modal parameters of the SFS is carried out using the Frequency Domain Decomposition (FDD) method proposed by Brincker et al. [24].

Figure 5-12 illustrates the singular value of the power spectral density matrix of the response of the SSI system to the ambient vibration before inducing scour. It can be observed that the system response at the various frequencies is dominated by the first singular value, and that the peaks corresponding to the first three modes are visible. These three vibration modes are illustrated in Figure 5-13 together with the corresponding modal vibration frequencies.

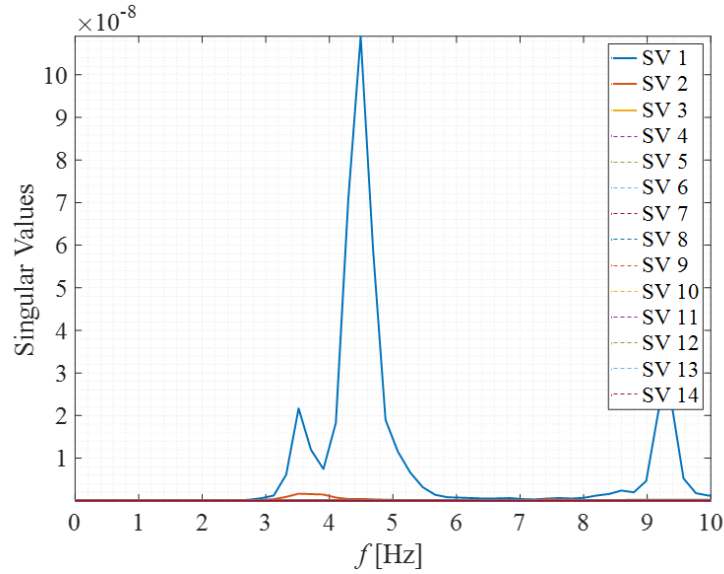


Figure 5-12: Singular values (SVs) of the PSD matrix of the response to ambient vibration in the case of no scour.

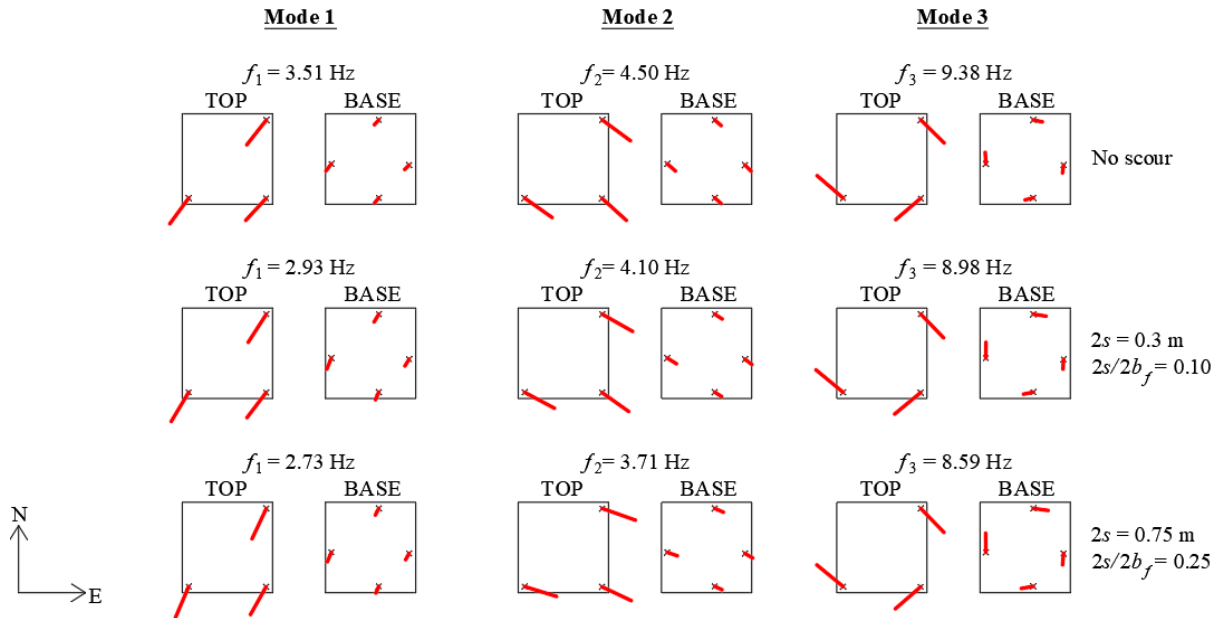


Figure 5-13: Experimental modal shapes for system with no scour, and normalised scour widths $2s/2b_f = 0.1$ m and $2s/2b_f = 0.25$ m. Plan view of top and base horizontal displacements.

The first two vibration modes correspond to the vibration of the system along two orthogonal directions that are rotated with respect to the principal axes of the superstructure (Figure 5-13). The third mode is associated with the torsion of the superstructure about the vertical axis. This may be due to a non-perfect contact between the base of the structure and the soil. Particularly, Figure 5-5ii illustrates the soil beneath the foundation after the removal of the structural prototype at the end of the experimental campaign. It can be observed that vegetation was found both in the area of the scour hole, and the southwest part of the foundation. This suggests that there was possibly a non-perfect contact between the soil and the foundation, resulting in water ingress and growth of vegetation where this contact was missing. This asymmetry in the foundation support could explain the differences between the simulated dynamic behaviour and the experimental one. This issue is discussed in detail in Section 5.4. Furthermore, this might explain the fact that the frequencies of the experimental first two modes of vibration (i.e., 3.51 Hz and 4.5 Hz) are, respectively, higher and lower than the value of 4.1 Hz reported in [2]. This value was obtained in a previous experimental campaign on the same prototype and could

be representative of the first two modes of vibrations, assuming that there was a perfect contact between the foundation and the soil.

It is noteworthy that for the purpose of performing the tests, the prototype was moved in another location, 20 m apart from the one of [2]. Thus, the differences in the frequency may also be explained by slight variations in the soil properties from one location to the other. The “x” symbols on the plan views of Figure 5-13 indicate the location of the accelerometers (Table 5-1) installed on the roof and foundation slab of EuroProteas.

Figure 5-14 illustrates the variation of the modal frequencies with the scour width normalized by the foundation width ($2s/2b_f$). It can be observed that all these frequencies vary linearly with $2s/2b_f$. The frequency of the first mode is more sensitive to scour, as expected due to the location of the scour hole. In the same figure, the vibration frequencies of the numerical models SFS_1, SFS_2 and SFS_3 are plotted. It is worth to note that results from the numerical models are not in a great agreement with those from the experimental tests. In particular, the numerical models overestimate the first vibration frequency for all the investigated $2s/2b_f$ values, whereas they underestimate the effects of scour in terms of frequency reduction in the case of the second mode. Moreover, it is noteworthy that the numerical models are characterized by two identical translation modes in the x and y directions in the case of no-scour whereas the experimental modes are different and coupled in the translational directions due to possible asymmetries in the foundation–soil contact area. It is also observed that the SFS_2 model cannot capture satisfactorily the frequency of the rotational mode shape, contrary to the SFS_1 model. Furthermore, it must be mentioned that SFS_1 results in slightly higher values of f_1 for $2s/2b_f \leq 0.1$, and of f_2 for all the investigated scour widths compared to SFS_2 and SFS_3, although the elastoplastic modelling of the soil domain. This is attributed to three factors: i) no plastic deformations are observed in the soil domain of SFS_1 for the investigated scour cases, which are expected to develop in larger scour widths, ii) the three-dimensional nature of SFS_1, which accounts for additional confinement and stress redistribution effects not fully captured in the plane-strain assumptions of SFS_2 and SFS_3, iii) the use of a lower value of Poisson’s ratio in SFS_3 for the estimation of the impedance functions ($\nu = 0.25$) compared to the models SFS_1 and SFS_2 ($\nu = 0.3$). Higher value of Poisson’s ratio would result in higher values of the impedance functions, and therefore a stiffer foundation response (see section 6.2). The reasons for the difference between the experimental and numerical results and the updating of the model to better capture the observed modal properties are discussed in detail in the next sections.

The effect of the scour hole shape on the dynamic behaviour of EuroProteas is investigated by comparing the results obtained with the models SFS_1, SFS_1_TS and SFS_1_SS, described in Section 5.2. Figure 5-15 shows the variation of the vibration frequencies vs the normalised scour width S/B for the various numerical models. The scour hole shape has only a minor effect on the variation of frequency of the system, which is mainly controlled by the normalised scour width. The triangular prism shape, which is more representative of real scour conditions, yields slightly higher frequencies than the rectangular one. Similarly, the case of SFS_1_SS, which simulates scour only by removing the contact between the foundation and soil rather than the soil elements under the foundation, yields results similar to the triangular prism shape.

Further analyses are made considering the case of embedded foundation. Table 5-3 compares the vibration frequencies obtained for the models SFS_1, SFS_1_TS, SFS_1_RS_E and SFS_1_TS_E. It can be observed that the models with embedded foundation exhibit higher vibration frequencies compared to the models with the shallow foundation. In addition, for the embedded foundation, the shape of the scour hole was found to have a negligible influence on the vibration frequencies.

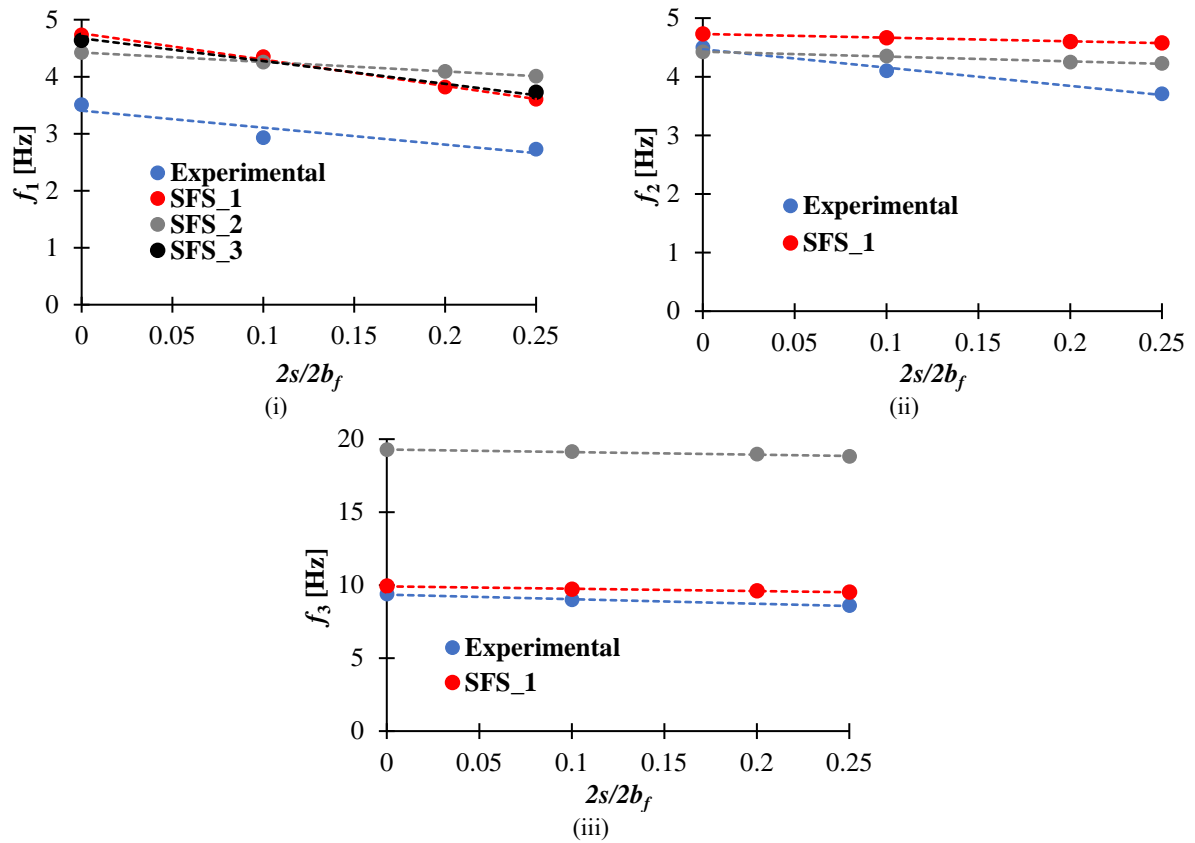


Figure 5-14: Variation of the vibration frequencies of the i) first, ii) second and iii) third monitored mode with the normalized scour width $2s/2b_f$ according to experimental and numerical results from the models SFS_1, SFS_2 and SFS_3.

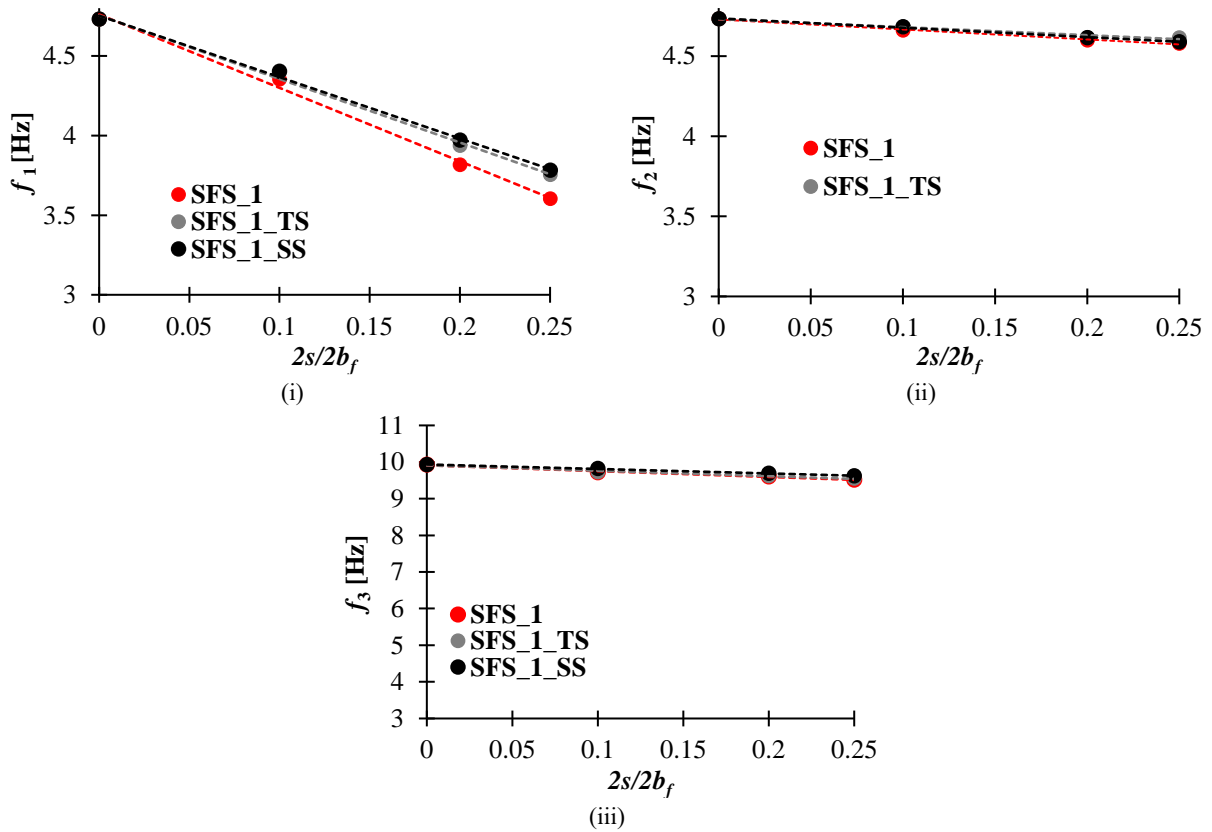


Figure 5-15: Comparison of monitored modes between the models SFS_1, SFS_1_TS and SFS_1_SS.

Table 5-3: Fundamental vibration frequencies of the models SFS_1, SFS_1_TS, SFS_1_RS_E and SFS_1_TS_E for increasing scour width.

Models	f_1 [Hz]				f_2 [Hz]				f_3 [Hz]			
	$2s/2b_f$				$2s/2b_f$				$2s/2b_f$			
	0	0.1	0.2	0.25	0	0.1	0.2	0.25	0	0.1	0.2	0.25
SFS_1	4.73	4.35	3.382	3.60	4.73	4.66	4.60	4.58	9.93	9.72	9.61	9.50
SFS_1_TS	4.73	4.44	3.94	3.75	4.73	4.68	4.62	4.59	9.93	9.73	9.62	9.55
SFS_1_RS_E	5.39	4.91	4.46	4.13	5.39	5.24	5.08	4.95	10.17	10.02	9.94	9.89
SFS_1_TS_E	5.39	4.89	4.45	4.08	5.39	5.12	4.95	4.87	10.17	10.02	9.96	9.90

Figure 5-16 compares the normalised vibration frequencies $f_{scour}/f_{no,scour}$ for increasing normalised scour width $2s/2b_f$ for the various models analysed. Similar to the models with surface foundations, the models with embedded foundation exhibit a linear reduction of the vibration frequencies for increasing scour width. However, the models with embedded foundation are slightly more sensitive to scour than the models with surface foundation, i.e., for the same value of the normalised scour width, slightly higher frequency reductions are observed. This is because for a given value of $2s/2b_f$, larger portions of soil, contributing to the stiffness of the system, are removed. For the sake of completeness, Table 5-4 shows the reduction of the vibration frequencies of the models SFS_1, SFS_1_TS, SFS_1_RS_E and SFS_1_TS_E for increasing scour widths with respect to the case of no scour.

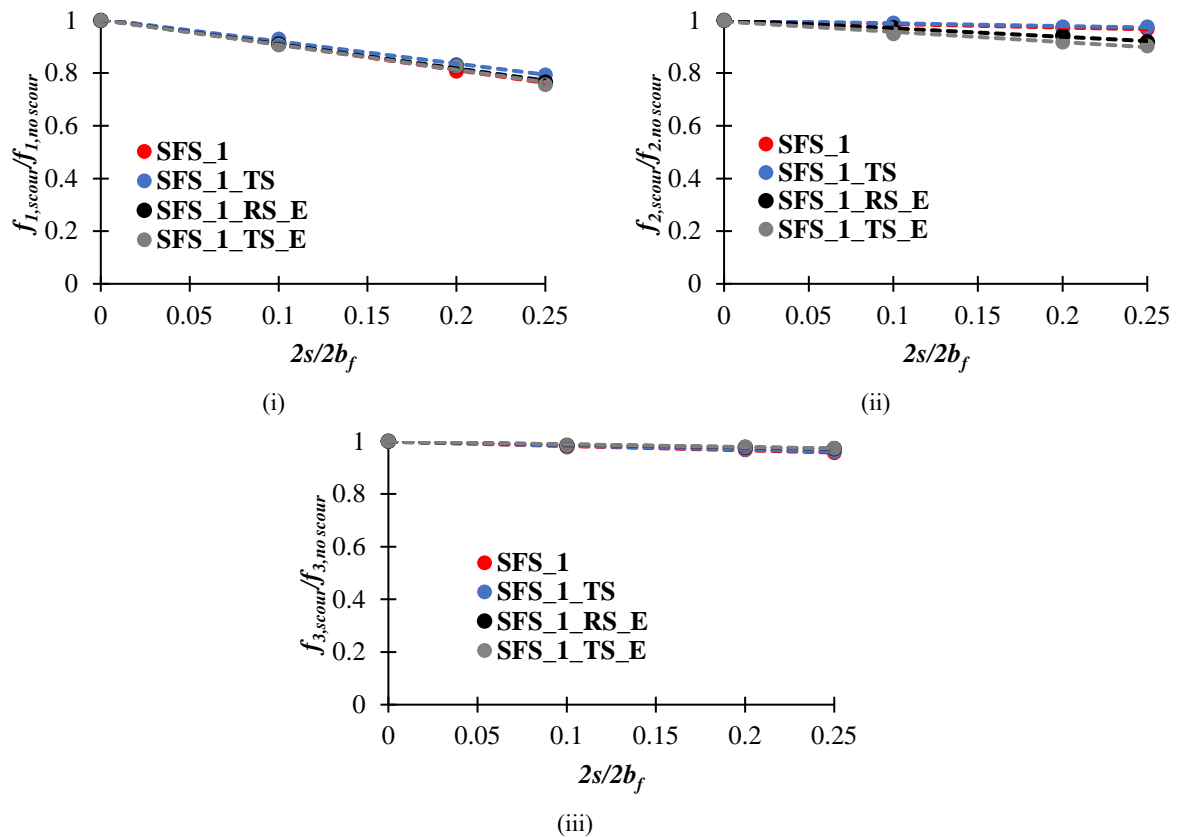


Figure 5-16: Comparison of the normalised vibration frequencies for increasing scour width between the models SFS_1, SFS_1_TS, SFS_1_RS_E and SFS_1_TS_E.

Table 5-4: Reduction of the vibration frequencies for increasing scour widths with respect to the case of no scour.

Models	Reduction of f_1 (%)			Reduction of f_2 (%)			Reduction of f_3 (%)		
	$2s/2b_f$			$2s/2b_f$			$2s/2b_f$		
	0.1	0.2	0.25	0.1	0.2	0.25	0.1	0.2	0.25
SFS_1	8.01	19.33	23.86	1.49	2.81	3.25	2.16	3.21	4.33
SFS_1_TS	7.07	16.79	20.66	1.04	2.43	2.48	2.01	3.12	3.82
SFS_1_RS_E	8.97	17.39	23.49	2.78	5.88	8.20	1.50	2.28	2.73
SFS_1_TS_E	9.41	17.40	24.44	5.11	8.31	9.80	1.48	2.11	2.66

The stress distribution of the soil in the vicinity of the scour hole is also investigated considering model SFS_1 to provide a more complete description of the effects of scour. Specifically, Figure 5-17 illustrates the vertical stresses in the soil surrounding the foundation for two different scour scenarios ($2s/2b_f = 0$ and $2s/2b_f = 0.25$). As it can be observed, scour affects the stress distribution at the soil beneath the foundation, which becomes not uniform, with high stresses localised under the foundation close to the scour hole. This is expected, due to the eccentricity between the resultant of the loads transmitted from the superstructure and the centre of the area of the foundation–soil interface providing a reaction. Nevertheless, these stresses are not expected to induce significant inelastic strains in a large portion of soil.

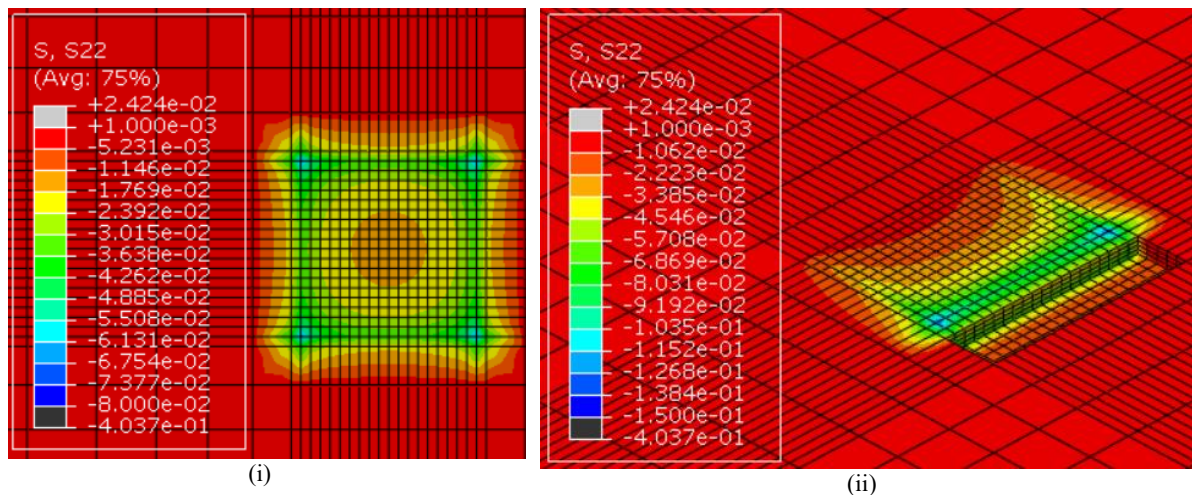


Figure 5-17: Vertical stresses distribution of the soil of the model SFS_1 for i) $2s/2b_f = 0$ and ii) $2s/2b_f = 0.25$ (unit of MPa).

In general, scour is expected to affect differently the vibration frequencies of different bridge typologies. To investigate this issue, some comparisons are made with the results obtained numerically in a previous study on Rubbianello bridge [19]. This is a multi-span masonry arch bridge with shallow foundations, which partially collapsed due to scour. Figure 5-18 compares the variation of the $f_{scour}/f_{no\ scour}$ ratio with the normalised scour width ratio $2s/2b_f$ obtained for EuroProteas (SFS_1) and for the Rubbianello bridge. It must be mentioned that in case of Rubbianello bridge only one pier is subjected to scour, and that the shallow foundation is embedded below the ground. Thus, the case of no scour (i.e., $2s/2b_f = 0$) corresponds to a scour depth equal the embedded depth of the foundation. It can be observed that in both the cases the reduction of frequency with the increase of the normalized scour width is linear.

However, in the case of the masonry arch bridge model, the rate of decay of the frequency is higher. This can be explained by the fact that the superstructure of EuroProteas undergoes an almost rigid movement and remains linear elastic even for large scour widths, whereas the masonry arch bridge undergoes severe damage and cracking. Thus, the change of frequency reflects not only the change of boundary conditions and reduction of support, but also the degradation of the system (i.e., reduction of tangent stiffness). It is also worth noting that seasonal temperature variations could affect the changes in natural frequency resulting from the variation of stiffness in the superstructure. Future work could

explore ways to distinguish these temperature-induced effects from those caused by scour to improve the reliability of vibration-based monitoring techniques. For instance, Borlenghi et al. [25] demonstrated how integrating tiltmeters with environmental sensors helps isolate temperature effects and identify scour-induced anomalies. To have more insight into how scour affects the changes of frequency in the case of different soil, foundation and superstructure properties, reference can be made to the results of the parametric study reported in Chapter 4.

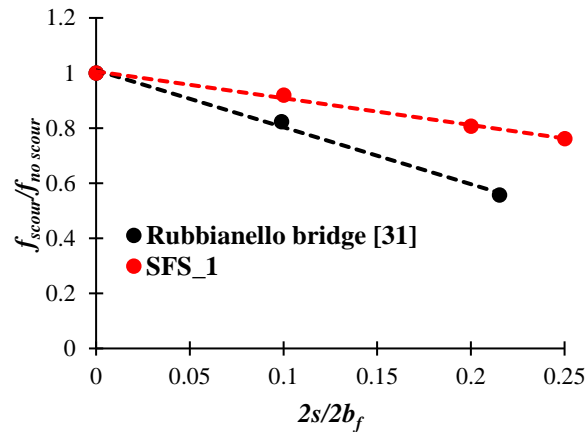


Figure 5-18: Comparison of the non-dimensional ratio $f_{scour}/f_{no\ scour}$ between EuroProteas and Rubbianello bridge.

5.4 Model updating

This subsection describes the updating of the numerical model SFS_1 carried out to obtain a better agreement with the experimental results. As discussed in Section 5.3, the presence of vegetation in the area of scour hole and under the southwest part of the foundation of EuroProteas suggests a explains the discrepancy in the dynamic behaviour of EuroProteas between the experiments and the numerical models based on a perfect soil–foundation contact. To study this issue, the model SFS_1 is considered in this section and updated to better simulate the obtained experimental results. Models SFS_2 and SFS_3 are not herein considered, although they are computationally more efficient than model SFS_1, because they cannot fully describe the dynamic behaviour of the system.

To simulate the lack of full support of the foundation at the beginning of the test, the soil elements of model SFS_1 are removed under the foundation at the location where vegetation was found (Figure 5-5ii) and modal analysis is run again on the updated model. Figure 5-19 illustrates the contact area between the soil and foundation for each of the examined scour scenarios.

The results of the modal analyses of the updated model are presented below and the consistency between the experimental and numerical results is investigated by both comparing resonance frequencies and mode shapes. As for the latter, the Modal Assurance Criterion (MAC) [24] is used to evaluate the matching of numerical and experimental mode shapes.

Figure 5-20 illustrates the corresponding modal shapes and vibration frequencies of EuroProteas. It can be noticed that the modal shapes are now in a very good agreement with the experimental ones, and the coupling is observed between the responses in the N–S and E–W directions

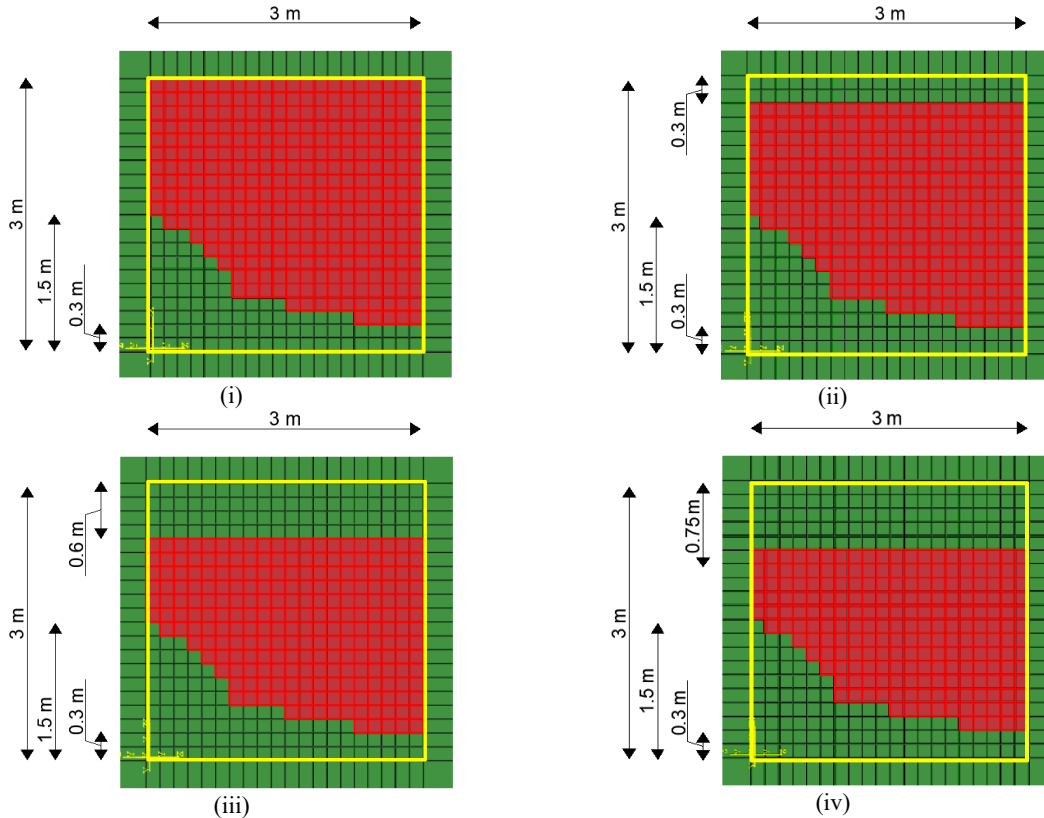


Figure 5-19: Contact area of soil-foundation interface for i) the case of no scour and for scour width ii) $2s = 0.3$ m iii) $2s = 0.6$ m and iv) $2s = 0.75$ m.

The Modal Assurance Criterion (MAC) is a useful tool for comparing pairs of modal shapes derived from numerical models to those obtained experimentally. In more detail, it is a statistical indicator sensitive to small differences in the modal shapes with values between 0 and 1, indicating null or absolute consistency between the compared pairs of mode shapes, respectively, while values higher than 0.8 indicate a satisfactory consistency. It must be mentioned that MAC must not be used for validation of the mode shapes, but solely for investigating the consistency. This is due to the fact that (i) it is unable to identify if the modal vectors are orthogonal or incomplete and (ii) it is unable to distinguish systematic errors from local discrepancies [24]. For this reason, it is important that the modal shapes to be matched are identified before applying the MAC.

Equation 5.10 expresses the MAC for two sets of mode vectors, φ_r and φ_q :

$$MAC(r, q) = \frac{|\varphi_r^T \varphi_q|^2}{(\varphi_r^T \varphi_r)(\varphi_q^T \varphi_q)} \quad (5.10)$$

where the symbol T denotes the transpose.

Table 5-5 shows the values of MAC between the experimental and numerical modes. A satisfactory consistency is achieved for all the modes and scour conditions investigated, with values significantly higher than 0.8. The torsional modal shape in particular is very well captured by the updated numerical model, whose performance generally improves for increasing levels of scour. Figure 5-21 illustrates the variation of the vibration frequencies of the updated system for increasing scour widths, together with the experimental ones. It can be noted that by updating the model SFS_1, there is also very good agreement in regards to the frequency variation. These results suggest that the assumption of a non-perfect contact between foundation and soil is valid and can explain the observed experimental results.

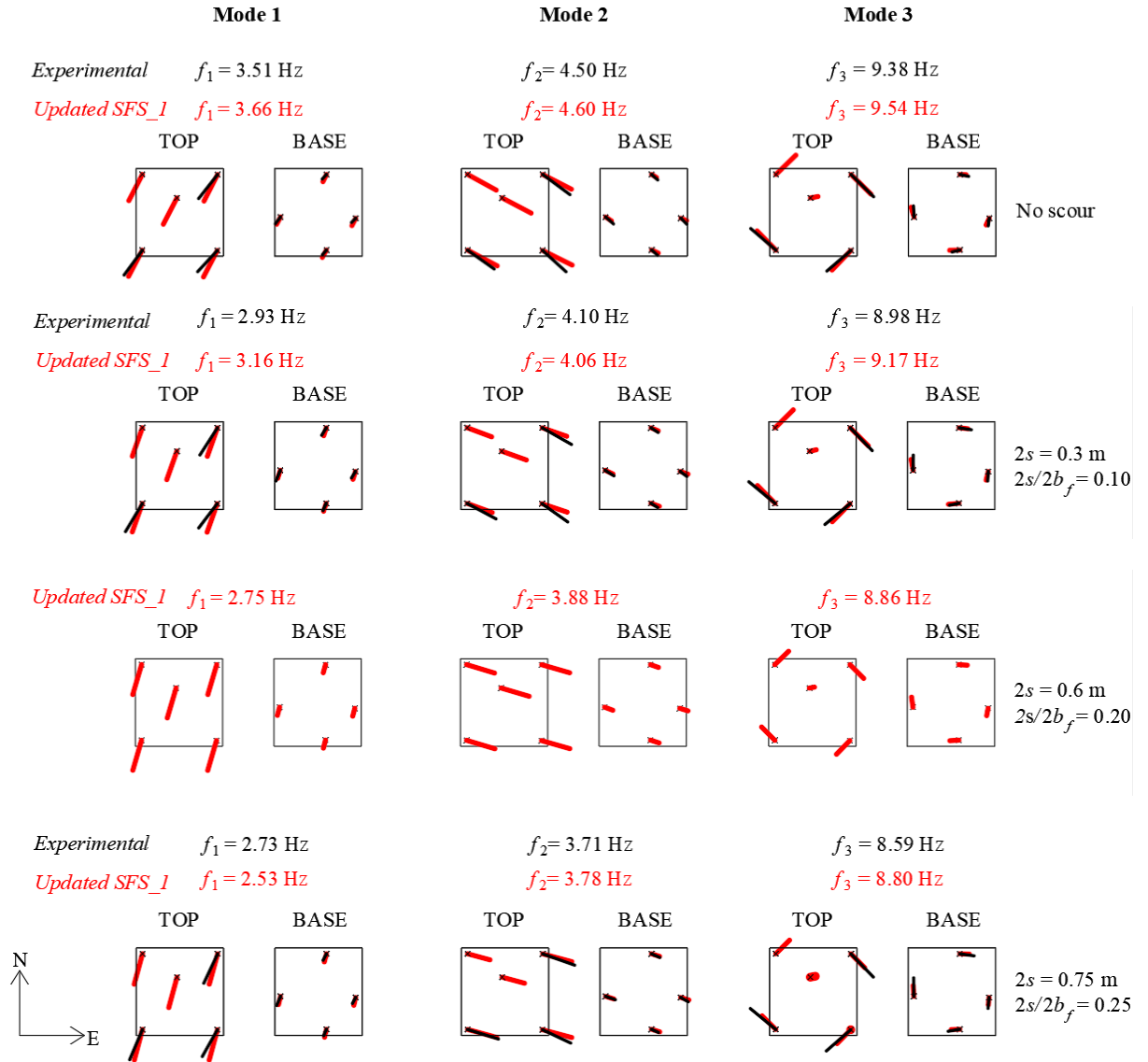


Figure 5-20: Numerical modal shapes for system with no scour, and normalised scour widths $2s/2b_f = 0.1$ m, $2s/2b_f = 0.2$ m and $2s/2b_f = 0.25$ m. Plan view of top and base horizontal displacements.

Table 5-5: MAC values between the experimental mode vectors and the matched numerical mode vectors.

$2s/2b_f$	MAC		
	Mode 1	Mode 2	Mode 3
0	0.95	0.96	0.99
0.1	0.94	0.95	0.99
0.25	0.96	0.99	0.99

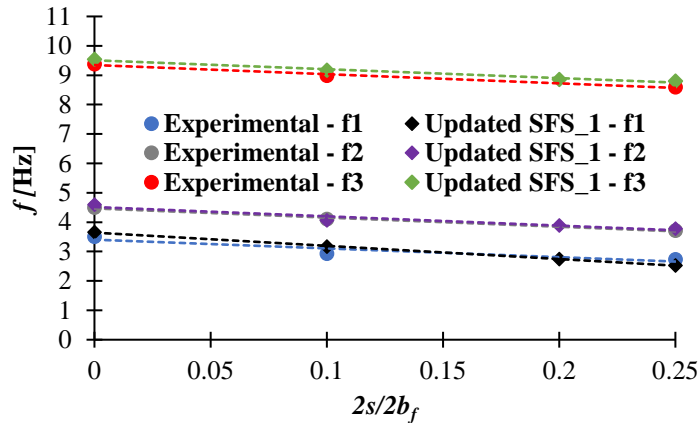


Figure 5-21: Variation of the vibration frequencies of the monitored modes with the normalized scour width $2s/2b_f$ derived by the updated SFS_1 model and experiments.

5.5 Conclusions

This paper has presented the results of an experimental campaign and numerical simulation aimed at evaluating the influence of scour on the dynamic behaviour of a structural prototype with shallow foundation. To the authors' best knowledge, this is the first study that investigates this through a full scale free-field experiment. The experimental testing campaign has also been complemented by extensive numerical analyses, investigating different modelling approaches for simulating the effects of scour on structural systems with shallow foundations.

The following observations can be made regarding the ambient vibration test results:

- a significant coupling was observed in the translational modes of vibration, even though the superstructure of EuroProteas is a symmetric system along both the horizontal principle axes. This was explained by the established non-uniform contact between the foundation and the soil. Although this result cannot be generalised and is out of interest, it is indeed very important and demonstrates the impact of the various uncertainties and not controllable/unexpected factors that accompany in-field testing.
- a linear reduction of the vibration frequencies of the three modes investigated (two translational plus one torsional) is observed for increasing scour widths. The reduction of frequency of vibration for 1/4 of scoured foundation width is of the order of 30%, 18% and 8%, respectively, for the first, second and third vibration mode.

Based on the simulation of the experimental tests, the following conclusions can be drawn:

- the investigated modelling approaches provide similar results in terms of reduction of vibration frequency of the system for increasing scour widths;
- the vibration frequencies of the system reduce significantly for increasing values of the normalised scour width, whereas they are not significantly affected by the scour hole shape (e.g., rectangular or triangular); the on the vibration frequency of the system and on the frequency reduction for increasing scour widths;
- the three dimensional modelling strategy, describing the soil as a continuum with absorbing boundaries, can provide very accurate estimates of the vibration modes and frequencies of the system for all the investigated scour scenarios, provided that the non-uniform contact between the soil and the foundation is modelled accurately.

These study results are very relevant for the development of strategies for monitoring bridges at risk of scour through vibration-based techniques. In this regard, it should be specified that the scour results in very different effects, in terms of change of vibration frequency, on different systems. For example, in the investigated case, characterised by a significant foundation rocking and a superstructure behaving linearly also for large scour widths, the frequency reduction due to scour is overall not very significant.

In more complex structural systems with the superstructure behaving nonlinearly due to damage and cracking even under moderate levels of scour, as in the case of masonry arch bridges, the frequency reduction is expected to be even more significant in comparison to the investigated case.

Finally, the experimental results and interpretation of the force–vibration tests will be the object of future studies, which will also investigate the influence of scour on the kinematic and inertial interaction of bridges with scoured shallow foundations under seismic input, by considering more realistic soil profile scenarios and bridge configurations. These studies will also explore the effects of temperature variations, material degradation, and cracking to better distinguish their impact on frequency changes from those caused by scour. Future studies will also investigate further the effects of scour on EuroProteas structure for higher scour widths by assuming a non-linear soil behaviour, where non-linear phenomena are expected to be significant. These results will be used to inform the design and assessment of bridges subjected to scour and earthquake hazards, and will provide evidence for the development of the next generation of Eurocode 8–2.

References

- [1] DYMOBRIS EU Project. Available: <http://www.infrastructuresilience.com/dymobris/>
- [2] D. Pitilakis, E. Rovithis, A. Anastasiadis, A. Vratsikidis, M. Manakou, "Field evidence of SSI from full-scale structure testing", *Soil Dynamics and Earthquake Engineering*, vol. 112, pp. 89-106, 2018.
- [3] A. Vratsikidis, D. Pitilakis, A. Anastasiadis, A. Kapouniaris, "Evidence of soil-structure interaction from modular full-scale field experimental tests", *Bulletin of Earthquake Engineering*, vol. 20, issue 7, pp. 3167-3194, 2022.
- [4] X. Wang, B. Ji, A. Ye, "Seismic Behavior of Pile-Group-Supported Bridges in Liquefiable Soils with Crusts Subjected to Potential Scour: Insights from Shake-Table Tests", *Journal of Geotechnical and Geoenvironmental Engineering*, vol 146, issue 5, 04020030, 2020.
- [5] G. G. Prasad, S. Banerjee, "The impact of flood-induced scour on seismic fragility characteristics of bridges", *Journal of Earthquake Engineering*, vol. 17, issue 6, pp. 803-828, 2013.
- [6] H. He, K. Wei, J. Zhang, S. Qin, "Application of endurance time method to seismic fragility evaluation of highway bridges considering scour effect", *Soil Dynamics and Earthquake Engineering*, vol. 136, 106243, 2020.
- [7] Y. Shang, A. Alipour, A. Ye, "Selection of Input Motion for Seismic Analysis of Scoured Pile-Supported Bridge with Simplified Models", *Journal of Structural Engineering*, vol. 144, issue 8, 04018099, 2018.
- [8] A. Fioklou, A. Alipour, "Significance of non-uniform scour on the seismic performance of bridges", *Structure and Infrastructure Engineering*, vol. 15, issue 6, pp. 822-836, 2019.
- [9] M.V. Manakou, D.G. Raptakis, F.J. Chávez-García, P.I. Apostolidis, K.D. Pitilakis, "3D soil structure of the Mygdonian basin for site response analysis", *Soil Dynamics and Earthquake Engineering*, vol. 30, issue 11, pp. 1198-1211, 2010.
- [10] D. Raptakis, N. Theodulidis, K. Pitilakis, "Data analysis of the euroseistest strong motion array in Volvi (Greece): standard and horizontal-to-vertical spectral ratio techniques", *Earthquake Spectra*, vol. 14, issue 1, pp. 203-224, 1998.
- [11] D. Raptakis, F. Chávez-García, K. Makra, K. Pitilakis, "Site effects at EuroSeistest-I. Determination of the valley structure and confrontation of observations with 1D analysis", *Soil Dynamics and Earthquake Engineering*, vol. 19, issue 1, pp. 1-22, 2000.
- [12] K. Pitilakis, D. Raptakis, K. Lontzetidis, T. Tika-Vasilikou, D. Jongmans, "Geotechnical and geophysical description of EUROSEISTEST, using field, laboratory tests and moderate strong motion records", *Journal of Earthquake Engineering*, vol. 3, issue 03, pp. 381-409, 1999.
- [13] S.O. Lee, I. Abid, S.H. Hong, "Effect of complex shape of pier foundation exposure on time development of scour", *Environmental Fluid Mechanics*, vol. 21, pp. 103-127, 2021.
- [14] Abaqus V. 6.14 Documentation, Dassault Systemes Simulia Corporation, 2014.
- [15] MATLAB and Statistics Toolbox Release 2012b, The MathWorks, Inc., Natick, Massachusetts, United States.
- [16] Seismic Engineering Research Infrastructures for European Synergies, Report on field testing for assessing input motion and SSI, Project No.: 227887, 2012.
- [17] R.L. Kuhlemeyer, J. Lysmer, "Finite element method accuracy for wave propagation problems", *Journal of the Soil Mechanics and Foundation Division*, vol. 99, issue 5, pp. 421-427, 1973.
- [18] E. Tubaldi, L. Macorini, B.A. Izzuddin, "Three-dimensional mesoscale modelling of multi-span masonry arch bridges subjected to scour", *Engineering Structures*, vol. 165, pp. 486-500, 2018.
- [19] F. Scozzese, L. Ragni, E. Tubaldi, F. Gara, "Modal properties variation and collapse assessment of masonry arch bridges under scour action", *Engineering Structures*, vol. 199, 109665, 2019.
- [20] G. Gazetas, "Formulas and charts for impedances of surface and embedded foundations", *Journal of Geotechnical Engineering*, vol. 117, issue 9, pp. 1363-1381, 1991.
- [21] J.P. Wolf, "Soil-Structure-Interaction Analysis in Time Domain", *Nuclear Engineering and Design*, vol. 111, issue 3, pp. 381-393, 1989.
- [22] Z. Hryniewicz, "Dynamic Response of a Rigid Strip on an Elastic Half-Space", *Computer Methods in Applied Mechanics and Engineering*, vol. 25, issue 3, pp. 355-364, 1981.

- [23] S. Tileylioglu, J.P. Stewart, R.L. Nigbor, “Dynamic stiffness and damping of a shallow foundation from forced vibration of a field test structure”, *Journal of Geotechnical and Geoenvironmental Engineering*, vol. 137, issue 4, pp. 344-353, 2011.
- [24] R. Brincker, L. Zhang, P. Andersen, “Modal identification of output-only systems using frequency domain decomposition”, *Smart Materials and Structures*, vol. 10, issue 3, pp. 441-445, 2001.
- [25] P. Borlenghi, G. Gentile, M. D’Angelo, F. Ballio, “Long-term monitoring of a masonry arch bridge to evaluate scour effects”, *Construction and Building Materials*, vol. 411, 134580, 2024.
- [26] M. Pastor, M. Binda, T. Harčarik, “Modal Assurance Criterion”, *Procedia Engineering*, vol. 48, pp. 543-548, 2012.

6 Dynamic behaviour and seismic response of scoured bridge piers

This study explores the transverse response of bridge piers in riverbeds under a multi-hazard scenario, involving seismic actions and scoured foundations. The combined impact of scour on foundations' stability and on the dynamic stiffness of soil-foundation systems makes bridges more susceptible to earthquake damage. While previous research has extensively investigated this issue for bridges founded on piles, this work addresses the less-explored but critical scenario of bridges on shallow foundations. A comprehensive soil-foundation structure model is developed to be representative of the transverse response of multi-span and continuous girder bridges, and the effects of different scour scenarios and foundation embedment on the dynamic stiffness of the soil-foundation sub-systems are investigated through refined finite element models. Then, a parametric investigation is conducted to assess the effects of scour on the dynamic properties of the systems and, for some representative bridge prototypes, the seismic response at scoured and non-scoured conditions are compared considering real earthquakes. The research results demonstrate the significance of scour effects on the dynamic properties of the soil-foundation structure system and on the displacement demand of the bridge decks.

From the analysis of the literature, it is evident that further research is needed to investigate the influence of scour on the dynamic behaviour and seismic response of bridges with shallow foundations. Building on the previous work carried out in Chapter 4, this chapter aims to fill this knowledge gap. In particular, the main novelty aspect of this study are: 1) a more complex and realistic superstructure model has been considered, by including more degrees of freedom for the superstructure compared to the model of Chapter 4 and Chapter 5, where the superstructure is treated as a SDOF system, 2) impedance functions have been derived by considering different values of the embedded depth of the foundation, as opposed to zero embedment in Chapter 4, 3) the analysis of the seismic response of bridge prototypes is carried out, whereas in Chapter 4 it was investigated only the variation of fundamental frequency.

Section 6.1 illustrates the investigated SFS system, and the modelling approach for the estimation of the foundation impedance functions, the dynamic behaviour and the seismic response of the SFS system for different scour scenarios. Section 6.2 presents the impedance functions for the various scour and embedded depth cases considered. Section 6.3 presents the result of an extensive parametric study investigating the effect of scour on the SFS system, for a wide range of superstructure mechanical and geometrical properties and soil conditions. Section 6.4 investigates the seismic response of some representative bridge prototypes by means of time-history analyses. The Conclusion section summarises the main findings of the study and future works needed. The content of this chapter is based on peer-reviewed journal publication, with minor modifications. The research was conducted in collaboration with Enrico Tubaldi, Sandro Carbonari, Fabrizio Gara and Francesca Dezi (Table 1-1).

6.1 Model description

This section describes the modelling approach followed to estimate the impedance functions of a massless rigid strip foundation rigidly resting on a homogenous elastic soil domain for various embedded depths and scour scenarios. The modelling approach, developed in Chapter 4, considers a more complex superstructure model and a shallow foundation with different embedded depths rather than one simply resting on the ground surface.

A substructure approach is employed, where the SFS system is divided into two parts, the soil medium and the superstructure. Firstly, the foundation impedance functions for the soil-foundation system are derived numerically by analysing in Abaqus [1] a massless rigid strip foundation resting on a homogeneous elastic soil domain. Then, the derived impedance functions are used to analyse the in-

plane dynamic behaviour and seismic response of a bridge pier, modelled as a multi-degree-of-freedom (MDOF) system.

6.1.1 Soil-foundation system and impedance functions

The frequency-dependent impedance functions governing the dynamic response of the soil-foundation system in the frequency domain are described by the following set of equations:

$$\begin{bmatrix} P(\omega) \\ Q(\omega) \\ M(\omega)/b_f \end{bmatrix} = \begin{bmatrix} k_{zz} + id_{zz} & 0 & 0 \\ 0 & k_{xx} + id_{xx} & k_{xy} + id_{xy} \\ 0 & k_{xy} + id_{xy} & k_{yy} + id_{yy} \end{bmatrix} \begin{bmatrix} w_0(\omega) \\ u_0(\omega) \\ \varphi_0(\omega)b_f \end{bmatrix} \quad (6.1)$$

where w_0 , u_0 are the displacement amplitudes along the z and x directions of the master node (i.e., the node at the centroid of the foundation at the level of the soil-foundation interface), and φ_0 is the rotation amplitude. Subsequently, P and Q denote the developing forces along the z and x directions at the master node respectively, whereas M denotes the overturning moment. The frequency-dependent quantities k_{ij} and $d_{ij}=c_{ij}\omega$ denote the real and the imaginary parts, respectively, of the impedance functions, describing the foundation response in the i -th direction due to the excitation in the j -th direction. Figure 6-1 illustrates forces and displacements along the various directions.

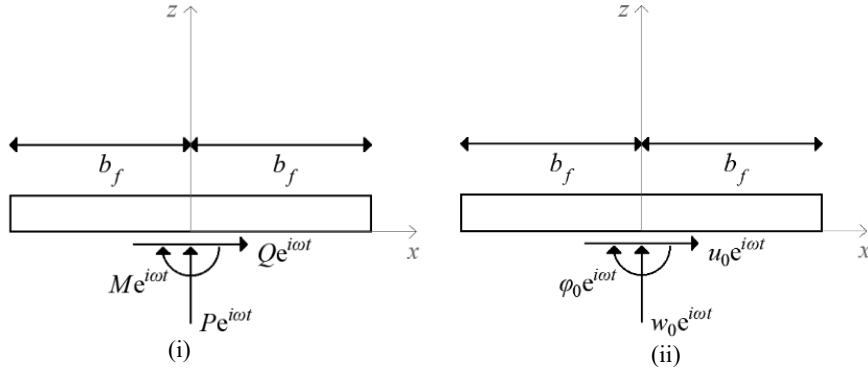


Figure 6-1: (i) Forces and (ii) displacements of the strip foundation.

The frequency dependent impedance functions are derived by considering a plain-strain finite element (FE) model of the soil domain, developed in Abaqus [1] for the various investigated embedment depth and scour scenarios. The soil beneath the foundation is assumed to be homogeneous and described by the shear modulus G , the shear wave velocity V_s , the density ρ_s and the Poisson's ratio ν . The ratio between the height and width of the foundation is assumed to be fixed and equal to $h_f/b_f = 0.3$, whereas the Poisson's ratio $\nu = 0.4$. The assumed values are representative of many real bridges with shallow foundation built on sandy soil. Furthermore, it must be noted that the use of a higher value of Poisson's ratio compared to 0.25 and 0.3 in Chapter 4 and 5 respectively, represents better the submerged and saturated soil conditions surrounding scoured bridge foundations, due to the increased lateral soil deformation under axial loading. This distinction ensures that the numerical analyses realistically capture the dynamic behaviour of SFS systems under real-world conditions. Further details about the FE modelling strategy can be found in Section 4.1.1.

A rigid body constraint is applied to the set of nodes at the interface between the soil and the foundation. For the embedded cases, the soil located adjacent to the bridge pier over the foundation is disregarded, by assuming that its contribution in terms of mass and stiffness is negligible with respect to that of the soil below the foundation. On the contrary, the soil located on the lateral sides of the foundation is assumed to be perfectly bonded to the foundation itself and contributes to the translational and rotational response of the soil-foundation system.

The impedance functions are evaluated with a steady-state analysis, by subjecting the master node to a harmonic unit amplitude displacement along a direction (while restraining the others) and by measuring the corresponding reaction forces along the various directions. It must be mentioned that the modelling approach was validated in Chapter 4. The validation was based on the comparison between the impedance functions derived numerically in Abaqus (Figure 6-2i) with those obtained by Hryniewicz [2] for a model with zero embedded depth and no scour, and for a Poisson's ratio $\nu = 0.25$. In the present study, the model considered in Chapter 4 is expanded by considering various embedded depths of the foundation for the estimation of the impedance functions (Figure 6-2ii). In particular, three more different embedded depths and three scour layouts are considered (see Section 6.2), for a total of 12 models. The scour hole is assumed to have a fixed triangular shape (Figure 6-3), which is defined by the portion of the foundation base that is undermined ($2s$). The assumed shape is based on flume tests (see [3] for a more in-depth discussion about this). Numerical analyses carried out in Chapter 5 suggest that the dynamic behaviour of structures with shallow foundations affected by scour is not significantly affected by the scour hole shape (e.g., rectangular or triangular), as long as they result in the same portion of the foundation being undermined. However, experimental studies carried out by Ciancimino et al. [4] on a model with caisson foundation have proven that the scour hole shape and the type of scour (i.e. general rather than local) have a strong influence on the dynamic response of bridge piers. Nevertheless, a thorough investigation of the influence of the scour hole shape on the dynamic impedances of the foundation, albeit very interesting, is out of the scope of the present study.

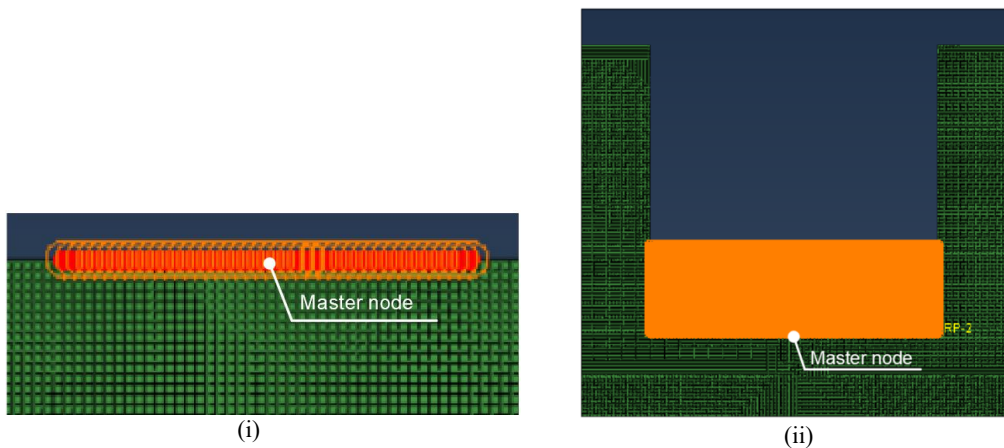


Figure 6-2: Rigid body constraint used to simulate the massless rigid strip foundation for the case of i) no embedment and ii) embedment depth.

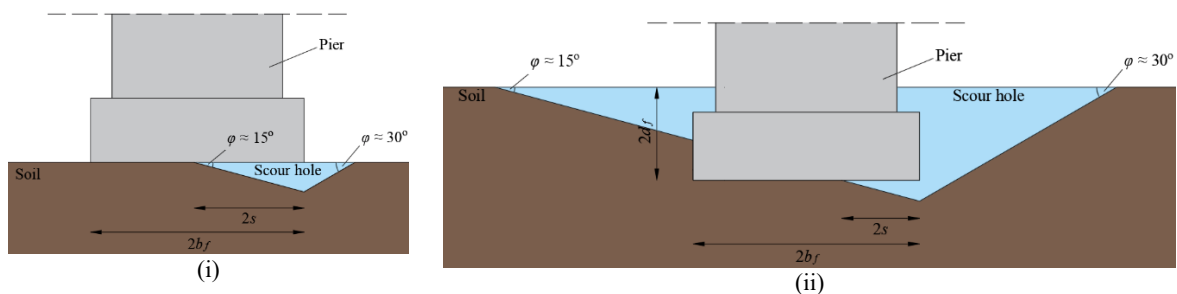


Figure 6-3: Geometry of the considered triangular scour hole for a i) no-embedded, ii) embedded foundation.

6.1.2 Superstructure

Figure 6-4 and Figure 6-5 illustrate the bridge pier and the analytical model of the SFS system considered in this work for studying the transverse response of the overall SFS system. To the authors' knowledge, this is the first study that investigates the influence of scour on the transverse dynamic behaviour of bridge piers with shallow foundations, by considering a Multiple Degree of Freedom (MDOF) model for describing the superstructure. The model is suitable to capture the transverse dynamic behaviour of piers in multi-span continuous bridges (sufficiently far from the abutments that may interact with the pier in carrying the lateral forces if equipped with fixed restraints in the transverse

direction) and to predict the longitudinal and transverse response of piers in multi-span simply supported bridges where each pier is responsible for its relative tributary mass (i.e the mass of one span).

The SFS system consists of a rigid foundation with mass m_f , a flexible pier with mass m_p lumped at the top and bottom nodes, a rigid pier cap with mass m_c , the bridge bearings with stiffness k_b (in case of isolated bridges), and the top mass, representative of the deck inertia m_d . The *dof* of the system are constituted by the transverse displacement of the bridge deck, the transverse displacement and rotation of the pier head and the transverse displacement and rotation at the bottom of the foundation. The soil-structure interaction is taken into account by the previously estimated impedance functions. The pier is treated as an Euler-Bernoulli beam element, having the following stiffness matrix \mathbf{K}_p :

$$\mathbf{K}_p = \begin{bmatrix} k_{11} & k_{12} & k_{13} & k_{14} \\ k_{21} & k_{22} & k_{23} & k_{24} \\ k_{31} & k_{32} & k_{33} & k_{34} \\ k_{41} & k_{42} & k_{43} & k_{44} \end{bmatrix} = \begin{bmatrix} \frac{12EJ}{h_p^3} & -\frac{6EJ}{h_p^2} & -\frac{12EJ}{h_p^3} & -\frac{6EJ}{h_p^2} \\ \frac{6EJ}{h_p^2} & 4EJ & \frac{6EJ}{h_p^2} & 2EJ \\ -\frac{12EJ}{h_p^3} & \frac{6EJ}{h_p^2} & \frac{12EJ}{h_p^3} & \frac{6EJ}{h_p^2} \\ -\frac{6EJ}{h_p^2} & 2EJ & \frac{6EJ}{h_p^2} & 4EJ \end{bmatrix} \quad (6.2)$$

where E and J are the elastic modulus and second moment of area of the cross-section of the pier, respectively.

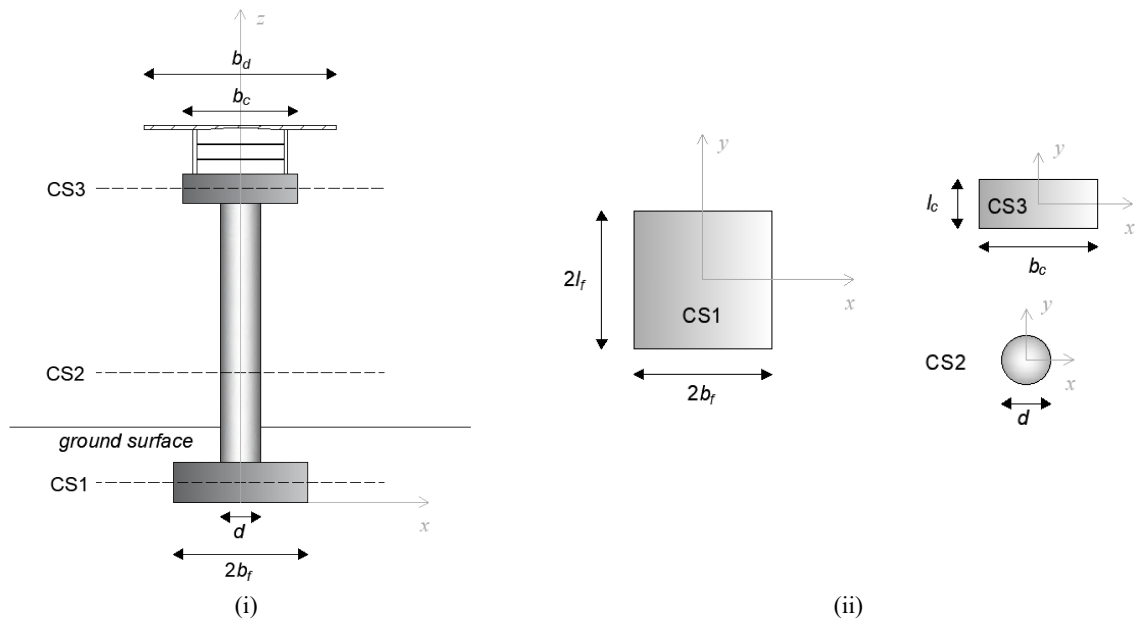


Figure 6-4: i) Considered bridge pier, ii) geometry of the system components.

$$\mathbf{M} = \begin{bmatrix} m_d & 0 & 0 & 0 & 0 \\ 0 & m_c + \frac{m_p}{2} & m_c \frac{h_c}{2} & 0 & 0 \\ 0 & m_c \frac{h_c}{2} & m_c \frac{h_c^2}{4} & 0 & 0 \\ 0 & 0 & 0 & \frac{m_p}{2} + m_f & m_p h_f + m_f h_f \\ 0 & 0 & 0 & m_p h_f + m_f h_f & 2m_p h_f^2 + m_f h_f^2 \end{bmatrix} \quad (6.8)$$

$$\mathbf{R} = \begin{bmatrix} 1 \\ 1 \\ 0 \\ 1 \\ 0 \end{bmatrix} \quad (6.9)$$

The natural frequency of the system can be estimated based on the Frequency Response Function (FRF). This can be obtained by evaluating the amplitude of $\bar{\mathbf{U}}$ under unit harmonic excitations with different frequencies. The peaks of the FRFs of the components of $\bar{\mathbf{U}}$ allow to identify the fundamental frequency of the SFS system.

6.2 Soil-foundation system impedance functions

This section illustrates the impedance functions of the soil-foundation system obtained following the modelling approach described in the previous section for four different embedded depths and various scour scenarios. The following values of the ratio of the embedded depth ($2d_f$) over the foundation width ($2b_f$) are considered: i) $d_f/b_f = 0$, ii) $d_f/b_f = 0.3$, iii) $d_f/b_f = 0.7$ and iv) $d_f/b_f = 1.0$. The scour hole scenarios are based on a triangular shape, illustrated in Figure 6-3 and Figure 6-6, They are hereafter labelled with: i) “NS”, i.e. no scour, ii) “TS1/4”, i.e. one fourth of the width of the foundation scoured, iii) “TS3/8”, i.e. three eighth of the width of the foundation scoured, and iv) “TS1/2”, i.e. half the width of the foundation scoured. The impedance functions are expressed in non-dimensional form as a function of the non-dimensional frequency $a_0 = \omega b_f / V_s$, where ω is the circular frequency of the excitation, and V_s is the soil shear wave velocity.

Figure 6-7 to Figure 6-10 illustrate the variation of the real and imaginary parts of the non-dimensional impedance functions as a function of the non-dimensional frequency a_0 for each embedded depth and scour scenario considered. Figure 6-11 to Figure 6-14 provide an alternative comparison of the impedance functions where the effect of the embedded depth is highlighted.

In general, in the case of zero embedment (Figure 6-7), both the real and the imaginary parts of the impedance functions decrease by increasing the scour width. Only the real and imaginary parts of k_{xry} and d_{xry} , namely the components expressing the coupling between the rotational and translational response, do not follow this trend, since they increase with scour, and particularly for the real component (k_{xry}) and for high values of the dimensionless frequency a_0 . The sign difference of the k_{xry} between the no scoured and scoured cases for high values of a_0 implies that when the no scoured foundation moves laterally, it tends to rotate in a counterclockwise direction, while the opposite occurs for the scoured foundations. The plots of Figure 6-7 for the case of zero embedment are very similar to those reported in Chapter 4, with only some differences in values due to the higher value of the Poisson’s ratio considered in this study (0.4 instead of 0.25). As a result of this, higher values are obtained for the real part of the impedance functions k_{xx} and k_{ryy} in this study.

With regards to the cases with embedded depth higher than zero, not considered in Chapter 4, in general there is also a significant reduction of the absolute terms of the real and imaginary parts of the impedance functions for increasing levels of scour width/foundation width ratio. Exception is the translational component k_{xx} for the case corresponding to $d_f/b_f = 0.3$, which increases for increasing scour width and depth for dimensionless frequency higher than 1.9. That means that the lateral

displacement of a foundation with a low embedded depth on a soft soil with a high excitation frequency is more significant in the case of no scour than in the case of scour. Furthermore, there is a dramatic decrease of the terms k_{xry} and d_{xry} of the scoured cases for the various embedded depths for increasing a_0 compared to the no scoured cases. This can be explained by the fact that the scoured foundation tends to behave as a foundation with no embedment due to the removal of the lateral soil contribution. A minor effect of the embedment level on the impedance functions of the scoured cases can be observed in Figure 6-12 to Figure 6-14. More in detail, the impedance functions of the system and their sensitivity to scour are significantly affected by the embedment depth. However, by increasing the level of embedment from $d_f/b_f = 0.3$ to 1, results are only mildly affected, leading to lower values of the components k_{xry} and d_{xry} and higher values of the components k_{ryry} and d_{ryry} . It is noteworthy that the scour hole geometry changes significantly with the embedment depth (Figure 6-3 and Figure 6-6).

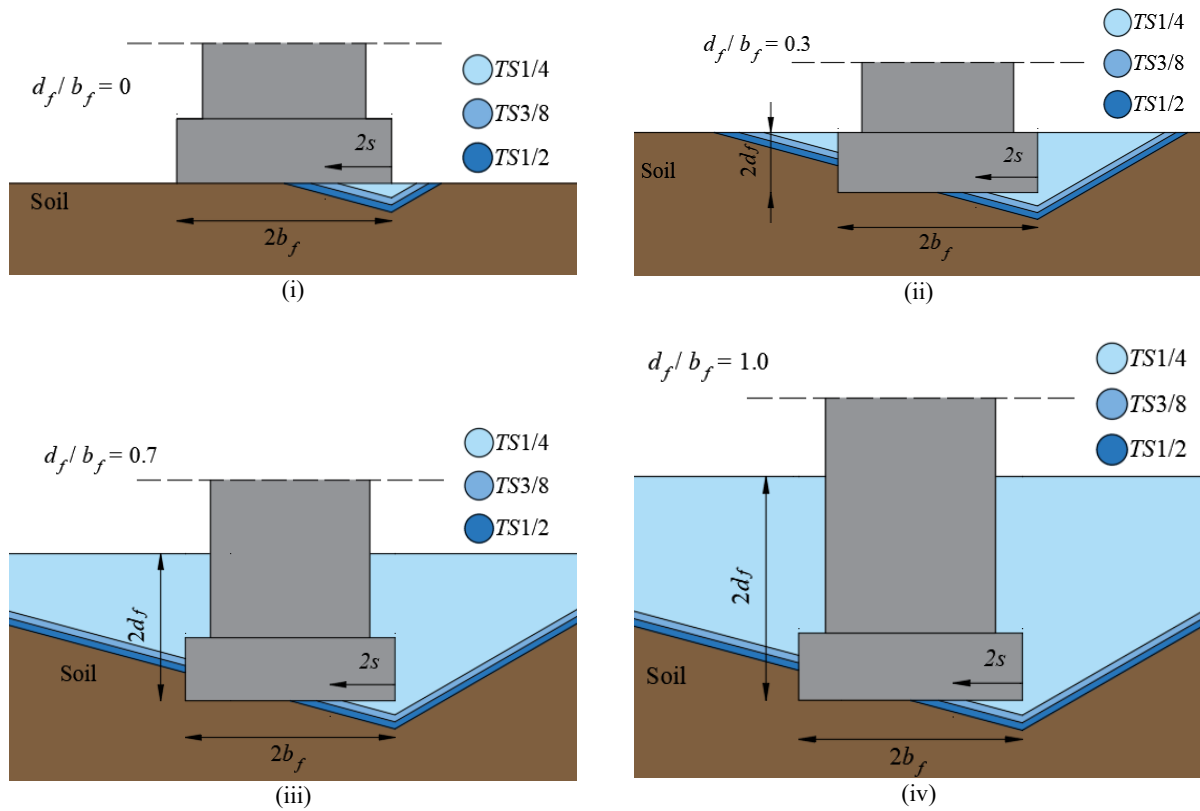


Figure 6-6: Scour scenarios investigated for different embedded depth i) $d_f/b_f = 0$ ii) $d_f/b_f = 0.3$ iii) $d_f/b_f = 0.7$ iv) $d_f/b_f = 1.0$.

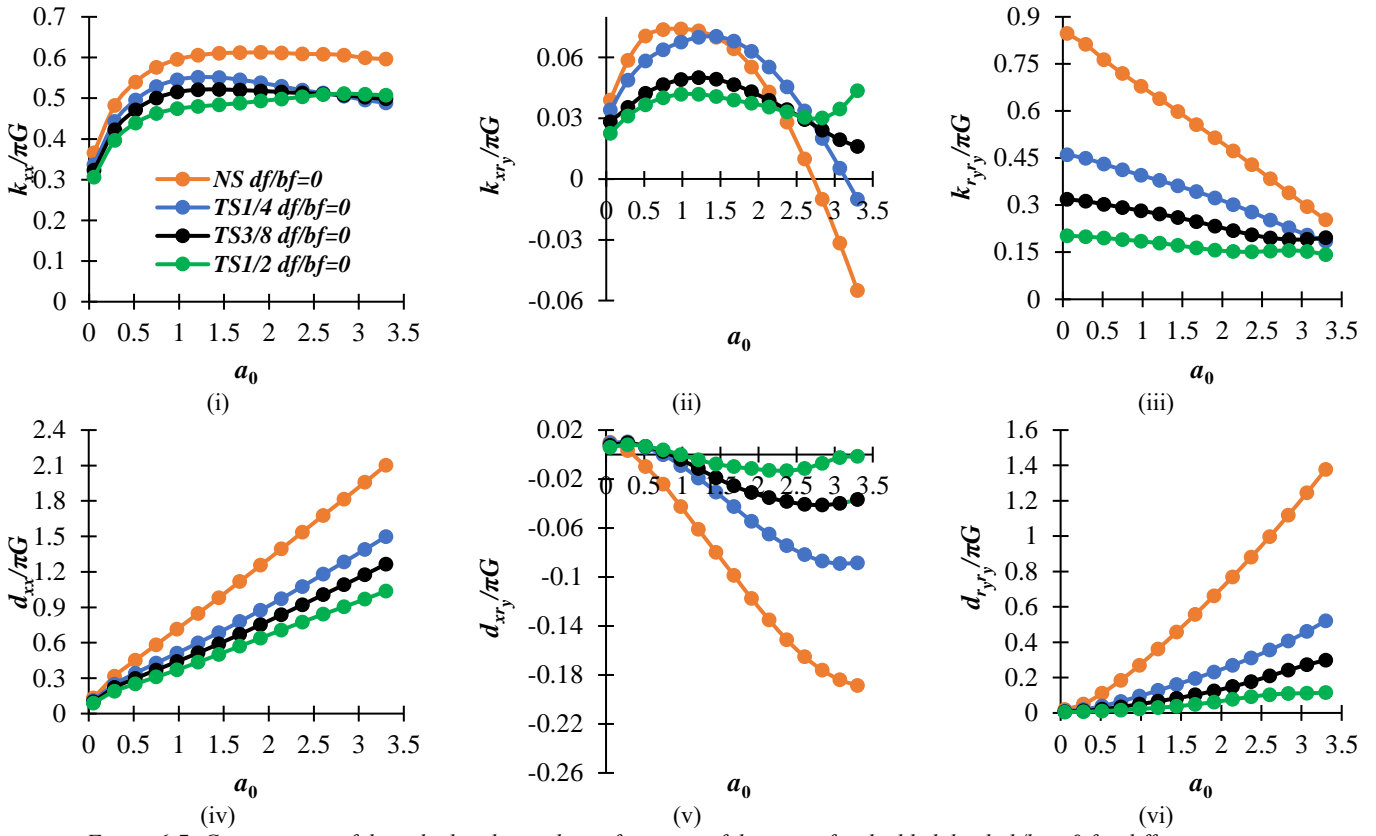


Figure 6-7: Comparisons of the calculated impedance functions of the case of embedded depth $d_f/b_f = 0$ for different scour scenarios i) k_{xx} ii) k_{xy} iii) k_{rxy} iv) d_{xx} v) d_{xy} vi) d_{rxy}

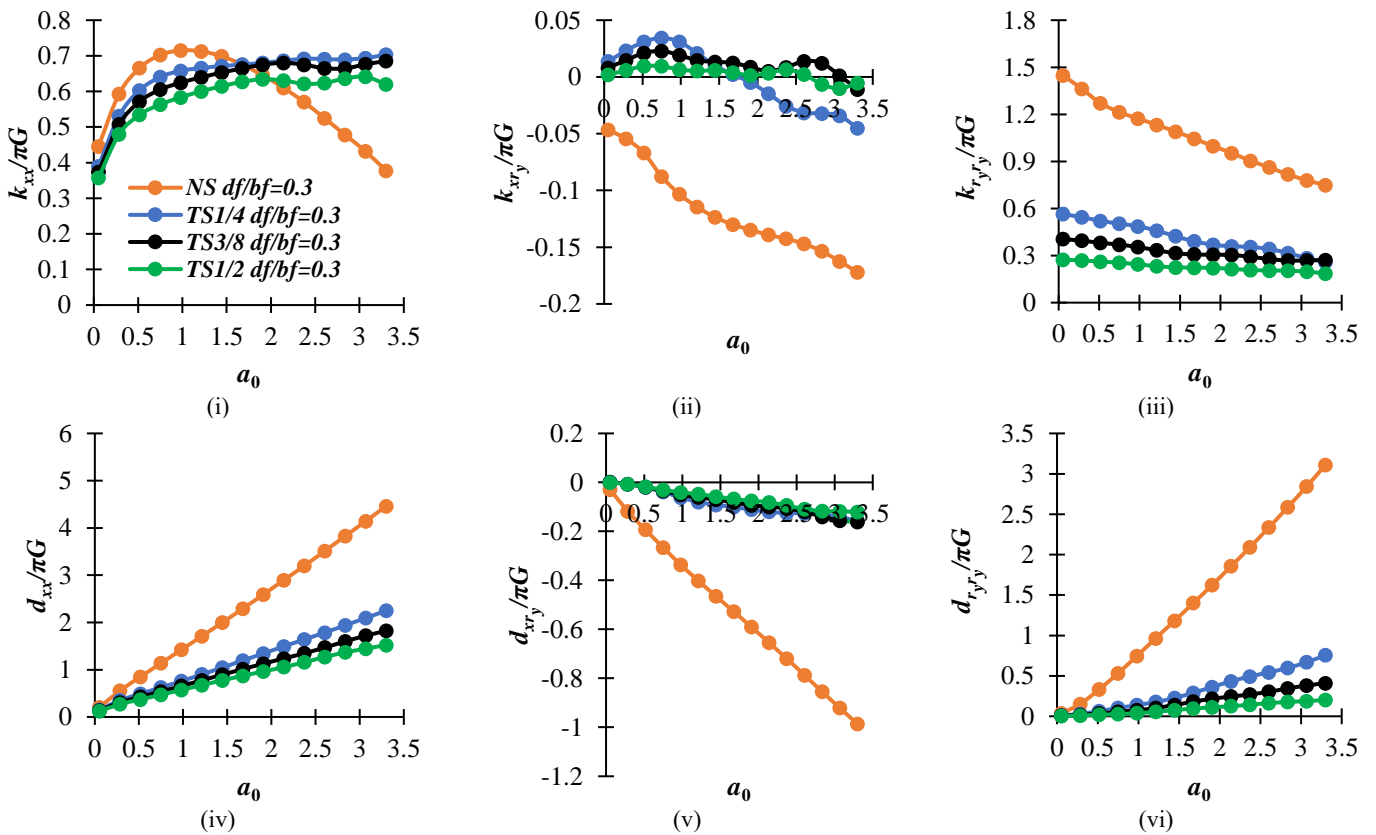


Figure 6-8: Comparisons of the calculated impedance functions of the case of embedded depth $d_f/b_f = 0.3$ for different scour scenarios i) k_{xx} ii) k_{xy} iii) k_{rxy} iv) d_{xx} v) d_{xy} vi) d_{rxy}

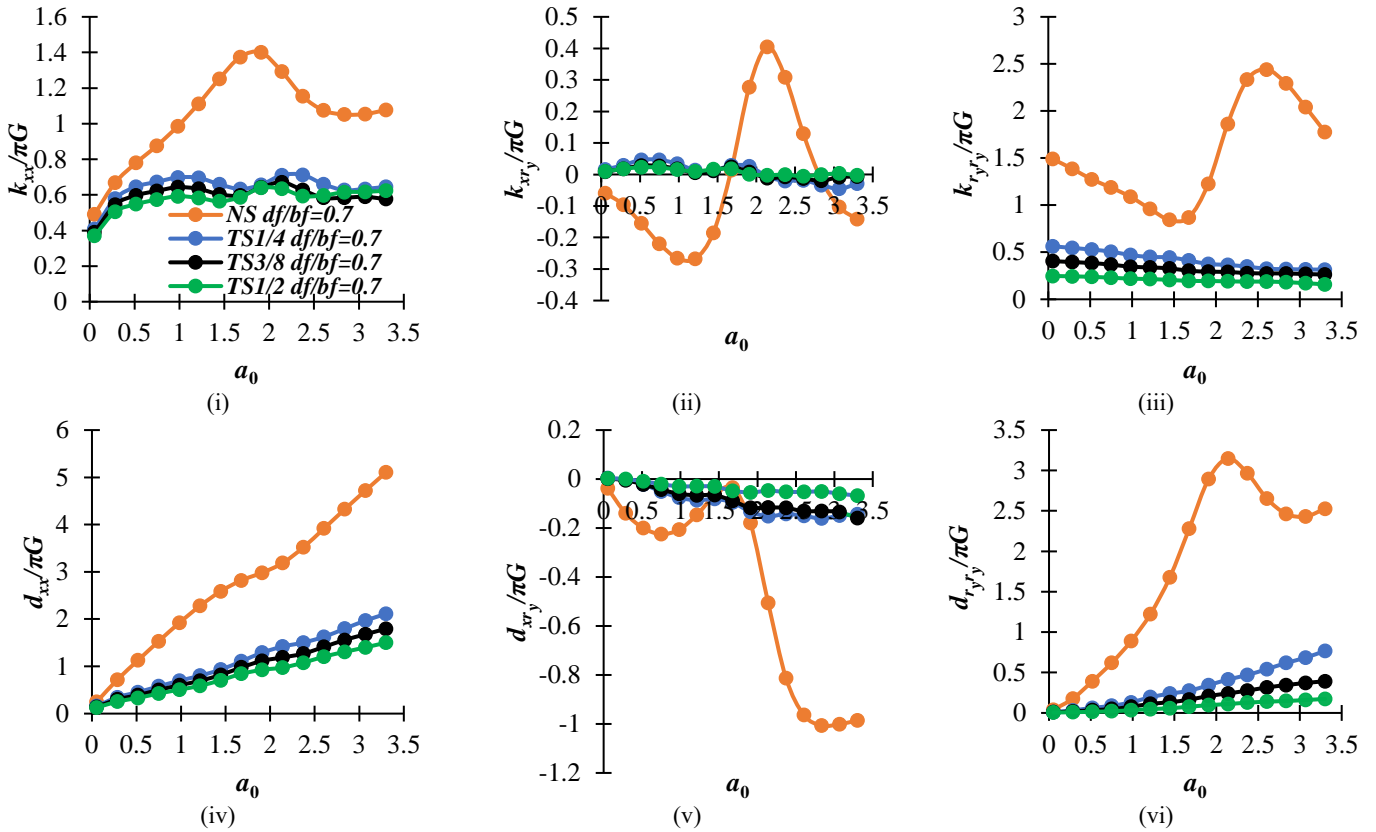


Figure 6-9: Comparisons of the calculated impedance functions of the case of embedded depth $d_f/b_f = 0.7$ for different scour scenarios i) k_{xx} ii) k_{xy} iii) k_{yy} iv) d_{xx} v) d_{xy} vi) d_{yy}

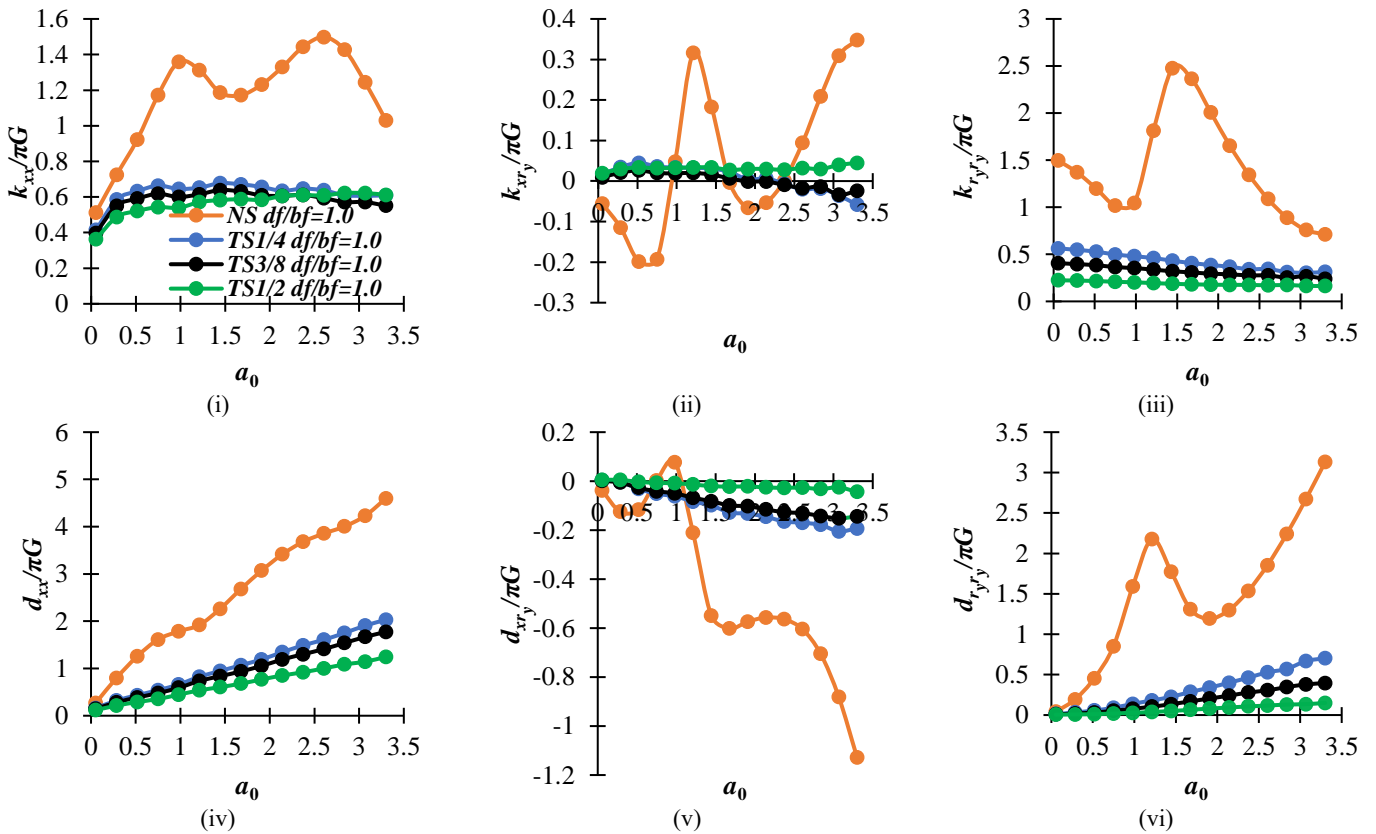


Figure 6-10: Comparisons of the calculated impedance functions of the case of embedded depth $d_f/b_f = 1.0$ for different scour scenarios i) k_{xx} ii) k_{xy} iii) k_{yy} iv) d_{xx} v) d_{xy} vi) d_{yy}

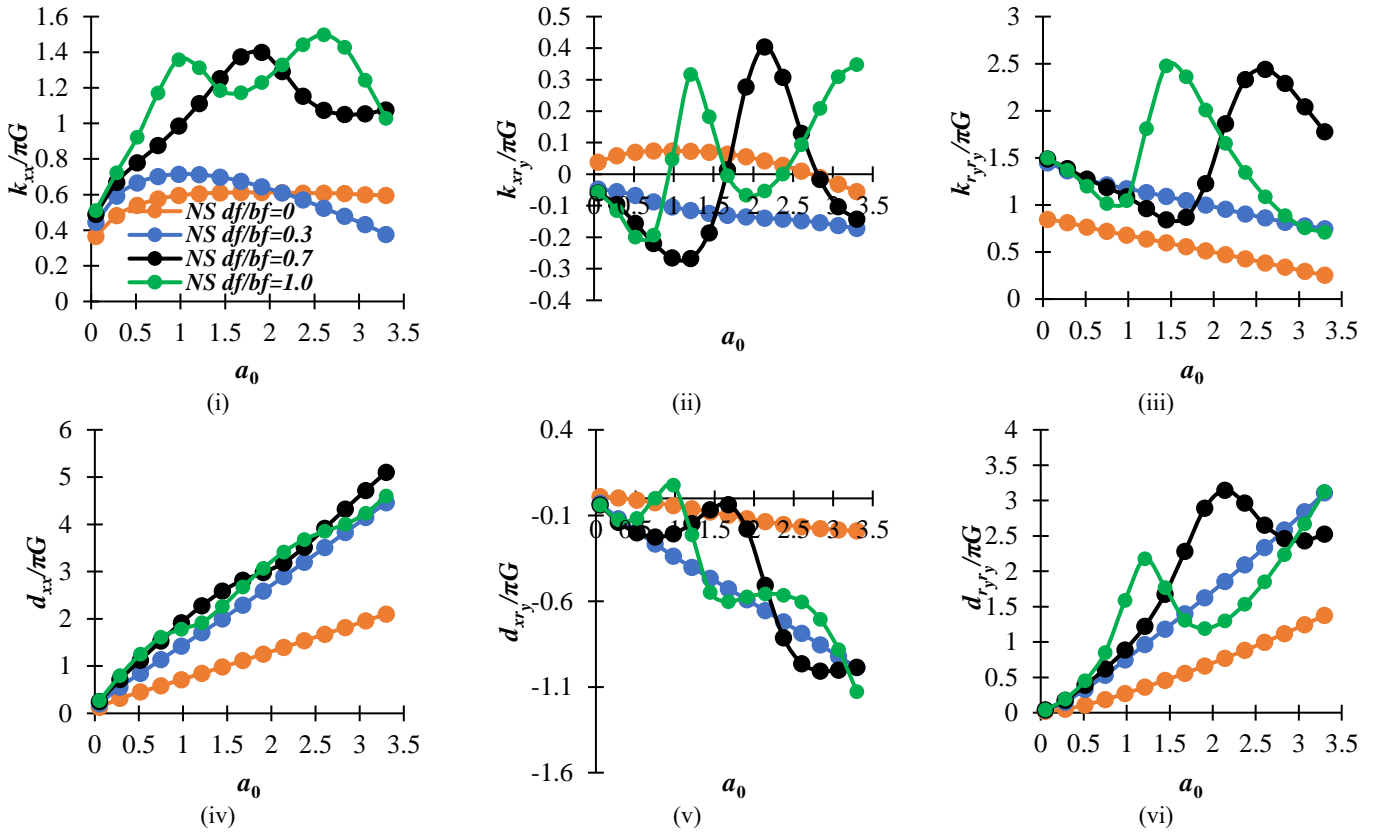


Figure 6-11: Comparison of the impedance functions of the case of NS for different embedded depths i) k_{xx} ii) k_{xy} iii) k_{yy} iv) d_{xx} v) d_{xy} vi) d_{yy}

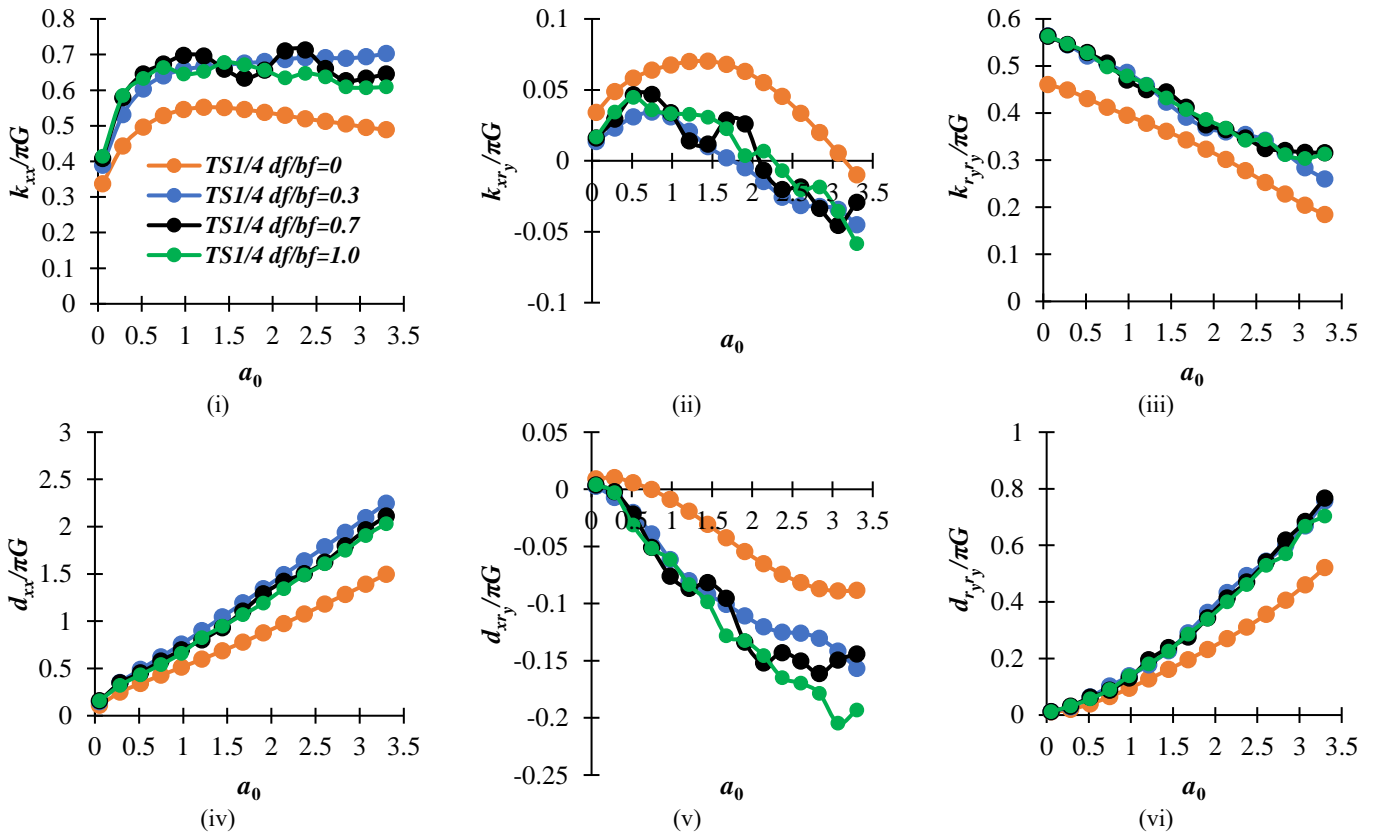


Figure 6-12: Comparison of the impedance functions of the case of TS1/4 for different embedded depths i) k_{xx} ii) k_{xy} iii) k_{yy} iv) d_{xx} v) d_{xy} vi) d_{yy}

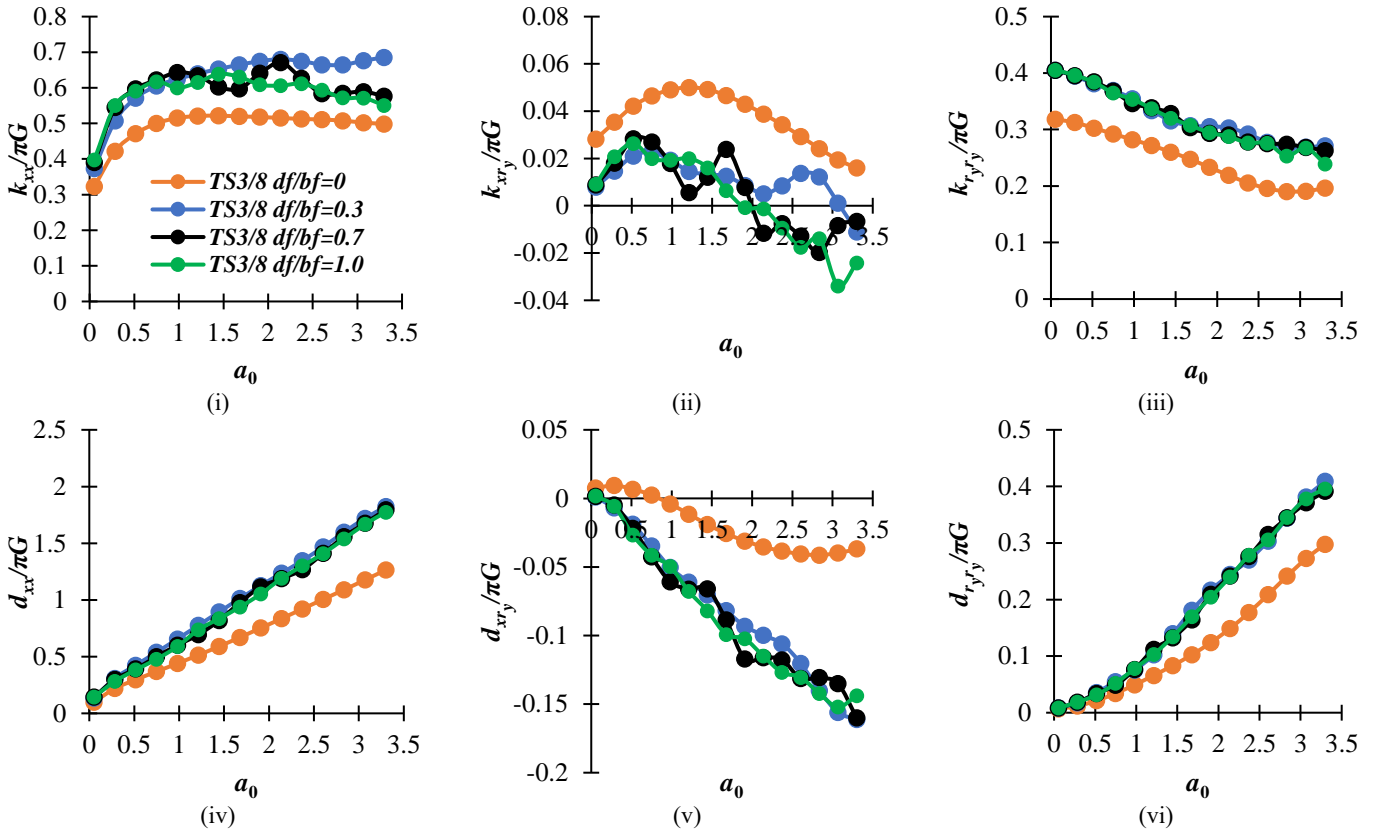


Figure 6-13: Comparison of the impedance functions of the case of TS3/8 for different embedded depths i) k_{xx} ii) k_{xry} iii) k_{ryy} iv) d_{xx} v) d_{xry} vi) d_{ryy}

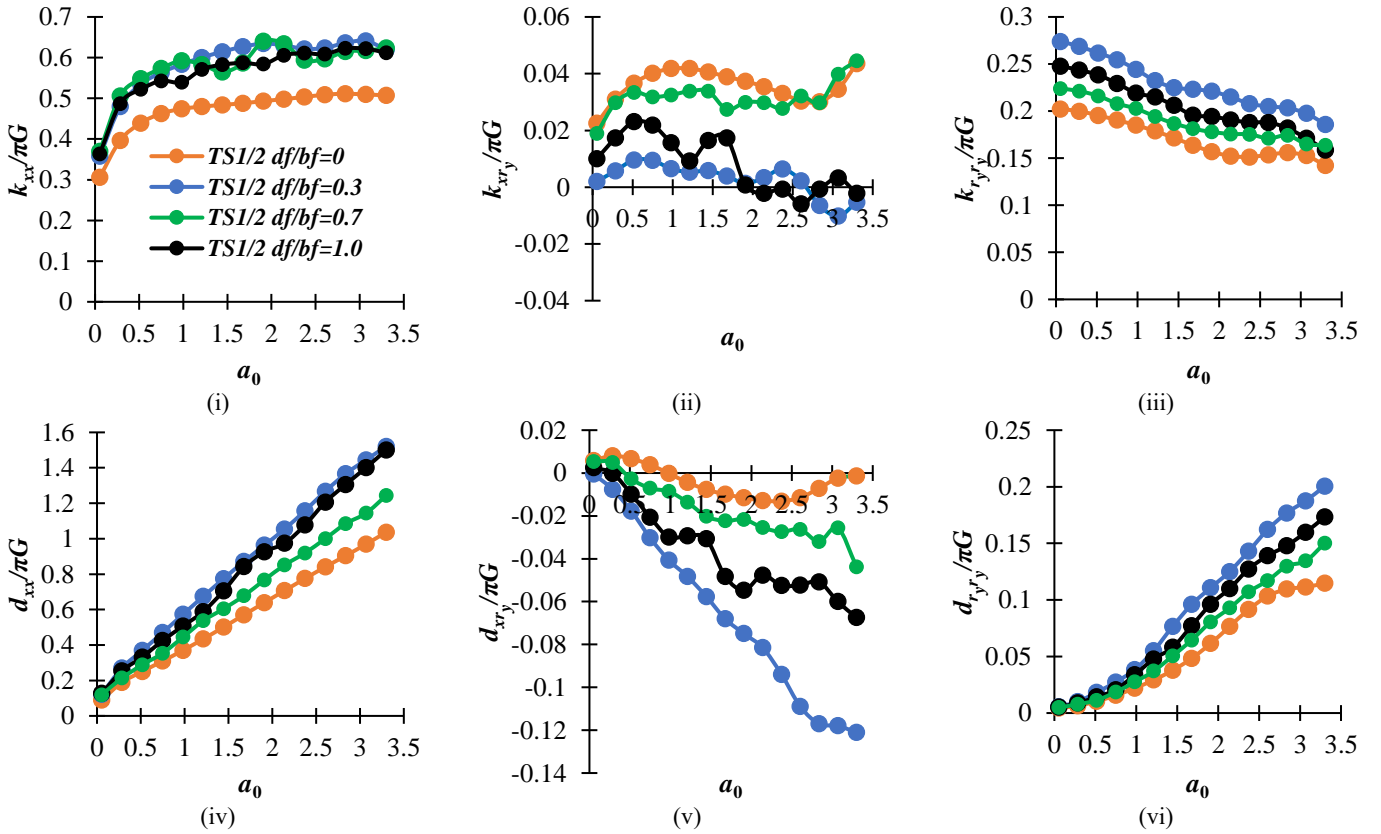


Figure 6-14: Comparison of the impedance functions of the case of TS1/2 for different embedded depths i) k_{xx} ii) k_{xry} iii) k_{ryy} iv) d_{xx} v) d_{xry} vi) d_{ryy}

6.3 Dynamic behaviour of SFS model

This section shows the results of a parametric study in which the previously derived impedance functions are used to evaluate the effect of scour on the dynamic response of the considered SFS system, for various foundation embedment depths and various geometrical, inertia and mechanical properties of the superstructure. The analysis expands the results shown in Chapter 4, where a simplified 3 degrees of freedom SFS model was considered for the case of foundation with no embedment. Similarly to Chapter 4, Buckingham theorem [5] is applied to reduce the numbers of the parameters that control the natural frequency $\tilde{\omega}$ of the SFS system of Figure 6-5. Specifically, $\tilde{\omega}$ can be expressed as a function of 14 parameters describing the superstructure, foundation and soil properties, with 3 reference dimensions, namely length [L], time [T] and mass [M]:

$$\tilde{\omega}=f(\omega_0, h_p, h_c, h_d, h_f, m_p, m_c, m_d, m_f, b_f, \rho, V_s, \nu, k_b) \quad (6.10)$$

The fixed base frequency of the superstructure, ω_0 , is controlled by the following parameters:

$$\omega_0=f(E, I, h_p, h_c, h_d, m_p, m_c, m_d, k_b) \quad (6.11)$$

According to Buckingham theorem, the number of the dimensionless Π parameters is equal to $15-3=12$ for the case of a foundation with no scour and no embedded depth. Two more parameters must be considered to account for the scour and embedded depth. The Π parameters obtained by choosing the variables b_f, ρ and V_s as the recurring set can be expressed as follows:

$$\begin{aligned} \Pi_\omega &= \frac{\tilde{\omega}}{\omega_0}, \Pi_{h_p} = \frac{h_p}{b_f}, \Pi_{h_c} = \frac{h_c}{b_f}, \Pi_{h_d} = \frac{h_d}{b_f}, \Pi_{h_f} = \frac{h_f}{b_f}, \Pi_{m_p} = \frac{m_p}{\rho b_f^3}, \Pi_{m_c} = \frac{m_c}{m_p}, \Pi_{m_d} = \frac{m_d}{m_p}, \\ \Pi_{m_f} &= \frac{m_f}{m_p}, \Pi_{\omega_0} = \frac{\omega_0 b_f}{V_s}, \Pi_{d_f} = \frac{2d_f}{2b_f}, \Pi_s = \frac{2s}{2b_f}, \Pi_k = \frac{k_b}{m_c \omega_0^2}, \nu \end{aligned} \quad (6.12)$$

Table 6-1: Units and dimensions of the involved parameters.

		Units	Dimensions
$\tilde{\omega}$	natural frequency of the SFS system	rad/s	[T ⁻¹]
ω_0	natural frequency of the fixed base system	rad/s	[T ⁻¹]
k_b	isolator stiffness on the pier	kN/m	[MT ⁻²]
h_p	pier height	M	[L]
h_c	pier cap height	M	[L]
h_d	65% of the deck height	M	[L]
h_f	half height of the foundation	M	[L]
m_p	pier mass	t	[M]
m_c	pier cap mass	t	[M]
m_d	deck mass	t	[M]
m_f	foundation mass	t	[M]
d_f	half embedment depth	m	[L]
s	half width of the scour-foundation interface	m	[L]
b_f	half width of the foundation	m	[L]
ρ	soil density	t/m ³	[ML ⁻³]
V_s	shear wave velocity	m/s	[LT ⁻¹]
ν	Poisson's ratio	-	-

It is noteworthy that the number of Π parameters is significantly increased compared the one of Chapter 4. This is the result of the more complex superstructure model and also of the consideration of the embedment depth of the foundation. In order to reduce the number of parameters to be varied in the

study, some simplifying assumptions are introduced. The values of the parameters Π_h , Π_{hc} , Π_{hd} and Π_{hf} are assumed to be fixed, and the bearings are assumed to restrain the relative motion between the top of the pier and the deck ($\Pi_k \rightarrow +\infty$). Furthermore, the width and depth of the pier cap are assumed as $b_c = 2b_f$ and $l_c = d$, respectively, while the width and the depth of the foundation are assumed to be equal. The ratio of the concrete density to soil density is assumed to be $\rho_c/\rho = 1.5$. Table 6-2 reports the values of the Π parameters considered in the parametric analysis. After introducing the above simplifying assumptions, the non-dimensional parameters that are varied in the parametric study are Π_h , Π_{mp} , Π_{mc} , Π_{mf} , Π_{ω_0} , Π_{df} , and Π_s . The parameter Π_{ω_0} varies from 0 to 4, whereas the parameter Π_h is assumed equal to either 1 or 5 in order to compare the behavior of tall and short piers. Once a value is chosen for Π_h , also the values of Π_{mp} , Π_{mc} , and Π_{mf} are fixed. Thus, the only parameters that is varied continuously in the analysis is Π_{ω_0} .

Figure 6-15 shows the variation of Π_{ω} for increasing values of Π_{ω_0} corresponding to the 4 scour case scenarios investigated for the different values of Π_{df} and Π_h considered. In general, the reduction of the vibration frequency of the SFS system due to scour is significantly different between the no-embedded and embedded scenarios, and particularly for taller piers. The effect of the embedment depth Π_{df} is generally low, with the exception of the case corresponding to $\Pi_s = 0.5$ and $\Pi_h = 5$, where an increase of the embedment depth leads to an increase of the effect of scour in terms of fundamental frequency reduction. On the other hand, both Π_{ω_0} and Π_h have a significant impact on the dynamic behavior of the SFS system, and increasing Π_{ω_0} and Π_h result in a reduction of the ratio of the natural frequency of the system due to scour. In other words, the taller the structure or the softer the soil, the higher the reduction of the natural frequency ratio due to scour. It is also interesting to observe that the reduction of natural frequency due to scour tends to approach an asymptotic value for high values of Π_{ω_0} .

Table 6-2: Assumed values and expressions of the investigated non-dimensional parameters.

$\Pi_k \rightarrow \infty$
$\Pi_h = 1, 5$
$\Pi_{hc} = 0.5$
$\Pi_{hd} = 0.5$
$\Pi_{hf} = 0.3$
$\Pi_{mp} = \frac{m_p}{\rho b_f^3} = \frac{A h_p \rho_c}{\rho b_f^3} = \frac{\rho_c \pi \left(\frac{d}{2}\right)^2 h_p}{\rho b_f^3} = \frac{1.5\pi \left(\frac{d}{2b_f}\right)^2}{4} \Pi_h$
$\Pi_{mc} = \frac{m_c}{m_p} = \frac{2b_f d h_c}{A h_p} = \frac{2b_f d h_c}{\pi \left(\frac{d}{2}\right)^2 h_p} = \frac{8b_f \Pi_{hc}}{\pi d \Pi_h}$
$\Pi_{md} = 4.7$
$\Pi_{mf} = \frac{m_f}{m_p} = \frac{4b_f^2 2h_f}{A h_p} = \frac{8b_f^2 h_f}{\pi \left(\frac{d}{2}\right)^2 h_p} = \frac{32b_f^2 \Pi_{hf}}{\pi d^2 \Pi_h}$
$\Pi_{\omega_0} = 0 - 4$
$\Pi_{df} = 0, 0.3, 0.7, 1$
$\Pi_s = 0, 0.25, 0.375, 0.5$
$\nu = 0.4$

In order to better highlight the effect of scour on the SFS system, Figure 6-16 illustrates the ratio of the natural frequency of the system with and without scour for increasing values of Π_s . The natural frequency ratio decreases almost linearly for increasing scour levels, and taller structures are found to be slightly more sensitive to scour effects. The variation of the frequency ratio with scour for different values of Π_{ω_0} above 1, tends to follow a single master curve. Thus, a self-similar behaviour is observed

for low values of shear wave velocity, for rigid superstructure, or for large foundations. Higher sensitivity to scour is observed for the case of embedded foundation corresponding to a foundation resting on the surface.

The results obtained for the case of zero embedment depth are quite similar to those obtained in Chapter 4 with a simpler superstructure system characterised by a single degree of freedom. It must be mentioned that the value of the Poisson's ratio of the soil in this study ($\nu = 0.4$) is different from the one considered in Chapter 4 ($\nu = 0.25$), whereas the term Π_h in this study is dependent on the pier height (h_p) compared to the one in Chapter 4 which is dependent on the total height of the SFS system. However, these differences have a negligible impact on the results.

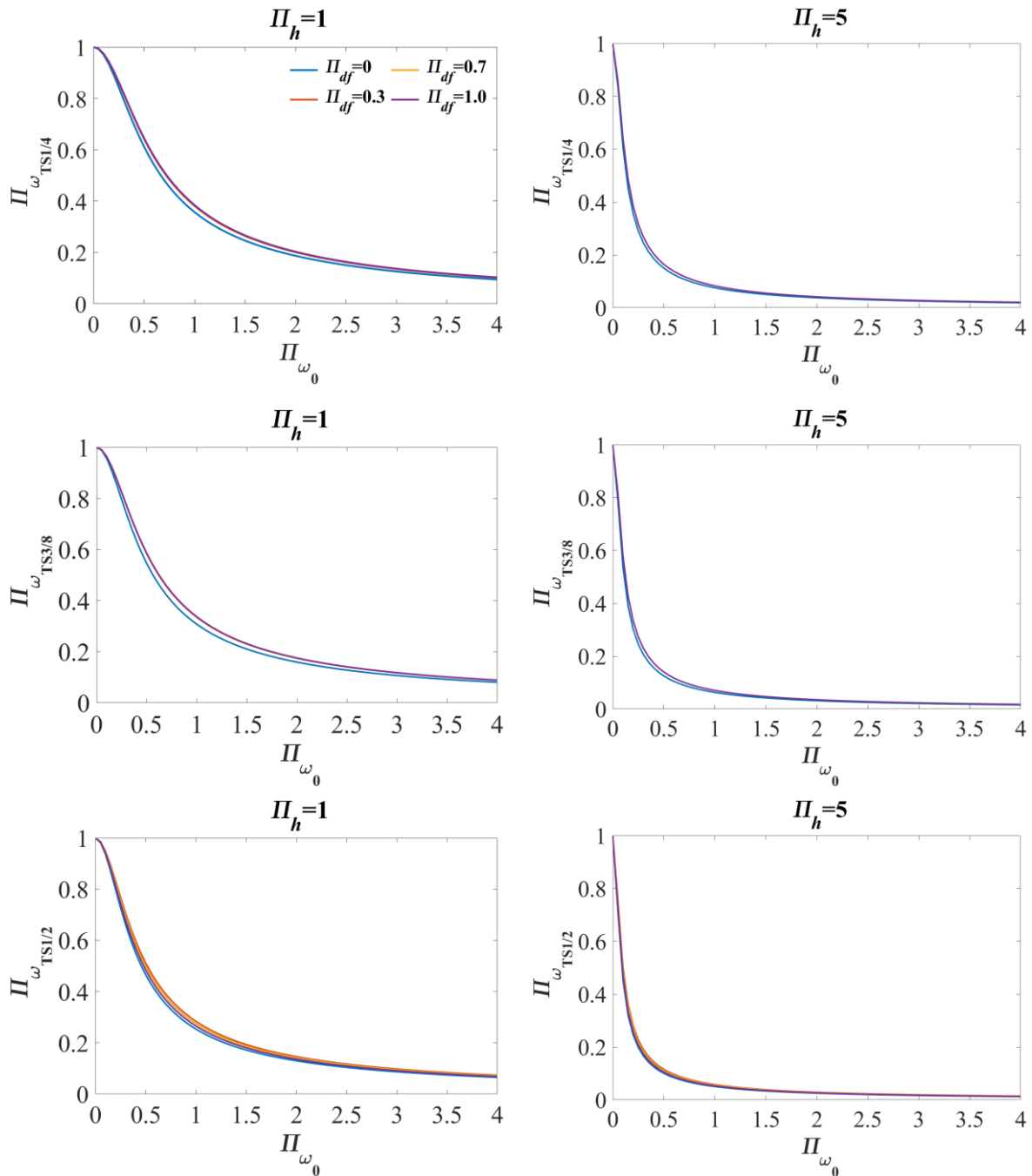


Figure 6-15: Variation of Π_{ω} for increasing values of Π_{ω_0} for various values of Π_{df} and Π_h .

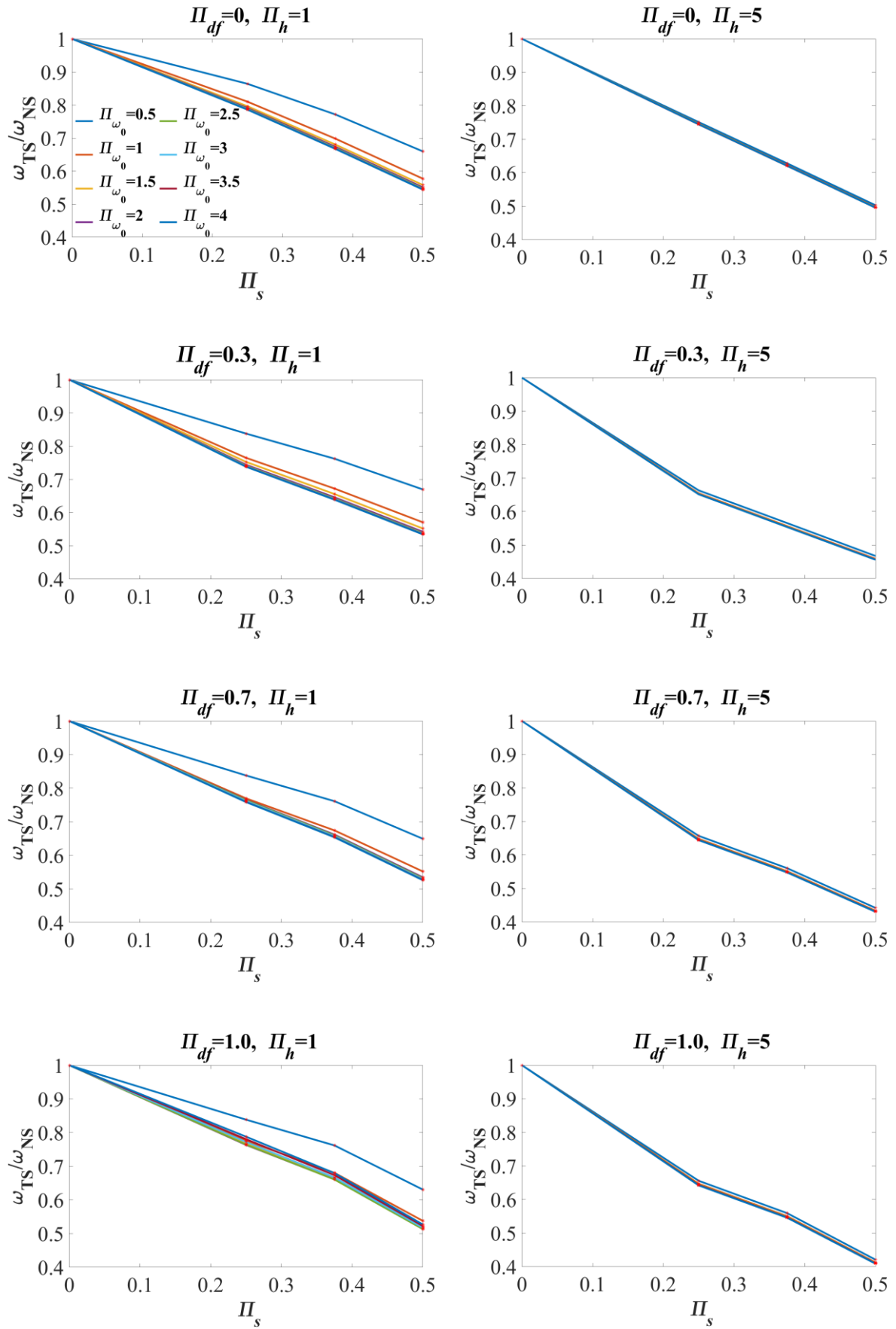


Figure 6-16: Ratio of the natural frequency of the system with and without scour for various levels of Π_{df} , Π_{ω_0} and Π_h .

6.4 Seismic response of SFS systems under scour hazard

In this section, the dynamic behaviour and the seismic performance of representative bridge piers with shallow foundation are investigated under various scour and embedded depths scenarios. Two different case studies are considered, corresponding to the SFS system of Figure 6-5, and differing only for the pier height. Table 6-3 reports the values of the parameters of the two investigated SFS systems, and Figure 6-17 shows the variation of the natural frequency of vibration for increasing levels of scour. The influence of the soil properties on the systems exposed to scour is also investigated, with three different values of the shear wave velocity considered, $V_s = 300, 500, 700$ (m/s). As expected, the tall pier has a lower natural frequency of vibration compared to the short pier. Moreover, there is an almost linear decrease of the natural frequency of the SFS systems for increasing scour levels and increasing the embedded depth increases the natural frequency and the sensitivity to scour only slightly.

Table 6-3: Geometry and properties of the examined SFS systems

Elastic modulus, $E =$	35GPa
Pier diameter, $d =$	2.1 m
Pier height, $h_p =$	5, 15 (m)
Foundation $2b_f \times 2b_f \times 2h_f =$	7 x 7 x 2.1 (m)
Pier cap $2b_c \times h_c \times d =$	7 x 1.75 x 2.1 (m)
Isolator stiffness, $k_b =$	$+\infty$
Deck mass, $m_d =$	610 ton
65 % of the deck height, $h_d =$	1.75 m
Soil density, $\rho =$	1600 kg/m ³
Shear wave velocity, $V_s =$	300, 500, 700 (m/s)

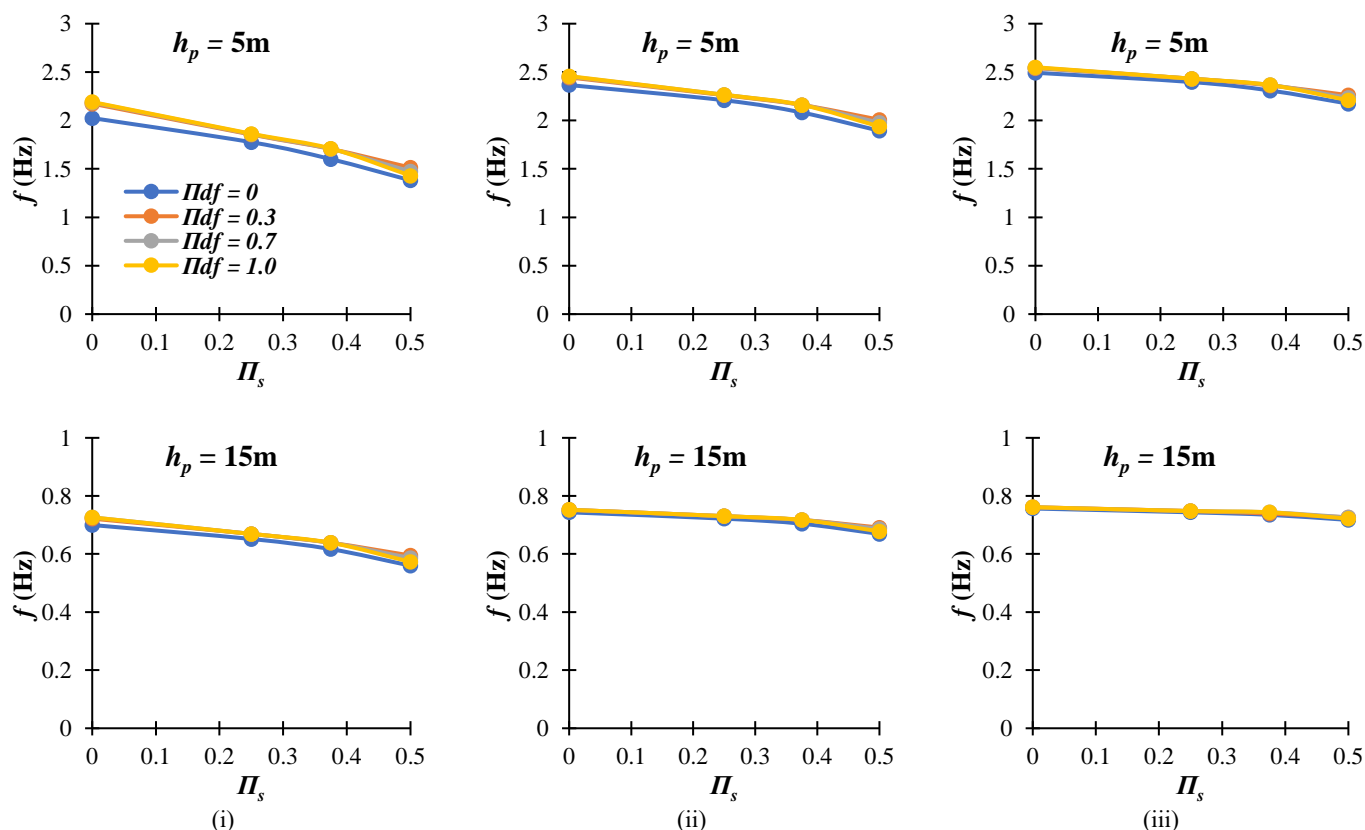


Figure 6-17: Vibration frequency estimates of the two investigated SFS systems for various scour and embedded depth scenarios and i) $V_s = 300$ m/s, ii) $V_s = 500$ m/s, iii) $V_s = 700$ m/s.

The seismic behaviour of the two SFS systems is analysed by performing time-history analyses under seven different ground motion records, selected with the Rexel software [6], and whose properties are reported in Table 6-4. The ground motions are characterized by an epicentral distance $25 < R < 37$, magnitude $5.5 < M < 6.3$ and shear wave velocity $360 \text{ m/s} < V_s < 760 \text{ m/s}$. The scaled records have been chosen so that the average acceleration elastic response spectrum matches the elastic response spectrum provided by Eurocode 8 [7] for soil Class C and $a_g = 0.19g$. Figure 6-18 illustrates the pseudo-acceleration spectrum of the single records obtained for a 5% damping ratio together with the average spectrum and the Eurocode 8 spectrum.

Table 6-4: Details of the picked ground motions via Rexel [6].

Earthquake	Station ID	Date	Magnitude M_w	Epicentral distance R (km)
Alkion	ST121	25/02/1981	6.3	25
Ishakli (aftershock)	ST856	03/02/2002	5.8	35
Izmit (aftershock)	ST3273	13/09/1999	5.8	25
Izmit (aftershock)	ST2571	11/11/1999	5.6	37
Cubuklu	ST65	20/04/1988	5.5	34
Adana	ST549	27/06/1998	6.3	30
Umbria Marche (aftershock)	ST223	14/10/1997	5.6	29

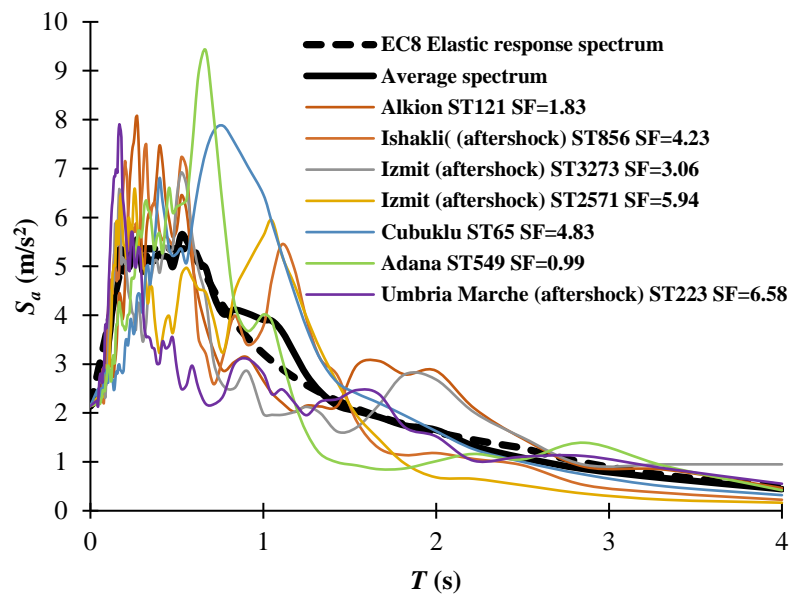


Figure 6-18: Response spectra of the ground motion records and corresponding scale factors (SF).

Figure 6-19 illustrates the seismic response of the two investigated SFS systems under various scour and embedment conditions for $V_s = 500 \text{ m/s}$ and for the ground motion recorded at Cubuklu. In particular, the time histories of the total displacement of the deck (u_d), the displacement of the foundation (u_f), and the contribution of the rotation of the foundation ($\varphi_f h_{total}$) are compared to each other in order to highlight the effect of soil-structure interaction on the response. It can be observed that the tall pier is characterized by significantly higher deck displacements, and a lower contribution to the response from soil-structure interaction, compared to the short pier. The peak deck displacement increases for increasing scour levels in the case of the short pier, whereas it does not increase significantly in the case of the tall pier. The contribution of the foundation rotation to the deck displacement response increases by increasing the scour level, as expected.

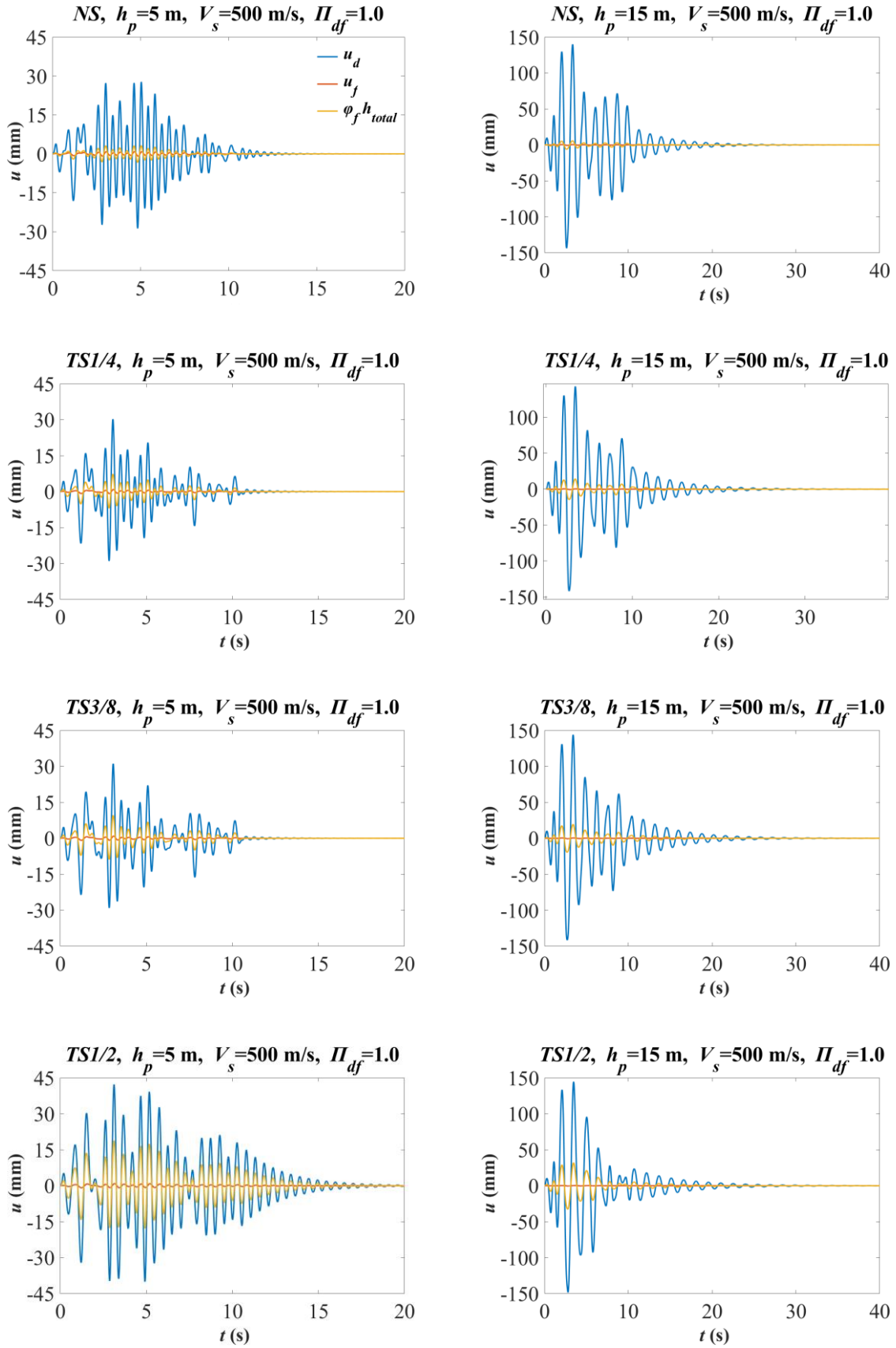


Figure 6-19: Seismic response of the examined SFS systems under Cubuklu earthquake for various scour and embedded depth scenarios and for $V_s = 500$ m/s.

Table 6-5 to Table 6-10 report the average peak seismic response of the SFS systems considering the 7 ground motions for all the above mentioned scour and shear wave velocity scenarios. In addition to the deck displacement and the base foundation displacement and rotation, the contribution of the pier flexure ($u_d - u_f - \varphi_f h_{total}$) is reported. In general, the peak deck displacement of the SFS systems increases by increasing the values of scour width, and so does the contribution of the base rotation to it, whereas the contribution of the base displacement and of the pier flexure does not change significantly. The contribution of the base rotation in presence of scour is more significant for the short pier than for the tall pier. By increasing the foundation embedment level, the peak deck displacement decreases in the case of no scour, whereas in the case of scour it is not possible to identify a clear trend. The effects of scour, in terms of peak deck displacement and contribution of the foundation rotation to it, are more significant for low values of V_s .

Table 6-5: Average peak response values of the SFS system for $h_p = 5$ m and $V_s = 300$ m/s under various scour and embedded depth scenarios.

$V_s = 300$ m/s	$\Pi_{df} = 0$				$\Pi_{df} = 0.3$			
	$\Pi_s = 0$	$\Pi_s = 0.25$	$\Pi_s = 0.375$	$\Pi_s = 0.5$	$\Pi_s = 0$	$\Pi_s = 0.25$	$\Pi_s = 0.375$	$\Pi_s = 0.5$
	u_d	23.48	34.91	37.56	40.84	19.09	32.72	35.80
u_f	1.62	1.89	1.72	1.32	1.48	1.90	1.90	1.95
$\varphi_f h_{total}$	8.31	17.45	22.22	28.40	4.94	14.90	19.14	26.52
$u_d - u_f - \varphi_f h_{total}$	13.70	15.72	13.79	11.24	12.78	16.13	14.88	14.01
$V_s = 300$ m/s	$\Pi_{df} = 0.7$				$\Pi_{df} = 1.0$			
	$\Pi_s = 0$	$\Pi_s = 0.25$	$\Pi_s = 0.375$	$\Pi_s = 0.5$	$\Pi_s = 0$	$\Pi_s = 0.25$	$\Pi_s = 0.375$	$\Pi_s = 0.5$
	u_d	18.64	32.69	35.87	43.01	18.31	32.85	36.01
u_f	1.31	1.76	1.81	1.63	1.21	1.74	1.78	1.34
$\varphi_f h_{total}$	4.81	14.92	19.22	28.10	4.75	14.99	19.30	28.42
$u_d - u_f - \varphi_f h_{total}$	12.63	16.18	14.97	13.53	12.46	16.28	15.04	12.44

Table 6-6: Average peak response values of the SFS system for $h_p = 5$ m and $V_s = 500$ m/s under various scour and embedded depth scenarios.

$V_s = 500$ m/s	$\Pi_{df} = 0$				$\Pi_{df} = 0.3$			
	$\Pi_s = 0$	$\Pi_s = 0.25$	$\Pi_s = 0.375$	$\Pi_s = 0.5$	$\Pi_s = 0$	$\Pi_s = 0.25$	$\Pi_s = 0.375$	$\Pi_s = 0.5$
	u_d	14.97	18.25	20.43	30.55	13.82	16.86	19.06
u_f	0.55	0.59	0.59	0.71	0.54	0.56	0.62	0.74
$\varphi_f h_{total}$	2.58	5.04	7.27	14.28	1.60	4.07	5.83	9.41
$u_d - u_f - \varphi_f h_{total}$	11.88	12.66	12.62	15.64	11.72	12.27	12.64	13.74
$V_s = 500$ m/s	$\Pi_{df} = 0.7$				$\Pi_{df} = 1.0$			
	$\Pi_s = 0$	$\Pi_s = 0.25$	$\Pi_s = 0.375$	$\Pi_s = 0.5$	$\Pi_s = 0$	$\Pi_s = 0.25$	$\Pi_s = 0.375$	$\Pi_s = 0.5$
	u_d	13.69	16.82	19.05	25.66	13.60	16.83	19.08
u_f	0.48	0.53	0.59	0.68	0.45	0.52	0.58	0.63
$\varphi_f h_{total}$	1.57	4.07	5.84	10.75	1.55	4.07	5.85	12.37
$u_d - u_f - \varphi_f h_{total}$	11.67	12.26	12.67	14.29	11.63	12.28	12.69	14.96

Table 6-7: Average peak response values of the SFS system for $h_p = 5$ m and $V_s = 700$ m/s under various scour and embedded depth scenarios.

$V_s = 700$ m/s	$\Pi_{df} = 0$				$\Pi_{df} = 0.3$			
	$\Pi_s = 0$	$\Pi_s = 0.25$	$\Pi_s = 0.375$	$\Pi_s = 0.5$	$\Pi_s = 0$	$\Pi_s = 0.25$	$\Pi_s = 0.375$	$\Pi_s = 0.5$
	u_d	13.42	14.78	16.46	19.27	12.73	14.27	15.33
u_f	0.29	0.30	0.30	0.31	0.29	0.30	0.32	0.36
$\varphi_f h_{total}$	1.30	2.44	3.69	6.02	0.81	2.01	2.87	4.42
$u_d - u_f - \varphi_f h_{total}$	11.84	12.07	12.50	12.96	11.65	11.98	12.18	12.64
$V_s = 700$ m/s	$\Pi_{df} = 0.7$				$\Pi_{df} = 1.0$			
	$\Pi_s = 0$	$\Pi_s = 0.25$	$\Pi_s = 0.375$	$\Pi_s = 0.5$	$\Pi_s = 0$	$\Pi_s = 0.25$	$\Pi_s = 0.375$	$\Pi_s = 0.5$
	u_d	12.67	14.25	15.31	18.14	12.64	14.25	15.31
u_f	0.26	0.28	0.30	0.32	0.25	0.27	0.30	0.29
$\varphi_f h_{total}$	0.79	2.01	2.87	4.95	0.78	2.01	2.87	5.49
$u_d - u_f - \varphi_f h_{total}$	11.64	11.98	12.18	12.89	11.63	11.99	12.18	13.03

Table 6-8: Average peak response values of the SFS system for $h_p = 15$ m and $V_s = 300$ m/s under various scour and embedded depth scenarios.

$V_s = 300$ m/s	$\Pi_{df} = 0$				$\Pi_{df} = 0.3$			
	$\Pi_s = 0$	$\Pi_s = 0.25$	$\Pi_s = 0.375$	$\Pi_s = 0.5$	$\Pi_s = 0$	$\Pi_s = 0.25$	$\Pi_s = 0.375$	$\Pi_s = 0.5$
	u_d	80.18	89.65	106.42	114.58	80.35	82.80	97.26
u_f	0.69	0.62	0.64	0.55	0.90	0.72	0.81	0.88
$\varphi_f h_{total}$	13.58	24.50	37.64	53.21	8.78	19.51	29.18	40.54
$u_d - u_f - \varphi_f h_{total}$	66.13	64.77	68.49	61.32	70.76	62.73	67.44	62.97
$V_s = 300$ m/s	$\Pi_{df} = 0.7$				$\Pi_{df} = 1.0$			
	$\Pi_s = 0$	$\Pi_s = 0.25$	$\Pi_s = 0.375$	$\Pi_s = 0.5$	$\Pi_s = 0$	$\Pi_s = 0.25$	$\Pi_s = 0.375$	$\Pi_s = 0.5$
	u_d	80.15	82.78	97.15	102.33	80.03	82.77	97.12
u_f	0.83	0.67	0.77	0.70	0.78	0.66	0.75	0.55
$\varphi_f h_{total}$	8.58	19.54	29.15	42.24	8.52	19.54	29.15	47.63
$u_d - u_f - \varphi_f h_{total}$	70.82	62.74	67.40	59.63	70.82	62.74	67.40	60.72

Table 6-9: Average peak response values of the SFS system for $h_p = 15$ m and $V_s = 500$ m/s under various scour and embedded depth scenarios.

$V_s = 500$ m/s	$\Pi_{df} = 0$				$\Pi_{df} = 0.3$			
	$\Pi_s = 0$	$\Pi_s = 0.25$	$\Pi_s = 0.375$	$\Pi_s = 0.5$	$\Pi_s = 0$	$\Pi_s = 0.25$	$\Pi_s = 0.375$	$\Pi_s = 0.5$
	u_d	71.37	74.44	74.34	74.19	70.22	73.50	74.89
u_f	0.27	0.23	0.20	0.18	0.33	0.28	0.29	0.30
$\varphi_f h_{total}$	4.89	8.91	12.25	17.64	2.98	7.36	10.06	13.75
$u_d - u_f - \varphi_f h_{total}$	66.28	65.39	62.00	56.52	66.95	65.93	64.61	59.57
$V_s = 500$ m/s	$\Pi_{df} = 0.7$				$\Pi_{df} = 1.0$			
	$\Pi_s = 0$	$\Pi_s = 0.25$	$\Pi_s = 0.375$	$\Pi_s = 0.5$	$\Pi_s = 0$	$\Pi_s = 0.25$	$\Pi_s = 0.375$	$\Pi_s = 0.5$
	u_d	70.17	73.50	74.89	73.24	70.14	73.49	74.88
u_f	0.30	0.26	0.27	0.24	0.28	0.25	0.27	0.18
$\varphi_f h_{total}$	2.91	7.37	10.06	14.86	2.88	7.37	10.07	16.23
$u_d - u_f - \varphi_f h_{total}$	66.99	65.93	64.62	58.24	67.01	65.93	64.63	57.61

Table 6-10: Average peak response values of the SFS system for $h_p = 15$ m and $V_s = 700$ m/s under various scour and embedded depth scenarios.

$V_s = 700$ m/s	$\Pi_{df} = 0$				$\Pi_{df} = 0.3$			
	$\Pi_s = 0$	$\Pi_s = 0.25$	$\Pi_s = 0.375$	$\Pi_s = 0.5$	$\Pi_s = 0$	$\Pi_s = 0.25$	$\Pi_s = 0.375$	$\Pi_s = 0.5$
	u_d	69.91	71.16	72.83	74.95	69.56	70.64	71.68
u_f	0.14	0.13	0.11	0.10	0.17	0.15	0.16	0.18
$\varphi_f h_{total}$	2.53	4.62	6.67	10.29	1.54	3.79	5.27	7.76
$u_d - u_f - \varphi_f h_{total}$	67.27	66.46	66.11	64.64	67.86	66.73	66.29	65.95
$\Pi_{df} = 0.7$				$\Pi_{df} = 1.0$				
$\Pi_s = 0$	$\Pi_s = 0.25$	$\Pi_s = 0.375$	$\Pi_s = 0.5$	$\Pi_s = 0$	$\Pi_s = 0.25$	$\Pi_s = 0.375$	$\Pi_s = 0.5$	
u_d	69.54	70.64	71.67	74.33	69.54	70.64	71.67	74.72
u_f	0.16	0.14	0.15	0.14	0.15	0.14	0.15	0.10
$\varphi_f h_{total}$	1.50	3.80	5.27	8.54	1.49	3.80	5.28	9.38
$u_d - u_f - \varphi_f h_{total}$	67.90	66.74	66.29	65.70	67.92	66.73	66.29	65.30

Figure 6-20 shows the ratio of the displacement due to the rotation of the foundation to the total displacement of the two investigated SFS systems for increasing scour widths and various embedded depths and shear wave velocities. The ratio increases almost linearly for increasing scour widths, whereas it reduces significantly for increasing values of shear wave velocity (i.e., stiffer soil). Moreover, the ratio is higher for the shorter pier, as already discussed above.

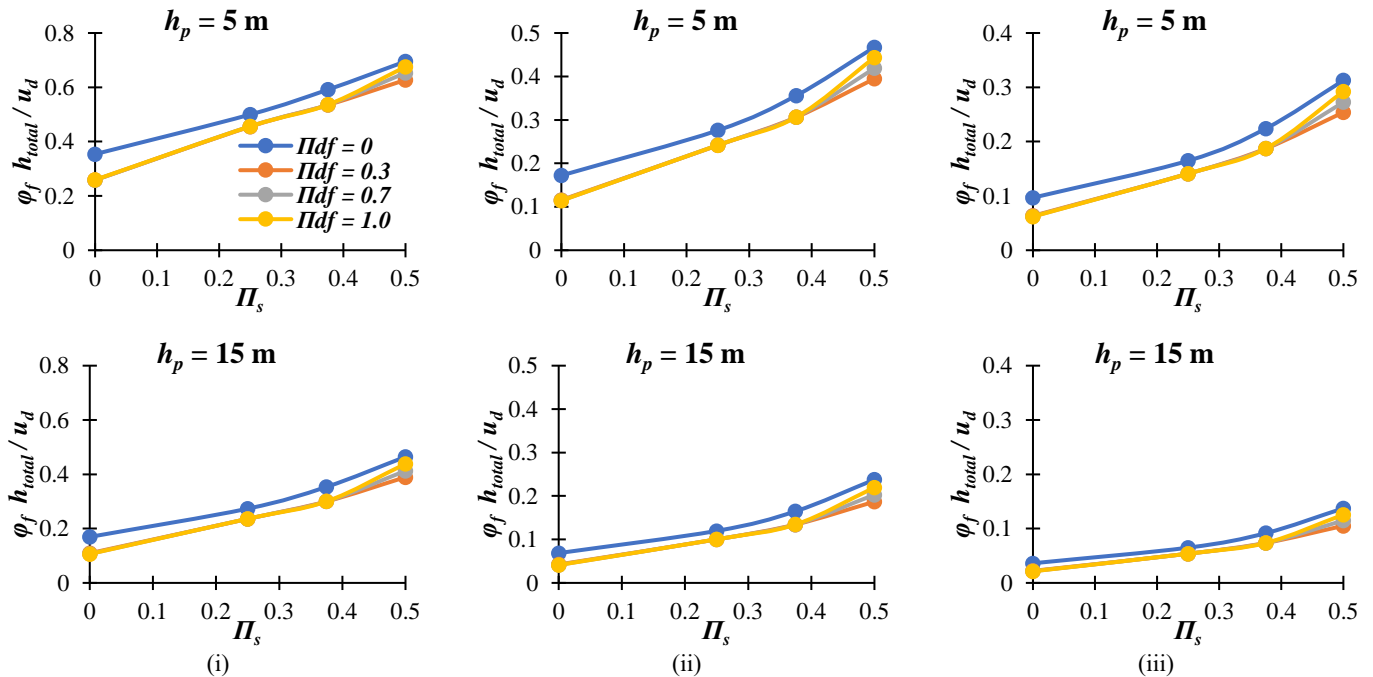


Figure 6-20: Contribution ratio of the rotational foundation displacement ($\varphi_f h_{total}$) to the total deck displacement (u_d) of the SFS systems for i) $V_s = 300$ m/s, ii) $V_s = 500$ m/s and iii) $V_s = 700$ m/s.

Figure 6-21 shows the contribution of the foundation displacement to the total displacement of the two SFS systems. Similarly, it is observed that the ratio is higher for the short pier. The displacement ratio decreases linearly for increasing scour width, and increasing values of V_s . However, it is worth mentioning that the contribution of the foundation displacement (u_f) to the overall deck displacement (u_d) is negligible. Figure 6-22 illustrates the contribution of the $u_d - u_f - \varphi_f h_{total}$ to u_d , which is representative of the flexural displacement of the pier. As expected, the ratio is higher for the taller pier, and it decreases almost linearly for increasing scour widths and increases for increasing values of V_s .

It is also interesting to observe that with the embedded depth Π_{df} increasing from 0 to 0.3 there is a dramatic reduction of the rocking phenomenon, whereas for values of Π_{df} increasing from 0.3 to 1 there is not a significant change. Thus, the rocking phenomenon is reduced dramatically by having an embedded foundation, with a minor role played by the depth of embedment. However, it must be mentioned that for the embedded cases ($\Pi_{df} > 0$) under severe scour, the higher the embedded depth, the higher the rocking phenomenon.

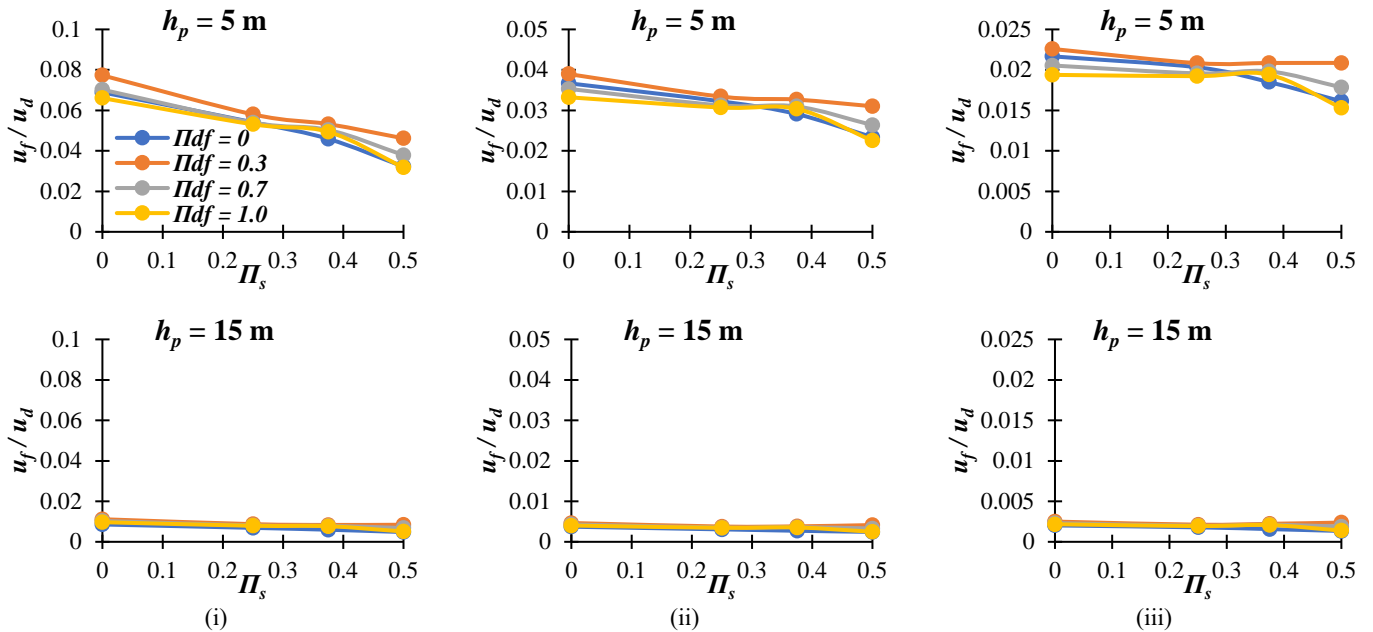


Figure 6-21: Contribution ratio of the foundation displacement (u_f) to the total deck displacement (u_d) of the SFS systems for i) $V_s = 300$ m/s, ii) $V_s = 500$ m/s and iii) $V_s = 700$ m/s.

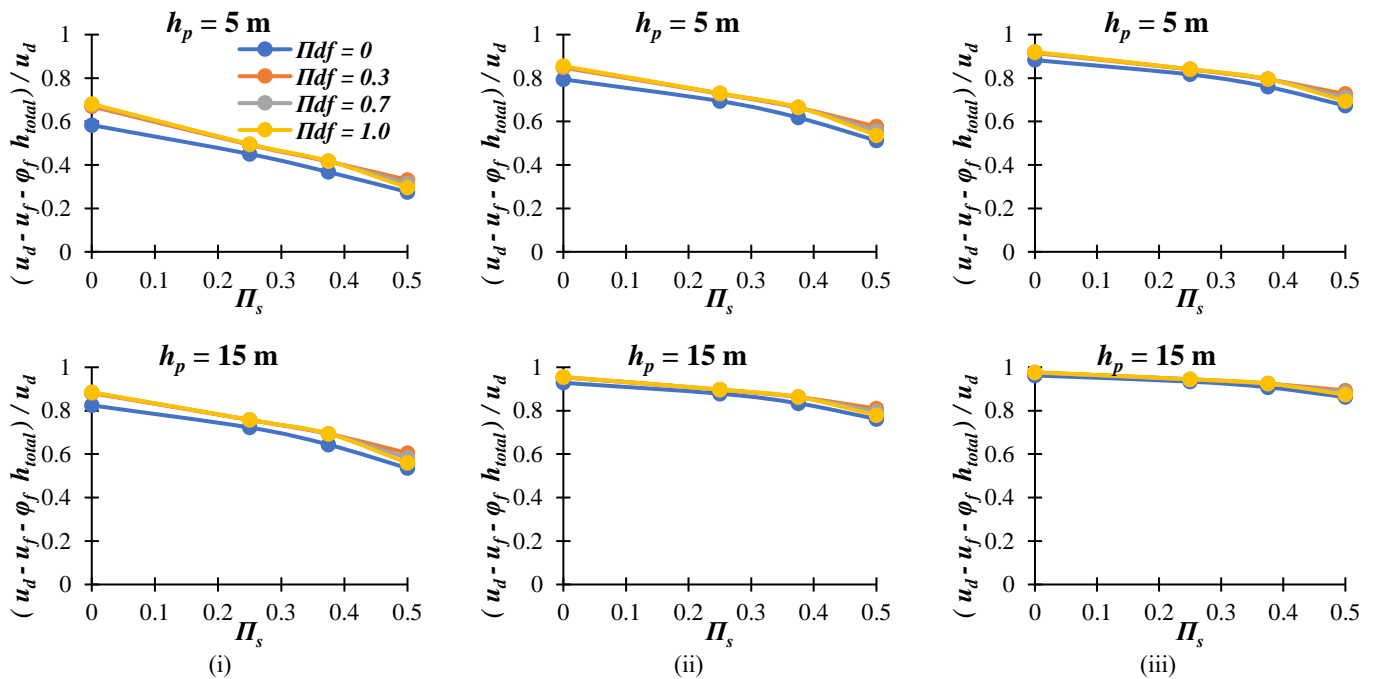


Figure 6-22: Contribution ratio of the $u_d - u_f - \phi_f h_{total}$ to the total deck displacement (u_d) of the SFS systems for i) $V_s = 300$ m/s, ii) $V_s = 500$ m/s and iii) $V_s = 700$ m/s.

It is important to note that, although this study does not compute FIM explicitly, its effects are indirectly considered through the impedance functions. The derived impedance functions account for SSI,

modifying the seismic response of bridge piers under different scour scenarios. The results indicate that scour affects FIM due to the foundation stiffness reduction and alters wave propagation (Figure 6-6 – Figure 6-14). The increased displacements and rocking of the foundation due to scour resulted from the time-history analyses further indicate deviation of FIM from free-field conditions. While this study primarily focuses on bridge response, future work will model FIM using kinematic interaction formulations to better quantify these effects.

6.5 Conclusions

This study has investigated the effect of scour on the dynamic behaviour and seismic response of bridges with shallow foundations. A multi-degree of freedom soil-foundation-structure (SFS) system, representative of the transverse response of continuous and simply supported girder bridges, has been analysed under various scour scenarios by considering different embedded depths of the foundation, and various soil and superstructure conditions. Initially, the frequency dependent impedance functions of a rigid strip foundation resting on an elastic soil domain have been numerically evaluated by performing analyses in Abaqus for different scour and embedded depths conditions. In general, increasing the scour width results in a significant reduction of the absolute values of the impedance functions for the case of no embedment. As for embedded cases, even though the presence of scour results in a dramatic reduction of the absolute values of the impedance functions, increasing scour width decreases them only slightly. Furthermore, the embedment depth has no significant effect on the impedance functions for all the scour scenarios, except for those related to the rotational behaviour, and the coupling between the translational and rotational behaviour of the foundation under severe scour conditions.

Subsequently, the dynamic behaviour of the SFS system has been investigated in an extensive parametric study considering wide ranges of values of the geometrical, mechanical and inertia properties of the soil and superstructure. The following results can be drawn:

- There is an almost linear reduction of the vibration frequency of the SFS system for increasing length of the foundation base undermined by scour.
- Higher sensitivity to scour is observed for the case of embedded foundation corresponding to a foundation resting on the surface. Increasing the embedded depth affects the results only slightly and yields a significant reduction of the vibration frequency for taller structures under extreme scour cases.
- In general, the reduction of the natural frequency of the SFS system due to scour is more significant for tall structures with soft soils.
- The variation with scour of the ratio of natural frequency of a SFS system with and without scour tends to a single master curve for low values of shear wave velocity, for rigid superstructure, or for large foundations.

Lastly, the seismic performance of two case studies with the same foundation and different pier height has been investigated by carrying out time history analyses under seven ground motion records and measuring the average peak seismic response of the components of the system. Based on the obtained results, the following conclusions are drawn:

- In general, the total displacement of the SFS system increases for increasing scour widths and for decreasing embedded depths. Particularly, this increase is more significant for SFS systems with softer soils.
- The embedded depth of the foundation affects only slightly the deck displacement and the sensitivity to scour.

- The relative contribution of the rocking of the foundation to the deck displacement is more significant for the shorter pier. Scour increases significantly this contribution. The response of the taller pier is dominated by pier bending also in the case of significant scour levels.
- The rocking phenomenon is reduced noticeably for embedded foundations. The embedment level affects the seismic response of the system only slightly.

The results of this study can be used to inform the development of structural health monitoring techniques for bridges with shallow foundations in seismic active and flood-prone areas. They also contribute to quantify the impact of scour on the seismic response of bridges with shallow foundations. While this work focuses on seismic response, the static effects of scour can also alter the boundary conditions and enhance the amplify rocking motions during seismic event. These factors, although not explicitly analysed here, could affect seismic performance. Future studies will investigate more realistic three-dimensional bridge models, by also taking into account the nonlinearity of the soil and of the superstructure. Additionally, future work will explore the explicit computation of Foundation Input Motion (FIM) to better quantify how scour modifies seismic input at the foundation level.

References

- [1] Abaqus V. 6.14 Documentation, Dassault Systemes Simulia Corporation, 2014.
- [2] Z. Hryniewicz, “Dynamic response of a rigid strip on an elastic half-space”, *Computer Methods in Applied Mechanics and Engineering*, vol. 25, issue 3, pp. 355-364, 1981.
- [3] E. Tubaldi, C.J. White, E. Patelli, S. Mitoulis, G. De Almeida, J. Brown, M. Cranston, M. Hardman, E. Koursari, R. Lamb, H. McDonald, R. Mathews, R. Newell, A. Pizarro, M. Roca, D. Zonta, “Invited perspectives: Challenges and future directions in improving bridge flood resilience”, *Natural Hazards and Earth System Sciences*, vol. 22, issue 3, pp. 795-812, 2022.
- [4] A. Ciancimino, L. Jones, L. Sakellariadis, I. Anastasopoulos, S. Foti, “Experimental assessment of the performance of a bridge pier subjected to flood-induced foundation scour”, *Géotechnique*, vol. 72, issue 11, pp. 998-1015, 2022.
- [5] T. Misic, M. Najdanovic-Lukic, L. Nesic, “Dimensional analysis in physics and the Buckingham theorem”, *European Journal of Physics*, vol. 31, issue 4, pp. 893, 2010.
- [6] I. Iervolino, C. Galasso, E. Cosenza, “REXEL: computer aided record selection for code-based seismic structural analysis”, *Bulletin of Earthquake Engineering*, vol. 8, pp. 339-362, 2010.
- [7] Eurocode 8: Design of structures for earthquake resistance – Part 1: General rules, seismic actions and rules for buildings

7 Conclusions and future work

Most of the existing research on bridge scour focuses on the case of bridges with deep foundations, leaving those the shallow foundations largely unexplored, despite their significance presence in earthquake-prone countries. Therefore, this lack of comprehensive studies had led to an undoubtedly gap in the current standards and monitoring strategies. This research aims to fill this knowledge gap by investigating both numerically and experimentally the impact of scour on the dynamic and seismic response of bridge with shallow foundations, and establish a quick, inexpensive, and remote approach able to capture scour extent by monitoring the vibration frequency of bridge piers.

One of the novelties of this study is the investigation of the impedance functions for shallow foundations under various scour conditions, which has been largely overlooked in previous studies. The frequency dependent impedance functions of a rigid strip foundation resting on an elastic soil domain are derived through a detailed finite element model and verified against analytical solutions to ensure accuracy of the results. Furthermore, they are presented in a non-dimensional form in relationship with the dimensionless frequency, making them applicable to different bridge configurations and soil conditions. In general, scour affects differently the various impedances, and the effects are also different for various frequencies investigated. For low frequencies, increasing scour width generally results in a reduction of the values of the impedance functions, while for high frequencies a clear trend cannot be identified. The impedance functions are also investigated for various embedded depths. When the foundation is embedded, even though the presence of scour leads to a dramatic reduction of the values of the impedance functions, increasing scour width decreases them only slightly. Additionally, the embedment depth has only a slight impact on the impedance functions for all the investigated scour scenarios, except for those related to the rotational behaviour, and coupling between the translational and rotational behaviour of the foundation under severe scour conditions.

Subsequently, extensive parametric analysis was conducted by using the derived impedance functions, to investigate the impact of scour on the dynamic behaviour of soil-foundation-structure (SFS) systems, considering a wide range of mechanical, geometrical and inertia properties of the soil and superstructure. Initially, a simplified single-degree-of-freedom (SDOF) system with a flexible base is used to investigate the impact of scour on the fundamental frequency variations. It is observed a linear reduction of the normalised fundamental frequency for increasing scour width, with more pronounced effects observed for tall piers on soft soils. Later, a more advanced multi-degree-of-freedom (MDOF) system with a flexible base, which is more representative of a bridge pier, is used to capture additional complexities of structural response and the effects of the embedment of the foundation. Systems with embedded foundation is observed to be more sensitive to scour compared to those with a foundation resting on the soil surface. Increasing the embedded depth affects the results only slightly, while it yields a significant reduction of the vibration frequency for taller structures under extreme scour cases. Furthermore, the variation with scour of the ratio of natural frequency of a SFS system with and without scour tends to a single master curve for low values of shear wave velocity, for rigid superstructure, or for large foundations.

Another novel contribution of this research is the first-ever full-scale free-field experiment, to the best author's knowledge, investigating the impact of scour on SFS systems with shallow foundations. Most of the experiments investigating scour effects in bridges with shallow foundations have been carried out in the laboratory, under controlled conditions, where it is impossible to fully recreate in-field conditions. The EuroProteas experimental campaign provides valuable insights into the effects of scour on the modal properties of bridges, filling a critical research gap by offering experimental validation for numerical strategies. The experimental testing campaign is complemented by both two-dimensional and three-dimensional numerical modelling strategies to identify the most effective approach for simulating the effects of scour on systems with shallow foundations. Specifically, i) a three-dimensional

model including the semi-infinite soil domain described by an elastoplastic behaviour, ii) a three-dimensional models where the soil is modelled through a set of distributed springs and dampers with aim of obtaining a simplified description of the soil-structure interaction problem, and iii) a simplified but robust two-dimensional model by using the derived impedance functions of this study, which is characterised by a significantly less computational cost and can replace traditional expensive scour monitoring techniques. Based on the results, all modelling strategies provide similar results in terms of the reduction of the vibration frequency of the system for increasing scour widths. The vibration frequencies of EuroProteas obtained by the numeral model reduce significantly for increasing scour widths, while they are in a great agreement with those obtained experimentally through vibration-based monitoring techniques. Particularly, the three-dimensional model describing the soil as a continuum with the absorbing boundaries can provide very accurate estimates of the modal properties of EuroProteas for all the investigated scour scenarios. Lastly, further numerical analyses conducted shows that the effect of scour hole (triangular or rectangular) have only a slight impact on the natural frequencies of EuroProteas for increasing scour widths.

This study also confirmed that scour-induced changes in the fundamental frequency significantly affects the seismic response of bridges by altering the rocking and translational contributions to total deck displacement. Time-history analyses of two bridge piers, differing only for the pier, subjected to real earthquake records shows that the total displacement of the SFS systems increases for increasing scour widths and for decreasing embedded depths, especially for SFS systems with softer soils. It is observed that the relative contribution of the rocking of the foundation to the total deck displacement is more significant for the shorter pier, while scour increases this contribution significantly. On the other hand, the seismic response of the taller pier is dominated by pier bending, especially under extreme scour conditions. Additionally, it is noticed that the embedded depth of the foundation has only a minor effect on the deck displacement and the sensitivity of the bridge piers to scour. The rocking phenomenon is reduced significantly for bridge piers with embedded foundations, while the embedment level affects their seismic response only slightly.

The findings of this research contribute to improving bridge design, scour monitoring, and maintenance strategies, providing a sound foundation for future studies that integrate scour and earthquake hazards. The developed strategies have important implications for the development of inverse techniques aimed at evaluating the extent of scour at bridge foundations based on the evaluation of the changes of the vibration frequency of SFS systems. This study advances the understanding of scour effects on bridges with shallow foundations, by filling fundamental knowledge gaps. Last but not least, the results provide insights into updating current bridge design codes, particularly in regions prone to flood and earthquake hazards, ensuring safety and resilience of brides against multi-hazards scenarios.

Despite the significant contributions of this research to the field, several limitations must be mentioned. The developed numerical models assume a linear behaviour of the soil (except the three-dimensional model using a semi-infinite soil domain which was described by an elastoplastic behaviour), and a linear superstructure response, which may lead to inaccuracies where material nonlinearities play a significant role, for example in extreme scour scenarios. Although a more realistic scour hole geometry was considered in the numerical analyses, the experimental investigation of EuroProteas in Chapter 5 included a rectangular scour hole, which is not representative of real scour conditions. Even though, the results demonstrated only a minor effect of the scour hole on the modal properties of EuroProteas for increasing scour widths, future experiments should investigate these effects further for larger scour widths. Furthermore, the impedance functions in Chapter 4 and 6 derived by assuming a bonded contact of the foundation-soil interface and do not account for soil-liquefaction or lateral spreading of the foundation, which may further impact the effects of scour on the dynamic behaviour and seismic response of bridges. Based on that, future studies should develop more advanced numerical modelling strategies to capture accurately the nonlinearities of soil and superstructure behaviour under coupled scour and earthquake hazards and validate them against further experimental tests. Lastly, seasonal

temperatures variation may also influence the natural frequency of systems, and therefore further long-term experimental and monitoring strategies are imperative to distinguish temperature-induced frequency variations from scour effects.

Data availability

All data supporting this thesis are available from the University of Strathclyde PURE repository in the following location:

<https://doi.org/10.15129/15b11bc4-5883-495b-8a09-4674308f5b86>